

**UNF Project  
Contract No. BDV34-977-01**

---

## **Empirical Deck for Phased Construction and Widening**

**Adel ElSafty, Ph.D., P.E. (Principal Investigator)**

**Kamal Tawfiq, Ph.D., P.E.**

**Ayman Okeil, Ph.D., P.E.**

---

**College of Computing, Engineering, and Construction  
University of North Florida  
Jacksonville, FL 32224-2645**

---

Sponsored by

**Florida Department of Transportation**



## **DISCLAIMER**

The opinions, findings, and conclusions expressed in this publication are those of the authors and not necessarily those of the State of Florida Department of Transportation.

## SI CONVERSION FACTORS

SYMBOL	WHEN YOU KNOW	MULTIPLY BY	TO FIND	SYMBOL
<b>LENGTH</b>				
<b>In</b>	inches	25.4	millimeters	mm
<b>Ft</b>	feet	0.305	meters	m
<b>yd</b>	yards	0.914	meters	m

SYMBOL	WHEN YOU KNOW	MULTIPLY BY	TO FIND	SYMBOL
<b>AREA</b>				
<b>in<sup>2</sup></b>	square inches	645.2	square millimeters	mm <sup>2</sup>
<b>ft<sup>2</sup></b>	square feet	0.093	square meters	m <sup>2</sup>
<b>yd<sup>2</sup></b>	square yard	0.836	square meters	m <sup>2</sup>

SYMBOL	WHEN YOU KNOW	MULTIPLY BY	TO FIND	SYMBOL
<b>VOLUME</b>				
<b>ft<sup>3</sup></b>	cubic feet	0.028	cubic meters	m <sup>3</sup>
<b>yd<sup>3</sup></b>	cubic yards	0.765	cubic meters	m <sup>3</sup>

NOTE: volumes greater than 1,000 L shall be shown in m<sup>3</sup>

SYMBOL	WHEN YOU KNOW	MULTIPLY BY	TO FIND	SYMBOL
<b>MASS</b>				
<b>oz</b>	ounces	28.35	grams	g
<b>Lb</b>	pounds	0.454	kilograms	kg

SYMBOL	WHEN YOU KNOW	MULTIPLY BY	TO FIND	SYMBOL
<b>FORCE and PRESSURE or STRESS</b>				
<b>lbf</b>	pound force	4.45	newton	N
<b>lbf/in<sup>2</sup></b>	pound force per square inch	6.89	kilopascals	kPa
<b>kip</b>	1,000 pounds force	4.45	kilonewton	kN

## TECHNICAL REPORT DOCUMENTATION

1. Report No.	2. Government Accession No.	3. Recipient's Catalog No.	
4. Title and Subtitle  <b>Empirical Deck for Phased Construction and Widening</b>		5. Report Date <b>February 2017</b>	
		6. Performing Organization Code	
7. Author(s) <b>Dr. Adel ElSafty, Dr. Kamal Tawfiq, Dr. Ayman Okeil</b>		8. Performing Organization Report No.	
9. Performing Organization Name and Address <b>University of North Florida School of Engineering, 1 UNF Drive Jacksonville, FL 32224</b>		10. Work Unit No. (TRAIS)	
		11. Contract or Grant No. <b>BDV34-977-01</b>	
12. Sponsoring Agency Name and Address <b>State of Florida Department of Transportation 605 Suwannee St. MS 30 Tallahassee, FL 32399</b>		13. Type of Report and Period Covered <b>Final Report March 2013 - September 2016</b>	
		14. Sponsoring Agency Code	
15. Supplementary Notes			
16. Abstract <p>Compressive membrane action behavior in bridge decks has been known for many years. Some countries, such as Canada, have adopted the empirical deck design method in the Canadian Highway Bridge Design Code after extensive studies and research. In the United States, the American Association of State Highway and Transportation Officials (AASHTO) LRFD Bridge Design Specifications has provisions that allow the use of the empirical deck design method; however, state departments of transportation (DOTs) often require that reinforced concrete decks be designed using the traditional method and disallow the use of the empirical method. This is due in part to the fact that some of the current conditions (e.g., it is imperative to have a sufficient overhang length) are impossible to satisfy in phased construction and future widening scenarios. Compressive membrane action, although more complex to analyze, is a more realistic design approach than the traditional method that assumes a pure bending behavior. The behavior and failure modes of reinforced concrete bridge decks clearly exhibit membrane action, assuming lateral restraint is sufficient among other conditions. Although both methods are conservative, studies have shown that assuming a flexural behavior in reinforced concrete bridge deck design leads to a larger increase in the reserve strength compared to the empirical deck design method. To investigate the performance of concrete bridge decks designed with the empirical design method, extensive experimental testing of a full-size specimen was conducted. The fabricated deck specimen mimicked a widening scenario, was 47 feet in length and 18.5 feet in width, and was supported on two prestressed concrete beams with a 14-foot spacing and a 2-ft overhang beyond the edge of one of the two beams. The two 36-inch-deep Florida I-Beams (FIB-36) were used to support the 8-inch concrete deck reinforced with two layers of No.5 rebar at 12-inch spacing in both directions. Nine service and failure tests were conducted at different locations along the bridge deck. Not only will the empirical deck approach decrease the required amount of deck reinforcement compared to the traditional method, it will also provide ease in design and constructability, which may decrease those associated costs even further. The test specimen used in this study provided desirable results in strength and serviceability (a concern for most agencies). The outcome of this research study provides information to the FDOT officials regarding the feasibility of using the empirical method in design of bridge decks under conditions not currently covered by AASHTO LRFD provisions.</p>			
17. Key Word <b>bridge, deck , empirical</b>		18. Distribution Statement <b>No restrictions</b>	
19. Security Classif. (of this report) <b>Unclassified</b>	20. Security Classif. (of this page) <b>Unclassified</b>	21. No. of Pages <b>274</b>	22. Price

## **ACKNOWLEDGEMENTS**

The authors would like to thank the Florida Department of Transportation for their support of this research. In particular, special thanks go out to Will Potter, Sam Fallaha, and David Wagner for their help and support throughout the project. The authors would also like to include special thanks to all the laboratory staff and the technicians at the Marcus H. Ansley Structures Research Center, Tallahassee, Florida.

## EXECUTIVE SUMMARY

Compressive membrane action behavior in bridge decks has been known for many years. Some countries, such as Canada, have adopted the empirical deck design method in the Canadian Highway Bridge Design Code after extensive studies and research. In the United States, the AASHTO LRFD Bridge Design Specifications has provisions that allow the use of the empirical deck design method; however, State Departments of Transportation (DOTs) often require that reinforced concrete decks be designed using the traditional method and disallow the use of the empirical deck design method. This is due in part to the fact that some of the current conditions (e.g., it is imperative to have a sufficient overhang length) are impossible to satisfy in future widening scenarios. Compressive membrane action, although more complex to analyze, gives a more realistic design approach than the traditional method that assumes a pure bending behavior.

An extensive experimental testing of a full-size specimen was conducted to investigate the performance of concrete bridge decks designed with the empirical design method. The fabricated deck specimen has a length of 47 feet and width of 18.5 feet and is supported on two prestressed concrete beams with a 14-foot spacing and a 2-ft overhang beyond the edge of one of the two beams. The two 36-inch-deep Florida I-Beams (FIB-36) were used to support the 8-inch concrete deck reinforced with two layers of No.5 rebar at 12-inch spacing in both directions. Nine service and failure tests were conducted at different locations along the bridge deck.

The behavior and failure modes of reinforced concrete bridge decks clearly exhibit membrane action assuming lateral restraint is sufficient among other conditions. Furthermore, studies have shown that assuming a flexural behavior in reinforced concrete bridge deck design leads to an increase in the reserve strength compared to the empirical deck design method. Not only will the empirical deck approach decrease the required amount of deck reinforcement compared to the traditional method, it will also provide ease in design and constructability, which may decrease those associated costs even further. The test specimen used in this study provided desirable results in strength and serviceability (a concern for most agencies). The outcome of this research study provides information to the FDOT officials regarding the feasibility and of using empirical design method in bridge decks.

# TABLE OF CONTENTS

<b>SI CONVERSION FACTORS</b> .....	iii
<b>TECHNICAL REPORT DOCUMENTATION</b> .....	iv
<b>ACKNOWLEDGEMENTS</b> .....	v
<b>EXECUTIVE SUMMARY</b> .....	vi
<b>LIST OF TABLES</b> .....	x
<b>LIST OF FIGURES</b> .....	xii
Chapter 1 Introduction.....	1
1.1 Objectives .....	2
1.2 Justification for the Research.....	2
1.1 Impact .....	2
1.2 Background.....	2
Chapter 2 Literature Review.....	5
2.1 Compressive Membrane Action in Slabs.....	6
2.2 Bridge Deck Design in the U.S.....	11
2.3 Deck Design in Canada.....	17
2.4 Methods of Predicting Deck Capacity .....	19
2.4.1 British Standard BS5400 Method .....	19
2.4.2 American Concrete Institute (ACI Method) .....	20
2.4.3 UK Highways Agency, BD81/02 Method .....	20
2.4.4 Taylor, Rankin, and Cleland’s Approach (TRC).....	21
Chapter 3 Design and Analysis of Test Specimen .....	26
3.1 Preliminary Design and Analysis of Deck.....	26
3.1.1 Analytical and Parametric Studies .....	26
3.1.2 Finite Element Modeling of Bridge Deck.....	33
3.2 Beam Design Information.....	45
3.3 Deck Design.....	47
Chapter 4 Experimental Program & Fabrication.....	48
4.1 Specimen Dimensions.....	49
4.1.1 Girder Details.....	50
4.2 Fabrication .....	50
4.2.1 Beam Fabrication .....	52

4.2.2	Bearing Pads-Type “D” .....	54
4.2.3	Formwork.....	55
4.2.4	Deck Steel Reinforcement .....	58
4.2.5	Concrete Deck.....	61
4.3	Instrumentation .....	66
4.3.1	Displacement Gauges.....	69
4.3.2	Embedded Strain Gauges on Steel Reinforcement .....	72
4.3.3	Concrete Deck Surface-Mounted Strain Gauges .....	78
4.3.4	Concrete Deck Surface-mounted Crack Width Gauges.....	78
4.3.5	Girder Surface-mounted Strain Gauges .....	80
4.4	Phased Widening .....	84
4.5	Loading and Testing .....	85
4.5.1	Load System.....	85
4.5.2	Load Cases .....	85
Chapter 5	Analysis and Interpretation of the Test Results .....	89
5.1	Service Results.....	92
5.1.1	Deflection Performance .....	92
5.1.2	Strain Readings .....	101
5.1.3	Crack Gauges and Widths.....	113
5.2	Failure Test Results.....	119
5.2.1	Overall Comparison .....	121
5.2.2	Deck Performance under Load Case F1 .....	127
5.2.3	Deck Performance under Load Case F2 .....	136
5.2.4	Deck Performance under Load Case F3 .....	142
5.2.5	Deck Performance under Load Case F4 .....	148
5.3	Mode of Failure.....	152
5.3.1	Load Case F1 .....	153
5.3.2	Load Case F2 .....	158
5.3.3	Load Case F3 .....	162
5.3.4	Load Case F4 .....	164
5.4	Results.....	168
Chapter 6	Comparison of Analytical, Finite Element, and Test Results.....	170

6.1	Comparison of the Finite Element Results and the Failure Test Results.....	170
6.2	Comparison of Analytical Results and the Failure Test Results.....	175
Chapter 7	Conclusions and Recommendations .....	176
7.1	Summary .....	176
7.2	Conclusions.....	178
7.3	Recommendations for Construction and Design .....	179
<b>References</b>	.....	<b>181</b>
<b>APPENDICES</b>	.....	<b>187</b>
	APPENDIX I: FORMWORK PICTURES.....	187
	APPENDIX II: MIX DESIGN.....	191
	APPENDIX III: FEA AND DESIGN CALCULATIONS .....	192
	APPENDIX IV: PHOTOS OF SPECIMEN AND TESTING.....	207
	APPENDIX V: INSTRUMENTATION.....	212
	APPENDIX VI: GAUGE LOCATIONS.....	218
	APPENDIX VII: CRACK MAPPING .....	234
	APPENDIX VIII: SERVICE PLOTS .....	241

# LIST OF TABLES

Table 2.1: Bridge Deck Design Method by State .....	15
Table 3.1: Summary of Predicted Capacities Using an 8-inch Slab ( $f'_c = 5$ ksi) .....	28
Table 3.2: Ultimate capacity of a bridge deck on FIB-36 girders analyzed using TRC ( $t_s = 8$ inch and $f'_c = 5$ ksi) .....	29
Table 3.3: Ultimate capacity of a bridge deck on AASHTO Type III girders analyzed using TRC ( $t_s = 7.5$ in and $f'_c = 5$ ksi).....	29
Table 3.4: Effect of compressive concrete strength on deck capacity using TRC method and FIB-36 girders .....	30
Table 3.5: Support beam lateral stiffness $K_b$ (kip/in) by varying beam type and beam spacing ..	32
Table 3.6: Required main reinforcing steel ratio for 8-inch-thick decks .....	37
Table 3.7: Initial beam spans and spacing's modeled in ANSYS prior to lab specimen selection .....	40
Table 3.8 Beam Design Information.....	45
Table 4.1: Slump Test Results .....	62
Table 4.2: Concrete Cylinder Strength for Deck .....	63
Table 4.3: Concrete Cylinder Strengths for Beams .....	64
Table 4.4: Data from Mill Test Reports for Deck Reinforcing Bars .....	64
Table 4.5: Gauge Count for S1, S2, S3, F1, F2, and F3 .....	67
Table 4.6: Gauge Count for S5 .....	67
Table 4.7: Gauge Count for S4/F4.....	68
Table 4.8: Typical Gauge Nomenclature .....	83
Table 4.9: Service Testing Notes .....	87
Table 4.10: Failure Testing Notes.....	88
Table 5.1: Deflection Comparisons .....	94
Table 5.2: Crack Location and Orientation for the bottom surface of the F1 Test.....	118
Table 5.3: Crack Widths for the bottom surface of the F1 Test .....	118
Table 5.4: Crack Location and Orientation for the bottom surface of the F4 Test.....	118

Table 5.5: Crack Widths for the bottom surface of the F4 Test .....	119
Table 5.6: Failure Test Deflection Results .....	123
Table 5.7: Testing Summary under service loads .....	169

# LIST OF FIGURES

Figure 1.1: Survey results for DOTs' preferred bridge deck design methodology (Nielsen, et al. 2010) .....	4
Figure 2.1: Wheel load transfer .....	6
Figure 2.2: Arching action and three-hinged arch analogy (Rankin 1982) .....	7
Figure 2.3: CMA effect (courtesy of Gvozdev 1939).....	8
Figure 2.4: Top Surface crack pattern of punching failure zone in model bridge deck test (Kirkpatrick, Rankin and Long 1984).....	9
Figure 2.5: Bottom surface crack pattern of punching failure zone in model bridge deck test (Kirkpatrick, Rankin and Long 1984).....	9
Figure 2.6: Reinforcement for cast-in-place deck.....	18
Figure 2.7: Details for cast-in-place deck slabs .....	19
Figure 3.1: Deck capacities by varying beam spacing and analysis method .....	27
Figure 3.2: Deck strength by varying deck thickness and beam spacing for decks on FIB-36 girders analyzed using TRC.....	30
Figure 3.3: Effect of span length on the bridge deck ultimate capacity .....	31
Figure 3.4: Relationship between ultimate capacity and equivalent stiffness of support system. 33	
Figure 3.5: Typical section for 14-foot beam spacing .....	34
Figure 3.6: Plate sign convention used in STAAD.Pro V8i .....	35
Figure 3.7: FIB-36 beam geometry in STAAD.Pro V8i.....	35
Figure 3.8: Three-dimensional finite element model.....	36
Figure 3.9: Finite element model showing maximum positive moment in the deck .....	36
Figure 3.10: Average ( $\rho$ ) vs beam spacing for 8-inch thick decks .....	38
Figure 3.11: FDOT guidelines for beam spacing to beam span for the FIB-36 .....	39
Figure 3.12: FE modeling of bridge span = 80' and beam spacing = 14' .....	41
Figure 3.13: FE modeling of bridge deck .....	41
Figure 3.14: Bridge modeling with span = 80' and beam spacing = 14' during widening phase	42
Figure 3.15: Load configuration during widening phase.....	43

Figure 3.16: Simulated tire patch footprints from pressure sensor film at different load levels ..	43
Figure 3.17: Variation of contact area with applied load.....	44
Figure 3.18: Tire contact pressure as function of applied load for different tire widths (Majumdar, et al. 2009) .....	44
Figure 3.19: Florida I-beam properties .....	45
Figure 3.20: Strand pattern .....	46
Figure 3.21: Shear stirrup spacing (symmetric about centerline).....	46
Figure 4.1: Fabricated specimen .....	48
Figure 4.2: Specimen dimensions .....	49
Figure 4.3: Testing locations.....	50
Figure 4.4: Transverse deck rebar extending beyond deck at the widening side .....	51
Figure 4.5: Specimen and load frame .....	51
Figure 4.6: FIB-36 Fabrication showing formwork and prestressing tendons .....	52
Figure 4.7: FIB-36 beams as delivered .....	53
Figure 4.8: FIB hanger brackets in top flange and views of completed beam.....	53
Figure 4.9: Bearing pad - FDOT Design Standard Index 20510 .....	54
Figure 4.10: Bearing pad in place .....	54
Figure 4.11: Deck hanger brackets .....	55
Figure 4.12: FIB-36 stirrups and overhang hanger brackets.....	56
Figure 4.13: Adjusting cantilever formwork system .....	56
Figure 4.14: Cantilever formwork .....	56
Figure 4.15: Deck formwork (clear span).....	57
Figure 4.16: Deck formwork during construction .....	57
Figure 4.17: Overall completed formwork .....	58
Figure 4.18: Transverse reinforcement (bottom layer centered) .....	59
Figure 4.19: Longitudinal reinforcement and cover (bottom layer centered).....	59
Figure 4.20: Plan view showing splice locations and lengths .....	60
Figure 4.21: Placed bottom mat .....	61
Figure 4.22: Placed top mat reinforcement.....	61

Figure 4.23: Deck pouring and curing .....	65
Figure 4.24: Concrete deck right after concrete pouring .....	65
Figure 4.25: Final specimen setup .....	66
Figure 4.26: Strain gauges on bottom mat reinforcement.....	68
Figure 4.27: Typical full-bridge crack gauge .....	69
Figure 4.28: S2/F2 surface strain gauges .....	69
Figure 4.29: Strand slip gauge locations.....	70
Figure 4.30 Displacement potentiometers on deck reinforcement on widening side .....	71
Figure 4.31: Laser displacement transducers (S1/F1 clouded).....	72
Figure 4.32: Horizontal girder displacement transducers .....	72
Figure 4.33: Bottom mat internal transverse strain gauges (for S1/F1, S2/F2 and S3/F3).....	73
Figure 4.34: Bottom mat internal transverse strain gauges read for S4/F4 test (originally installed for S3/F3) .....	74
Figure 4.35: Lower mat internal longitudinal strain gauges .....	75
Figure 4.36: Top mat internal strain gauges on transverse bars (for S1/F1, S2/F2 and S3/F3)....	75
Figure 4.37: Top mat internal transverse gauges read for S4/F4 test (originally installed for S3/F3).....	76
Figure 4.38: Typical laser deflection instrumentation .....	76
Figure 4.39: Vertical laser displacement transducers read for S1/F1 .....	77
Figure 4.40: Deck surface gauges for measuring strains before and after cracking .....	78
Figure 4.41: Bottom deck surface gauges (crack and foil) .....	79
Figure 4.42: Top deck surface gauges (crack and foil).....	79
Figure 4.43: Section A-A.....	80
Figure 4.44: Section B-B .....	80
Figure 4.45: Section C-C .....	81
Figure 4.46: Elevation showing sections .....	82
Figure 4.47: Detail 1 for Section C-C.....	82
Figure 4.48: Effect of girder rotation on deck deformations .....	86

Figure 5.1: Example of load vs. deformation for failure test using two methods of deformation measurements.....	90
Figure 5.2: Example of vertical load and difference in deflection measurements ( $\delta$ ).....	90
Figure 5.3: Comparison between raw and extrapolated vertical deformation vs. applied load for test F1.....	91
Figure 5.4: Typical location of D5b.....	93
Figure 5.5: Schematic of loads applied on test specimen.....	95
Figure 5.6: Service test load deflection D8b.....	96
Figure 5.7: Service test load deflection D9b.....	97
Figure 5.8: Service test load deflection D10b.....	98
Figure 5.9: S4 Laser deflection gauge for D9b, midspan.....	99
Figure 5.10: S4 Laser deflection gauge for D10b, midspan.....	100
Figure 5.11: Load-deflection plots for D5b under service load levels.....	101
Figure 5.12: Service test S1 load strain for TB10-TB16.....	103
Figure 5.13: Service test S2 load strain for TB10-TB16.....	104
Figure 5.14: Service test S3 load strain for TB10-TB16.....	105
Figure 5.15: Service test S4 load strain for TB10-TB16 (S3 gauges read).....	105
Figure 5.16: Service test S1 longitudinal rebar strains for LB2-LB5.....	106
Figure 5.17: Service test S2 longitudinal rebar strains for LB1-LB5.....	107
Figure 5.18: Service test S3 longitudinal rebar strains for LB1-LB5.....	107
Figure 5.19: Service test S4 longitudinal rebar strains for LB1-LB5 (S3 gauges read).....	108
Figure 5.20: Service tests top deck strains - Gauge S3t.....	109
Figure 5.21: Service tests top deck strains - Gauge S4t.....	109
Figure 5.22: Service tests top strains - Gauge S11t (S14t for S3).....	110
Figure 5.23: Service tests top strain gauge S14t (S11t for S3).....	111
Figure 5.24: Service tests bottom strain gauge S7b.....	111
Figure 5.25: Service tests bottom strain gauge S8b.....	112
Figure 5.26: Service tests bottom strain gauge S9b.....	112
Figure 5.27: Service test S1 bottom crack gauges.....	113

Figure 5.28: Service test S2 bottom crack gauges .....	115
Figure 5.29: Service test S2 top crack gauges .....	115
Figure 5.30: S1 crack gauge vs. transverse gauge .....	116
Figure 5.31: Crack pattern underneath the F1 test (dark circle represents load center) .....	117
Figure 5.32: Failure test ultimate loads.....	119
Figure 5.33: Failure tests load vs. strain, displaying TB13 .....	122
Figure 5.34: Load vs. deflection from failure tests for D7b .....	123
Figure 5.35: Load vs. deflection from failure tests for D8b (load cases F1, F2, and F3) & D10b (load case F4).....	124
Figure 5.36: Load vs. deflection from failure tests for D9b .....	125
Figure 5.37: Load vs. deflection from failure tests for D10b .....	125
Figure 5.38: Load vs. deflection relations up to failure (raw readings from actuator displacement gauge before corrections).....	126
Figure 5.39: F1 Transverse cross-section of bottom transverse strain TB10-TB16.....	127
Figure 5.40: F1 Transverse cross-section of bottom transverse strain TB5-TB9.....	128
Figure 5.41: F1 Transverse cross-section of bottom transverse strains TB2-TB4 .....	128
Figure 5.42: F1 Longitudinal cross-section view of bottom transverse strains (TB1, TB3, TB7, and TB13) .....	129
Figure 5.43: F1-retest transverse cross-section view of bottom transverse strains (TB10-TB16) .....	130
Figure 5.44: F1-retest transverse cross-section view of bottom transverse strains (TB5-TB9) .	130
Figure 5.45: F1-retest transverse cross-section view of bottom transverse strains (TB2-TB4) .	131
Figure 5.46: F1 re-test longitudinal cross-section view of bottom transverse strains (TB1, TB3, TB7, and TB13) .....	132
Figure 5.47: F1 Load vs. deflection with extrapolated curve .....	133
Figure 5.48: F1 deflection profile at 100 kip .....	134
Figure 5.49: F1 Load vs. horizontal displacement of girder flanges .....	135
Figure 5.50: F2 Transverse cross-section view of bottom transverse strains (TB10-TB16).....	136
Figure 5.51: F2 Transverse cross-section view of bottom transverse strains (TB5-TB9).....	137
Figure 5.52: F2 Transverse cross-section view of bottom transverse strains (TB2-TB4).....	137

Figure 5.53: F2 Longitudinal cross-section view of bottom transverse strains .....	138
Figure 5.54: F2 Transverse cross-section view of top transverse strains (TT1-TT5).....	139
Figure 5.55: F2 Transverse cross-section view of top transverse strains (TT6-TT8).....	139
Figure 5.56: F2 Longitudinal cross-section view of bottom longitudinal strains .....	140
Figure 5.57: F2 Load-deflection .....	141
Figure 5.58: F2 Load vs. horizontal displacement of girders flanges.....	142
Figure 5.59: F3 Transverse cross-section view of bottom transverse strains TB10-TB16.....	143
Figure 5.60: F3 Transverse cross-section view of bottom transverse strains TB5-TB9.....	143
Figure 5.61: F3 Transverse cross-section view of bottom transverse strains TB2-TB4.....	144
Figure 5.62: F3 Longitudinal cross-section view of bottom transverse strains (TB1-TB13).....	145
Figure 5.63: F3 Longitudinal cross-section view of longitudinal bottom strains (LB1-LB5)....	145
Figure 5.64: F3 Transverse cross-section view of top transverse strains (TT1-TT5).....	146
Figure 5.65: F3 Transverse cross-section view of top transverse strains (TT6-TT8).....	146
Figure 5.66: F3 Load-deflection .....	147
Figure 5.67: F3 Load vs. horizontal displacement of girders flanges.....	148
Figure 5.68: F4 Strain cross-section (TB2-TB4) .....	149
Figure 5.69: F4 Strain cross-section (TB5-TB9) .....	149
Figure 5.70: F4 Transverse cross-section view of bottom transverse strains (TB10-TB16).....	150
Figure 5.71: F4 Longitudinal cross-section view of bottom transverse strains (TB1, TB3, TB7, TB13) .....	151
Figure 5.72: F4 Longitudinal cross-section view of bottom longitudinal strains (LB1-LB5)....	151
Figure 5.73: F4 Load vs. deflection (D9b) .....	152
Figure 5.74: Typically observed cracks at failure.....	153
Figure 5.75: Load Case F1 – Test location close-up .....	154
Figure 5.76: Load Case F1 – Test location .....	154
Figure 5.77: Load Case F1 – Failure ellipse area from bottom slab: 87 in. (7.25 ft) x 96 in. (8 ft) .....	155
Figure 5.78: Load Case F1 – Failure at load point from top of slab.....	155
Figure 5.79: Load Case F1 – Longitudinal cracking on top of slab near overhang.....	156

Figure 5.80: Load Case F1 – Longitudinal crack extending roughly 80 inches from center line of load to farthest visible crack towards F2 location .....	157
Figure 5.81: Load test Load Case F2 – Test location .....	158
Figure 5.82: Load Case F2 – Test location close-up .....	159
Figure 5.83: Load Case F2 – Failure at the top of slab.....	159
Figure 5.84: Load Case F2 – Tracing cracks at top of slab .....	160
Figure 5.85: Load Case F2 – Top slab cracking near widening side.....	160
Figure 5.86: Load Case F2 – Longitudinal cracking near overhang.....	161
Figure 5.87: Load Case F2 – Close-up of failure at top of slab under load point.....	161
Figure 5.88: Load Case F2 – Close-up of failure at top of slab under load point.....	162
Figure 5.89: Load Case F2 – Failure at bottom of slab .....	162
Figure 5.90: Load Case F3 – Test location .....	163
Figure 5.91: Load Case F3 – Failure at load point .....	163
Figure 5.92: Load Case F3 – Extent of failure surface at bottom of slab .....	164
Figure 5.93: Load Case F4 – Test location .....	165
Figure 5.94: Load Case F4 – Failure .....	165
Figure 5.95: Load Case F4 – Failure at top of slab.....	166
Figure 5.96: Load Case F4 – Extent of failure surface at bottom of slab .....	167
Figure 5.97: Load Case F4 – Extent of top deck cracking.....	167
Figure 6.1: Empirical and traditional FEA model for S1 and F1-test, loading at mid span .....	171
Figure 6.2: Empirical and traditional FEA model for S1 and F1-test, loading near the overhang .....	171
Figure 6.3: Deformation of the empirical slab.....	172
Figure 6.4: Deformation of the traditionally designed slab .....	172
Figure 6.5: Laboratory test results and FEA results of F1-Test.....	173
Figure 6.6: Vertical deformations from laboratory and FEA models for F1-Test.....	174
Figure 6.7: Top and bottom slab crack distribution and failure (F1-test).....	174
Figure 6.8: Crack distribution from FEA-empirical slab.....	175
Figure 7.1: Typical widening taken from FDOT SDG.....	178

Figure 7.2: Proposed widening detail ..... 180

It has been recognized for several years that bridge deck slabs have inherent enhanced strength and that laterally restrained slabs exhibit strengths much higher than those predicted by most design codes. The enhanced strength is attributed to the presence of arching action or compressive membrane action (CMA). The degree of arching action is highly dependent on the magnitude of the external restraint among other factors.

Concrete deck slabs resist wheel loads by a complex internal mechanism and not just by flexure. This internal mechanism (arching action) is sustained by in-plane membrane forces that develop because of the lateral confinement provided by the concrete bridge deck and supporting components acting in tandem with the deck. Contrary to the traditional assumption that continuous deck slabs behave purely as flexural members, experimental tests indicated that the deck failure usually occurs as a result of overstraining around the perimeter of the wheel footprint, with a punching shear mode of failure. The inclination of the fracture surface is much less than 45 degrees due to the presence of large in-plane compressive forces associated with arching. As a result of membrane arching action and the punching shear research, the Ontario Highway Bridge Design Code (OHBDC) and some U.S. Departments of Transportation (DOTs) adopted a simple empirical design approach for bridge decks. This empirical deck design method can be used when specific requirements are fulfilled that pertain to slab thickness, transverse span-to-depth ratio, transverse span, diaphragms, overhangs, and other parameters. It is much simpler than the traditional design method as it does not require performing structural analysis for finding the load effects. According to AASHTO LRFD C9.7.2.1 (AASHTO 2012), both the traditional method and the empirical method are conservative with a significant factor of safety of 10 for the traditional method and 8 for the empirical method, thus providing a considerable reserve strength.

The AASHTO LRFD Bridge Design Specifications has provisions that allow state departments of transportation (DOTs) to use the empirical deck design method as well as the traditional design method. Compressive membrane action (what the empirical method is based on), although more complex to analyze, gives a more realistic design approach than the traditional method that is covered in the Florida Department of Transportation (FDOT) Structures Design Guidelines (FDOT 2014) and AASHTO LRFD. On the other hand, design calculations in the traditional method are based on a typical unit width strip, thus assuming a purely flexural approach rather than the membrane action that is exhibited in bridge decks provided that certain conditions are met. Although both methods are conservative, using the traditional method (flexural approach) in design leads to an excessive use of steel reinforcement and an excessive factor of safety when compared to the empirical deck design method. Not only will the empirical deck approach decrease the amount of reinforcement required compared to the traditional method, it also provides ease in design and constructability, which may decrease the associated costs even further.

## 1.1 Objectives

The main objectives of the research study are to

1. Evaluate the soundness of using the empirical design method for design of bridge deck slabs and its implications for potential future widening or phased construction and associated traffic control impact.
2. Develop bridge deck design recommendations for the FDOT.

## 1.2 Justification for the Research

There is potential for cost savings if economical methods can be completed to ensure that the empirical design will satisfy design requirements during phased construction and/or widening. In Florida, all deck slabs are currently required to be designed according to AASHTO's Traditional Design Method (AASHTO LRFD 9.7.3). The traditional design method typically results in a higher ratio of steel reinforcement than the empirical method in the final stage. At this time, the empirical design method for deck slabs as per AASHTO LRFD 9.7.2 is not allowed in Florida as per Structures Design Guidelines 4.2.4 (FDOT 2014). According to the SDG (FDOT 2014), the empirical design method is not permitted because of the potential for future widening or phased construction and associated traffic control impact in order to comply with AASHTO LRFD 9.7.2.4. This research project investigates the adequacy and feasibility of using the empirical design for bridge decks during phased construction and/or widening, which has potential for cost savings.

### 1.1 Impact

The main outcome of this research study is to provide information to the Department regarding the empirical design method for the Departments bridges. Upon acceptance that the results of this research show the use of the empirical deck satisfies Objective 1, a modification to the Structures Design Guidelines would be required. Utilization of the empirical method for deck design will generate cost savings to the FDOT on new bridge construction projects.

### 1.2 Background

Currently, the FDOT Structures Design Guidelines 4.2.4 (FDOT 2014) directs engineers to use the AASHTO LRFD Traditional Design Method 9.7.3. The use of the empirical design method for deck slabs as per AASHTO LRFD 9.7.2 is not permitted by the FDOT partly because of the potential for future widening or phased construction and associated traffic control impact in order to comply with AASHTO LRFD 9.7.2.4. Generally, the use of the empirical method to design concrete bridge decks has not been widely adopted by state transportation agencies. In addition to the concerns of using the empirical design method in a phased construction or widening scenario, one other matter of apprehension is its capacity to control deck cracking.

Traditionally, reinforced concrete bridge deck design has been conducted using an equivalent strip method (AASHTO 1996). This procedure defines an assumed section, with a specified width called the equivalent strip to carry the live-load bending moment. Loading is then assigned using the specified design vehicles, and the deck is assumed to be a continuous beam across the supporting girders. Primary flexural reinforcement transverse to the girders, is then selected based on traditional procedures for the design of one-way reinforced concrete slabs. Additional reinforcement is placed orthogonally to assist with load distribution to the primary reinforcement and for temperature/shrinkage control.

A main concern that the empirical method provides a less effective design to control transverse cracking in bridge decks. However, researchers from the Michigan and New York transportation departments (MDOT and NYDOT respectively) have investigated the adequacy of the empirical method and have recommended using it where the deck falls within AASHTO's empirical bridge deck provisions. The NYDOT (New York Department of Transportation 2011) did not notice any change in transverse cracking in the deck due to using the empirical design method and attributed deck cracking to other causes beside the used design method. The NYDOT (New York Department of Transportation 2011) indicated that the empirical decks were found to be performing satisfactorily, with no spalling or delamination. It also indicated that cracking was minor with regards to serviceability. It reported that longitudinal cracking was a larger percentage of the total crack density for the empirical decks and transverse cracking was a larger percentage of the total crack density for the conventional decks. When considering deck age, the transverse cracking was found to be equivalent for the empirical and conventional designs, while the empirical design exhibited slightly higher longitudinal cracking than conventional design.

The MDOT (Michigan Department of Transportation 2012) reported that the stresses due to dead load and live load were less than the required stress to initiate deck cracking. However, the developed tensile stresses in the deck due to restrained shrinkage could exceed the modulus of rupture of the deck concrete depending on the composite section geometry, stiffness, and spacing of the girders. Therefore, it was recommended that the steel reinforcement be increased for empirical decks on deeper steel girders and AASHTO Type IV prestressed concrete beams. Also, MDOT (Michigan Department of Transportation 2012) reported that crack widths and crack densities were comparable between the two designs, with empirical decks exhibiting less transverse cracking and more longitudinal cracking than conventional decks. It also reported that the cracking was proportional with beam spacing and volume of truck traffic for both deck design methods. It concluded that the performance of the empirical design was found to be satisfactory and comparable to the conventional design. Therefore, they recommended to continue using the empirical design method where cost savings are realized.

Contrary to the position of MDOT and NYDOT, other researchers (Barth & Frosch 2001; Frosch, et al 2003) maintain a reinforcement ratio of 0.6 percent obtained from the AASHTO traditional deck design method is still necessary for adequate crack control. Apparently, there is some disagreement as to how much steel is required in bridge decks to control cracking. Some say a longitudinal and transverse reinforcement ratio of 0.3 percent is sufficient, while others suggest a minimum reinforcement ratio of 0.6 percent. Most states currently utilize a reinforcement ratio closer to 0.6 percent. Survey results obtained by Nielsen, et al. signify the discrepancy between the state highway agencies in choosing between the two methods of design, as shown in Figure 1.1.

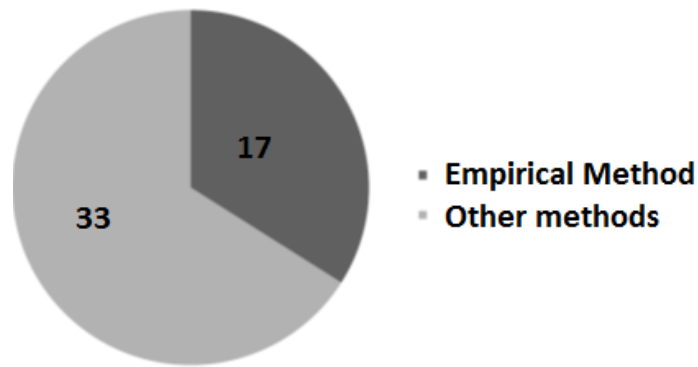


Figure 1.1: Survey results for DOTs' preferred bridge deck design methodology (Nielsen, et al. 2010)

The FDOT has several bridges in use that were designed and constructed with the empirical design method. There are three bridges located in the northern part of Florida that have been built with the empirical deck method used for CIP deck. After 7 years, these bridges were recently inspected and showed minimal serviceability issues, even with heavy traffic. One of the bridges is close to Jacksonville and the other two are in Ebro. The bridge in Jacksonville carries State Road 21 (Blanding Blvd) over North Fork Black Creek and was completed in 2010. The bridges in Ebro (460118 & 460119) were built in 2009. Both bridges look good and both receive heavy traffic. The west bridge (460119) is in the best shape, with just a single longitudinal crack running the length of the bridge roughly 3 - 4 ft into the outside lane, from the shoulder side. The east bridge (460118) has more longitudinal cracks present but they mimic the edges of beam lines, not the steel reinforcement. The only cracking that may mimic rebar lines was seen at the NE corner of the east bridge, nowhere else. There were a couple of cracks at the north end of the approach span with a 12-inch spacing. Only few "crescent" shaped cracks were seen at the ends of the spans, starting at construction joints and working their way to the girder line in a diagonal fashion. They were about 30 - 40 inches long. One transverse crack was seen on the east bridge roughly 5 ft into the span. The maintenance engineer on site questioned the pour sequence of the deck having something to do with the cracking.

AASHTO LRFD states that the available test data indicates that there is a factor of safety of at least 10 for decks designed according to the flexure design method and 8 for decks designed according to the empirical deck method. Therefore, serviceability and durability are the critical factors when evaluating the two design methods. If it can be proven through experimental testing and refined analyses, that the empirical design method may also be used during phased construction and/or widening, there is potential that this method will be more widely accepted for cost savings from reduced reinforcement quantities, as well as design and construction man hours.

According to AASHTO LRFD Section 9.6.1 AASHTO 2012, bridge decks are allowed to be analyzed using the following three methods:

1. Tradition method, also known as Elastic method or Equivalent strip method.
2. Empirical method, also known as the Ontario method.
3. Refined method, or finite element modeling.

In the empirical deck design, if the deck meets certain criteria the minimum amount of transverse reinforcing steel shall be  $0.27 \text{ in}^2$  per foot in the bottom layer and  $0.18 \text{ in}^2$  per foot in the top layer. The commentary in AASHTO LRFD explains that these amounts correspond to a 7.5 inch thick deck slab using 0.3% of the gross area for bottom mat and 0.2% of the gross area for the top mat. For an 8 inch thick deck, and using the same rule of thumb in the AASHTO LRFD commentary C9.7.2.5, this corresponds to a reinforcing steel ratio of  $0.29 \text{ in}^2$  per foot in the bottom layer and  $0.19 \text{ in}^2$  per foot in the top layer. Arching Action is defined in the AASHTO LRFD as “A structural phenomenon in which wheel loads are transmitted primarily by compressive struts formed in the slab”. In order to use the empirical design for bridge decks, the concrete deck is assumed to resist the concentrated wheel loads through internal membrane stress, also known as internal arching, and not through traditional flexural resistance. The arching action takes place when cracks develop in the positive moment region of the reinforced concrete deck which results in shifting the neutral axis toward the compression zone. The arching action is resisted by in-plane membrane forces that develop as a result of lateral confinement provided by the surrounding concrete deck, rigid accessories, and supporting components acting compositely with the deck.

In the traditional method, the deck is divided into strips (typically 1 foot in width) and analyzed as a reinforced concrete flexural element. Based on the AASHTO LRFD, the traditional design method shall apply to concrete decks that have four layers of reinforcement, two in each direction. The positive and negative bending moments due to dead loads can be calculated by assuming the deck continuous over three supports. Since in any typical reinforced concrete deck, the slab spans primarily in the transverse direction or perpendicular to the traffic, the live bending moments should be based only on the axles of the AASHTO HL-93 design truck or design tandem, per AASHTO LRFD 3.6.1.3.3. The live load effect may be determined using the approximate method of analysis or the refined methods of analysis i.e. finite element modeling. In the approximate method of analysis, the deck is divided into strips perpendicular to the main longitudinal girders. The deck reinforcement is designed for its maximum positive and negative moments. The equivalent width of an interior strip of a deck may then be calculated. For ease of use, the positive and negative moments in the deck due to the vehicular loads have been calculated and shown in Table A4-1 in AASHTO LRFD.

In the finite element design method, the deck is modeled using detailed three-dimensional shells or plate elements. The flexural and torsional deformation of the deck should be considered and the vertical shear deformation may be neglected (AASHTO LRFD 4.6.3.2). The deck can be assumed to act as an isotropic plate element where the thickness is uniform and the stiffness is

almost equal in all directions. It could be assumed to act as an orthotropic plate element, where the flexural stiffness may be uniformly distributed along the cross-section of the deck and the torsional rigidity is not contributed by a solid plate only. The refined orthotropic deck analysis could also be used where direct wheel loads are applied to the deck structure. Three dimensional shell or solid finite element model could be used for the refined orthotropic deck model utilizing the following simplifying assumptions: linear elastic behavior, plane sections remain plane, small deflection theory, residual stresses and imperfections are neglected (AASHTO LRFD, 4.6.3.2.4).

### 2.1 Compressive Membrane Action in Slabs

Bridge decks have been traditionally designed using a one foot distribution width with live load moment equations provided as a function of a design truck wheel load based on the AASHTO Standard Specifications for Highway Bridges (AASHTO 2002). However, numerous tests reported in the literature have led to the understanding that traditional design methods tend to be overly conservative. This leads to an unnecessarily high amount of reinforcement in the design (Batchelor & Hewitt 1976; Fang 1985; B.D. Batchelor 1990; Lee & Chen 1994; Fang et. al 1990; S.E Taylor 2000). One of the main factors for the overdesign of slabs can be attributed to the presence of an internal “arching action” (Figure 2.1 and Figure 2.2) that can significantly enhance overall strength. Figure 2.2 shows the arching action and three-hinged arch analogy (G. I. Rankin 1982). The “arching action” occurs due to the restraint of the slab in the transverse direction. Restraint is provided by the bridge girders and by other parts of the bridge system. The added strength gained from this “arching action” allows for a reduction in reinforcing steel requirements. The slabs resist concentrated wheel loads by the internal arching which is a complex internal membrane stress state; not by flexure alone.

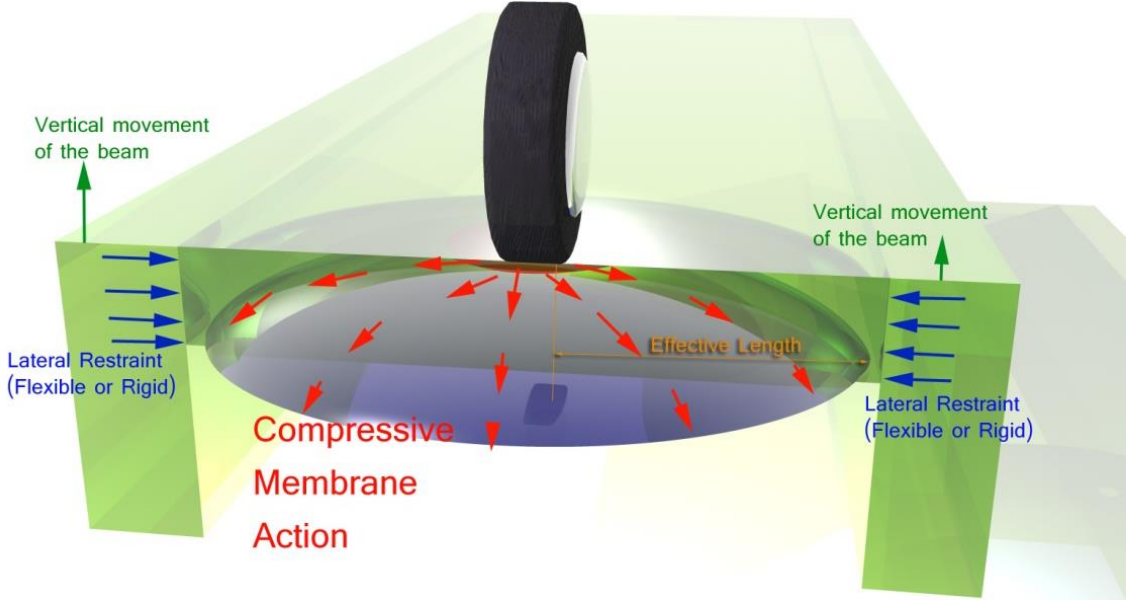


Figure 2.1: Wheel load transfer

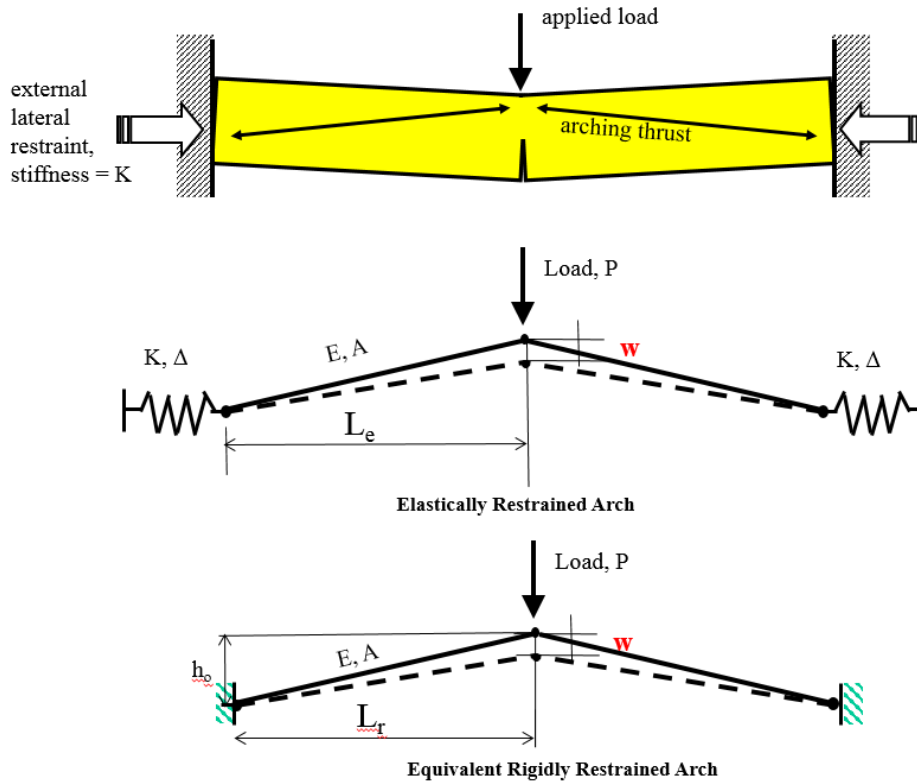


Figure 2.2: Arching action and three-hinged arch analogy (Rankin 1982)

The concept of “arching action” in slabs was recognized by engineers for many decades. Turner (1980) indicated that a slab will behave like a flat dome and a slab combined. There have been many efforts to rationalize Compression Membrane Action (CMA) in analysis taking into account arching action (Gvozdev 1939). Figure 2.3 shows the effect of arching action on deck strength enhancement. Ockleston (1955) published the full-scale loading test results from a slab in a building in Johannesburg. The measured failure loads were considerably higher than those predicted by yield line theory, which had become globally accepted at the time.

Christiansen (1963) developed a theory for one-way spanning slabs restrained by a flexible boundary. Additionally, Christiansen and Frederiksen (1983) postulated a simplified approach to assess the strength of laterally restrained slabs based upon the consideration that flexural and arching effects were independent of one another. Thus, for predicting the peak load, the following relationship can be used:

$$P_m = P_{\text{test}} - P_j$$

where  $P_m$  = load due to compressive membrane action

$P_{\text{test}}$  = maximum total load on the slab

$P_j$  = Johansen’s loads (i.e. flexural capacity using yield line analysis)

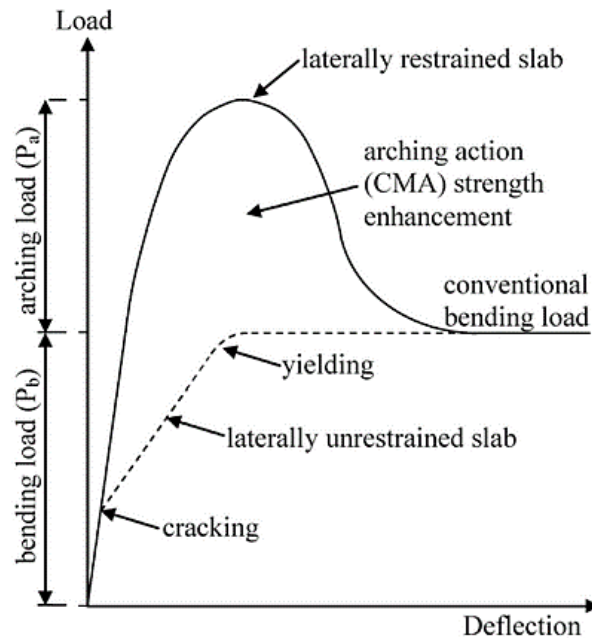


Figure 2.3: CMA effect (courtesy of Gvozdev 1939)

Taylor and Hayes (1965) carried out tests on 22 unreinforced and reinforced square slabs in pairs. They concluded that the enhancement in strength was greatest in the pairs where the simply supported model had been close to flexural failure prior to punching, that is, in the slabs with a lower percentage of reinforcement.

Compressive membrane action (CMA) received significant attention in 1971. The American Concrete Institute (ACI 318-14) held a seminar which was aimed at bringing together researchers in the field of concrete slab systems. The special publication (Hung & Nawy 1971) contains several papers devoted to CMA. Park (1965) presented the lateral stiffness and strength required to enhance membrane action. He also presented a theory to determine the ultimate moment of a rigid-plastic strip, based upon a yield line pattern and using horizontal equilibrium combined with geometric compatibility. Park concluded that, due to the sensitivity to the concrete strength, the strength of restrained slabs is highly dependent upon the stress diagram employed in the calculations. He used Hognestad's relationship, which assumed an elastic-plastic material property. Later, he presented a refined theory which included an adjustment for the lateral restraint and axial strain, caused by shrinkage and creep in the concrete. Park (1965) presented the results of tests on twenty small-scale mortar models where the span to depth ratio varied between 18 and 30. Park refined his theory and summarized the many years of work in his book (Park & Gamble 1980) and his method is discussed later.

Rankin [ (G. I. Rankin 1982), (Rankin and Long 1997)] published his theory including the effects of compressible membrane action. Rankin provided a relatively simple method for the prediction of flexural and shear punching strengths of interior slab column specimens and he showed that the theory provided more realistic values for the actual strength compared to the design codes. While there is general agreement for the bending strength of slabs there are major discrepancies between the design codes for the prediction of shear strength.

Kirkpatrick et al. (1984) investigated arching effects in the deck slabs of M-beam (a prestressed beam type in the UK) bridge deck slabs, as shown in Figure 2.4 and Figure 2.5. This included both field and laboratory tests and is summarized in several papers. The first paper (Kirkpatrick, Rankin & Long 1984) described tests carried out on four bridges, and a subsequent paper (Kirkpatrick, Rankin & Long 1986) presented the punching strength test results on a third scale model of another bridge. The analysis of punching was developed by modifying Rankin's model to develop the arching capacity.

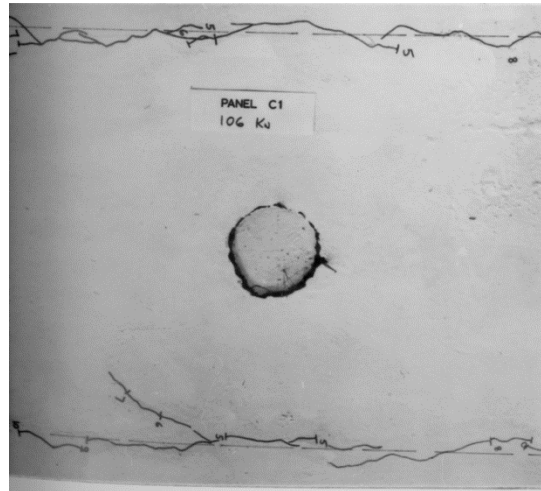


Figure 2.4: Top Surface crack pattern of punching failure zone in model bridge deck test (Kirkpatrick, Rankin and Long 1984)

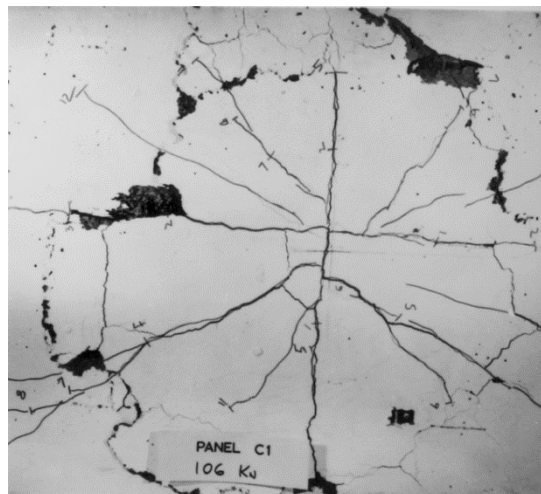


Figure 2.5: Bottom surface crack pattern of punching failure zone in model bridge deck test (Kirkpatrick, Rankin and Long 1984)

It was postulated that the arching effect could be equated to an “equivalent” reinforcement percentage which had a similar effect on the depth of the neutral axis. By the substitution of the equivalent reinforcement index into the equation for the punching shear strength the enhanced punching strength was established. The theory showed good agreement for thick slabs (span to

depth ratio less than 15) with near rigid restraint and showed that the then current design codes were highly conservative. Fang (1985) conducted an experimental and analytical study on two types of concrete decks; cast-in-place and precast decks. The study showed that the results predicted by the analytical models correlated with the experimental findings. Also, Fang (1985) also tested full-scale bridge decks (cast-in-place and precast) on steel girders, that was designed in accordance with the empirical method, and having only about 60% of the reinforcing steel required by the AASHTO traditional method. The test indicated that the deck performed satisfactorily under the AASHTO design loads. Also, the deck behavior was linear under service and overload conditions and was not affected by fatigue loading. Another experimental and analytical study was conducted by Tsui et al. (1986) that dealt with the negative moment behavior and ultimate capacity of the deck under concentrated loads. Compared to the experimental results, the analytical model generally overestimated the girder deflections except at the midspan of the interior girder. However, since the deflections were very small, the analytical results agreed with the experimental ones. The results showed that the general punching shear model gives the closest prediction. Researchers later accumulated and presented an overview of these tests on bridge decks (Long & Rankin 1989; Long, Kirkpatrick & Rankin 1995). It was concluded that the percentage of reinforcement in the deck slab could be reduced to 0.6% with a beam spacing between 5 ft and 6.5 ft. This represented a 35% saving in the cost of a typical bridge deck.

Over the course of several studies, Taylor et al. (2002; 2003; 2007) has presented the effects of CMA in high strength concrete bridge decks. It is known that the compressive strength of concrete has a significant effect on the strength of laterally restrained slabs. This research extended the existing knowledge of compressive membrane action for concrete with compressive strengths up to 14,500 psi, and by utilizing the advantages of high performance concrete it was possible to produce decks with very low percentages of reinforcement. Fifteen one-way slabs typical of a section of bridge deck were tested. The variables included concrete strength, degree of edge restraint and the percentage, position and type of reinforcement. The extent of arching action is dependent upon the degree of lateral restraint and this has proved difficult to quantify. Taylor (2000) provided a method for assessing the degree of lateral restraint by using a restraint model. Taylor et al. (2002), developed a method for predicting the ultimate load carrying capacity of bridge deck type slabs with a range of boundary conditions. The proposed method was found to more accurately predict the strength of these slabs compared to current methods.

Hewitt and Batchelor (1975) presented a rational theory for membrane action. They implemented tests on bridge models and suggested a theory, based upon Christiansen's concept of a combined flexural and arching moment. Batchelor et al. (1976) set out a detailed test program to assess the endurance limit of slabs with various amounts and arrangements of reinforcement. Five models of a steel/concrete composite type bridge, at 1/8 scale, were tested. Subsequently the design code (Ontario Ministry of Transportation 1979) was changed to allow a reduction in reinforcement to 0.3% in the deck slabs provided certain boundary conditions existed. In the 1970s and 1990s research into the behavior of bridge decks continued to be conducted. In 1992, Bakht and Jaeger summarized the results of tests on short span simply supported "slab on girder" bridges. The transverse distribution of loads appeared to improve at higher loads. The FEA (Finite Element Analysis) packages adopted were capable of modelling arching by incorporating sufficient degrees of freedom to allow for the in-plane restraint. Mufti et al. (1993) carried out tests on 1/2 scale bridge models containing no conventional

reinforcement. The third model included external straps welded to the underside of the top flanges. This provided sufficient lateral restraint to ensure a punching failure at a load far in excess of the required ultimate bridge loading. However, these steel straps were equivalent to a 1.4% area of conventional reinforcement, which was over three times the recommended steel area provided in the Canadian bridge code at the time (OHBDC 1979).

## 2.2 Bridge Deck Design in the U.S.

AASHTO LRFD includes both traditional and empirical deck design approaches. Adoption of deck design methods varies by state. A summary of bridge deck design on different states is presented as follows:

1. The Alabama Department of Transportation Bridge Bureau Structures Design and Detailing Manual – January 1, 2008 provides a table that shows the required deck thickness and reinforcement based on girder type and girder spacing. The table was furnished by the State Bridge Engineer and any exceptions will require prior approval. The table shows a deck thickness that varies from 7" minimum to 7 ¾" maximum with girder spacing varying from 4.0' to 10.0'. The main transverse reinforcing steel is always No. 5 bar with spacing between 6½ and 4½ inches. This corresponds to a reinforcement ratio of 0.68 to 0.98.
2. The Arizona Department of Transportation 2012 Bridge Design Guidelines Section 9.6.1 allows the reinforced concrete deck to be designed following an approximate elastic method which is referenced in the AASHTO LRFD traditional design method. Refined method of analysis or finite element modeling is only allowed for complex bridges with prior approval from the ADOT Bridge Group.
3. The California Department of Transportation 2011 Bridge Design Practice, Chapter 10 Concrete Decks, allows the design of reinforced concrete decks as transverse strip flexure members which is based on the Approximate or Traditional Method of Analysis (AASHTO LRFD, 4.6.2.1). The refined method of analysis, based on AASHTO LRFD 4.6.3, is recommended for more complex decks which would require a more detailed analysis i.e. curved decks. The empirical design method, based on AASHTO LRFD 9.7.1 is not permitted for now until further durability testing is completed.
4. The Colorado Department of Transportation 1989 Bridge Design Manual, Section 8 provides a table that shows the minimum deck thickness and reinforcing steel size and spacing based on the effective span length. The deck thickness varies between 8 in and 9 in with increments of a quarter inch. The main transverse reinforcing steel is No. 5 bar with spacing between 9 in and 5 in which corresponds to a reinforcement ratio of 0.43 to 0.69. This table is based on the Load Factor Design.
5. The Connecticut Department of Transportation 2011 Bridge Design Manual, Section 8.1.2.2 allows the use of the empirical design method based on the AASHTO LRFD Specifications.
6. The Delaware Department of Transportation 2005 Bridge Design Manual, Section 5.3.1.2 does not allow using the empirical design method for decks and references AASHTO LRFD Section, 4.6.2, Approximate Method of Analysis for applying wheel loads.

7. The Georgia Department of Transportation 2012 Bridge and Structures Design Manual uses the Service Load Design for bridge decks to provide a stiffer deck with less cracking. It provides a deck chart showing the bar size and spacing using the BRSLAB07 design program. It also assumes the deck is continuous over 3 or more supports with a continuity factor of 0.8 and a minimum deck thickness of 7 inches.
8. The Idaho Transportation Department 2005 LRFD Bridge Design Manual, Section 9.7.2 allows the use of the empirical design method for bridge decks and provides a design aid for determining the deck thickness based on the type of beam used.
9. The Illinois Department of Transportation 2012 Bridge Manual Design Guides, Section 3.2.1 is based on the traditional method. Illinois DOT Bridge Manual provides a chart to determine the spacing for No. 5 bars in top and bottom mats.
10. The Indiana Department of Transportation 2012 Design Manual Chapter 404, Bridge Deck allows the use of the approximate method of analysis, commonly referred to as the equivalent strip method or traditional method, in accordance with AASHTO LRFD 4.6.2. The Indiana DOT does not mention whether the empirical deck design method is allowed.
11. The Iowa Department of Transportation 2012 LRFD Bridge Design Manual recommends using the strip method for deck design based on AASHTO LRFD 4.6.2.1. The empirical method is to be used only with permission of the Bridge Engineer.
12. The Kansas Department of Transportation 2012 LRFD Bridge Design Manual, Section 3.9.4 uses the traditional design method for bridge decks and does not use the empirical method.
13. The Louisiana Department of Transportation and Development 2008 LRFD Bridge Design Manual allows the use of both the empirical deck design and the traditional design method. It also lists special provisions related to the concrete material, curing method and deck thickness when using the empirical deck design.
14. The Maine Department of Transportation 2003 Bridge Design Guide Chapter 6 provides two tables that show the minimum deck thickness and reinforcing steel size and spacing based on the maximum girder spacing. The deck thickness varies from 7 in to 11 in with a half inch increment. The main transverse reinforcing steel is No. 5 bar with a 6 inch spacing which corresponds to a reinforcement ratio of 0.47 to 0.74. The Maine DOT Bridge Design Manual does specify what method the design is based on.
15. The Massachusetts Department of Transportation LRFD Bridge Manual, 2009 Part II provides design tables showing the required steel reinforcement and deck thickness. Section 3.5.2 of Part I requires using the traditional method of analysis when the beam spacing is outside the table limits. The empirical deck design is not allowed.
16. The Michigan Department of Transportation 2012 Design Manual – Bridge Design – Chapter 7 LRFD Section 7.01.19 allows the use of the empirical design method according to AASHTO LRFD 9.7.2.
17. The Minnesota Department of Transportation 2013 LRFD Bridge Design Manual Section 9.2.1 allows the use of the traditional approximate method of analysis only. The empirical deck design method shall not be used.

18. The Missouri Department of Transportation 2013 Category 751 LRFD Bridge Design Guidelines Section 751.10.1.4 recommends the use of the equivalent strip method and does not mention the empirical design method.
19. The Montana Department of Transportation 2002 Structures Manual, Chapter 15 provides a table that shows the slab thickness and reinforcing steel based on the beam spacing. This table is based on the equivalent strip method.
20. The Nebraska Department of Roads Bridge Office Policies & Procedures (BOPP) Manual, 2013, Section 3.1.1, requires the deck be designed using the empirical design method in accordance with current AASHTO LRFD Bridge Design Specifications. It also provides the required deck thickness based on the effective span. The top mat shall have No. 4 bars at 12 inches in both directions while the bottom mat shall have No. 5 bars at 12 inches in both directions.
21. The Nevada Department of Transportation 2008 Structures Manual, Chapter 16, allows the use of the traditional approximate method of analysis only. The empirical deck design method shall not be used.
22. The New Jersey Department of Transportation 2009 Design Manual for Bridges and Superstructure, 5<sup>th</sup> Edition, Section 9.7.2, allows the use of the empirical design if the bridge structure entails straight longitudinal superstructure members.
23. The New Mexico Department of Transportation Bridge Procedures and Design Guide, 2013, uses the 1979 Bridge Design and Detailing Instructions. The main reinforcing steel used is No. 5 at 6 in for the top and bottom mats.
24. The New York State Department of Transportation Bridge Manual, 2011, Section 5.1.5.1, allows the use of the empirical design method for isotropic decks that meet the following conditions:
  - a. There must be four or more girders in the final cross-section of the bridge. (A stage construction condition with three girders is permissible; however, the temporary overhangs must be reinforced traditionally.)
  - b. The maximum center-to-center spacing of the girders is 11 ft, and the minimum spacing is 5 ft.
  - c. Design slab thickness shall be a minimum of 8 inches, and the total standard deck thickness shall be a minimum of 9½ inches. An 8½-inch-thick deck may be used with solid stainless steel and stainless-steel-clad reinforcement.
  - d. The deck is fully cast-in-place and water cured. Only permanent corrugated metal and removable wooden forms shall be permitted (prestressed concrete form units are not allowed).
  - e. The supporting components are made of spread steel or concrete I-girders.
  - f. The deck shall be fully composite in both positive and negative moment regions. In negative moment regions, composite section property computations shall only include the area of the longitudinal steel.

- g. Isotropic reinforcement may be used with spread concrete box beams provided the reinforcement is adequate to resist flexure for the clear span between beam units.
  - h. The minimum overhang, measured from the centerline of the fascia girder to the fascia, is 2 ft 6 in. If a concrete barrier composite with the deck is used, the minimum overhang is 2 ft.
  - i. Skew angles up to 45°. Note: For skews above 30° isotropic reinforcement becomes very congested at the end of the slab. Traditional deck slab reinforcement is recommended for skews greater than 30°.
25. The North Carolina Department of Transportation 2013 Structures Design Manual Section 6.2.2 does not mention whether the deck is designed using a specific method. It rather provides tables that show the deck thickness and reinforcement based on beam spacing.
  26. The North Dakota Department of Transportation 2004 LRFD Bridge Design Specifications uses the traditional approximate method of analysis for deck design. The empirical deck design method shall not be used.
  27. The Ohio Department of Transportation 2012 Bridge Design Manual Section 300 requires the deck to be designed with the approximate elastic method of analysis in accordance with AASHTO LRFD also known as the traditional design method. The refined method of analysis and the empirical design method, AASHTO LRFD 9.7.2 are prohibited.
  28. The Oregon Department of Transportation 2012 Bridge Design and Drafting Manual, Section 1.1.20 does not allow the use of the empirical design method. It states that excessive deck cracking, apparently due to under reinforcement, precludes the use of this method until further notice.
  29. The Rhode Island Department of Transportation LRFD Bridge Design Manual, 2007 Section 9.5 uses the approximate elastic method of analysis for design of concrete decks. The refined method of analysis shall be used only when approved by the Managing Bridge Engineer. The empirical method of analysis will be considered by the Managing Bridge Engineer on a case-by-case basis.
  30. The South Carolina Department of Transportation Bridge Design Manual, 2006 Section 17.2 allows the use of the strip method only. The use of the empirical deck design is prohibited.
  31. The Pennsylvania Department of Transportation 2012 Design Manual Part 4 Structures requires the concrete decks be designed in accordance with the traditional design method. The refined method and the empirical method are only allowed if approved by the Pennsylvania DOT Chief Bridge Engineer.
  32. The Texas Department of Transportation Bridge Design Manual – LRFD, 2015 allows the empirical design method specified in Article 9.7.2 with certain conditions. It also allows the Traditional Design method specified in Article 9.7.3.

33. The Agency of Transportation in Vermont 2010 Structures Design Manual does not mention whether the deck is designed using a specific method. Section 9.1 provides tables that show the deck thickness and reinforcement based on beam spacing.
34. The Virginia Department of Transportation 2012 Structures and Bridge Manuals Volume V Part 2, does not allow the use of the empirical design method. It also provides a table that shows the required deck thickness, reinforcing steel area and bar spacing for steel beams and prestressed concrete beams based on the beam spacing.
35. The Washington State Department of Transportation 2011 Bridge Design Manual LRFD Section 5.7 requires that the deck be designed using the traditional design of AASHTO LRFD 9.7.3.
36. The West Virginia Department of Transportation Bridge Design Manual, 2006 Section 3.2.1 allows the use of the empirical design method provided all required design conditions are met based on AASHTO LRFD 9.7.2.4.
37. The Wisconsin Department of Transportation 2011 Bridge Manual Chapter 17.3.C allows the use of the empirical design method with additional conditions to the AASHTO LRFD requirements. Wisconsin DOT has imposed the following additional conditions in an attempt to eliminate the longitudinal cracking:
  - a. For an 8-inch slab the maximum girder spacing is 7 feet.
  - b. For an 8.5-inch slab the maximum girder spacing is 8 feet.
  - c. For a 9-inch slab the maximum girder spacing is 9 feet.
38. The Wyoming Department of Transportation 2012 Bridge Design Manual Chapter 2 uses the traditional design based on AASHTO LRFD 9.7.3. It also provides a deck reinforcing steel table that shows the deck thickness, the girder spacing, the bar size, positive and negative moments based on 12-inch spacing for transverse bars and maximum longitudinal bar spacing. The design is based on the HL93 Design Loading.

Table 2.1 shows the deck design method by state. Only 10 states allow the use of the empirical deck design, note that Figure 1.1 reflects results from an older study.

Table 2.1: Bridge Deck Design Method by State

<b>Bridge Deck Design Method by State</b>		
<b>State</b>	<b>Abbreviation</b>	<b>Empirical/Traditional*</b>
ALABAMA	AL	Traditional
ALASKA	AK	N/A

Table 2.1 continued

ARIZONA	AZ	Traditional
ARKANSAS	AR	N/A
CALIFORNIA	CA	Traditional
COLORADO	CO	N/A
CONNECTICUT	CT	Empirical
DELAWARE	DE	Traditional
FLORIDA	FL	Traditional
GEORGIA	GA	N/A
HAWAII	HI	N/A
IDAHO	ID	Empirical
ILLINOIS	IL	Traditional
INDIANA	IN	Traditional
IOWA	IA	Traditional
KANSAS	KS	Traditional
KENTUCKY	KY	N/A
LOUISIANA	LA	Empirical
MAINE	ME	N/A
MARYLAND	MD	N/A
MASSACHUSETTS	MA	Traditional
MICHIGAN	MI	Empirical
MINNESOTA	MN	Traditional
MISSISSIPPI	MS	N/A
MISSOURI	MO	Traditional
MONTANA	MT	Traditional
NEBRASKA	NE	Empirical
NEVADA	NV	Traditional
NEW HAMPSHIRE	NH	N/A
NEW JERSEY	NJ	Empirical
NEW MEXICO	NM	N/A

Table 2.1 continued

NEW YORK	NY	Empirical
NORTH CAROLINA	NC	N/A
NORTH DAKOTA	ND	Traditional
OHIO	OH	Traditional
OKLAHOMA	OK	N/A
OREGON	OR	Traditional
PENNSYLVANIA	PA	Traditional
RHODE ISLAND	RI	Traditional
SOUTH CAROLINA	SC	Traditional
SOUTH DAKOTA	SD	N/A
TENNESSEE	TN	N/A
TEXAS	TX	Empirical
UTAH	UT	N/A
VERMONT	VT	N/A
VIRGINIA	VA	Traditional
WASHINGTON	WA	Traditional
WEST VIRGINIA	WV	Empirical
WISCONSIN	WI	Empirical
WYOMING	WY	Traditional

\*N/A: No design manual available or design provided by state DOT

### 2.3 Deck Design in Canada

The 2006 Canadian Highway Bridge Design Code Clause 8.18.1 allows the use of the empirical design method for decks where decks do not need to be analyzed, except for the negative moment region in the overhang and in the continuous spans over the supports. It also gives the option of using flexural design methods as an alternative to the empirical method. In order to use the empirical design method, the deck must meet all of the following conditions from Clause 8.18.4.1:

1. The deck thickness between the fascia beams must be uniform.
2. The deck is made composite with the supporting beams.
3. The supporting beams are parallel to each other and the beams' bearing lines are also parallel.
4. The beam spacing to deck thickness ratio is less than 18.0.
5. The beam spacing is less than 13.0 feet (4 m).

6. The deck extends sufficiently beyond the fascia beams to provide the full development length for the transverse reinforcement.
7. The longitudinal reinforcement shall be provided in the deck in the negative moment region for continuous spans.

Cast-in-place decks, based on Clause 8.18.4.2, shall meet the requirements listed above and the following conditions:

1. The deck shall contain two mats of reinforcing steel near the top and bottom faces, with a minimum reinforcement ratio,  $\rho$ , of 0.003 in each direction, Figure 2.6.
2. When the deck is supported on parallel beams, the reinforcement bars closest to the top and bottom faces are placed perpendicular to beam lines or are placed on a skew parallel to the bearing lines, as shown in Figure 2.7.
3. The reinforcement ration,  $\rho$ , may be reduced to 0.002 where the deck with the reduced reinforcement can be satisfactorily constructed and the reduction of  $\rho$  below 0.003 is approved.
4. Where the transverse reinforcing bars are placed on a skew, the reinforcement ratio for these bars is not less than  $\rho/\cos^2\theta$ , where  $\theta$  is the skew angle.
5. Where the unsupported length of the edge stiffening beam,  $S_e$ , exceeds 16.5 ft (5 m), the reinforcement ratio,  $\rho$ , in the exterior regions of the deck slab is increased to 0.006.
6. The spacing of the reinforcement in each direction and in each assembly does not exceed 12 in (300 mm).

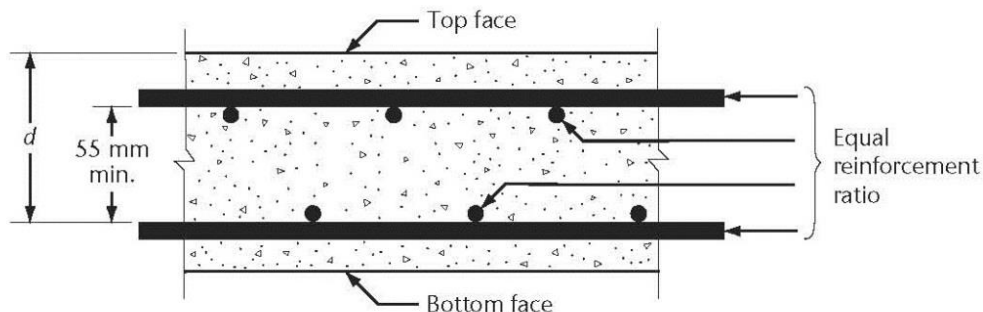


Figure 2.6: Reinforcement for cast-in-place deck

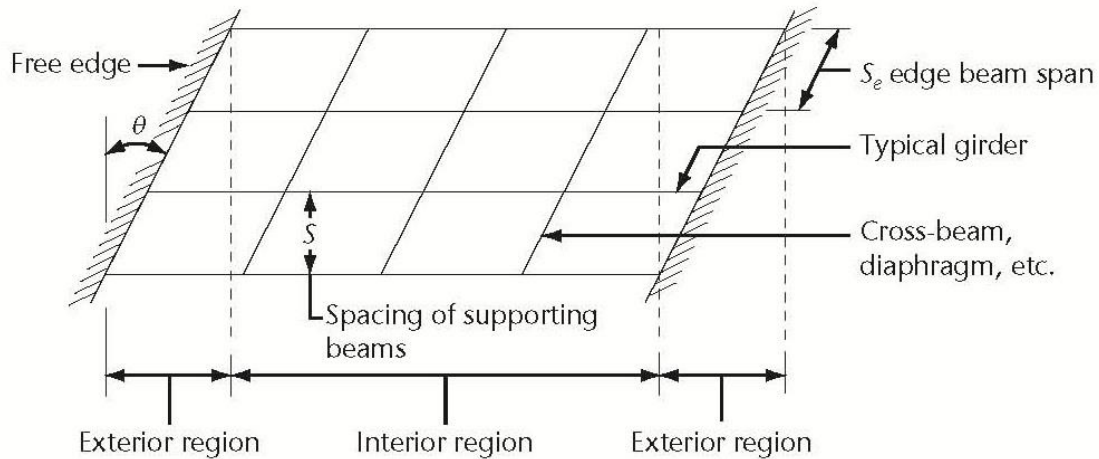


Figure 2.7: Details for cast-in-place deck slabs

## 2.4 Methods of Predicting Deck Capacity

From literature, several methods were used to investigate and predict the ultimate capacity of bridge decks. These methods included British Standard (BS5400), American Concrete Institute (ACI 381-14), UK Highways Agency (BD81/02), and Taylor, Rankin and Cleland's approach (2002; 2003).

### 2.4.1 British Standard BS5400 Method

In this design of the bridge deck slab, the predominant factor is the bending capacity (British Standards Institute 1990). The BS5400 method (British Standards Institute 1990) recommends the use of Pucher charts which uses influence surfaces of elastic plates for the predicted flexural and punching shear capacity. The local effect of the concentrated wheel load is represented as shown in Equation 1.

$$M = A_s f_y d \left( 1 - \frac{0.746 A_s f_y}{f_{cu} b d} \right) \quad \text{Eq. 1}$$

Where,

$A_s$  : Area of steel reinforcement

$f_y$ : Yield stress

$d$ : Effective depth

$b$ : Cross section width

$f_{cu}$ : Standard concrete cube's compressive strength.

The Pucher Charts are used to establish the predicted flexural failure load from the maximum allowable internal moment (British Standards Institute 1990). The relationship between the bending moment and the applied load is shown in Equation 2 (British Standards Institute 1990).

$$M = 0.08P \text{ kN} \cdot \text{m}/\text{m} \quad \text{Eq. 2}$$

The punching shear strength (British Standards Institute 1990) is given by Equation 3

$$P_{vs} = 0.79 \cdot \sqrt[3]{100 \cdot \frac{A_s}{bd}} \cdot \sqrt[3]{\frac{f_{cu}}{25}} \cdot \sqrt[4]{\frac{500}{d}} \cdot b_o \cdot d \quad \text{Eq. 3}$$

#### 2.4.2 American Concrete Institute (ACI Method)

The bending capacity and the local effect of a concentrated load can be represented by Equations 4 and 5 (all factors of safety are removed) (ACI 318-14).

$$M = \rho \cdot f_y \cdot d^2 \left( 1 - \frac{0.5\rho f_y}{\beta \cdot f'_c} \right) \quad \text{Eq. 4}$$

The same Pucher Chart was used to find the flexural capacity with the ACI method, since the ACI 318-14 punching shear capacity formula deduces that the slab has been already correctly designed for flexure. The ACI formula for punching strength is shown in Equation 5.

$$P_{vs} = 4 \cdot \sqrt{f'_c} \cdot b_o d \quad \text{Eq. 5}$$

where  $b_o$  is the perimeter of the punching shear failure surface.

#### 2.4.3 UK Highways Agency, BD81/02 Method

This method takes into account the development of the compressive membrane action developed in the slab. It assumes that the type of slab failure is punching shear and that it has an effective rigid restraint system (UK Highway Agencies 2002). The method first accounts for an ideal elastic-plastic concrete stress block derived as in Equation 6, where  $\varepsilon_c$  is the plastic strain value for an idealized elastic-plastic concrete and  $f'_c$  is the concrete equivalent cylinder strength.

$$\varepsilon_c = (-400 + 60f'_c - 0.33f'^2_c) \times 10^{-6} \quad \text{Eq. 6}$$

This enabled the estimation of McDowell's non-dimensional parameter  $R$  for the arching moment of resistance, (Equation 7), where  $L_r$  is the half span of the slab strip with boundary restraint (mm) and  $h$  is the overall slab depth (mm).

$$R = \frac{\varepsilon_c L_r^2}{h^2} \quad \text{Eq. 7}$$

Considering the moment ratio  $M_r$  and the deformation  $u$ , the maximum value for the arching moment ratio was derived as shown in Equations 8 and 9.

$$M_r = 4.3 - 16.1\sqrt{3.3 \times 10^{-4} + 0.1243 R} \quad \text{Eq. 8}$$

$$u = -0.15 + 0.36\sqrt{0.18 + 5.6R} \quad \text{Eq. 9}$$

This led to the calculation of the non-dimensional maximum arching moment coefficient  $k$  (Equation 10) used to find the effective flexural reinforcement ratio  $\rho_e$ , given by Equation 11, where  $d$  is the average effective depth to tensile reinforcement (mm).

$$k = 0.0525(4.3 - 16.1\sqrt{3.3 \times 10^{-4} + 0.1243R}) \quad \text{Eq. 10}$$

$$\rho_e = \frac{k \cdot f'_c \cdot h^2}{240d^2} \quad \text{Eq. 11}$$

Finally, the effective reinforcement ratio was substituted into Long's equation for the punching strength, as shown in Equation 12, where  $c_x$  is the diameter of loaded area (mm).

$$P_{pv} = 1.52 \cdot (c_x + d) \cdot d \cdot \sqrt{f'_c} \cdot (100\rho_e)^{0.25} \quad \text{Eq. 12}$$

Subsequent research done by Queen University led to adjustments of the plastic strain value to incorporate high-performance concrete, as explained in the following approach.

#### 2.4.4 Taylor, Rankin, and Cleland's Approach (TRC)

##### 1. Effective width of loaded slab

An effective width of slab subjected to arching forces is described by Equation 13

$$b_{eff} = c_y + 2 \cdot L_e + 2h \quad \text{Eq. 13}$$

Where,

$b_{eff}$ : effective width of loaded slab

$L_e$ : half the span of the arch length =  $\frac{L}{2} - \frac{c_x}{2}$

$c_y$ : width of patch load perpendicular to slab span

$c_x$ : width of patch load parallel to slab span

$L$ : spacing between supporting beams

$h$ : depth of slab

##### 2. Stiffness parameters

The width of the supporting beams has a significant influence on the strength of the deck slab (Taylor, Rankin & Cleland 2002). Considering that the supporting beams are related to a spring with an equivalent stiffness, the 'equivalent area' of lateral stiffness,  $A_b$ , gives an external stiffness of  $EA_b/L_e$ , as shown in Equations 14 - 17.

$$E_c = 4.23 \sqrt{f'_c} \quad \text{Eq. 14}$$

$$K_s = \frac{E_c h b_{eff}}{L_e} \quad \text{Eq. 15}$$

Calculate the second moment of area of the support beam about the vertical axis ( $I_{yb}$ )

$$A_b = \frac{\zeta L_e I_{yb}}{b_{eff}^3} \quad \text{Eq. 16}$$

where  $\zeta$  = constant support condition ( $\zeta = 114.5$  for simply supported or  $\zeta = 985$  for fixed ends)

$$K_b = \frac{A_b E_c}{L_e} \quad \text{Eq. 17}$$

A similar approach was made in assessing the restraint inherent in a bridge deck slab (Equation 18), where  $A_d$  is the sum of diaphragm area and the area of slab outside the effective width.

$$K_d = \frac{\Sigma A_d E_c}{L_e} \quad \text{Eq. 18}$$

The combined flexibility of the total restraint is expressed in Equation 19.

$$K_r = \frac{1}{\frac{1}{K_b} + \frac{1}{K_d}} \quad \text{Eq. 19}$$

Where,

$E_c$ : concrete elastic modulus

$K_s$ : stiffness of slab within effective width

$A_b$ : equivalent area of support beam

$K_b$ : equivalent stiffness of support beam

$K_d$ : stiffness of diaphragm and slab

$K_r$ : combined stiffness of restraint

### 3. Bending capacity

The bending capacity is estimated by taking into account the equivalent rectangular stress block as listed in Equations 20 to 24.

$$\text{Depth of stress block, } \beta = 1 - 0.003 f' c \text{ but } \leq 0.9 \quad \text{Eq. 20}$$

$$\text{Depth of neutral axis, } x = \frac{f_y A_s}{0.67 f' c \beta b} \quad \text{Eq. 21}$$

$$\text{Lever arm, } z = d - 0.5 \beta x \quad \text{Eq. 22}$$

$$M_b = f_y A_s z \quad \text{Eq. 23}$$

$$P_b = k_b M_b \quad \text{Eq. 24}$$

Where,

$\beta$ : proportional depth of stress block (= 0.9 in BS)

x: depth of concrete compression zone  
b: width of section  
 $f_y$ : reinforcement yield strength  
 $A_s$ : area of steel reinforcement  
 $M_b$ : flexural moment of resistance at principal section  
 $P_b$ : predicted ultimate flexural capacity  
 $k_b$ : static moment coefficient for a strip under uniform loading

#### 4. Arching Section

The arching section may be estimated by using Equation 25.

$$2d_1 = h - 2x\beta \quad \text{Eq. 25}$$

New  $d_1$  is from previous iterations, where  $d_1$  is half of the arching depth.

#### 5. Affine Strip

Equations 26 and 27 are used to determine the affine strip.

$$A = \alpha b d_1 \quad \text{Eq. 26}$$

$$L_r = L_e \sqrt[3]{\left(\frac{EA}{KL_e} + 1\right)} \quad \text{Eq. 27}$$

Where,

A: cross-sectional area

$L_r$ : half the span of the rigidly restrained arch

#### 6. Arching parameters

The arching parameters in Equations 28 – 33 are estimated considering the plastic strain formula. This is determined through the non-dimensional parameter for the arching moment of resistance  $R$  from previous research by McDowell et al. (1956).

$$\varepsilon_u = 0.0043 - [(f'_c - 60)2.5 \times 10^{-5}] \quad \text{but } < 0.0043 \quad \text{Eq. 28}$$

$$R = \frac{\varepsilon_u L_r^2}{4d_1^2} \quad \text{Eq. 29}$$

$$\varepsilon_c = 2\varepsilon_u(1 - \beta) \quad \text{Eq. 30}$$

Where,

$\varepsilon_u$ : concrete maximum compressive strain

$\varepsilon_c$ : concrete compressive plastic strain value

R: McDowell's non-dimensional parameter (elastic deformation)

## 7. Deformation

$$R > 0.26 \rightarrow u = 0.31 \text{ (constant)} \quad \text{Eq. 31}$$

$$0 < R < 0.26 \rightarrow u = -0.15 + 0.36\sqrt{0.18 + 5.6R} \quad \text{Eq. 32}$$

Where u is McDowell's non-dimensional parameter (deflection)

## 8. Contact depth

The refined contact depth  $\alpha$  is given in Equation 33.

$$\alpha = 1 - \frac{u}{2} \quad \text{Eq. 33}$$

$\alpha$  and  $d_1$  are used to refine arching action section (see Eq. 26) until the value remains constant.

Where  $\alpha$  is the proportion of  $d_1$  in contact with the support

## 9. Arching capacity

The arching capacity for the section is determined by the maximum value for the arching moment  $M_r$ , as shown in Equations 34 – 38.

$$R > 0.26 \rightarrow M_r = \frac{0.3615}{R} \quad \text{Eq. 34}$$

$$0 < R < 0.26 \rightarrow M_r = 4.3 - 16.1\sqrt{3.3 \times 10^{-4} + 0.1243R} \quad \text{Eq. 35}$$

$$M_a = 0.168bf'c d_1^2 M_r \left( \frac{L_e}{L_r} \right) \quad \text{Eq. 36}$$

$$[\text{for maximum arching } L_e = L_r, M_{ar} = 0.168f'c d_1^2 M_r] \quad \text{Eq. 37}$$

$$P_a = k_a M_a \quad \text{Eq. 38}$$

Where,

$M_r$ : moment ratio (non-dimensional)

$M_{ar}$ : arching moment of resistance of rigidly restrained slab strip

$M_a$ : arching moment of resistance

$P_a$ : predicted ultimate arching capacity

$k_a$ : static moment coefficient under concentrated mid-span loading

## 10. Flexural punching capacity

The flexural punching capacity is established by taking into account the bending and the arching capacity (Equation 39).

$$P_{pf} = P_a + P_b \quad \text{Eq. 39}$$

### 11. Shear punching capacity

An equivalent area of reinforcement is estimated in order to determine the shear punching capacity as shown in Equation 40,

$$\rho_e = (\rho_e + \rho) \left( \frac{f_y}{320} \right) = \left( \frac{M_a + M_b}{M_b} \right) \left( \frac{f_y}{320} \right) \rho \quad \text{Eq. 40}$$

Where,

$\rho_e$ : effective reinforcement ratio at principal section

$\rho$ : reinforcement ratio at principal section

The shear punching strength is quantified in terms of the equivalent area of reinforcement due to the combined effect of bending and arching (Equation 41), where  $r_f$  is the shape factor.

$$P_{pv} = \frac{0.43}{r_f} \sqrt{f'c} (\text{critical perimeter}) d (100\rho_e)^{0.25} \quad \text{Eq. 41}$$

Critical perimeter is at 0.5d from face of loaded area

### 12. Ultimate capacity

The ultimate capacity for the bridge deck slab was determined according to the lesser of the flexural and shear punching capacities as shown in Equations 42 and 43.

$$\text{If } P_{pf} < P_{pv} \rightarrow P_p = P_{pf} \quad \text{Eq. 42}$$

$$\text{If } P_{pf} > P_{pv} \rightarrow P_p = P_{pv} \quad \text{Eq. 43}$$

Where  $P_p$  is the ultimate capacity

Regarding the effect of lateral stiffness on the ultimate capacity of bridge deck, studies have shown that the TRC approach presents more precise predictions when compared to the experimental strengths (Taylor, Rankin & Cleland). This can be attributed to the fact that the method considers the variations of the external restraint stiffness. In this study, it was determined to perform more analysis based on varying the external restraint factors using the TRC approach. As shown in the following chapter, this analysis provided a more thorough characterization of the structural response of the bridge deck as a result of changing the lateral stiffness of the supporting beams.

## Chapter 3          Design and Analysis of Test Specimen

Several methods were used to analyze the bridge deck. These methods included conducting finite element (FE) analyses and an analytical method. The FE analyses were performed using commercial finite element packages (STAAD and ANSYS) to investigate the effect of several variables including deck thickness, beam spacing, bridge span, reinforcement ratio, and concrete compressive strength. First, the bridge superstructures were modeled using STAAD and a parametric study was conducted. Then, a more refined analysis was conducted using ANSYS. At the same time, the investigation using an analytical method was carried out to assess the effect of lateral stiffness on the strength of the bridge deck slab. This analytical method used the approach of Taylor et al. (2007), which considers not only flexural capacity, but also punching shear capacity on one-way slab strips. After performing these analyses, a design of the lab test specimen was performed to simulate a realistic behavior of bridge decks. The design of the test specimen included both the Florida I-beam (FIB) and the deck, which was designed following the empirical deck design method provisions as stated in AASHTO LRFD. After testing, a calibration of the ANSYS FE model was conducted.

### 3.1 Preliminary Design and Analysis of Deck

Several methods were used to design and analyze the lab specimen and to predict the ultimate load carrying capacity of the bridge deck. These methods included a simplified analytical method and a finite element analysis. The analytical method assessed the effect of lateral stiffness on the strength of the bridge deck slab. It used the approach of Taylor et al. (2007), which considers not only flexural capacity, but also punching shear capacity on one-way slab strips. The proposed method by Taylor et al. 2007 considered the compressive membrane action capacity acting in the bridge deck and was found to better predict the slab strength compared to other methods. The aforementioned procedure considers a restraint system where the supporting edge beams and surrounding area of unloaded slab were equated to a spring with an equivalent stiffness.

#### 3.1.1 Analytical and Parametric Studies

To investigate the effect of different parameters on the lateral stiffness and ultimate capacity of the deck, this study conducted a detailed comparison between the following four methods: British Standard (BS5400), ACI 318-14, UK Highways Agency BD81/02, and Taylor, Rankin, and Cleland's approach, referred to as TRC (2002). The following parameters were used in the comparative analysis to analyze their effect on the predicted ultimate capacity of bridge deck.

- 5 different deck slab thicknesses (7.5 in, 8 in, 8.5 in, 9 in, and 9.5 in)
- 5 different support beam spacing (6 ft, 8 ft, 10 ft, 12 ft, and 14 ft)
- Steel reinforcement ratio of 0.454% and 0.630%
- Bridge span length of 50, 60, 70, 80, and 90 ft
- Beam type including FIB-36, AASHTO Type III, and two steel W-shape girders: W44x335, and a Built-up steel girder
- Compressive concrete strength of 4 ksi, 5 ksi, and 8 ksi
- Reinforcement yield strength of 60 ksi

Table 3.1 summarizes some of the results obtained from the MathCAD sheet developed for this study which used a 0.454% reinforcement ratio and 8-in deck thickness. Evaluation was performed to determine the effect of different beam spacing and deck thickness on the bridge deck ultimate capacity. The capacity values, listed in Table 3.2, for the 8-in deck with 14-ft beam spacing are slightly different than those in Table 4.8 due to the change in concrete compressive strength. The predicted capacity in Table 3.2 was based on  $f'_c$  of 5,000 psi. However, the concrete compressive strength of the experimentally tested deck reached 8,500 psi. Figure 3.1 represents graphical interpretations for the comparison between the different methods. The TRC method estimates a lower capacity than the BD81/02 method. However, the ACI 318-14 and the BS5400 standard codes were significantly more conservative than the BD81/02 and the TRC approach. This discrepancy can be attributed to the different factors that each method considers. For instance, ACI 318-14 and BS5400 methods take into account both the flexural and the shear punching capacity, and the BD81/02 only takes into account the latter. The ACI 318-14 and BS5400 methods do not consider the spacing while the BD81/02 method considers it. Nevertheless, the TRC approach does not only take into consideration the flexural and shear punching, and the spacing between beams, but it also considers a series of different stiffness parameters that contribute to the development of the compressive membrane action. The BD81/02 also accounts for the compressive membrane action, but does not take into consideration the lateral restraint provided by the supporting beams, end diaphragms, and surrounding area, as does the TRC approach. It was observed that when the support beam spacing increased, the predicted ultimate capacity decreased. This was more drastically observed for the TRC approach than for the other three methods.

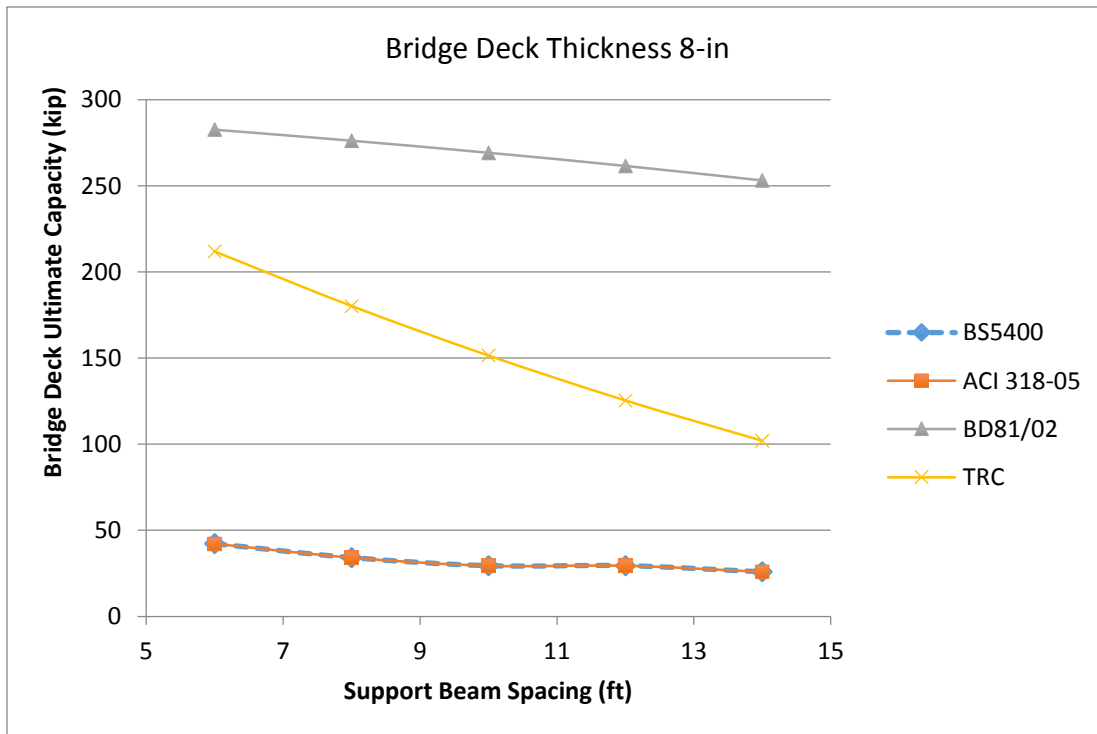


Figure 3.1: Deck capacities by varying beam spacing and analysis method

Table 3.1: Summary of Predicted Capacities Using an 8-inch Slab ( $f'_c = 5$  ksi)

SPACING (ft)	THICKNESS (in)	Method	Flexural Capacity	Shear Capacity	Ultimate Capacity	Type of Failure
			Kip			
6	8	BS5400	42.245	105.05	42.245	Flexural
		ACI-318	42.178	133.117	42.178	Flexural
		BD81	-	282.585	282.585	Shear
		TRC	211.876	222.876	211.876	Flexural
8		BS5400	34.155	105.05	34.155	Flexural
		ACI-318	34.1	133.117	34.1	Flexural
		BD81	-	276.174	276.174	Shear
		TRC	180.215	213.541	180.215	Flexural
10		BS5400	29.457	105.05	29.457	Flexural
		ACI-318	29.411	133.117	29.411	Flexural
		BD81	-	269.178	269.178	Shear
		TRC	151.451	202.78	151.451	Flexural
14		BS5400	25.896	105.05	25.896	Flexural
		ACI-318	25.855	133.117	25.855	Flexural
		BD81	-	253.108	253.108	Shear
		TRC	101.963	177.366	101.963	Flexural

Using the TRC approach, analysis was conducted on several specimen configurations and varying parameters, as shown in Table 3.2 and

Table 3.3.

Table 3.2: Ultimate capacity of a bridge deck on FIB-36 girders analyzed using TRC ( $f'_c = 5$  ksi)

FIB- 36				Flexural Arching	Punching Shear	Ultimate Capacity	Type of Failure
Length (ft)	Spacing (ft)	Thickness (in)	$\rho\%$ empirical	kip			
50	14	8	0.454	101.529	177.078	101.529	Flexural
60				101.735	177.216	101.735	Flexural
70				101.869	177.304	101.869	Flexural
80				101.963	177.366	101.963	Flexural
90				102.032	177.412	102.032	Flexural
			$\rho\%$ traditional	kip			
50			0.63	122.258	182.905	122.258	Flexural
60				122.432	183.011	122.432	Flexural
70				122.544	183.08	122.544	Flexural
80				122.622	181.128	122.622	Flexural
90	122.68	183.164		122.68	Flexural		

Table 3.3: Ultimate capacity of a bridge deck on AASHTO Type III girders analyzed using TRC ( $f'_c = 5$ ksi)

AASHTO TYPE III				Flexural Arching	Punching Shear	Ultimate Capacity	Type of Failure
Length (ft)	Spacing (ft)	Thickness (in)	$\rho\%$ empirical	kip			
50	14	8	0.454	75.899	156.79	75.899	Flexural
60				75.906	156.797	75.906	Flexural
70				75.91	156.801	75.91	Flexural
80				75.913	156.804	75.913	Flexural
90				75.916	156.807	75.916	Flexural
			$\rho\%$ traditional	kip	kip	kip	
50			0.63	100.598	167.843	100.598	Flexural
60				100.605	167.848	100.605	Flexural
70				100.608	167.851	100.608	Flexural
80				100.611	167.853	100.611	Flexural
90	100.613	167.855		100.613	Flexural		

The effect of steel reinforcement ratio was also investigated. Table 3.2 and

Table 3.3 show the effect of increasing the steel reinforcement ratio on the ultimate load capacity. When comparing the results in Table 3.2 and

Table 3.3, the ultimate load capacity varied greatly with beam type. This is attributed to the difference in lateral stiffness each girder type provided the slab.

Figure 3.2 represents the impact of beam spacing on the bridge deck considering varying slab thickness. The slab ultimate capacity was inversely proportional to the beam spacing. However, it was directly proportional to the slab thickness. This can be attributed to the reduction of the lateral stiffness when increasing the beam spacing. Table 3.4 shows the effect of the compressive concrete strength on the capacity of a bridge deck supported by FIB-36 girders as calculated by the TRC method.

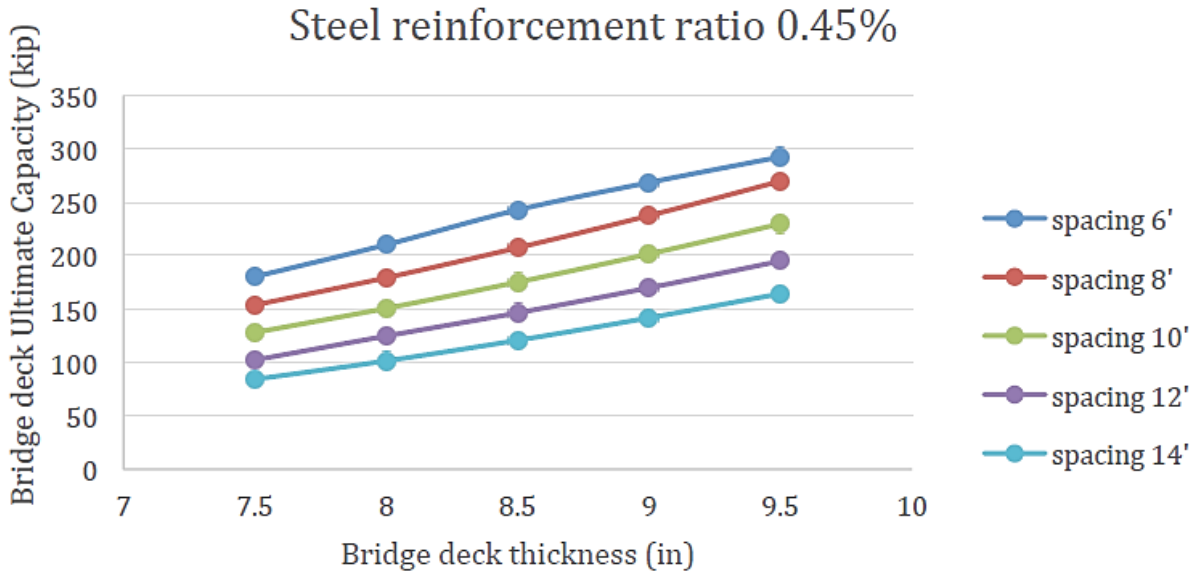


Figure 3.2: Deck strength by varying deck thickness and beam spacing for decks on FIB-36 girders analyzed using TRC

Table 3.4: Effect of compressive concrete strength on deck capacity using TRC method and FIB-36 girders

FIB-36					Flexural Arching	Punching Shear	Ultimate Capacity	Type of Failure
f'c (ksi)	Length (ft)	Spacing (ft)	Thickness (in)	ρ% empirical	kip			
4	80	12	7.5	0.45	92.898	146.676	92.898	Flexural
5					105.344	170.799	105.344	Flexural
8					119.593	224.327	119.593	Flexural

The effect of bridge span length on deck capacity was also investigated and shown to be negligible for the selected range of span lengths. This is due to the fact that the span length of the bridge has minimal influence on increasing stiffness in the transverse direction due to two reasons. First, longer span lengths require larger girder sizes, and even though the flange sizes are identical for all FIB sections, a deeper girder would still have larger lateral stiffness. Second, and more importantly, a large component of the lateral stiffness is due to the restraint of the deck within the effective strip width; i.e. area influenced by the load, according to Taylor’s method. Therefore, the lateral restraint provided by the deck will not vary greatly with the span length since variation in the effective strip width is not significant for different span lengths. This can also be observed from the results using FIB-36 girders and a compressive concrete strength of 5 ksi, as shown in Figure 3.3.

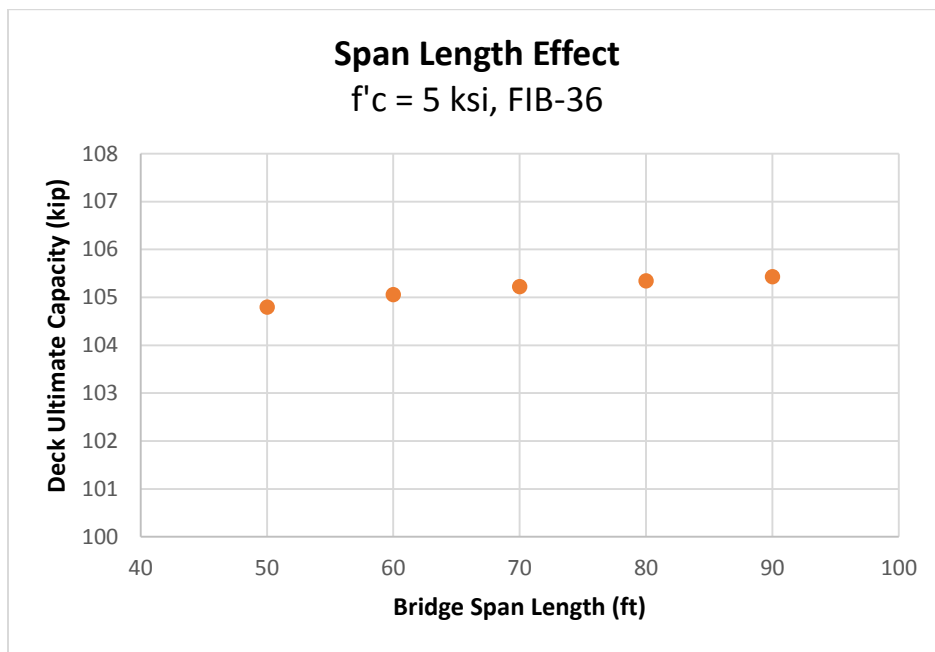


Figure 3.3: Effect of span length on the bridge deck ultimate capacity

The effect of the lateral restraint in structural slab systems on the arching action and the load-carrying capacity of the deck was investigated. Laterally restrained deck slabs developed axial compressive forces that result in a significant increase in flexural stiffness and load capacity of the deck. To explain the deck behavior, the reinforced concrete deck will deflect under loading with cracking in the concrete on the tension face and stretching of the reinforcement. The deflected slab attempts to expand laterally outward. However, this impulse is prevented, to some degree, by the lateral stiffness of the supporting beams, diaphragms, and the area of the slab adjacent the loaded segment. FIBs have wider flanges than AASHTO beams, beams, and higher lateral stiffness than a beam of the same height. The TRC method considers a restrained system where the supporting edge beams, end diaphragm, and surrounding area of unloaded slab are modeled as a spring of an equivalent stiffness. Equations 17 and 18, respectively derive how the TRC method accounts for beam and slab restraint. The total restraint,  $K_r$ , considers both the

stiffness of the slab ( $K_a$ ) and the stiffness of the support beams ( $K_b$ ). For every deck thickness, analysis was performed to determine the effect of beam type and beam spacing on the beam lateral stiffness  $K_b$  and the deck ultimate capacity. Table 3.5 lists the results specific to an 8 inch thick slab.

Table 3.5: Support beam lateral stiffness  $K_b$  (kip/in) by varying beam type and beam spacing

8-inch Deck Thickness										
50-ft Span										
	6-ft beam spacing		8-ft beam spacing		10-ft beam spacing		12-ft beam spacing		14-ft beam spacing	
	$K_b$ (kip/inch)	Capacity (kip)	$K_b$ (kip/inch)	Capacity (kip)	$K_b$ (kip/inch)	Capacity (kip)	$K_b$ (kip/inch)	Capacity (kip)	$K_b$ (kip/inch)	Capacity (kip)
W44X335	8399	155.3	3756	121.8	1992	95.4	1181	80.4	756.572	74.7
AASHTO III	10620	162.1	4748	127.9	2519	100.8	1493	82.9	956.473	75.9
BUILT-UP STEEL	20190	180.7	9028	145.7	4789	116.8	2839	92.9	1819	80.8
FIB 36	70510	210.3	31530	179.4	16730	150.7	9915	124.8	6352	101.5

Figure 3.4 shows the relationship between the lateral stiffness of the supporting beam,  $K_b$ , and the bridge deck ultimate capacity for various beam types and beam spacing. Figure 3.4 shows higher ultimate capacity for decks supported on FIB-36 beams which have the highest lateral stiffness of the test group. The behavior of increased deck capacity when using FIB-36 beams vs. other beams of AASHTO and built-up steel beams was consistent for every investigated beam spacing ranging from 6 to 14 feet.

In conclusion, the results indicated that the beam lateral stiffness has a direct effect on the ultimate capacity of the bridge deck. It was observed that the FIB-36 girder provided higher lateral stiffness compared to the other girders (AASHTO Type III, steel built-up section, and W44x335). This resulted in greater lateral restraint that enhanced the compressive membrane action, thus increasing the ultimate load capacity of the bridge deck. Varying the bridge span length had little impact on the deck's ultimate capacity. It was observed that increasing the support beam spacing decreased the deck capacity because of the reduction in lateral stiffness of the deck. However, increasing the deck thickness increased the stiffness and the ultimate strength.

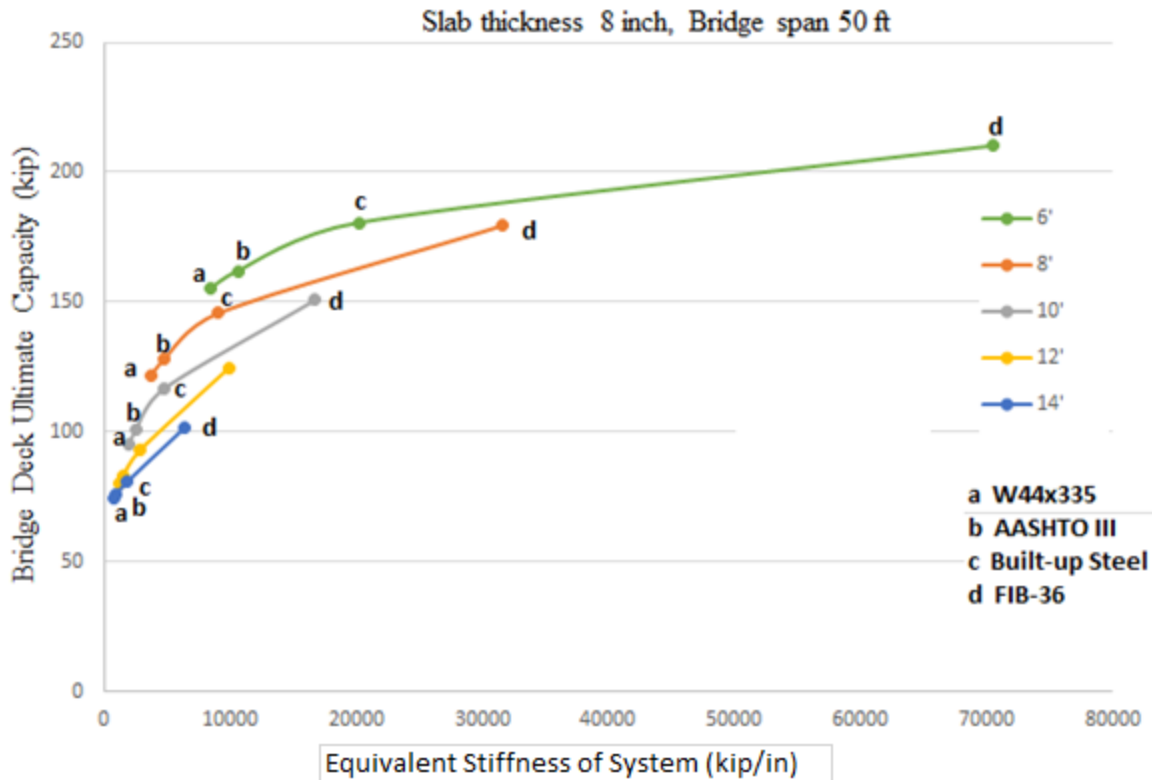


Figure 3.4: Relationship between ultimate capacity and equivalent stiffness of support system

### 3.1.2 Finite Element Modeling of Bridge Deck

#### 3.1.2.1 STAAD Finite Element Analysis

In this project, a study was conducted to verify the feasibility of the empirical design method. Fifteen bridge models were designed following the FDOT SDG requirements for bridge deck thickness of 8 inches. The bridge superstructures consisted of FIB-36 beams designed based on FDOT Design Standard 20036 and the Instructions for Design Standards (IDS) 20010.

Finite element models were partnered with a parametric study, analyzing the 15 bridge models. These models were differentiated by use of three different span lengths of 70 ft, 80 ft, and 90 ft, with varying beam spacing of 6 ft, 8 ft, 10 ft, 12 ft, and 14 ft. The effect different deck thicknesses had was also incorporated into the study. Five different typical beam sections were used to carry a minimum of 3 design lanes (AASHTO LRFD, 3.6.1.1.1) and a constant overhang of 4 feet on both sides. Each typical section was input as a unit model with 3 different span lengths of 70, 80, and 90 feet. Each unit model had a total length of 240 feet with 3 simply supported spans and Type K typical section based on LRFD Table 4.6.2.2.1-1. Figure 3.5 shows one of the investigated sections set at a beam spacing of 14 ft.

All 15 models were initially designed using the commercial software, SmartBridge, to obtain the layout of prestressing strands, their debonding, and the shear reinforcement. Live load deflections were calculated by running the AASHTO HL-93 vehicular load over the models. The environmental classification was assumed to be Extremely Aggressive based on the FDOT SDG

Table 1.4.3-1 which requires a Class IV deck concrete. The concrete strength used was 5,500 psi, based on the FDOT *Standard Specifications for Road and Bridge Construction* (FDOT Standard Specs) Section 346-3, for Class IV concrete. The concrete used for the Prestressed FIB-36 beams was Class VI with a concrete strength of 8,500 psi, based on the FDOT SDG Table 1.4.3-1, and the FDOT Specs Section 346-3. The reinforcing steel used for the deck and for the prestressed FIB-36 beams' shear reinforcement was ASTM A615, Grade 60 as per the FDOT SDG 1.4.1-B. The shear reinforcement layout at the ends of the FIB-36 beams was in accordance with FDOT Index 20036, and the other regions were designed following the beam elevation details shown in FDOT Index 20036. The prestressing strands used in the FIB-36 beams were ASTM A416, Grade 270, low-relaxation in accordance with Section 4.3.1-A of the FDOT SDG.

The models were analyzed with *STAAD.Pro V8i* to obtain the dead load moments, future wearing surface moments, and live load moments in the deck. The decks were then designed as a reinforced concrete flexural element. The steel reinforcing ratio obtained from the finite element analysis was compared to that obtained from the empirical design and the traditional design methods; each method getting its own bridge model. The 15 bridges were checked to verify they met the criteria for use of the empirical method based on AASHTO LRFD, Section 9.2.7.4. As described earlier in Section 3.2 of this report, the steel reinforcing area came out to be  $0.31 \text{ in}^2$ ; a little higher than required by AASHTO LRFD. The bridges were then analyzed using three-dimensional linear finite element models that include all elements of the structure such as traffic railings, deck, girders, and substructure. The required reinforcing steel ratios ( $\rho$ ) obtained from all three methods were compared to make recommendations on whether the empirical method would provide adequate deck designs with minimal cracking.

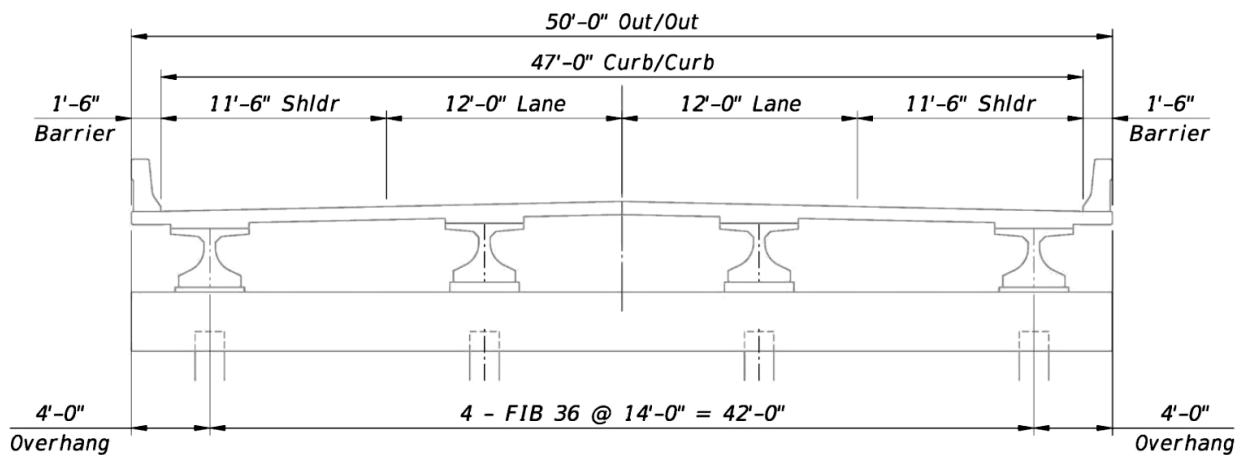


Figure 3.5: Typical section for 14-foot beam spacing

The decks were modeled as 4-noded (quadrilateral) plates with varying thicknesses based on the beam spacing and span. Figure 3.6 shows the element and the sign convention used. The deck plates used were 2'x2' and were generated in *STAAD.Pro V8i* using the mesh generation facility.

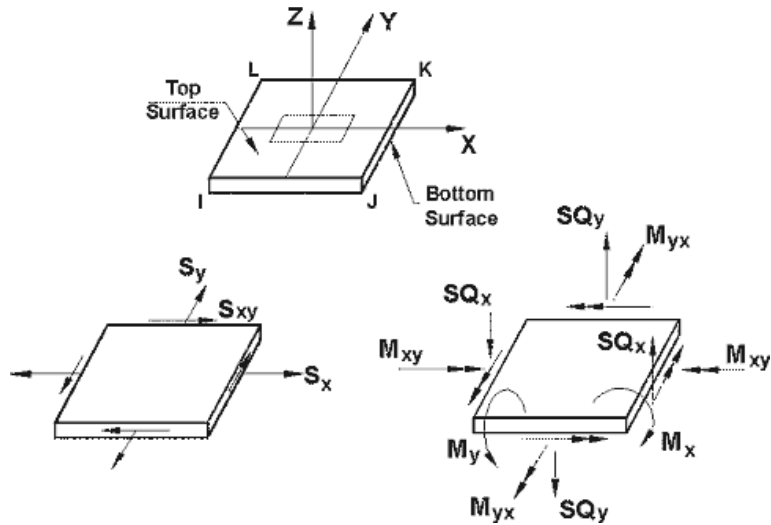


Figure 3.6: Plate sign convention used in STAAD.Pro V8i

The FIB-36 beams, the FDOT F-Shape barrier, the bent cap, and the piles were modeled as beam/column elements in *STAAD.Pro V8i*. The FIB-36 beams and the F-Shape barrier were built as special elements using the user defined table (Figure 3.7) with geometry matching the FDOT Design Standards Index 20036 and Index 420 for the FIB-36 and F-Shape barrier, respectively.

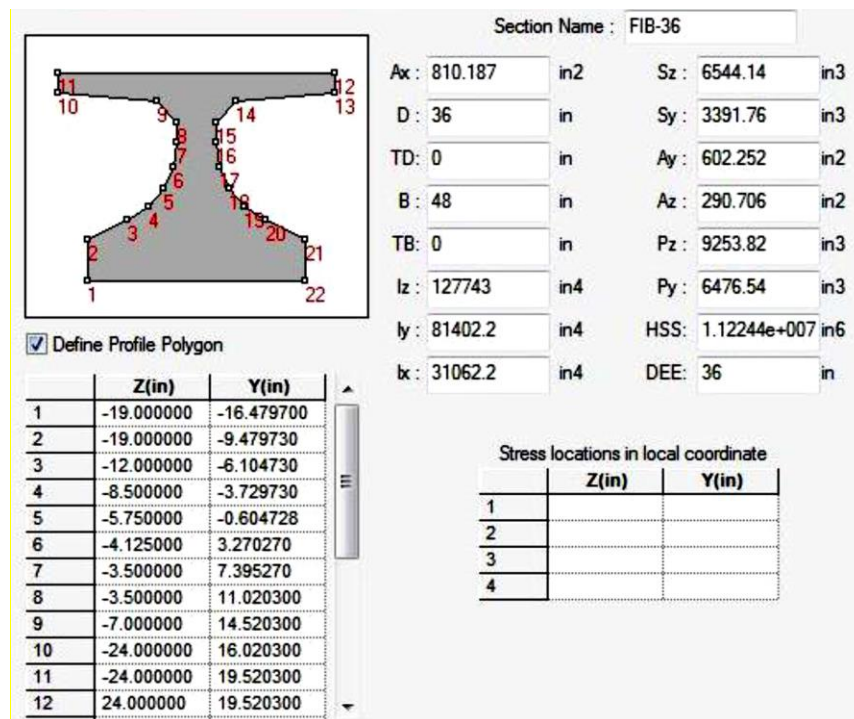


Figure 3.7: FIB-36 beam geometry in STAAD.Pro V8i

The dead loads applied in the finite element models included the self-weight of all the element of the structure. The stay-in-place forms load was applied as a uniform pressure between the top flanges of beams (between beam lines) while the future wearing surface load was applied as a

uniform pressure between the curb lines. In order to obtain the maximum live load effect, the HL-93 design truck was modeled as a moving load on the deck surface in the longitudinal and transverse directions at one foot increments. Figure 3.8 represents the 3-D finite element model. Figure 3.9 shows the positive moments developed in the deck.

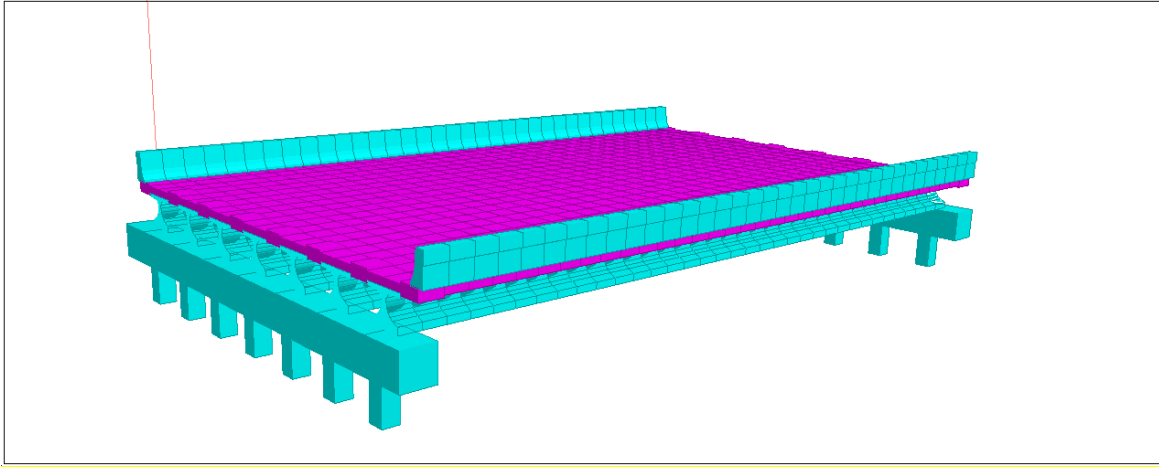


Figure 3.8: Three-dimensional finite element model

The service moments due to live load, dead loads (including stay-in-place forms) and future wearing surface were extracted from the output of *STAAD.Pro V8i* and imported to a Mathcad sheet. A design of the deck flexural reinforcement was performed. Also, deck cracking and steel tensile stresses were checked.

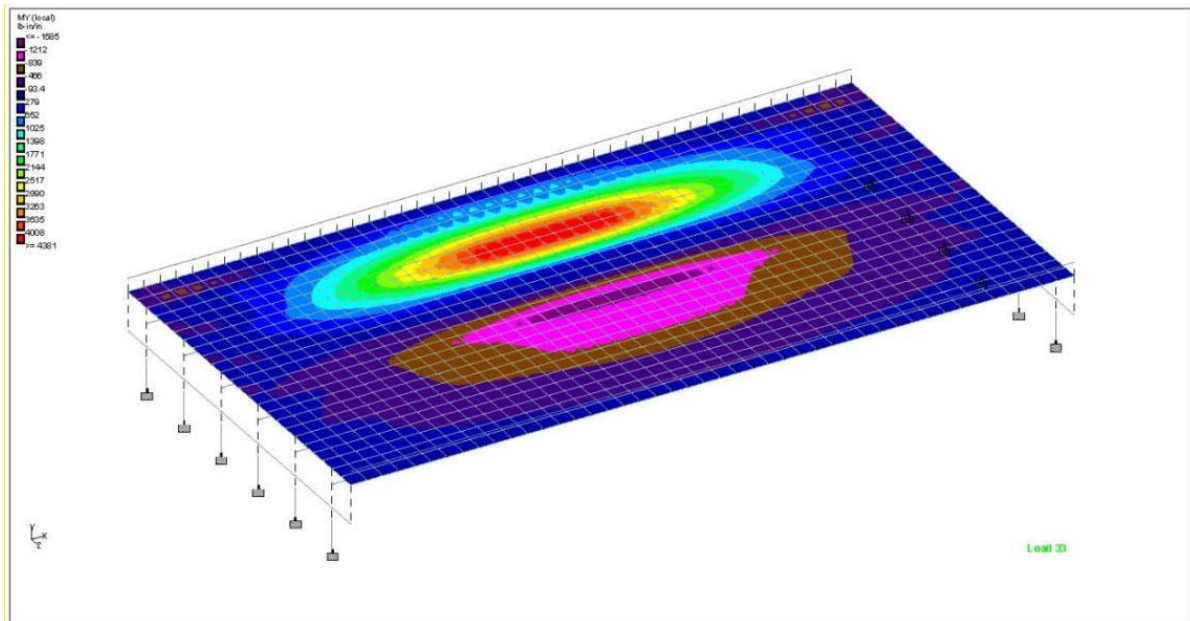


Figure 3.9: Finite element model showing maximum positive moment in the deck

The FDOT IDS 20010 provides a figure indicating the FIB-36 maximum span lengths for each beam spacing. Table 3.6 shows some of the investigated span lengths that exceed the span limitations provided in the FDOT IDS 20010.

The average reinforcing steel ratio ( $\rho$ ), for the 8-inch thick decks, was plotted versus the beam spacing. It showed that the required reinforcing steel ratio obtained from the finite element models is between the required reinforcing steel ratios obtained from the traditional method and the empirical method, as shown in Figure 3.10. A more refined finite element analysis was required to verify the findings. Therefore, it was decided to further perform finite element analysis in ANSYS.

Table 3.6: Required main reinforcing steel ratio for 8-inch-thick decks

Required Main Reinforcing Steel Ratio / Layer ( $\rho$ )							
Beam Spacing (ft)	Span Length (ft)	Deck Thickness (in)	Overhang (ft)	Bar Size	Required Traditional Design	Required Empirical Design	Required Finite Element Design
6	70	8.00	4	No. 5	0.530%	No Good*	0.424%
	80	8.00	4	No. 5	0.530%	No Good*	0.424%
	90	8.00	4	No. 5	0.530%	No Good*	0.488%
8	70	8.00	4	No. 5	0.634%	0.454%	0.439%
	80	8.00	4	No. 5	0.634%	0.454%	0.513%
	90	8.00	4	No. 5	0.634%	0.454%	0.584%
10	70	8.00	4	No. 5	0.777%	0.454%	0.498%
	80	8.00	4	No. 5	0.777%	0.454%	0.583%
	90**	8.00	4	No. 5	0.777%	0.454%	0.665%
12	70	8.00	4	No. 5	0.931%	0.454%	0.529%
	80	8.00	4	No. 5	0.931%	0.454%	0.628%
	90**	8.00	4	No. 5	0.931%	0.454%	0.727%
14	70**	8.00	4	No. 5	1.065%	0.454%	0.528%
	80**	8.00	4	No. 5	1.065%	0.454%	0.655%
	90**	8.00	4	No. 5	1.065%	0.454%	0.760%

\* Does not meet all empirical design conditions

\*\* Falls outside the FDOT IDS 20010 limitations

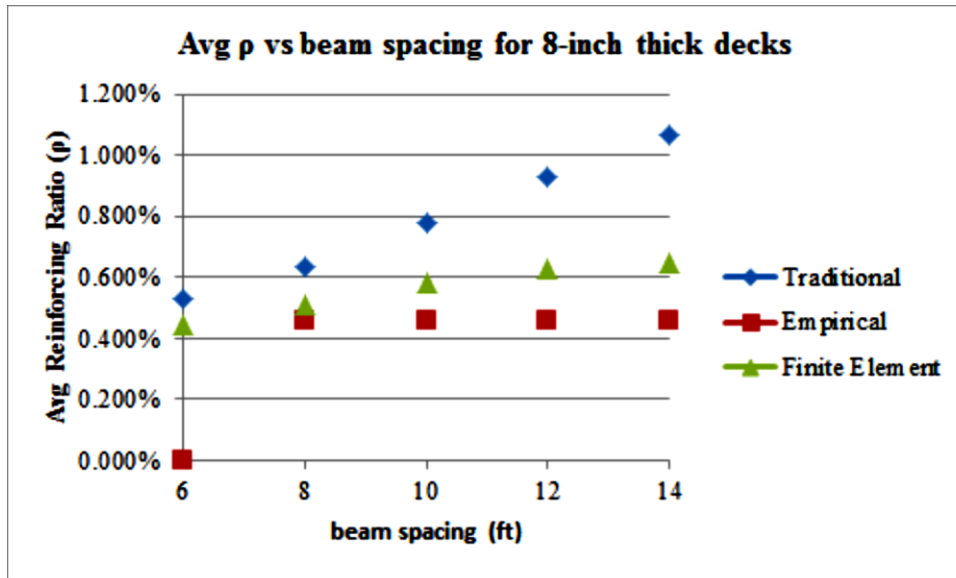


Figure 3.10: Average ( $\rho$ ) vs beam spacing for 8-inch thick decks

### 3.1.2.2 ANSYS Finite Element Analysis

Originally, it was decided to develop several finite element models for hypothetical bridges which consisted of seven FIB girders with various beam spans and beam spacing. The chart based on the FDOT estimated span and spacing of FIB-36 (Figure 3.11 was used as a guideline to establish the geometries of the hypothetical bridges.

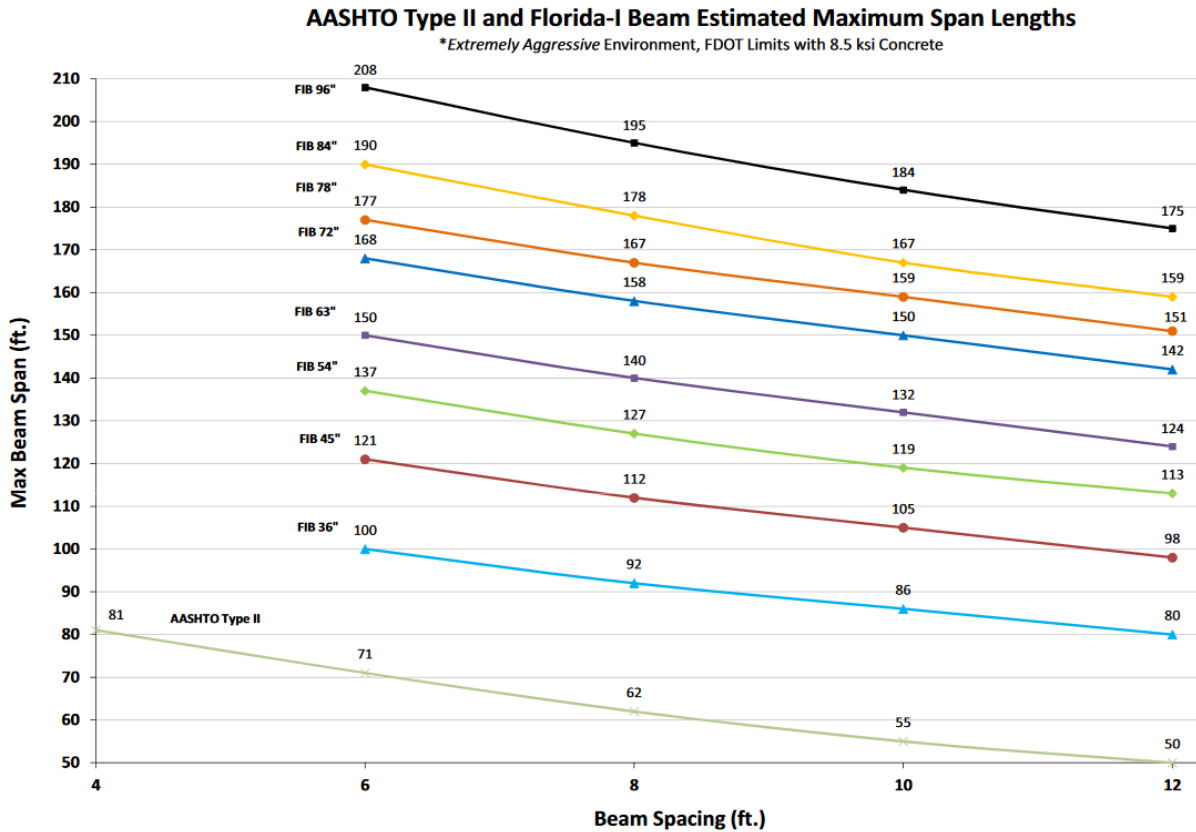


Figure 3.11: FDOT guidelines for beam spacing to beam span for the FIB-36

Figure 3.11 indicates the design assumptions for an interior beam design, a final beam concrete strength of 8.5 ksi and 6.0 ksi at release, and a deck concrete strength of 4.5 ksi. Table 3.7 shows the beam spans and spacing for the finite element models.

Table 3.7: Initial beam spans and spacing's modeled in ANSYS prior to lab specimen selection

Model No.	Beam Span (ft) vs. Beam Spacing (ft)	
	Traditional Design	Empirical Design
1	80 x 14	80 x 14
2	80 x 12	80 x 12
3	90 x 8	90 x 8
4	90 x 10	90 x 10
5	90 x 12	90 x 12
6	100 x 8	100 x 8
7	100 x 6	100 x 6

Initially, seven finite element models were developed based on the geometries shown in Figure 3.11. A hypothetical bridge was considered at the beginning of this study (Figure 3.12) and before starting the design and construction of the full-scale specimen for laboratory testing. The main reason for selecting these FEA models was mainly to have a better understanding of the slab/beam characteristics needed in the full-scale laboratory specimen. Such a full-scale specimen could be very costly and time consuming to develop and test. Therefore, it was important to develop and analyze a hypothetical bridge using FEA models prior to making the final decision about the following characteristics of the full-scale specimen:

- Proper geometries
- Material properties
- Design methods (Traditional vs. Empirical)
- Stress distributions and deformations of the bridge deck and FIB beams
- The potential development of crack initiation and propagation during load applications
- Simulation of bridge deck construction and widening conditions
- Schemes of surface and embedded instrumentations of the specimen/s
- The effect of boundary conditions on the development of Compression Membrane Action (CMA) in the bridge deck.

Figure 3.13 shows the finite element model configuration of a typical slab.

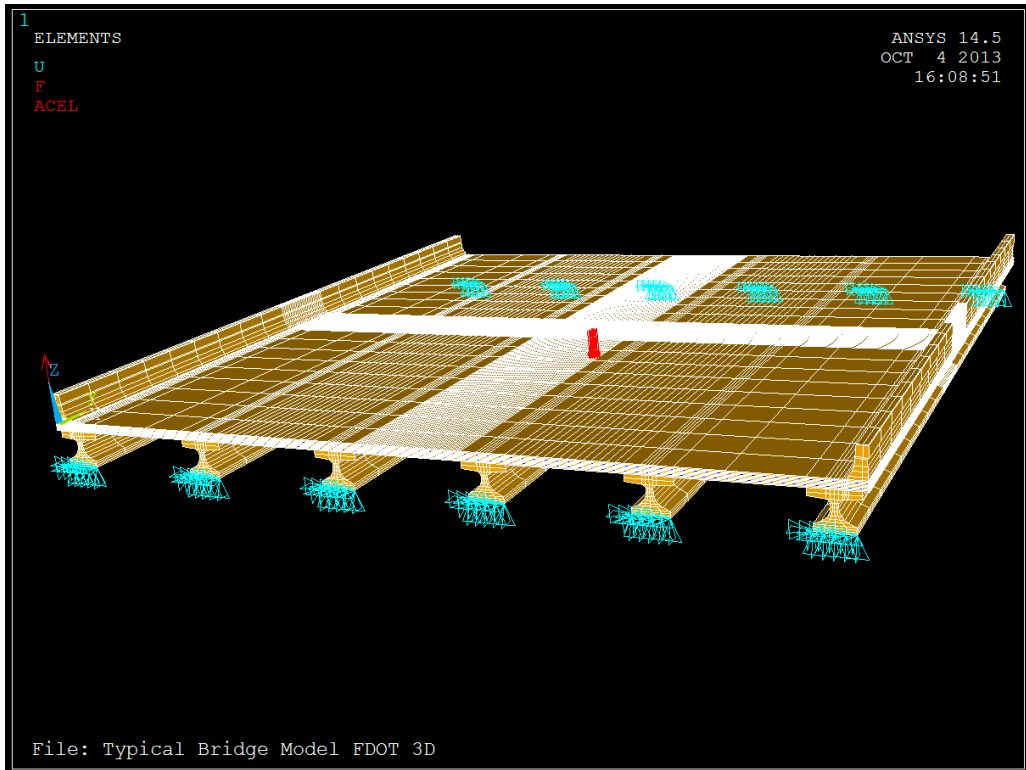


Figure 3.12: FE modeling of bridge span = 80' and beam spacing = 14'

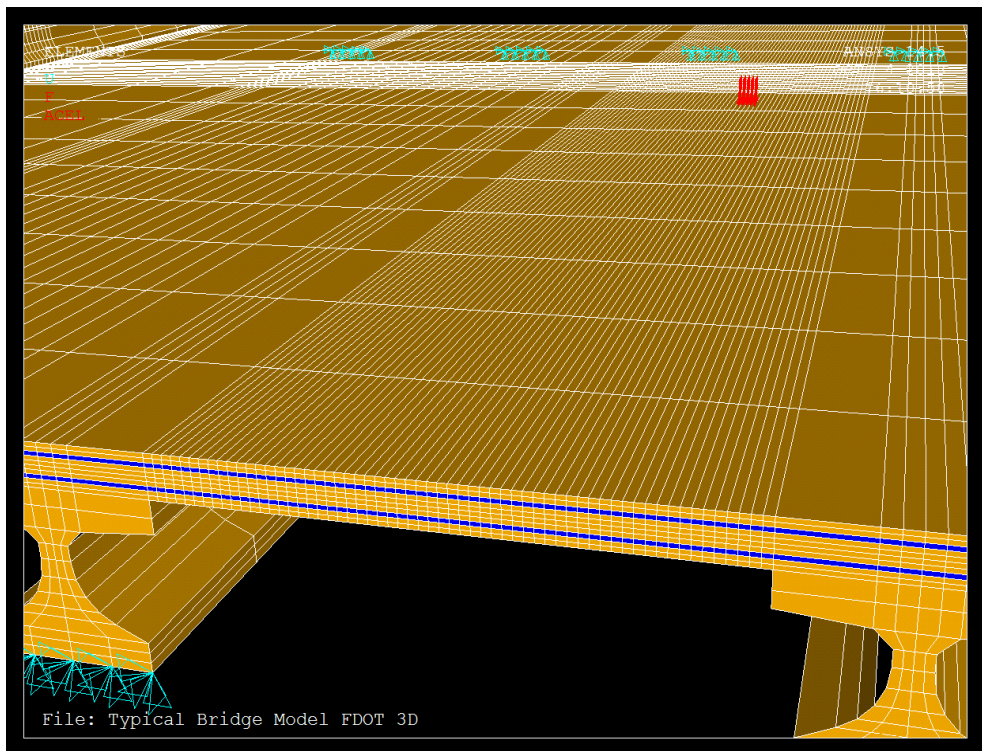


Figure 3.13: FE modeling of bridge deck

### 3.1.2.3 Determining the Steel Reinforcement Ratios in Traditional and Empirical Deck Designs

Mathcad solutions were obtained for each beam spacing and presented in Appendix III. Slab thicknesses of 8-in, 9-in, and 10-in were considered in the calculations. Another round of FEA was conducted to determine the stress distribution in bridge slabs for 14 bridge models simulating the widening and phased construction. Figure 3.14 and Figure 3.15 show one variation of the modeling. To apply the wheel load from HL-93 design truck on the finite element models, it was necessary to estimate the load distribution of a typical wheel on the nodes of the bridge slabs. For that purpose, a study conducted by Majumdar et al. (2009) was used to determine the proper simulated tire patch (Figure 3.16). Figure 3.17 and Figure 3.18 show the contact area and pressure for several truck tire widths, as a function of applied load. The FE models used both the entire truck load and one wheel load to simulate the laboratory testing setup. In one of the models a line load was applied to simulate the load of a barrier during the slab widening construction.

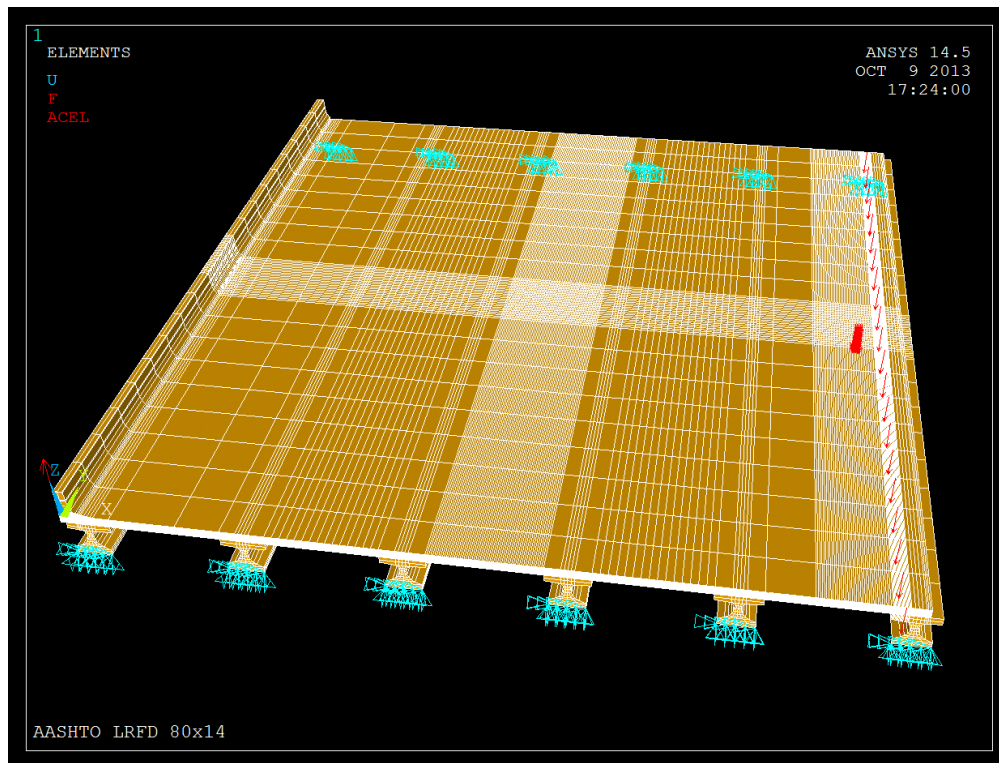


Figure 3.14: Bridge modeling with span = 80' and beam spacing = 14' during widening phase

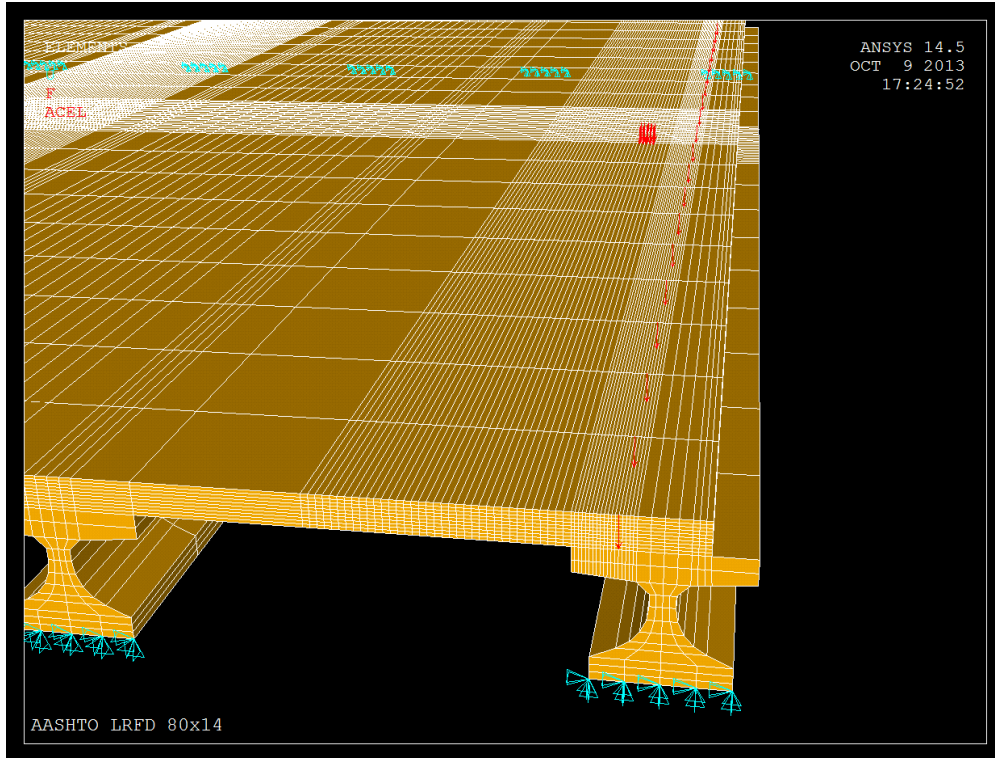


Figure 3.15: Load configuration during widening phase

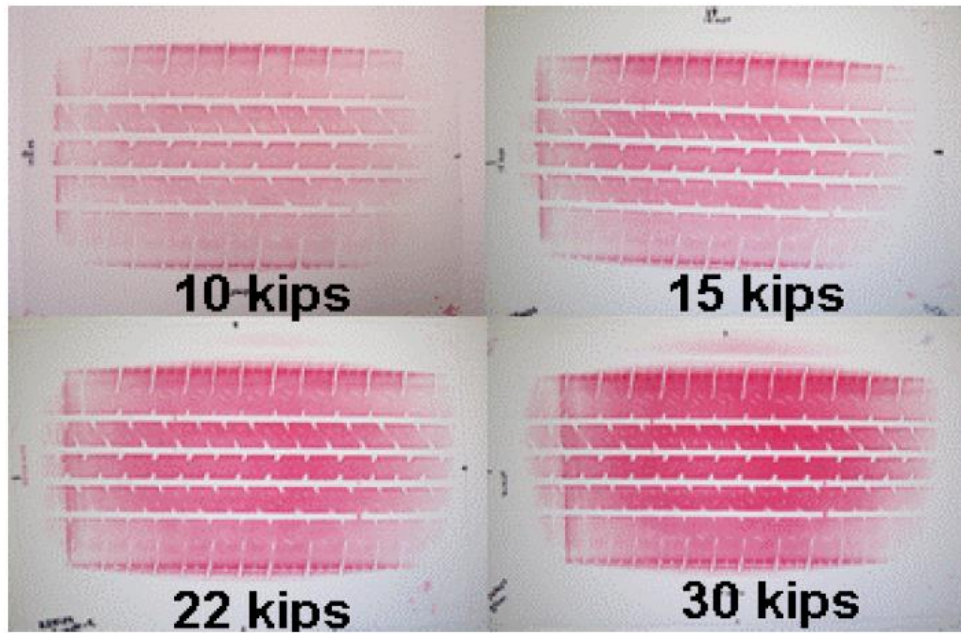


Figure 3.16: Simulated tire patch footprints from pressure sensor film at different load levels

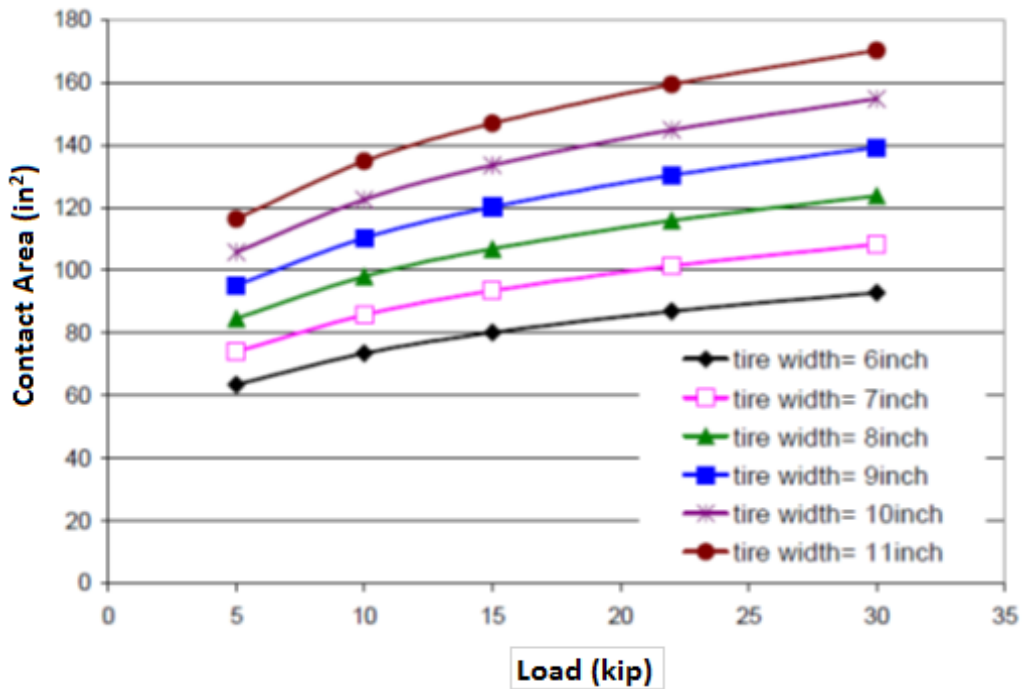


Figure 3.17: Variation of contact area with applied load

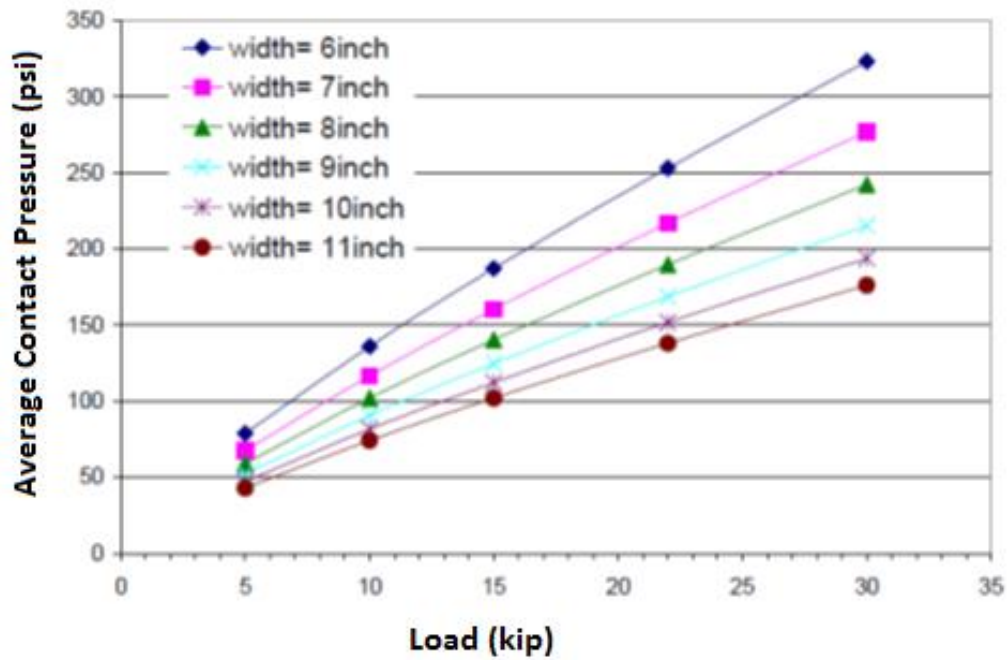


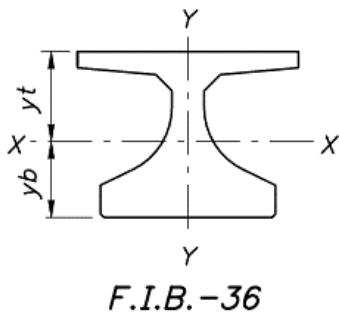
Figure 3.18: Tire contact pressure as function of applied load for different tire widths (Majumdar, et al. 2009)

### 3.2 Beam Design Information

The smallest Florida I-beam (FIB-36) was sufficient for satisfying both flexure and shear limits to cover a 47-foot span at a beam spacing of 14 feet with an 8-inch-thick deck. The beam length was set to be 47 feet to accommodate conducting multiple tests at several locations on the specimen without affecting their respective results. The 36-inch Florida I-Beam was designed in accordance with the 2014 FDOT SDG and 2014 FDOT Design Standard Index 20036. Figure 3.19 shows geometric beam properties and the cross-sectional shape of the FIB-36, while Table 3.8 lists other detailed information. Figure 3.20 displays the strand pattern selected for best results. The stirrup spacing shown in Figure 3.21, was conservatively set to prevent premature shear failure during testing.

Table 3.8 Beam Design Information

Beam Information	
Design Compressive Strength	8,500 psi (Class VI)
Beam Length	47 feet
Strands	Twenty-six, fully bonded, 0.6 inch diameter, grade 270k, low-relaxation strands stressed at 44 kip each, straight strands



Florida I-Beam Geometric Properties	
Area ( $in^2$ )	806.58
Perimeter ( $in$ )	206.57
$I_{xx}$ ( $in^4$ )	127,545
$I_{yy}$ ( $in^4$ )	81,070
$y_t$ ( $in$ )	19.51
$y_b$ ( $in$ )	16.49

Figure 3.19: Florida I-beam properties

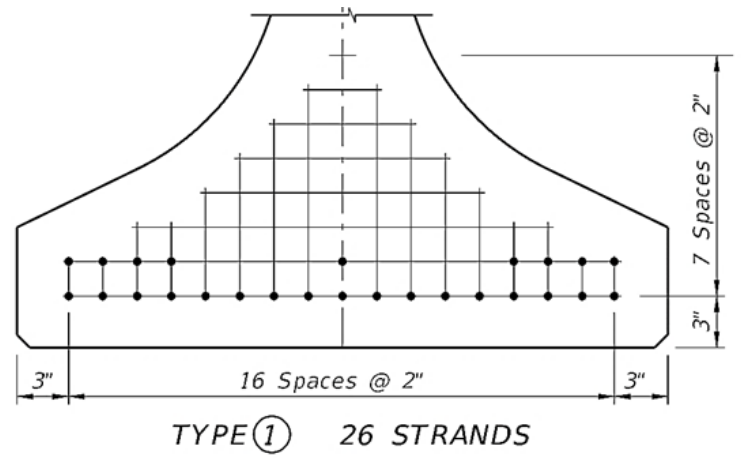


Figure 3.20: Strand pattern

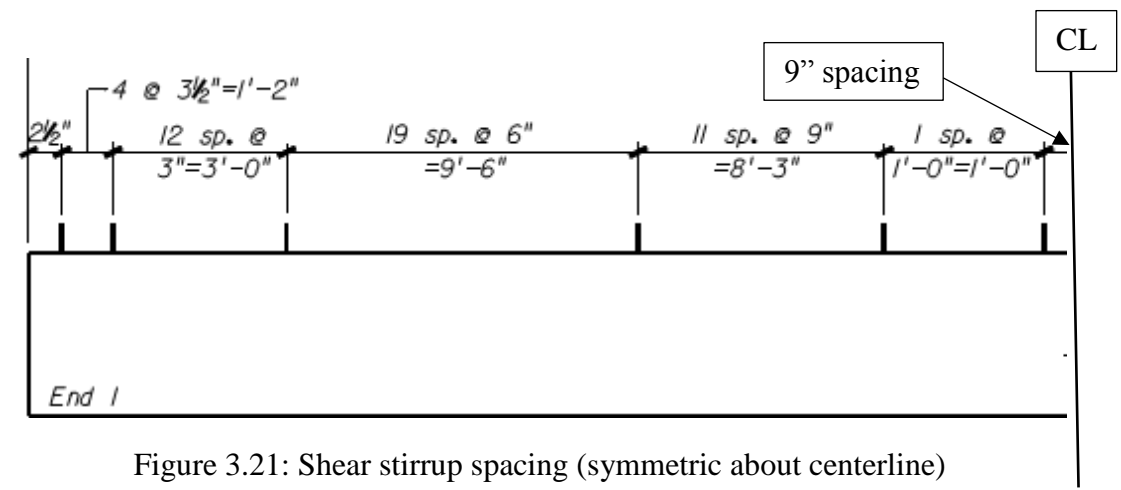


Figure 3.21: Shear stirrup spacing (symmetric about centerline)

### 3.3 Deck Design

The minimum depth of slab according to section 9.7.1.1 in AASHTO LRFD is 7 inches. However, according to section 4.2.2 of FDOT SDG, a minimum design depth of 8 inches is specified for new construction of both short and long bridges. For new construction of long bridges, FDOT SDG specifies the minimum thickness of cast-in-place (CIP) bridge decks on beams to be 8.5 inches with the top 0.5 inch being sacrificial. For new construction of short bridges, it specifies the minimum thickness of bridge decks cast-in-place (C.I.P.) on beams to be 8 inches. In order to satisfy some design conditions and be in compliance with section 4.2.2 of the FDOT SDG, the deck was specified to be 8 inches which overrides the AASHTO minimum deck thickness of  $t_s = 7$  inches.

Section 9.7.2.5 of AASHTO LRFD indicates that the reinforcement requirements for the empirical deck followed a minimum of  $0.27 \text{ in}^2/\text{ft}$  for each bottom layer and  $0.18 \text{ in}^2/\text{ft}$  for each top layer with those values corresponding to a 7.5-inch slab. For the 8-inch slab specified for the test specimen, the values are then adjusted to  $0.288 \text{ in}^2/\text{ft}$  for the bottom layer and  $0.192 \text{ in}^2/\text{ft}$  for the top layer. Based on analysis, No. 5 steel reinforcement bars spaced at 12 inches was chosen for each layer giving a ratio of  $0.31 \text{ in}^2/\text{ft}$  for the top and bottom layer thus, going above the minimum requirements for empirical deck design conditions per AASHTO. Additionally, the layers were staggered by 6 inches for better distribution; avoiding two bars being in the same plane, which minimizes the concrete discontinuity.

## Chapter 4

## Experimental Program & Fabrication

The test specimen developed for studying the performance of the empirical bridge deck was designed in accordance with AASHTO LRFD, FDOT SDG and FDOT Standard Specs. Laboratory testing was conducted in the FDOT Marcus H. Ansley Structures Research Center (MHA-SRC) in Tallahassee, FL. The available testing facility allowed for building a full-size specimen. The tested specimen was chosen to meet the goals of the project by mimicking realistic bridge dimensions and configurations rather than relying on reduced scale or component like specimens. In particular, the specimen design was chosen to provide data on the performance of the tested concrete bridge deck in widening scenarios, which is not currently covered by AASHTO LFRD, yet is often encountered by bridge engineers. In typical widening scenarios, the existing barrier, and deck overhang get removed back halfway across the top flange of the exterior girder. In the process, the embedded deck reinforcement is exposed and prepared for creating lap splices with new bars that will reinforce the widened portion of the deck. A temporary barrier is usually installed to protect workers and traffic during deck widening.

The overall specimen size was decided to have a length of 47 feet to allow for multiple tests to be conducted at several locations without one test/failure zone significantly affecting another. Load frame anchor points in the lab floor, being set at a 6-ft spacing, also had to be considered when choosing the specimen length. It was decided that the specimen would consist of a concrete bridge deck that is supported on two prestressed concrete girders at the desired spacing of 14 ft as shown in Figure 4.1 which depicts the final condition of the specimen before testing. A third girder line would have made the specimen much larger for little added benefit since the considered loading was a wheel load at midspan in between two girders. The deck was extended beyond one of the girders and weight blocks were placed along the edge of the overhang to simulate the effect of continuity a third girder line, and the deck in between the two, would have provided. It was determined through analysis that the developed specimen was adequate for evaluating overall deck behavior.



Figure 4.1: Fabricated specimen

## 4.1 Specimen Dimensions

For the chosen two-line girder bridge specimen, Figure 4.2 shows a sketch of the specimens used in the experimental program. The fabricated deck specimen has a length of 47 feet and width of 18.5 feet and is supported on two prestressed concrete beams with a 14-foot spacing. The two FIB-36 beams were used to support the 8 inch concrete deck reinforced with two layers of No.5 rebar at 12-inch spacing in both directions. This reinforcement choice more than satisfies the AASHTO LRFD (9.7.5.2) reinforcement criteria of 0.27 in.<sup>2</sup>/ft for each bottom layer and 0.18 in.<sup>2</sup>/ft for each top layer. The higher reinforcement amounts were chosen as per FDOT recommendations. The choice of the maximum girder spacing of 14-foot was intentional because of the difficulty of repeating such a large and expensive test. A specimen built with girders set at the maximum allowable spacing can be considered the worst case scenario. Successful performance of the deck in the configuration shown in Figure 4.2, will simultaneously garner acceptance of the deck design for design for girders at a tighter spacing more typically used in construction. Extensive analyses were run before the described specimen was finalized (see Chapter 3 for details about these analyses).

Throughout this report, terms such as S1 and F1 refer to the type of test that was conducted. For example, S1 signifies the first service test location as shown in Figure 4.3, F1 signifies a failure test at the same location. A plan view of the specimen and failure testing locations is shown in Figure 4.3. S1 is in the same place as F1, typical for the rest of the tests.

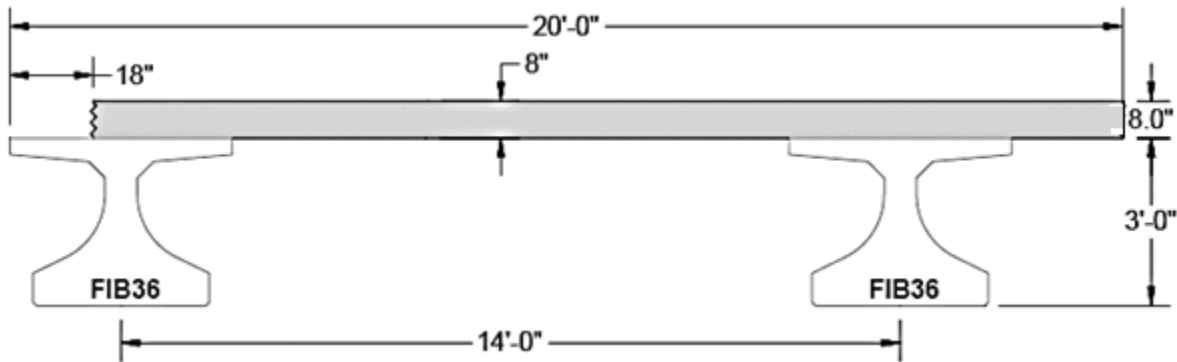


Figure 4.2: Specimen dimensions

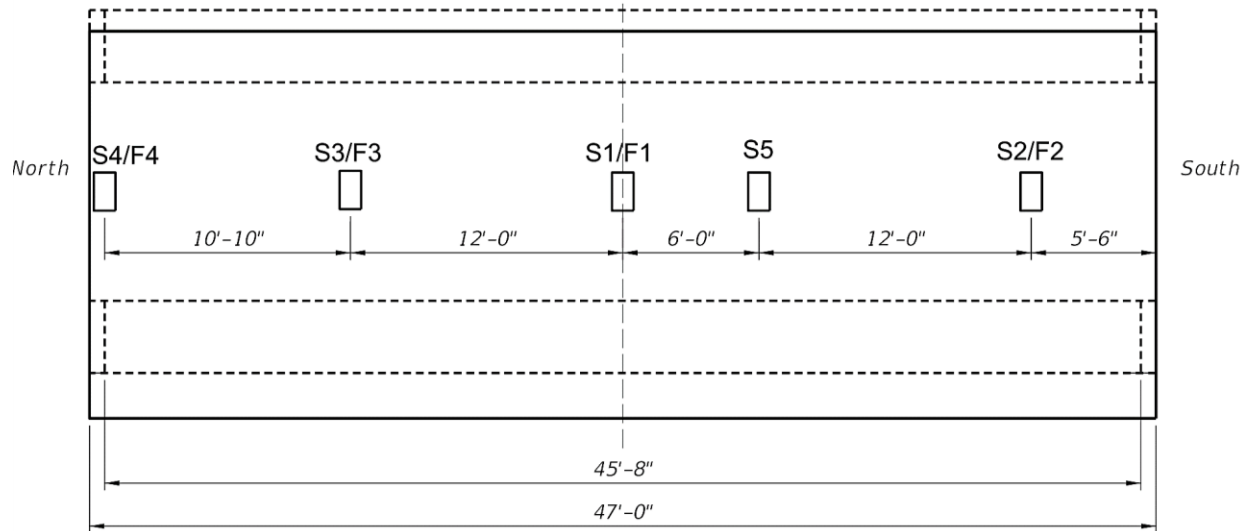


Figure 4.3: Testing locations

#### 4.1.1 Girder Details

The smallest Florida I-beam (FIB-36) size was sufficient for both flexural, shear, and torsional limits to cover a 47-foot span at a spacing of 14 ft. The FDOT charts for sizing FIB girders based on spacing and span length were used as a starting point for initial design (example Figure 3.11). According to the 2015 FDOT Design Standards (Index No 20510), for beams without diaphragms the edge of bearing pad should be 4 inches in from the end of the beam. Since the bearing pad used was 32-in wide and 8-in long, the span length was 45-ft-8-in from center to center of the bearing pads. The focus of this study was on the performance of the concrete deck. Therefore, the girders were designed to avoid premature failure by having a capacity to resist higher loads than the anticipated deck failure loading according to preliminary calculations that showed the failure load would exceed the design wheel load.

## 4.2 Fabrication

Construction means and methods used in actual bridges were followed in the construction of the test specimen. This includes the detailing of the girder reinforcement, rebar in the deck, and formwork for the CIP concrete deck. The chosen specimen was constructed in four main steps:

1. Fabrication and casting of prestressed concrete FIB beams,
2. Delivering of precast beams to the FDOT MHA-SRC and setting the girders on the supports,
3. Building the formwork and placing the concrete deck reinforcement,
4. Adhering strain gauges to the reinforcement and routing cabling, and
5. Pouring the deck concrete.

It should be noted that the girders were supported on neoprene bearing pads. Also, the transverse deck reinforcement was extended outside of the deck edges on the side, simulating a widening scenario (Figure 4.4) as this is the current practice for widening existing bridges. After the concrete is properly cured, the specimen construction is complete (Figure 4.5) and is ready for loading. The edge of concrete deck for the specimen at its widening location was established 6 inches from the girder centerline. This differs from the common practice of cutting and bringing the concrete edge to centerline of the girder top flange. It was justified because of the wide flange of the FIB.

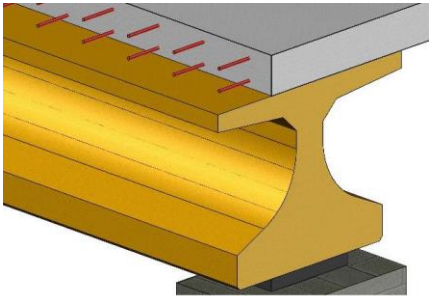


Figure 4.4: Transverse deck rebar extending beyond deck at the widening side

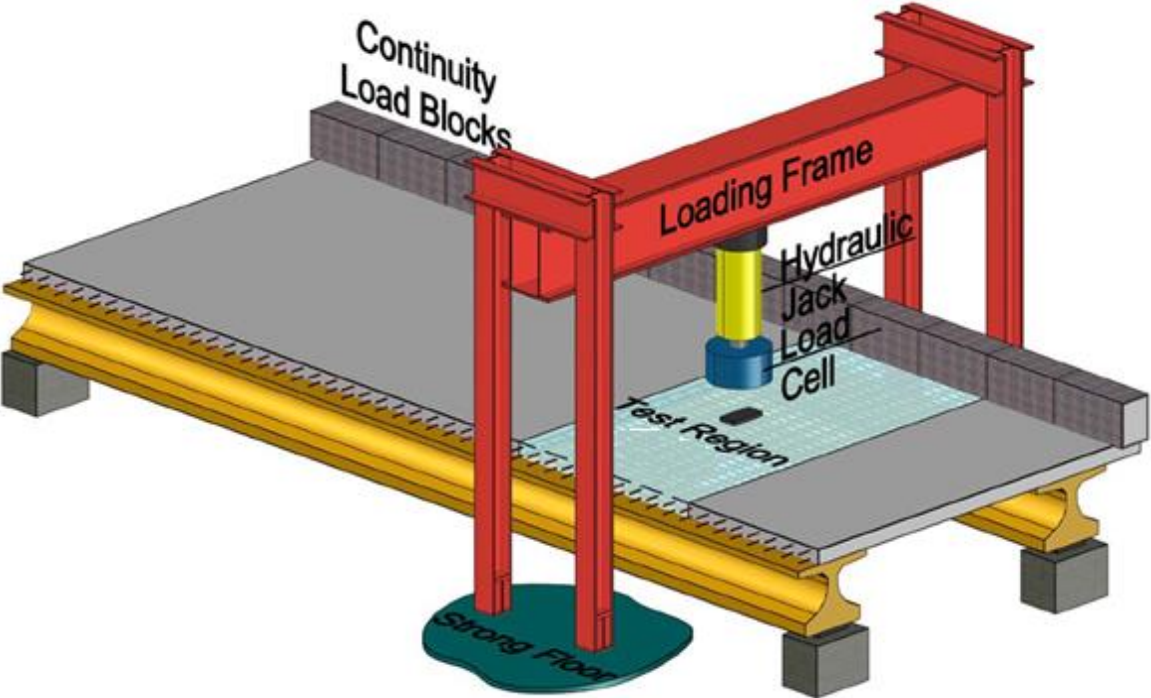


Figure 4.5: Specimen and load frame

#### 4.2.1 Beam Fabrication

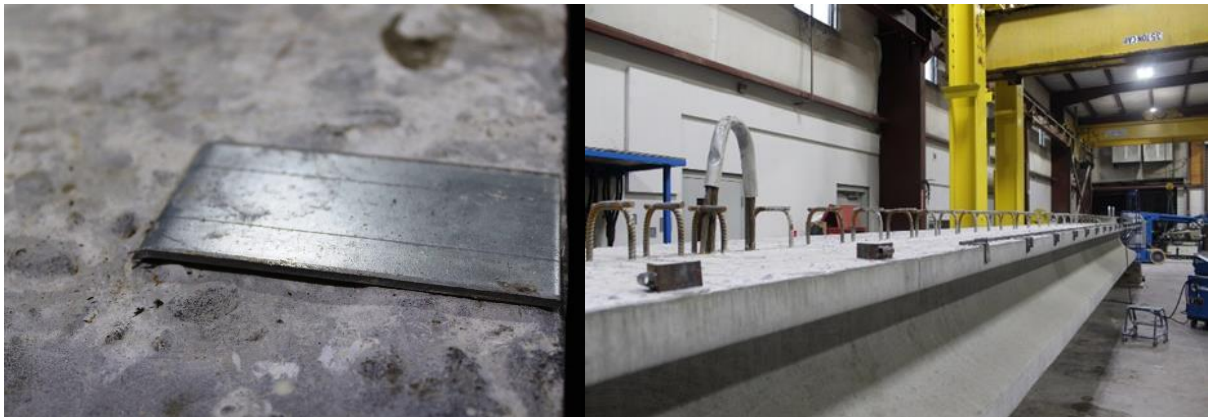
Based on the analyses presented in Chapter 3, the two FIB-36 beams designed to support the deck were fabricated at a casting yard with twenty six 0.6-in prestressing strands stressed to 43.9 kip as can be seen in Figure 4.6. Four additional top flange dormant prestressing strands per beam were added to prevent tensile cracking. The fabricated prestressed FIB-36 followed Index 20036 of the 2014 FDOT Design Standards. Shear reinforcement was designed to avoid premature shear failure of the specimen girders as shown in Figure 3.21. All stirrups were extended above the top flange elevation to obtain composite action with the deck when cast in the lab, as shown in Figure 4.12. Figure 4.6 shows the beam fabrication along with its formwork. Figure 4.7 shows beams as delivered to the FDOT MHA-SRC. Figure 4.8 shows the stay-in-place hanger brackets that were installed in order to connect the formwork for the deck.



Figure 4.6: FIB-36 Fabrication showing formwork and prestressing tendons



Figure 4.7: FIB-36 beams as delivered



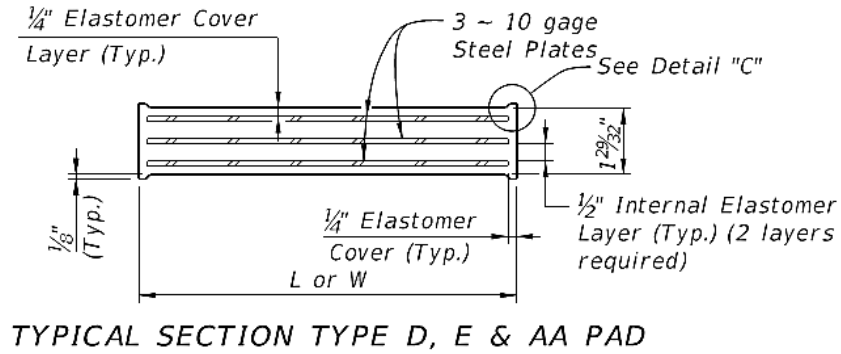
a) Close-up of bracket on top flange

b) Overall view of brackets

Figure 4.8: FIB hanger brackets in top flange and views of completed beam

#### 4.2.2 Bearing Pads-Type "D"

In accordance with the 2014 FDOT Design Standards (Index 20510), neoprene bearing pads of the dimensions shown in Figure 4.9 were chosen to support the FIB-36 girders. Figure 4.10 shows the bearing pads in place under the beams.



PAD TYPE (See Note 1)	BEAM TYPE	BEARING PAD DIMENSIONS		*BEVELED BEARING PLATE DIMENSIONS	
		L	W	C	D
D (G=110psi)		8"	2'-8"	1'-0"	3'-0"

Figure 4.9: Bearing pad - FDOT Design Standard Index 20510



Figure 4.10: Bearing pad in place

### 4.2.3 Formwork

Usually, stay-in-place (SIP) forms are used for concrete deck construction. They add additional dead load since they are kept in place permanently after the deck is poured and because of the additional concrete that fill the SIP form corrugations. The decks are cured on site and the formwork is fabricated so that the beams are resisting the additional weight. However, it should be noted that for this project, stay-in-place forms were not used as they would have blocked access and thus prevented obtaining crack width information and deck deflection measurements and would have increased the stiffness and reinforcement of the deck. Therefore, removable wood formwork was used, which created a flat bottom deck profile. In order to keep the project as realistic as possible, the beams were used to support the deck and removable wood formwork dead load during the production of the deck. The used formwork followed the requirements from the 2015 FDOT Standard Specifications for Road and Bridge Construction, section 400. Figure 4.13 through Figure 4.17 show different components of the formwork during construction at various locations of the specimen. Note the custom formwork-to-beam connections fabricated to make use of the embedded SIP bracket clips (Figure 4.1- Figure 4.15). Additional photos showing formwork fabrication are located in Appendix 1.



a) Bracket with tube for bolt

b) Tensile connection



c) Bottom connection

d) Side view

e) Top connection

Figure 4.11: Deck hanger brackets



Figure 4.12: FIB-36 stirrups and overhang hanger brackets



Figure 4.13: Adjusting cantilever formwork system



Figure 4.14: Cantilever formwork



Figure 4.15: Deck formwork (clear span)



Figure 4.16: Deck formwork during construction



Figure 4.17: Overall completed formwork

#### 4.2.4 Deck Steel Reinforcement

Typically in reinforced concrete bridge decks, rebars were placed in two layers, a top and a bottom layer. As stated earlier, No. 5 rebar spaced at 12 in. was chosen for the deck specimen, which satisfies AASHTO LRFD requirements. The reinforcement was staggered to allow for better distribution of steel throughout the section, which also allowed for easier installation of embedded strain gauges. Another possible benefit of staggering the reinforcement was for better flow and compaction of the concrete during the deck pour. To achieve the stagger, the bottom mat was centered by positioning the first transverse bar at midspan and longitudinal bar halfway between the FIBs. Conversely, the top mat was placed by shifting the longitudinal and transverse bars 6-in either way in comparison to the bottom mat bars, as shown in Figure 4.18 and Figure 4.19. Due to available rebar being sold in 20, 30, and 40 ft lengths, a lap splice was necessary in all lines of longitudinal reinforcement. Two splices were called out for the longitudinal bar in the bottom layer running along the line of test locations in order to avoid interference with strain gauges to be placed on the rebar, this splice line occurred at the center of the beam spacing. Lap splice locations for the bottom mat are shown in Figure 4.20. The top and bottom layers were placed such that the transverse rebars had a 2-inch clear concrete cover as per Florida SDG for an 8-inch deck. Figure 4.21 and Figure 4.22 show pictures of the reinforcement layers for the deck slab during placement.

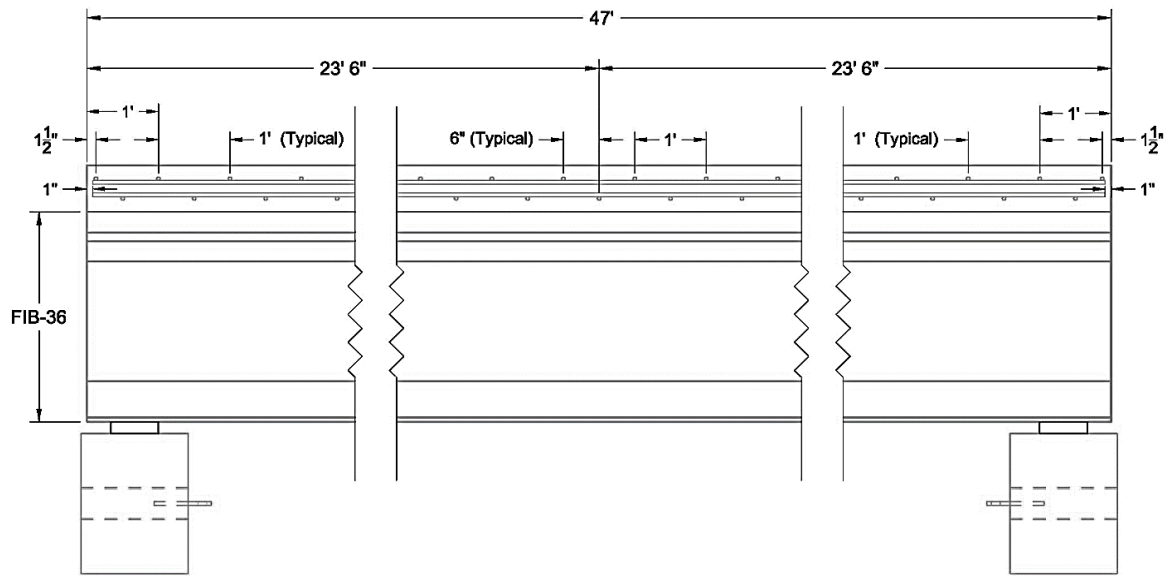


Figure 4.18: Transverse reinforcement (bottom layer centered)

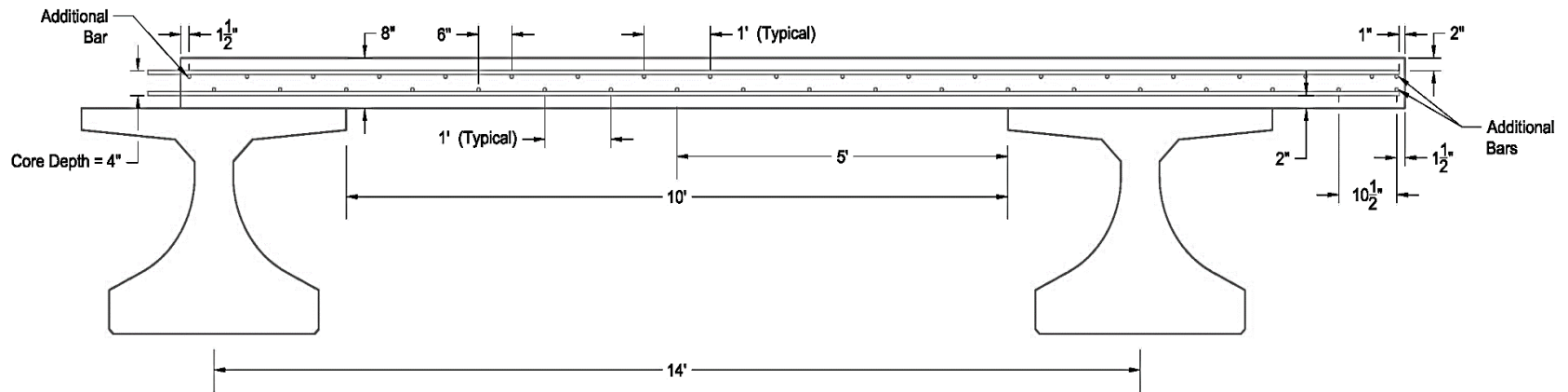
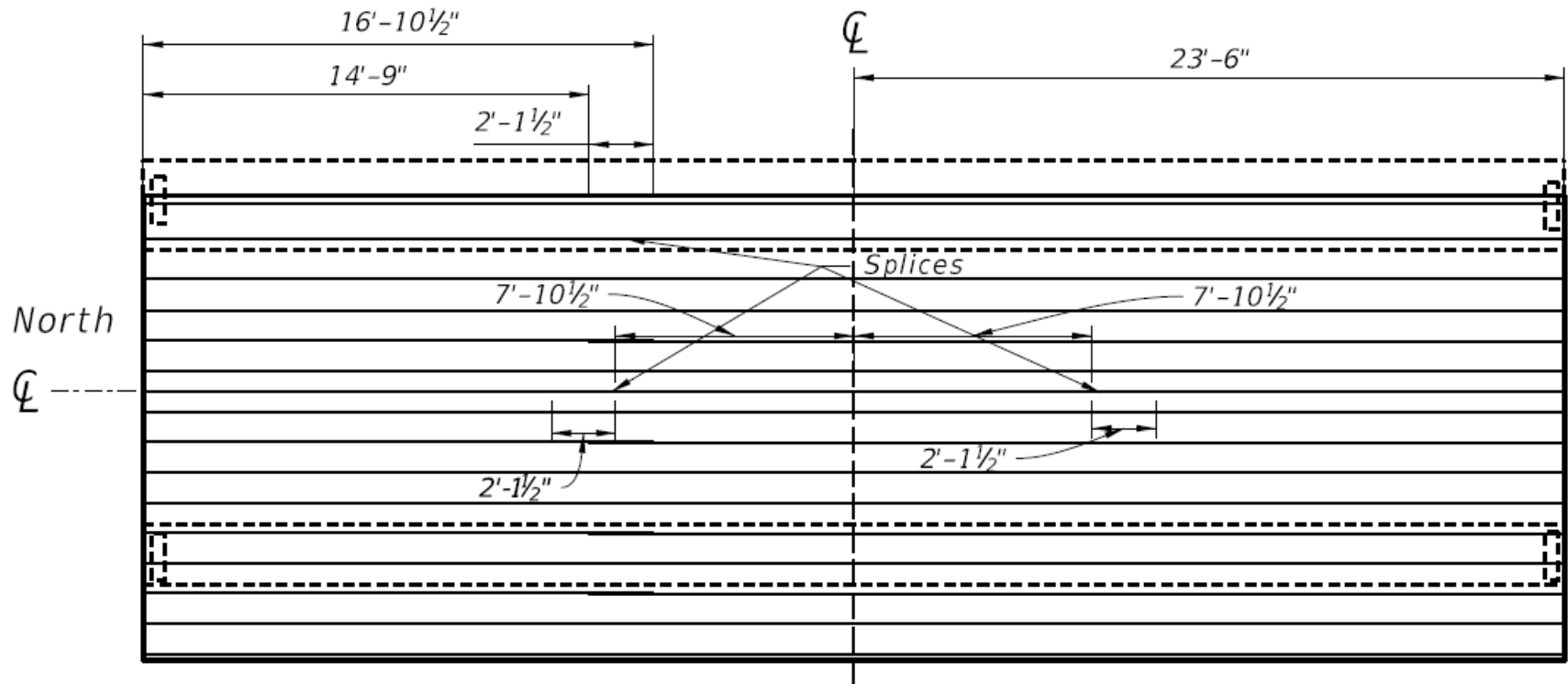


Figure 4.19: Longitudinal reinforcement and cover (bottom layer centered)



BOTTOM LONGITUDINAL REBAR MAT WITH SPLICES

Figure 4.20: Plan view showing splice locations and lengths



Figure 4.21: Placed bottom mat



Figure 4.22: Placed top mat reinforcement

#### 4.2.5 Concrete Deck

The concrete deck fabrication followed the FDOT Standard Specs, Section 400. Due to the large size of the deck pour, a pump truck was employed to place the wet concrete (Figure 4.23a). Placing the concrete followed the FDOT Standard Specs, Section 400.7. The pump crew experienced an issue with their lines clogging at the start of the pour resulting in the loss of a few yards from the first truck. This loss resulted in a fourth truck needing to be ordered to fill in a small portion of the deck at the north-west corner of the specimen. This small section was accessible by the delivery truck, and therefore placed via its shoot.

Section 400-16.4 states the cast-in-place concrete must be allowed to cure for at least seven days. Moreover, the specification states to begin applying the curing compound immediately after the initially placed concrete has been floated, straight-edged, textured and a damp surface condition exists and to place a curing blanket on all exposed surfaces. The curing compound used was a white Type 2 curing compound applied to all exposed surfaces at a uniform coverage using a compressor driven sprayer per the specification section 400-16.2. Additionally, the cylinder molds were all sprayed with curing compound and placed under the north edge of the specimen providing a similar curing environment as the specimen. Table 4.2 and

Table 4.3 list the compressive strength results obtained from the cylinders for the deck and girder concrete respectively. These tests were performed to obtain as tested strength. The tests were carried out at the FDOT MHA-SRC according to ASTM C39 (Standard Test Method for Compressive Strength of Cylindrical Concrete Specimens).

Slump tests were performed for each truck and water was added as necessary to reach a slump that could be pumped. Table 4.1 shows the results of the slump tests. It should be noted that the fourth truck arrived with a 6-inch slump and did not require additional water. During placement, concrete was sampled from the pump hose for all of the first three trucks for later compressive strength testing. Concrete from the fourth truck, however, was sampled straight from the shoot. A total of thirty four 6-in x 12-in cylinder molds were prepared. Twelve cylinder molds came from each of the first two trucks (10 yard trucks) and six molds from the third truck which was a 3 yard truck. Finally, four molds were obtained from the fourth truck. Table 4.2 and Table 4.3 list results from standard testing of deck and girder concrete cylinders, respectively.

Table 4.1: Slump Test Results

<b>Final Slump Before Pumping</b>	
<b>Truck 1</b>	5.25 inches
<b>Truck 2</b>	5.5 inches
<b>Truck 3</b>	3.75 inches

The placing/curing of the concrete are shown in Figure 4.23. Figure 4.24 shows the completed pour just before texturing and application of the curing compound. The test specimen was inspected after curing and prior to testing and revealed no early age cracking. A copy of the mix design provided by Argos is included in Appendix II. The completed test specimen after curing can be seen in Figure 4.25. Table 4.4 lists the mill test results for the #5 bars used in reinforcing the deck.

Table 4.2: Concrete Cylinder Strength for Deck

Specimen ID	Pour Date	Specimen Age (days)	Avg. Diameter (in)	Avg. Length (in)	Weight (lb)	Unit Weight (lb/ft <sup>3</sup> )	Strength (psi)
Emp Deck Truck 1-1	8/14/2015	69	5.9375	11.8125	27.32	144.34	8461.7
Emp Deck Truck 1-2	8/14/2015	69	5.9375	11.875	27.52	144.63	8806.6
Emp Deck Truck 1-3	8/14/2015	69	5.9375	11.875	27.12	142.53	8144.6
Emp Deck Truck 2-1	8/14/2015	69	5.96875	11.875	27.54	143.22	8365.8
Emp Deck Truck 2-2	8/14/2015	69	5.9375	11.75	26.9	142.88	8567.9
Emp Deck Truck 2-3	8/14/2015	69	5.9375	11.75	27.18	144.36	8062.6
Emp Deck Truck 3-1	8/14/2015	69	5.9375	11.8125	27.38	144.66	8752.4
Emp Deck Truck 3-2	8/14/2015	69	5.9375	11.75	27.28	144.89	8193.7
Emp Deck Truck 3-3	8/14/2015	69	5.9375	11.75	27.38	145.43	8811.6
Emp Deck Truck 4-1	8/14/2015	69	5.9375	11.8125	27.18	143.60	8052.5
Emp Deck Truck 4-2	8/14/2015	69	5.9375	11.6875	26.92	143.75	8056.1
Emp Deck Truck 4-3	8/14/2015	69	5.875	11.8125	27.10	146.24	8154.3

Table 4.3: Concrete Cylinder Strengths for Beams

Specimen ID	Pour Date	Specimen Age (days)	Avg. Diameter (in)	Avg. Length (in)	Weight (lb)	Unit Weight (lb/ft <sup>3</sup> )	Strength (psi)
UNF-FIB-36 1	11/3/2015	353	4	7.6875	8.02	143.46	9079.8
UNF-FIB-36 2	11/3/2015	353	4	7.6875	7.98	142.74	9241.3
UNF-FIB-36 3	11/3/2015	353	4	7.8125	8.28	145.74	9963.9

Table 4.4: Data from Mill Test Reports for Deck Reinforcing Bars

Specimen ID	Yield Stress (psi)	Tensile Strength (psi)	Elongation (%)
NUCOR Steel - #5 (1 <sup>st</sup> Batch)	69,000	110,400	12.0
NUCOR Steel - #5 (1 <sup>st</sup> Batch)	82,000	115,700	10.0



a) Pouring concrete



b) Soaker hoses and curing compound applied



c) Concrete Curing



d) Cylinders Curing

Figure 4.23: Deck pouring and curing



Figure 4.24: Concrete deck right after concrete pouring



Figure 4.25: Final specimen setup

### 4.3 Instrumentation

The developed instrumentation plan was designed to capture the major attributes of deck behavior. In addition to the load cell that measured the applied load, the plan included embedded as well as surface-mounted gauges and instrumentation to measure strain, deflection, slip of reinforcement, and crack growth. The purpose of the installed instrumentation was to capture:

- Strains in the transverse and longitudinal deck reinforcement
- Strain measurements at top and bottom deck surfaces near the load point throughout testing (quarter-bridge foil gauges)
- Vertical displacement of the deck under load
- Vertical and lateral girder movement in line with the applied load
- Crack gauges also provided strain measurements at top and bottom deck surfaces near the load point throughout testing (full-bridge strain gauges)
- Strand or bar slip of the girder prestressing steel, or the rebar from the widening side

Foil strain gauges (5-mm gauge length) were used to capture longitudinal and transverse steel reinforcement strains on both the bottom and top steel mats (Figure 4.26). A small part of the rebar was ground flat at the centroid of the bar, where the strain gauges were to be placed before the concrete was poured. The bottom mat transverse gauges were positioned 2-5/16 inches above the bottom surface of the concrete deck, the bottom mat longitudinal gauges at 2-5/16 inches. Similarly, the top mat transverse gauges were positioned 2-5/16 inches below the top surface of the concrete deck, along the top transverse reinforcement.

Crack gauges (200-mm gauge length) were also installed on the bottom and top of the deck surface (Figure 4.27). Additionally, 60-mm foil gauges were placed on the surface of the deck, oriented transverse to the specimen length (Figure 4.28). For tests S1, S2, S3, F1, F2, and F3, readings from 119 gauges were recorded. For S4/F4, and S5, data from 76 gauges were recorded. Table 4.5 and Table 4.6 list the breakup of the types of gauges recorded for each of the service and failure tests. The installed strain gauges for S1/F1 testing location are shown in the following figures along with their associated positions. Figure 4.33 through Figure 4.39 show details of the instrumentation plans. Instrumentation was also placed on the beams and under the deck. Because of the size and uniqueness of the specimen built for this study, it lent itself as an opportunity to also monitor some girder attributes. Strain gauges were installed on the webs of the girder to assess whether the lack of diaphragms would lead to high bending stresses in the web due to out-of-plane moments caused by deck slab deformations. Laser deflection gauges were also used to record girder vertical and horizontal displacements. Horizontal gauges measured displacement of the top and bottom girder flanges along the transverse line where the load was applied. Finally, slippage of prestressing strands at girder ends was recorded for six strands using slip gauges with special clamps. Figure 4.43 through Figure 4.29 shows the instrumentations on the beams. Figure 4.3 shows the locations of the load tests conducted in this study which may be referenced to as necessary. As stated earlier service load tests (labeled “S”) are denoted S1 through S5 and the strength (failure) load tests (labeled “F”) were denoted F1 through F4. More details about the instrumentation plan can be found in Appendix V and VI.

Table 4.5: Gauge Count for S1, S2, S3, F1, F2, and F3

Gauge Type	Gauge Count
Load Cell	2
Foil Strain	87
Crack Strain	6
Deflection	18
Strand Slip	6
TOTAL	119

Table 4.6: Gauge Count for S5

Gauge Type	Gauge Count
Load Cell	2
Foil Strain	50
Crack Strain	0
Deflection	18
Strand Slip	6
TOTAL	76

Table 4.7: Gauge Count for S4/F4

<b>Gauge Type</b>	<b>Gauge Count</b>
<b>Load Cell</b>	2
<b>Foil Strain</b>	50
<b>Crack Strain</b>	6
<b>Deflection</b>	18
<b>Strand Slip</b>	6
<b>TOTAL</b>	76



Figure 4.26: Strain gauges on bottom mat reinforcement



Figure 4.27: Typical full-bridge crack gauge



Figure 4.28: S2/F2 surface strain gauges

### 4.3.1 Displacement Gauges

#### 4.3.1.1 Actuator Displacement

A string pot displacement transducer was attached to the main housing of the Enerpac RR-40018 actuator with its string attached to the moving head of the actuator itself. This displacement gauge became very important during the latter part of the failure tests since it continued to

provide displacement of the deck after the main deflection gauge assembly (D7b - D11b & D13b; Figure 4.38) was removed. The laser displacement transducers were removed before subjecting the specimen to high load levels in order to protect them from being damaged as the test zone experienced failure. It should be noted that raw string pot measurements had to be adjusted since they included other deformations due to load system flexibility caused by components such the elastomeric load/bearing pads and load frame deformations. Details of this adjustment are discussed later in Chapter 6.

#### 4.3.1.2 Displacement Potentiometers

Displacement potentiometers were also used to record strand slip in the beams and rebar slip on the widening side, as shown in Figure 4.29. Figure 4.30 shows the transverse deck reinforcement extended beyond the deck edge and the installed slip gauges. Six slip gauges were installed at the ends of the beams to check if the strands will slip during testing. Figure 4.29 shows the configuration and strand-slip gauge locations. A special bracket was used to keep the slip gauges attached to the exposed strand ends protruding from the beam ends. No strand slip displacement was detected or reported.

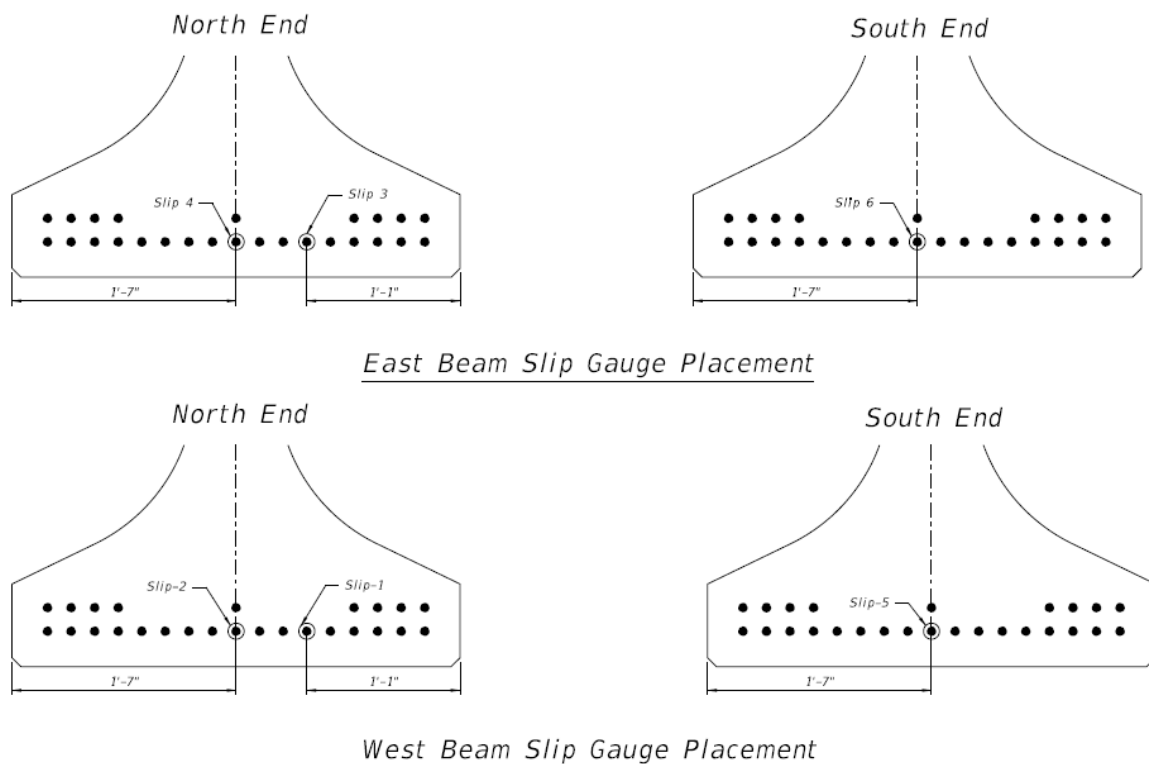


Figure 4.29: Strand slip gauge locations

#### 4.3.1.3 Laser Displacement Transducers

Displacement information was collected using laser transducers from MTI Instruments. The sensors were positioned to provide information about the global specimen movement, as well as

the movement of the deck and girders in the vicinity of the applied load for each of the test cases. A cluster consisting of laser displacement transducers was placed under the deck as seen in Figure 4.31. This cluster was repeated for all loading positions as shown in Figure 4.31 except for load case S4/F4 whose proximity to the deck's edge imposed a different gauge configuration. Figure 4.38 and Figure 4.39 show the displacement gauge names and exact locations for S1/F1 load tests.

In addition to the vertical movement, displacement gauges were placed to measure horizontal girder flange movement. The purpose of these horizontal gauges is to assess the lateral stiffness provided by the girders. Figure 4.32 shows a cross-section in line with one of the test locations showing the horizontal gauge locations.

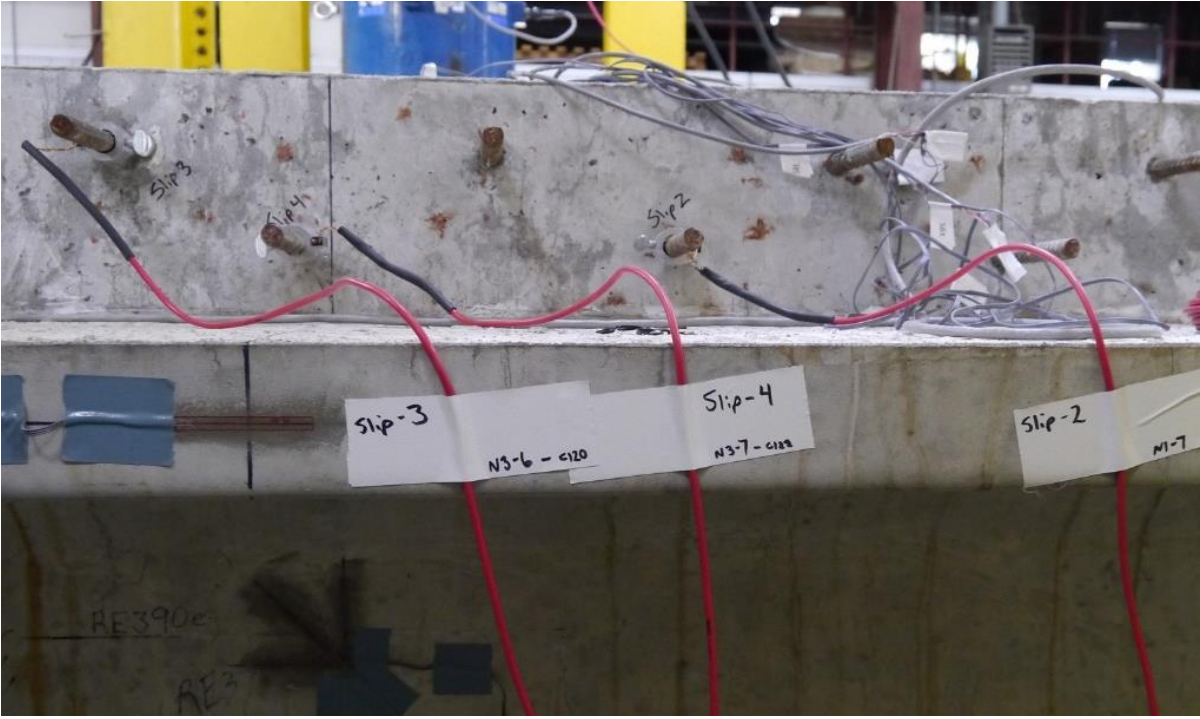


Figure 4.30 Displacement potentiometers on deck reinforcement on widening side

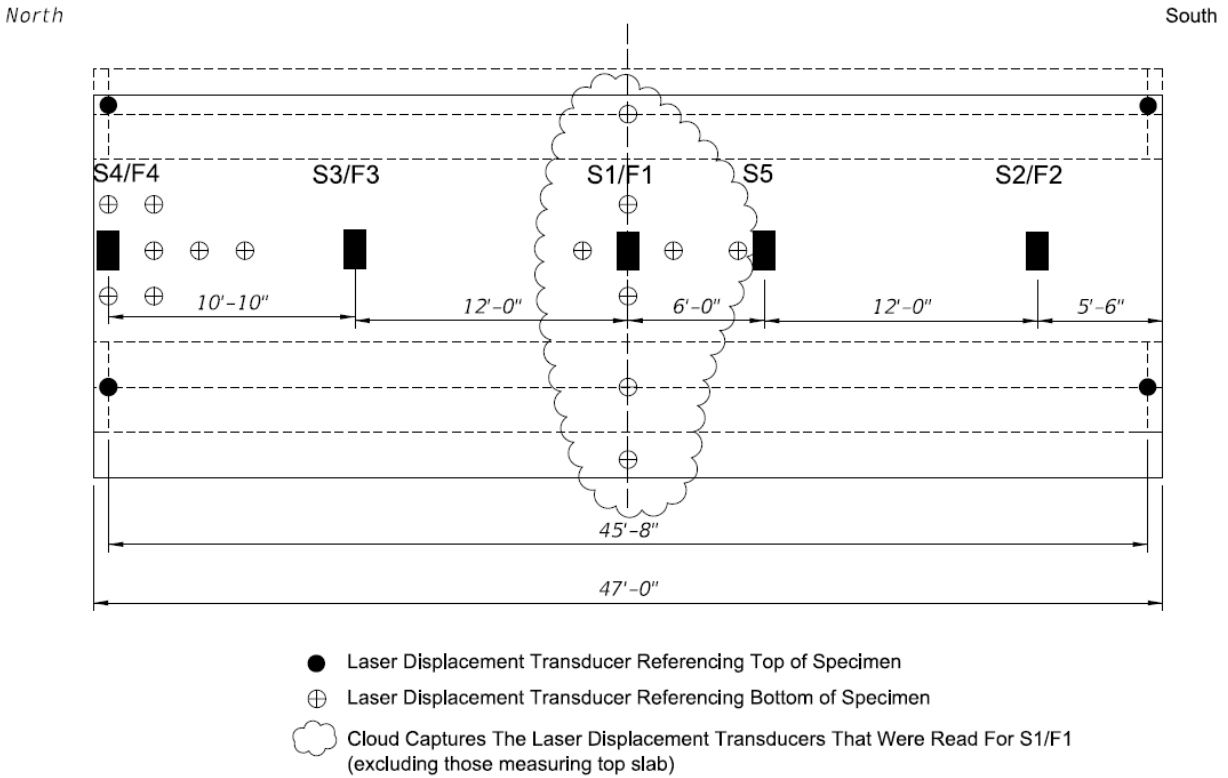


Figure 4.31: Laser displacement transducers (S1/F1 clouded)



Figure 4.32: Horizontal girder displacement transducers

#### 4.3.2 Embedded Strain Gauges on Steel Reinforcement

Transverse (main) and longitudinal (secondary) rebars were instrumented with foil strain gauges at each loading position. The distribution of the transverse strain gauges was chosen to provide the most data in line with the load, transverse to the centerline of the deck. Figure 4.33 through Figure 4.37 show the general layout of strain gauges installed on steel reinforcement. Five longitudinal gauges, designated LB (Longitudinal Bottom Mat), were distributed along the rebar centered under the load point. TT and TB (Transverse Top Mat and Transverse Bottom Mat respectively) were placed in a similar fashion each capturing the most data in line with the load

point. A fewer number of strain gauges were installed away from the applied load location as shown in Figure 4.33 through Figure 4.37. This arrangement was employed on one side of the load only to limit the number of required resources. The gauge arrangement provides information about the extent of the influence area due to the load. This strain gauge arrangement was used for both the service and failure load tests with the exception of the S4/F4 test which did not have gauges on the steel reinforcement directly below. For the S4/F4 test, instrumentation was placed on the deck surfaces and the gauges on the steel reinforcement from the S3/F3 test were read during the testing of S4 and F4.

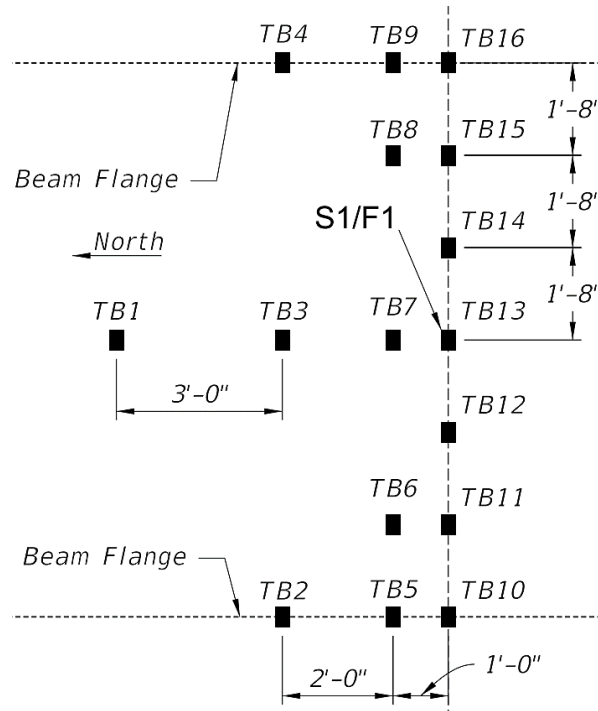


Figure 4.33: Bottom mat internal transverse strain gauges (for S1/F1, S2/F2 and S3/F3)

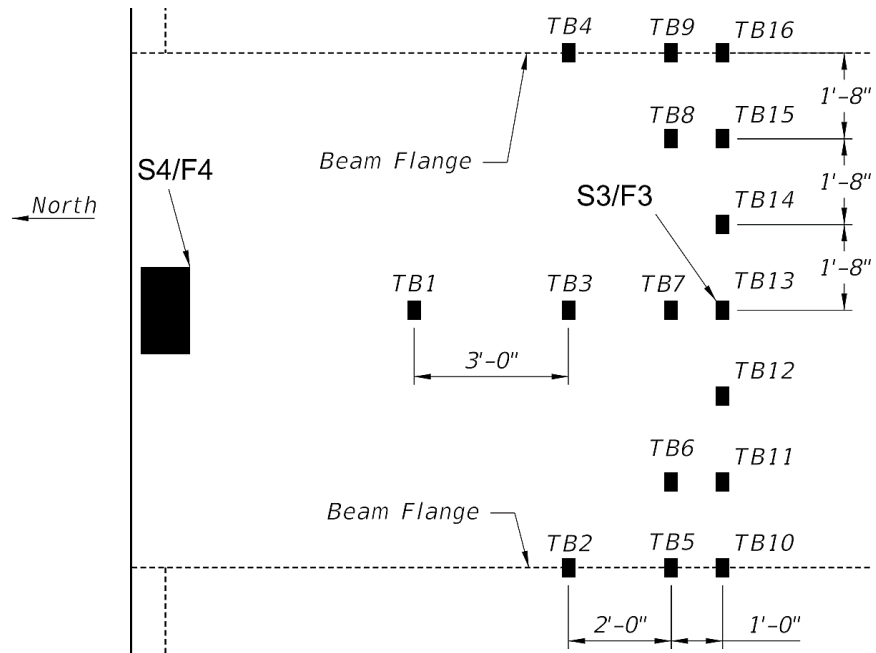


Figure 4.34: Bottom mat internal transverse strain gauges read for S4/F4 test (originally installed for S3/F3)

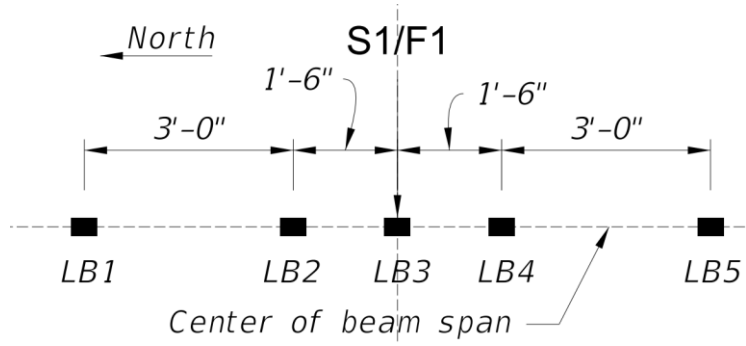


Figure 4.35: Lower mat internal longitudinal strain gauges

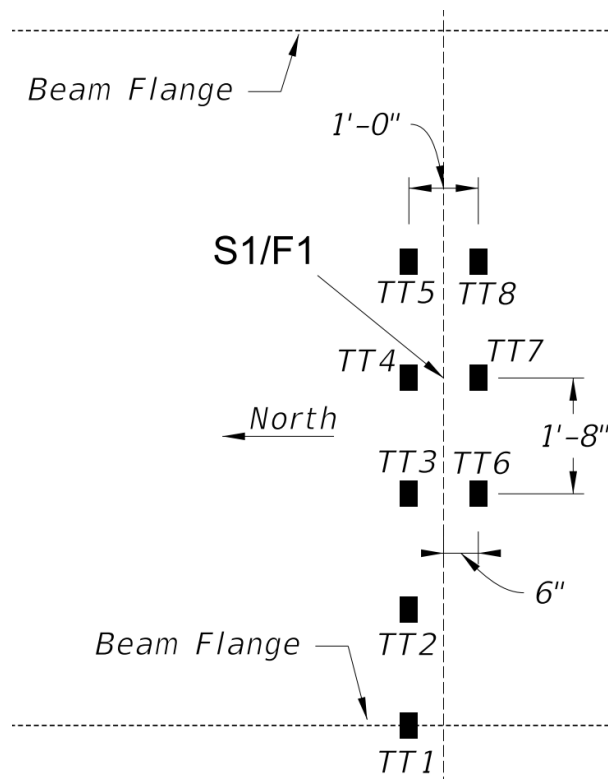


Figure 4.36: Top mat internal strain gauges on transverse bars (for S1/F1, S2/F2 and S3/F3)

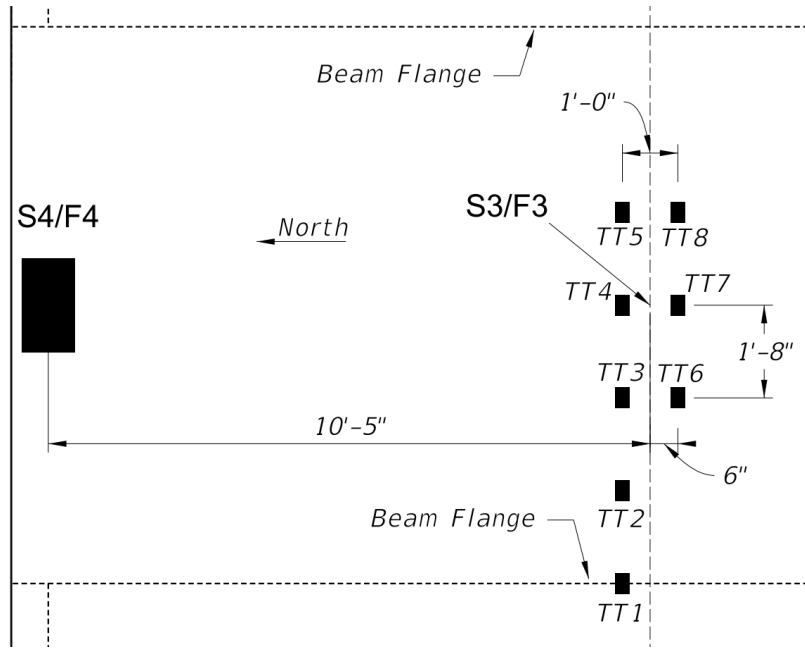


Figure 4.37: Top mat internal transverse gauges read for S4/F4 test (originally installed for S3/F3)

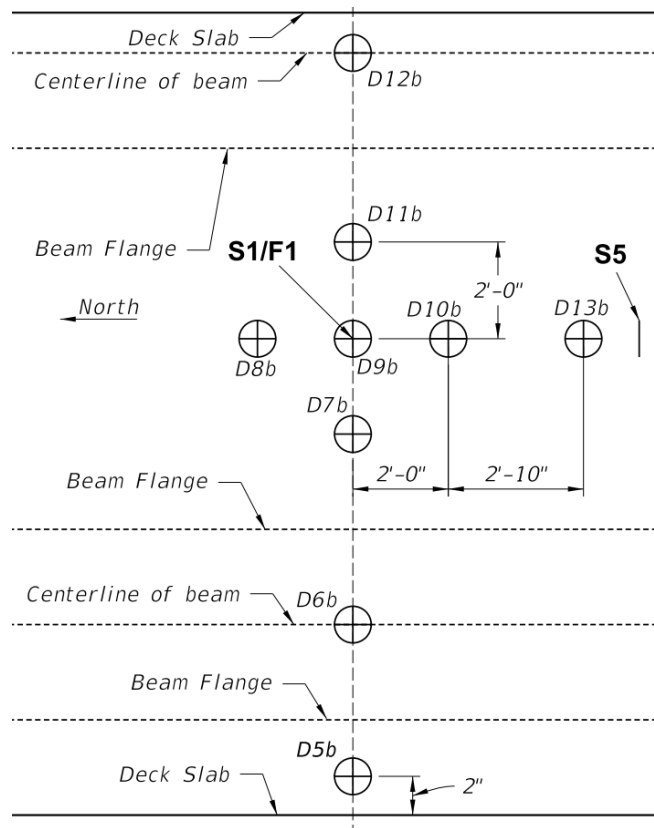


Figure 4.38: Typical laser deflection instrumentation

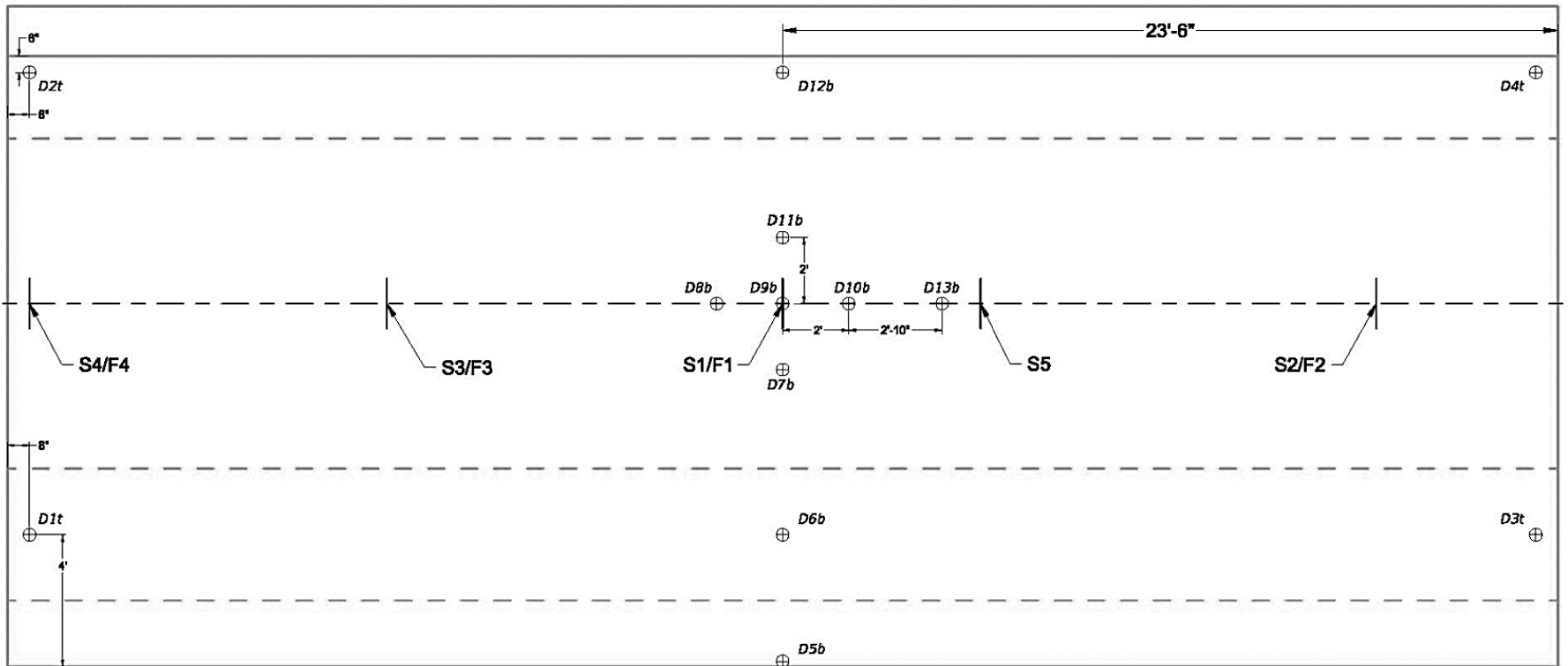


Figure 4.39: Vertical laser displacement transducers read for S1/F1

### 4.3.3 Concrete Deck Surface-Mounted Strain Gauges

Surface strains were measured using foil strain gauges attached to the top and bottom surfaces of the deck. More gauges were placed on the top surface than the bottom one because of anticipated cracking on the bottom side, which would render the gauges unuseful early during the test. Figure 4.40 is a cross section of the specimen at a typical load line showing the transverse positions of the installed surface gauges. For each cluster, 12 foil gauges were placed on the top surface around the load point. On the bottom surface, only three strain gauges were placed transversely in line with the load. This layout was repeated for each of the strength loading positions, F1, F2, F3, and F4. Figure 4.41 and Figure 4.42 show the bottom and top surface clusters of strain and crack gauges, respectively.

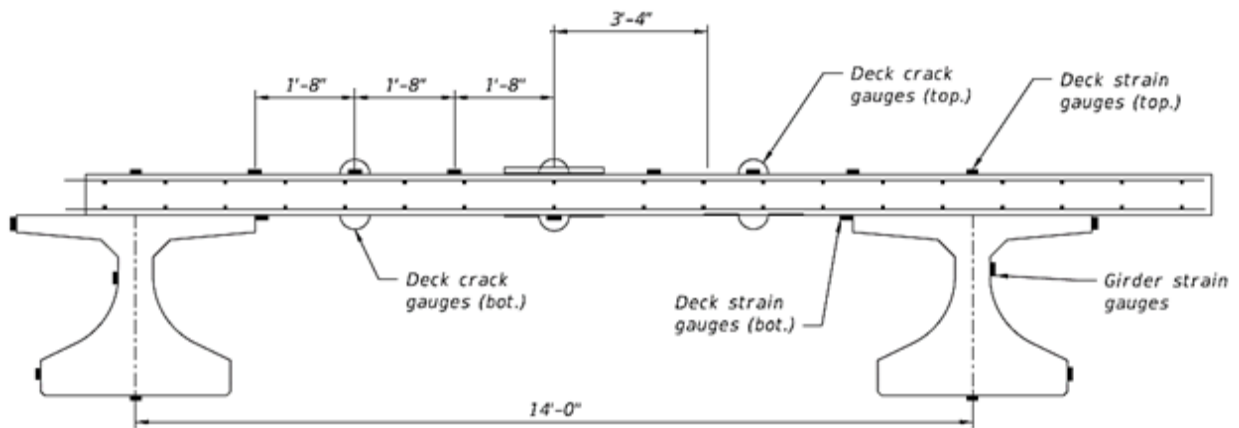


Figure 4.40: Deck surface gauges for measuring strains before and after cracking

### 4.3.4 Concrete Deck Surface-mounted Crack Width Gauges

Crack width gauges were placed on both sides (top and bottom) in anticipation of cracking around the applied load position. Because of the existence of the other strain gauges, the crack width gauges had to be shifted away from the loading pad by 12 inch as shown in Figure 4.41 and Figure 4.42.

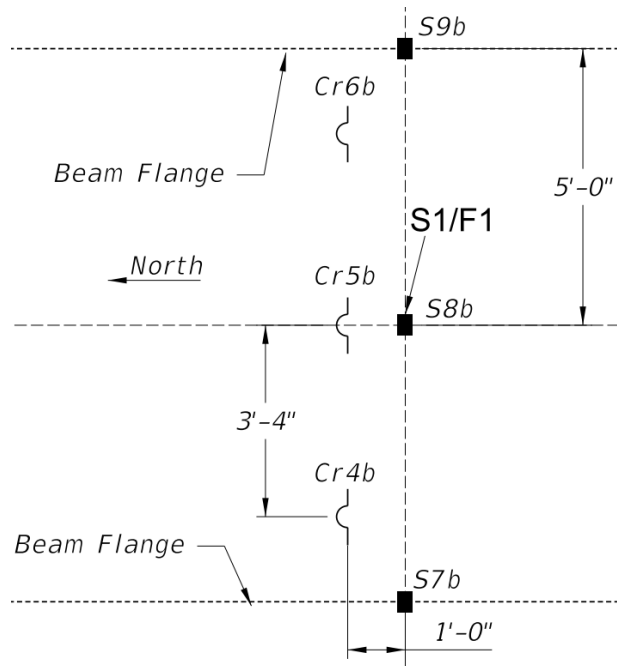


Figure 4.41: Bottom deck surface gauges (crack and foil)

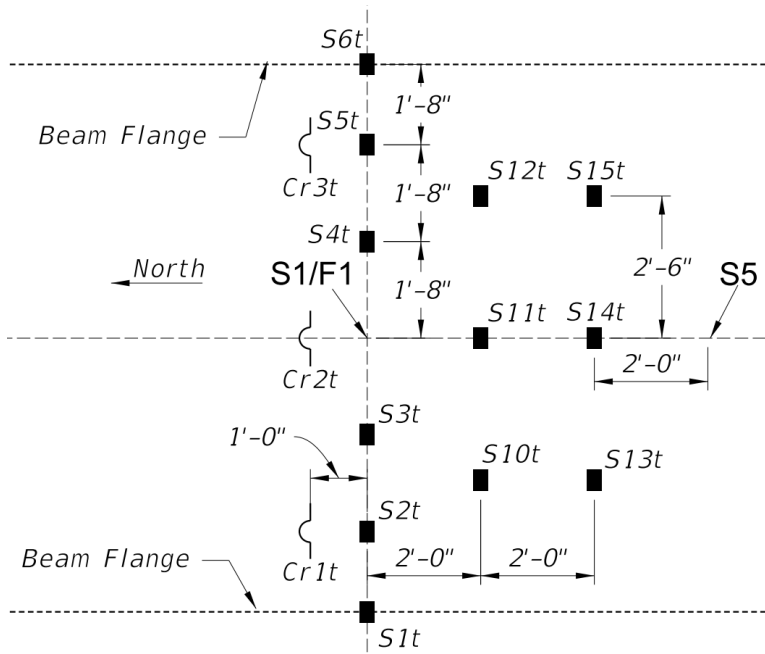


Figure 4.42: Top deck surface gauges (crack and foil)

### 4.3.5 Girder Surface-mounted Strain Gauges

Both supporting girders were instrumented with strain gauges to monitor their performance. Longitudinal strain gauges were attached to the top and bottom flanges, while both sides of the webs were instrumented with either a rosette or a vertical strain gauge. Rosettes were centered on the flattest, most vertical part of the web. The gauges on the girders were read during all tests. Figure 4.43 through Figure 4.2947 show the location of the girder strain gauges used in this study. Table 4.8 shows the typical strain gauge nomenclature used during the testing which is also shown in Appendix V. Refer to Figure 4.46 for locations of cross-sections.

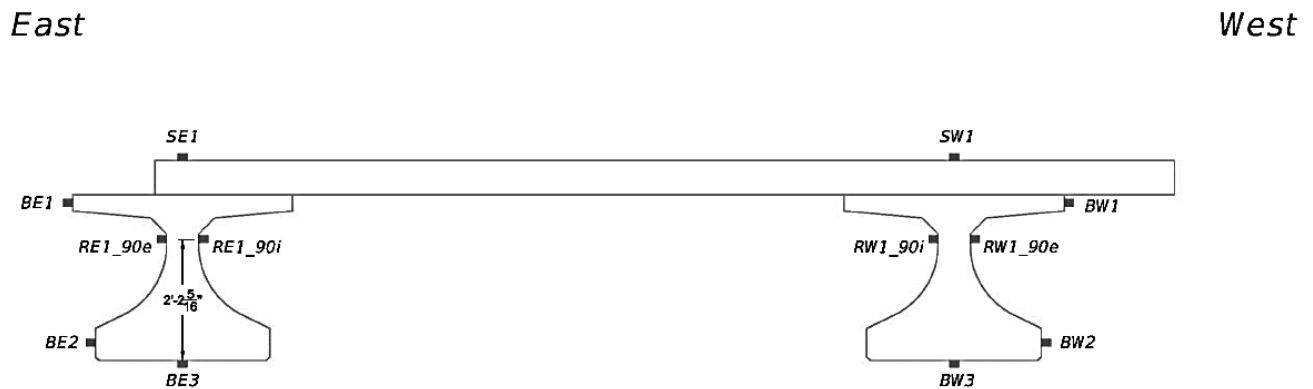


Figure 4.43: Section A-A

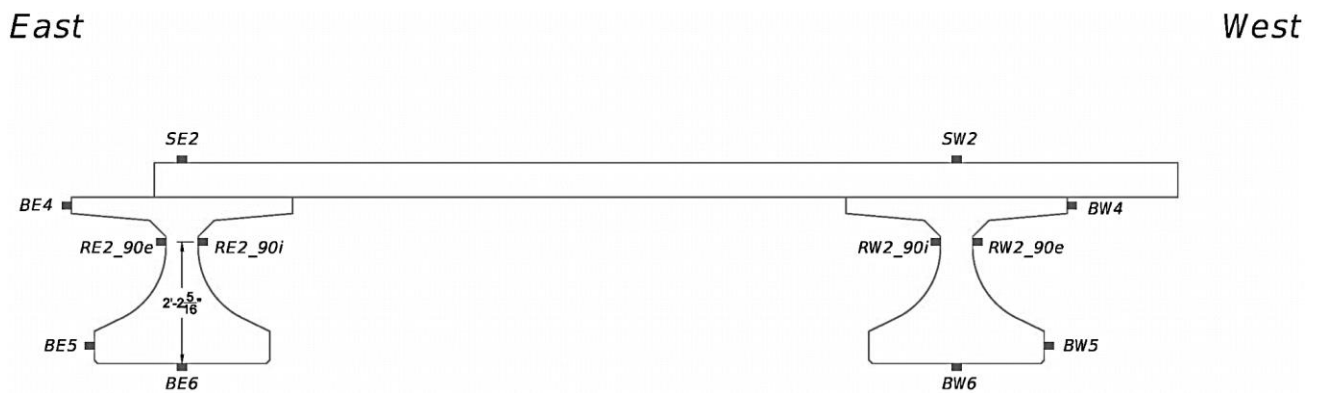


Figure 4.44: Section B-B

East

West



Figure 4.45: Section C-C

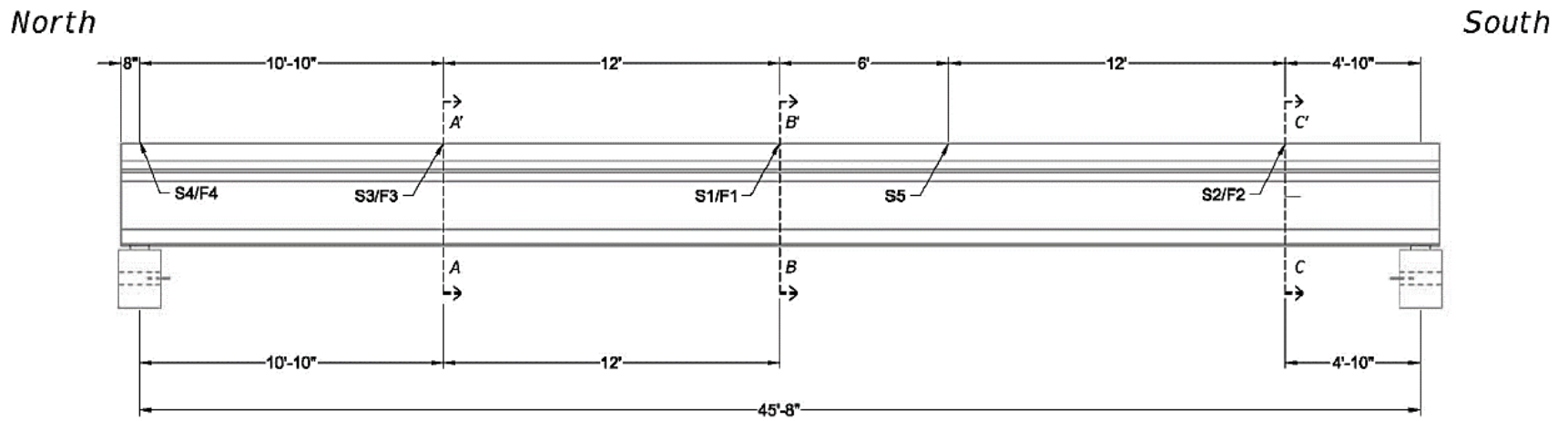


Figure 4.46: Elevation showing sections

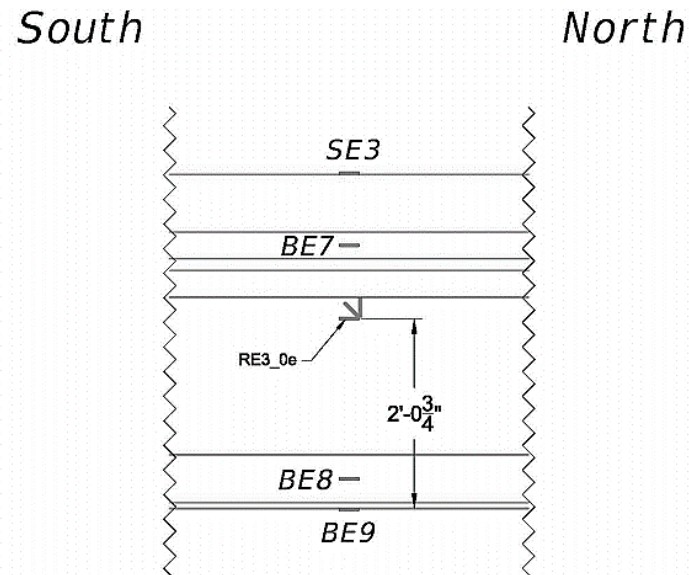


Figure 4.47: Detail 1 for Section C-C

Table 4.8: Typical Gauge Nomenclature

Meaning	Label
Transverse Rebar, Bottom	TB#
Transverse Rebar, Top	TT#
Longitudinal Rebar, Bottom	LB#
Surface Strain Gauge, Top of Slab	S#t
Surface Strain Gauge, Bottom of Slab	S#b
Crack Strain Gauge, Top of Slab	Cr#t
Crack Strain Gauge, Bottom of Slab	Cr#b
Surface Strain Gauge Top of Slab above East Beam	SE#
Surface Strain Gauge Top of Slab above West Beam	SW#
East Beam Surface Strain Gauge	BE#
West Beam Surface Strain Gauge	BW#
East Beam Rosette Longitudinal Direction, exterior	RE#_0e
East Beam Rosette Vertical Direction, exterior	RE#_90e
East Beam Rosette 45° between L & V, exterior	RE#_45e
West Beam Rosette Longitudinal Direction, interior	RW#_0i
West Beam Rosette Vertical Direction, interior	RW#_90i
West Beam Rosette 45° between L & V, interior	RW#_45i
Slip displacement attached to strand or rebar	Slip-#
Displacement on Top of Slab	D#t
Displacement on Bottom of Slab	D#b
Displacement on Girder Flanges, Lateral Orientation	D#h
Optional String Pot Crack Monitoring Gauge	DisCr#

Notes on Gauges:

- S3/F3 gauge readings were monitored during the F4 test.
- Two of the horizontal displacement gauges on the west girder were switched on the S1 test. (D15h was referencing the top beam flange while D14h was referencing the bottom flange.). The issue was corrected in the subsequent tests.

## 4.4 Phased Widening

In the 2016 FDOT Standard Design Guidelines, it is suggested to perform removal of existing decks back to center of the cross-section of the exterior beam during a widening project (Figure 7.1). Because Florida I-Beams have a much wider top flange, it was decided to bring the formwork away from center of the cross-section for constructability. Moving the location at which deck removal ends ensures that girder stirrups will remain untouched, thus keeping the composite action between the deck and the girder intact. Therefore, the deck in the lab specimen was not formed to the center-of-beam cross-section of the “exterior” girder (the girder without the overhang), and the end of the deck was constructed to be approximately 6-in off of center. Accordingly, the entire deck became approximately 18.5-ft wide. Transverse deck rebars were extended beyond the deck end at the widening side to simulate exposed deck rebars after removal the overhang.

After removal of the deck overhang in a real-world widening process, the exterior deck span becomes continuous on one side (interior) only. Continuity develops a negative moment that should enhance the deck’s resistance to positive moments at the middle of the span on the widening side. Simulating the continuity accurately in a laboratory setup is challenging. The research team considered two options: Tie-down anchors (Clamping), or Edge Load. In the tie-down anchors (clamping) approach, the extended part of the deck specimen would be clamped to the strong floor or a similar restraint. As such, continuity moments would increase as the applied test load increased due to the increase in deck rotation, which leads to an increase in the clamping force. The edge load approach is simpler, and it entails adding a distributed load in the form of weighted steel/concrete blocks along the edge of the extended part of the deck specimen. The developed negative moment is therefore constant regardless of the applied test load in this approach. For simplicity, the research team decided to adopt the edge load approach since the magnitude of the distributed load can be adjusted based on what level of negative continuity moment needs to be achieved. As a result, the distributed load was chosen to only simulate the effect of the dead load of the deck, rather than the effect of the dead load and a wheel load in the adjacent span. The effect of the dead load was achieved by using 24 in. x 18 in. x 48 in. steel loading blocks weighing ~1,940 lb - 1,960 lb on average resting on their 24 in x 48 in side. Twelve loading blocks were set flush with the west end of the deck (part extending beyond interior girder). The blocks protruded 6 inches from the north and south ends of the deck. Given these dimensions and weight, the blocks developed a negative moment equal to ~1.5 kip·ft/ft in the deck at the centerline of the girder on the continuity side. As stated earlier, this moment is less than what would develop in an actual bridge, hence, it represents a more conservative option. For the transverse span loading on the deck, applying the testing load at the center of the transverse span was performed to obtain the most critical scenario and produce the largest vertical slab deformation and the largest horizontal beam deformations.

## 4.5 Loading and Testing

### 4.5.1 Load System

An 800-kip hydraulic jack was used to load the specimen. The load was applied on the deck through a neoprene bearing pad with dimensions equal to the footprint of a typical tire contact area of 10 in x 20 in, according to AASHTO LRFD Bridge Design Specifications section 3.6.1.2.5. The loading pad was centered between the beams to cause the maximum effect in the deck. The hydraulic jack was attached to a steel loading frame that was connected to the strong floor in the laboratory. The loading frame spanned the specimen transversely; i.e., short direction. One of the benefits of the relatively long span specimen used in this study is that it could be used multiple times to produce results under different deck supporting conditions since girder flexibility affects the performance of concrete decks. This is especially true for arching action behavior, which is greatly affected by the lateral stiffness of the deck supporting girders. Therefore, girder flexibility around midspan is different in comparison with girder flexibility at and near the support locations. Girder flexibility is one of the parameters that is studied in this research, which was varied by placing the applied load at five different locations in the longitudinal direction. A typical loading rate of 250 lb/sec was implemented in all tests conducted for this study. The load was applied with a load-controlled hydraulic jack that was continuously monitored by the data acquisition system (DAQ). Figure 4.5 shows a depiction of specimen configuration before one of the conducted tests.

### 4.5.2 Load Cases

Successful implementation of decks designed using the empirical method should encompass satisfactory performance under service, strength, fatigue, and long-term effects. The scope of this study is on the first two of these four conditions; i.e., service and strength. The importance of validating the behavior of concrete decks under service conditions stems from the fact that lower reinforcement ratios may lead to large crack widths, which are known to expedite the deterioration of bridge decks, especially in aggressive environments. Strength capacity is important for ensuring the structural integrity and safety of the bridge to the public. The research team devised a test plan to cover these two conditions by loading the specimen at various locations. The difference in behavior between the various locations is related to the lateral girder stiffness by which the girders support the deck, which is directly related to the arching action that can develop in the deck. Figure 4.48 shows a schematic of girder rotations at two different locations along the bridge span. At midspan, the girder rotations will be higher because of the less restraint to such movement when compared to sections closer to the support. Furthermore, failure modes controlled by punching shear, which often take place in concrete bridge decks, are sensitive to proximity to edges. The chosen test locations would highlight any differences in wheel load capacity. To simulate the effect of continuity, the deck was extended beyond one of the girders and weight blocks were placed at the edge of the overhang as mentioned previously.

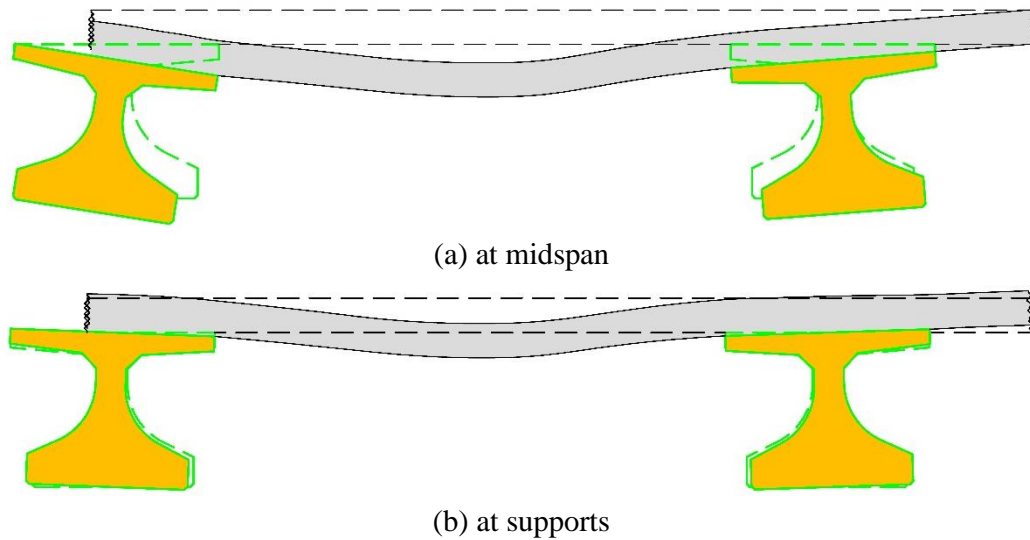


Figure 4.48: Effect of girder rotation on deck deformations

The effective width of a wheel load was first calculated according AASHTO LRFD per the traditional method. It was found that a distance equal to ~10 ft in the longitudinal direction (5 ft on each side of the applied load) would fall under the influence of loading at a certain location. This influence area is especially important at higher load levels where irreversible material damage may take place and can affect the performance of other locations. Under service conditions, the load levels are not sufficient to introduce such irreversible nonlinear behavior and a closer load spacing can be used. Therefore, five service load and three strength load tests were planned. In deciding on loading locations, the 6-foot pattern of the anchorage points in the laboratory strong floor where the loading framing would be anchored was considered. The spacing between the service load test locations was at least 6 ft whereas it was at least 12 ft between the closest strength load tests, which is more than twice the distance to the edge of the calculated influence area. As can be seen from Figure 4.3, each of the chosen load locations was unique for both service and strength cases. Considering the symmetry of the specimen, it can be said that the service load cases were at 0, 6, 12, and 18 ft from the midspan of the supporting girders. Strength cases were at 0, 12, and 18 ft from midspan. It should be noted that an additional fourth strength and service load (S4/F4) test was conducted before the testing on the S3/F3 location since the S4/F4 location was less than 12 ft from the S3/F3 location and located in-line with the center of the north supports. This was to help obtain an uncompromised test location for the weakest point in the specimen; i.e., deck at bridge span ends with no transverse diaphragms or thickened slab.

A summary of the load cases showing the load levels and number of times loaded is shown in Table 4.9 and Table 4.10. The stops at certain loading points indicated that the deck was being checked for cracks. Before failure, the load was decreased to a safe level so lab staff could move the central laser displacement gauges out of the failure area to protect them for future tests. The failure modes for each test location were exhibiting a membrane type of failure. Additionally, it

should be noted that concrete strengths for the deck were much higher than the design strength. Table 4.2 and

Table 4.3 show the concrete cylinder strengths for deck and beams, respectively. Table 4.9 shows the load applied up to the service load level of 21.3 kip which is calculated based on an HL-93 wheel load including dynamic load allowance (1+IM), which translates into (1.00) (16k) (1.0 + 33%) = 21.3 kip according to AASHTO LRFD. The corresponding Strength-I design wheel load is (1.75) (16k) (1.0 + 33%) = 37.2 kip. Loads were held at intermittent load levels as shown in the “History” column to check for cracking and their respective widths. It should also be noted that the service load levels were repeated several times for some tests to confirm the consistency of the slab behavior. The expected cracking load for the deck slab is approximately 23 kip, accounting for a girder spacing of 14 feet without considering continuity. When considering the continuity or negative moment developed over the supports (girders) due to the load blocks on the overhang, the expected cracking load increases to be around 25 kip.

Table 4.9: Service Testing Notes

Service Test	Service Load (kip)	Test Load Reached (kip)	Times Loaded	History (numbers represent load in kip)
S1	21.3	21.88	3	Load to 8, 10 then 21.3, unload to 0. Repeat to service load two more times
S2	21.3	21.92	3	Load to 9, 12, 15, 18, and 21.3, unload to 0. Repeat service load two more times.
S3	21.3	21.68	4	Load to 10, then 21.3 Repeat to service load three more times.
S4	21.3	40.24	1	Load to service load Then ramp to 40.24
S5	21.3	21.65	3	Load to 21.3, unload to 0 Repeat two more times

Load levels during service tests were low compared to failure loads, and therefore, there were no concerns of damage to the laser gauges. Several load cycles (three or four) were applied to the specimen to capture any cracking under service load levels. The dates when the service tests were conducted were as follows (not in order of testing):

- S1- 10/20/15- Tested three times to service load level.
- S2- 10/23/15- Tested three times to service load level.
- S3- 10/30/15 - Tested four times to service load level.
- S5- 11/03/15 - Tested three times to service load level.
- S4- 12/18/15 - Tested once to 40 kip while pausing slightly near service level to obtain crack width information.

Table 4.10: Failure Testing Notes

Service Test	Max Calculated Flexural Capacity Load (kip)	Calculated Failure Load due to Punching (AASHTO & ACI) (kip)	Expected Failure load by Taylor et al. (kip)	Test Load Reached (kip)	Times Loaded
F1*	26.5	175	108	100.9	2
F1-retest	26.5	175	108	218.1	2
F2	26.5	175	108	165.4	2
F3	26.5	175	108	183.3	2
F4	26.5	120	108	80.3	2

\*Failure did not occur

The load during failure tests was initially applied in increments of 5 kip to 10 kip. The specimen was loaded twice during failure tests. In the first cycle, the applied load exceeded service load levels by three to four times. It was then dropped to a safe load level (around 20 kip) to remove the instruments directly beneath the deck to prevent them from damage at failure. In all cases, the load increments were decreased at higher load levels to allow for more opportunities to inspect the specimen's behavior prior to failure.

Failure tests were conducted in the following order: F1 (test to 100 kip), F2, F1 Reloading (two ramps one to 30 kip for crack width and one to complete failure at 218 kip), F4, and F3. The laser gauges were removed and relocated to a safer location once a certain load level (between 60 to 100 kip) was reached during failure tests. The dates that the failure tests were conducted were (not in order of testing):

- F1- 11/13/15 (First test to 100 kip)
- F1 Re-Test - 12/09/15 (failure [218 kip]).
- F2- 11/25/15
- F3- 12/22/15
- F4- 12/18/15 Note that F1 and F2 were already tested to complete failure. F1 may have influenced F4 results.

## Chapter 5 Analysis and Interpretation of the Test Results

Analysis of experimental results is presented and discussed in this chapter. First, a section is dedicated to assessing the performance of reinforced concrete decks that follow the empirical design provisions in AASHTO LRFD under service load levels. This section is followed by a section that addresses the performance of the deck under elevated load levels up to failure.

The results presented in this chapter are the major indicators of the behavior observed during the experiments. These results were selected for the evaluation of the empirical design methodology. A thorough set of results, including the ones presented in this chapter, can be found in Appendix VIII, which is provided for completeness. As is typical with instrumentation embedded in reinforced concrete, a few of the embedded strain gauges that were installed on the steel reinforcement acted erratically. These gauges were not used to interpret results and were omitted.

Strain relations for F1 were plotted using the initial test that was conducted on 11/13/15 to have a more original strain result that was not affected by any previous high load test (if strain was used from the 12/09/15 testing date, the results would have been altered by the high strain levels already experienced in the transverse reinforcement when it was previously loaded to 100 kip). Deflection for the F1 test was used from the testing date of 12/09/15 for a complete load-deflection plot all the way up to failure.

Deflection measurements were recorded using both laser and actuator displacement gauges. In the raw data files for deflection, positive deformation indicated the specimen moving away from the laser gauge while negative meant the specimen moved towards the instrumentation. For the following figures, the deflection readings that were given from the laser gauges were negated so that positive deformation would be towards the laser. The vertical deflection measurement from the actuator needed to be corrected for several potential sources of error that introduce additional deformations on top of the actual specimen deformation. These errors included the possible uneven deformation of the Neoprene loading and girder bearing pads, the compressibility of the hydraulic system, and the deflection of the jacking beam the actuator was attached to which spanned 24 ft. The laser gauges were removed from the vicinity of the respective test location after a relatively high load level was reached causing the need to rely on an interpolation of the load deflection results. A correction factor was obtained by comparing the difference between the laser gauges and actuator displacement at early load levels. Both gauge types were reading the deformations up to 100, 70, 80, and 60 kip, for failure tests F1 through F4, respectively. For example, Figure 5.1 shows that the laser gauges measured lower deflections than the string potentiometer gauge installed on the actuator. The laser gauges were removed at load levels ranging between 60 to 100 kip. It was decided to determine the differences in the deflection measurements,  $\delta$  from actuator and the laser gauges. The magnitude of each  $\delta$  reading was then plotted vs. the vertical load increment. The final relationship of Load vs.  $\delta$  is shown in Figure 5.2 for F1.

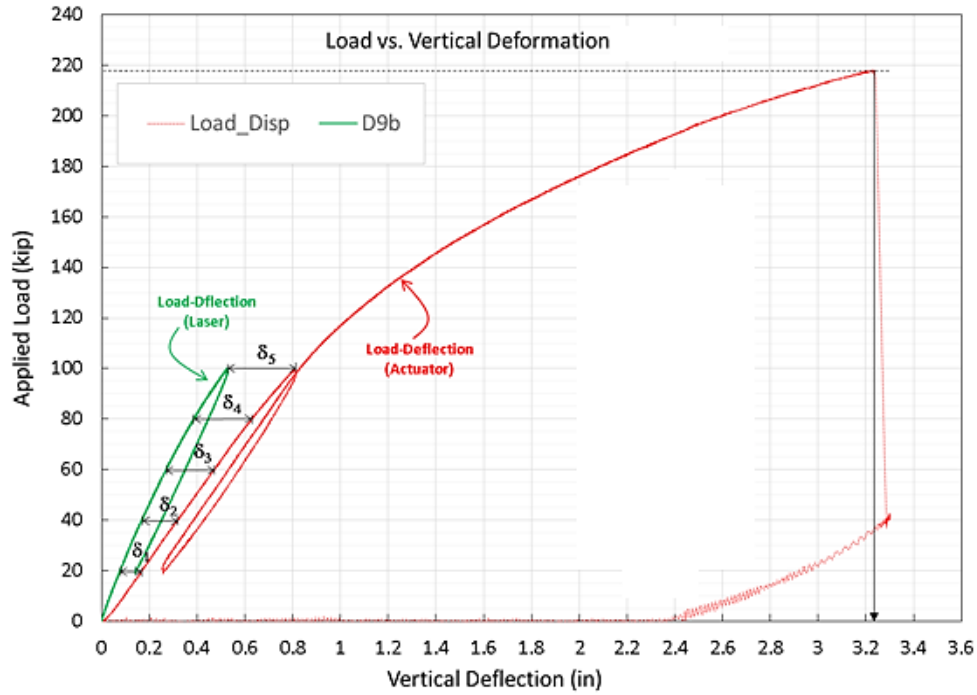


Figure 5.1: Example of load vs. deformation for failure test using two methods of deformation measurements

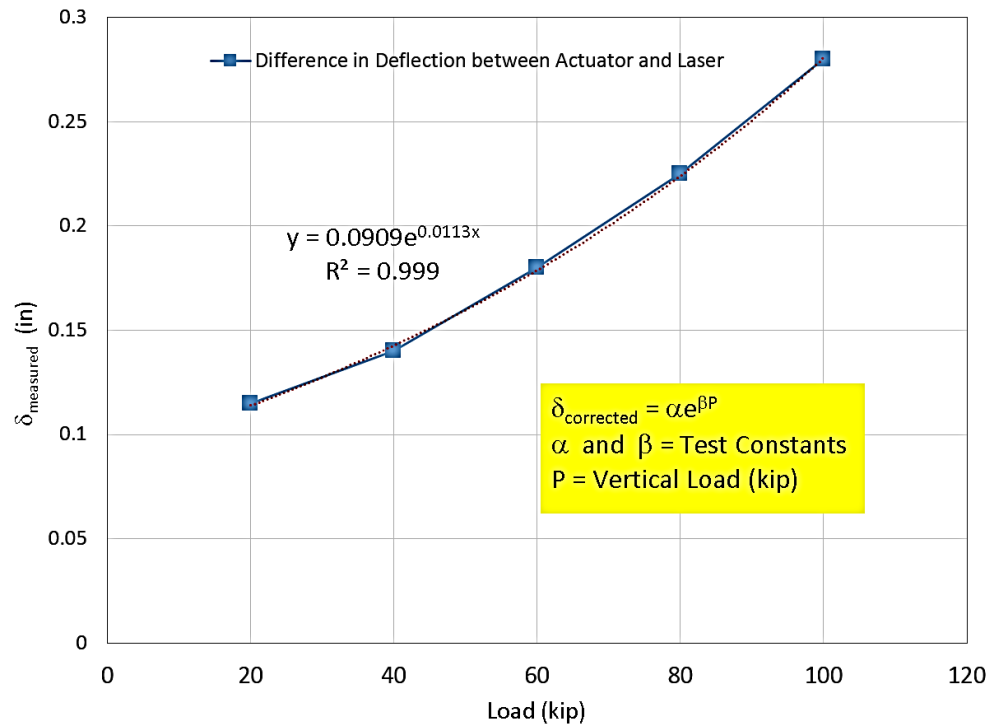


Figure 5.2: Example of vertical load and difference in deflection measurements ( $\delta$ )

As can be seen from the above relationship, the Load vs.  $\delta$  relationship can be represented by the following equation, Equation 44:

$$\delta_{\text{corrected}} = \alpha e^{\beta P} \tag{Eq. 44}$$

where

$\delta_{\text{corrected}}$  = Actual measured differences between actuator and laser readings (inch)

$\alpha$  and  $\beta$  = Test constants

P = Vertical Load (kip)

By using this equation, it was possible to extrapolate the relationship between vertical load and laser deflection measurements. The extrapolated relationship is shown in Figure 5.3, for test F1.

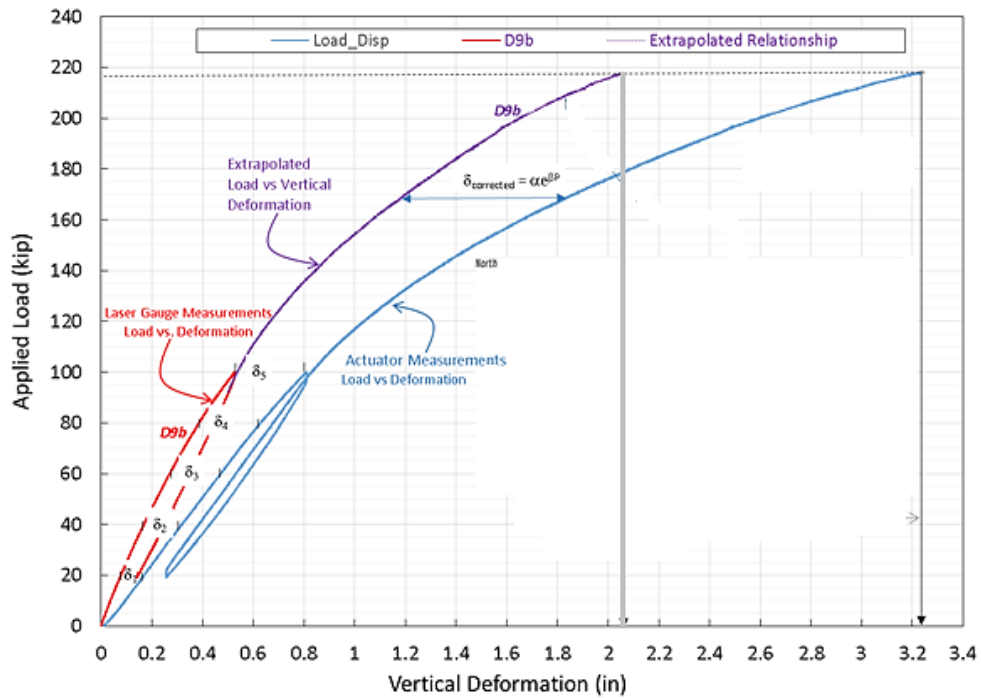


Figure 5.3: Comparison between raw and extrapolated vertical deformation vs. applied load for test F1

The test constants  $\alpha$  and  $\beta$  were determined for each test. For F1 test, it was found that  $\alpha = 0.0909$  and  $\beta = 0.0113$ . By using this relationship, it was possible to extrapolate the values obtained from the laser gauges up to the failure load. This method was then used to predict the vertical load vs. vertical deflection relationships for the other conducted tests.

## 5.1 Service Results

Load levels reached during the service load tests were limited to approximately 22 kip. This load level exceeds a typical design wheel load (16 kip) after applying a dynamic impact magnification factor (IM) of 33%. The importance of this set of tests stems from the fact that decks designed following the empirical deck design method have to perform adequately at service load levels and not only be capable of resisting ultimate load levels. Crack widths should be limited to avoid accelerated deterioration of the lower amount of embedded steel reinforcement in an empirical deck design. Excessive deflections under service conditions may lead to a host of problems (e.g. ponding and rider discomfort) that can be avoided if the limit set by AASHTO LRFD is not exceeded. Strain levels in embedded reinforcement and deck concrete extremities will also be discussed to assess if any overstressing took place under service conditions.

### 5.1.1 Deflection Performance

Four gauges were selected for assessing the deflection performance of the deck. With the exception of the S4/F4 test, the location of the first three gauges, D8b, D9b, and D10b, were under the applied load with D9b being aligned with the load and the other two at 2 feet away in longitudinal direction. The S4/F4 case being unique, with a different gauge layout for deflection because of the edge constraint. The fourth gauge, D5b, was positioned on the overhang as can be seen in Figure 5.4. The service test load deflection plots for all four gauges can be seen in Figure 5.6 through Figure 5.11. It should be noted that the plotted deflections are with respect to the rigid laboratory strong floor as a reference. Therefore, these deflections are not net deck deflections, but include the effect of girder movement as well, which renders the outcomes presented in this chapter as conservative.

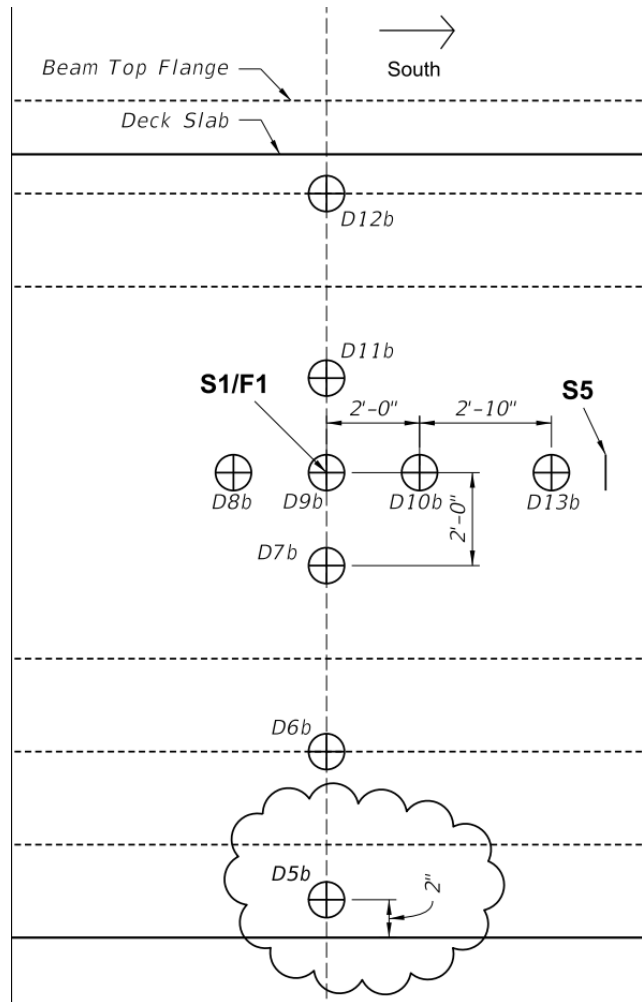


Figure 5.4: Typical location of D5b

It can be seen from the plots for D8b, D9b, and D10b that there was very little difference in the deflection between these three gauges with D9b experiencing a slightly higher deflection of 0.055 in. (1.4 mm). The only exception to this trend is S4, whose deflections were noticeably higher, 0.2 in. (5.1 mm), and the difference between the two gauges on S4 was more pronounced compared to the other service tests. The observed higher deflection is expected for S4 which is the most critical loading case where the applied load is positioned along the edge of the deck, hence, load distribution is limited to one side only.

The maximum deflection limit for light weight metal and concrete decks with no pedestrian traffic is  $L/800$  in AASHTO LRFD (9.5.2), where  $L$  is the span length. This limit translates into 0.21 in. (5.3 mm). By comparing the presented results to this limit, it can be stated that the design wheel load including dynamic magnification meet the AASHTO LRFD requirements for all interior service load cases, namely S1, S2, S3, and S5, with a huge margin. The critical edge case, S4, also meets AASHTO LRFD deflection limit, however, the margin is much smaller. If a higher margin against deflection is desired, thickening of the deck as is currently required by the FDOT SDG may be necessary. Results for the S4 test are plotted separately to be able to adequately distinguish the other service test results from each other.

Table 5.1 reflects measured deflections from all service load tests in addition to AASHTO LRFD allowable deflection for the span length of the lab specimen. According to AASHTO LRFD section 4.6.2.1.6, the design section for negative moments may be taken as one-third the flange width but not exceeding 15 in from the centerline of the support. To be conservative, the full centerline to centerline spacing of 14 ft was selected for the transverse span length. This shows that the worst case satisfies the allowable deflection limit even for the edge loading case; S4.

Table 5.1: Deflection Comparisons

<b>Reference</b>	<b>Deflection (in)</b>
<b>AASHTO LRFD 2012 (L/800, no pedestrian)</b>	0.21
<b>S1</b>	0.053
<b>S2</b>	0.045
<b>S3</b>	0.047
<b>S4</b>	0.21 (using second ramp)
<b>S5</b>	0.050

The difference between the deflections of different interior service load cases is minimal and is mainly due to the difference in girder deflection at each loaded position. For example, deflections for S1 also include the girder deflection, which is highest at this location as it is in the middle of the girder’s span length. Deflections for other locations (S2, S3, and S5) are slightly less, which is a result of the lower girder deflection at these locations.

Using the equivalent strip method, the expected cracking load for the deck slab was calculated to be about 23 kip accounting for a girder spacing of 14 feet without including the effect of continuity. When considering the continuity effect (or developed negative moment) due to the load blocks on the overhang (see Figure 5.5), the expected cracking load will be approximately 25 kip.

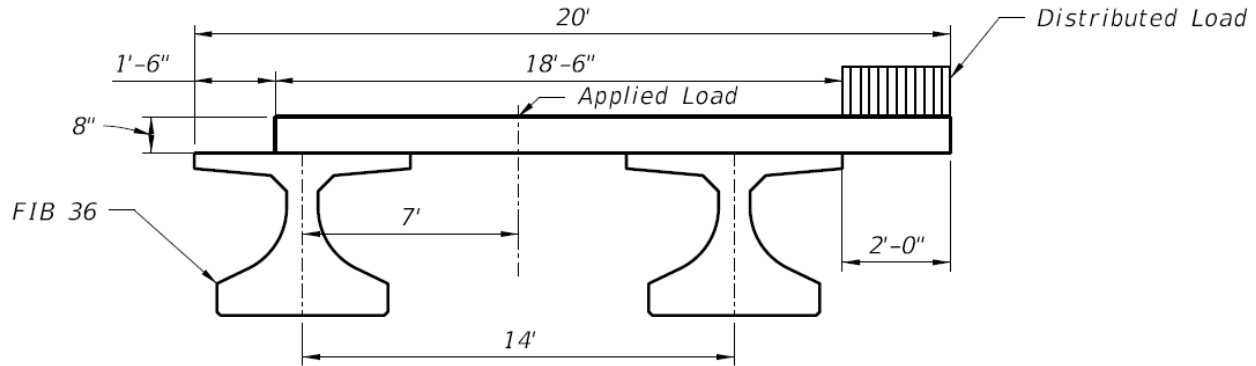


Figure 5.5: Schematic of loads applied on test specimen

S4 test results are shown separately in most deflection comparison plots because of the different gauge layout and because of the fact that large differences in recorded deflections make such a comparison challenging using a plot with the same scale. Figure 5.6 shows deflections for service tests S1, S2, S3, and S5 for the D8b displacement gauge under the slab. The behavior for S3 displacement appears to be erratic with intermittent resets while maintaining the similar linear trend observed for the other gauges. This may be an indication of a problem in the fixture holding the gauge or in the floor on which the fixture stood. It was deemed more appropriate to keep the recorded plot as is, nevertheless, it is clear that removing these abrupt resets would result in a deflection close to that recorded by the same gauge for service test S2. It should be noted that in the presented deflection plots, positive and negative readings indicate downward and upward movement, respectively.

The maximum deflections were recorded using gauge D9b, which was positioned directly under the applied load. Figure 5.7 shows that the displacements recorded using this gauge D9b whose maximum values are given in Table 5.1. Figure 5.8 shows displacement data from D10b near the load point for service tests, which confirm a linear behavior like the other gauges. Figure 5.9 and Figure 5.10 show the displacements for the S4 test from D9b and D10b respectively. Both plots show a linear behavior up to the maximum applied service load.

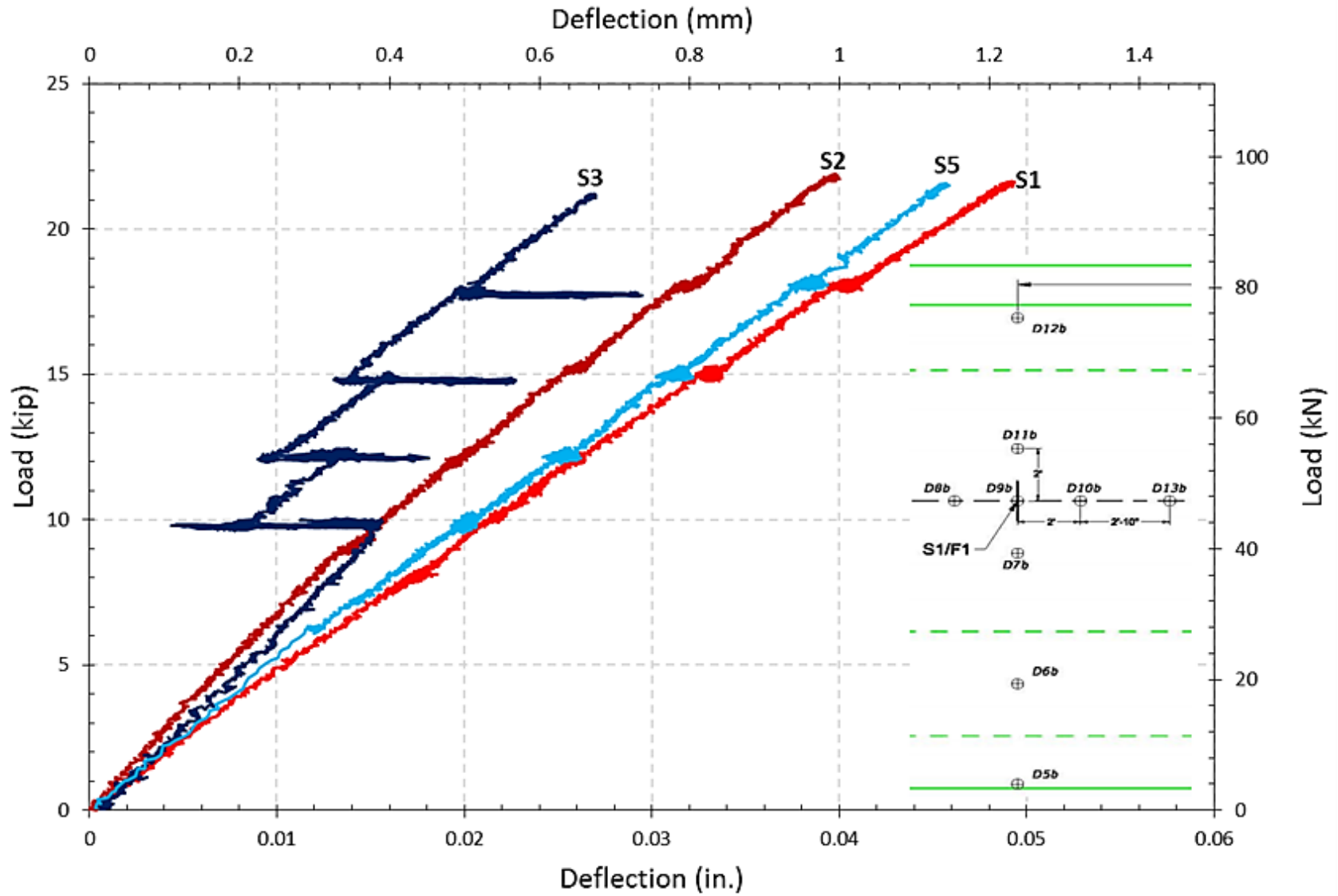


Figure 5.6: Service test load deflection D8b

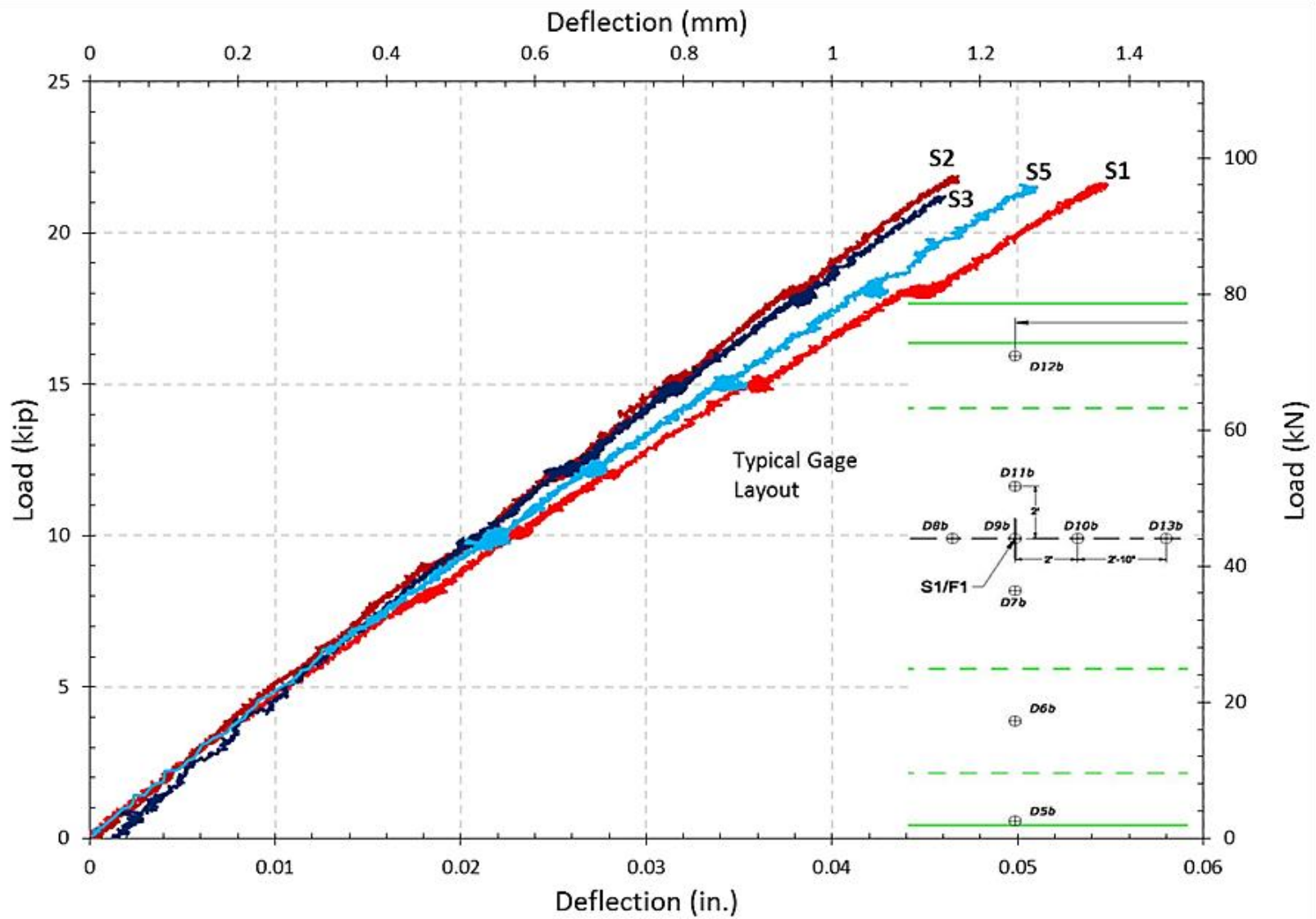


Figure 5.7: Service test load deflection D9b

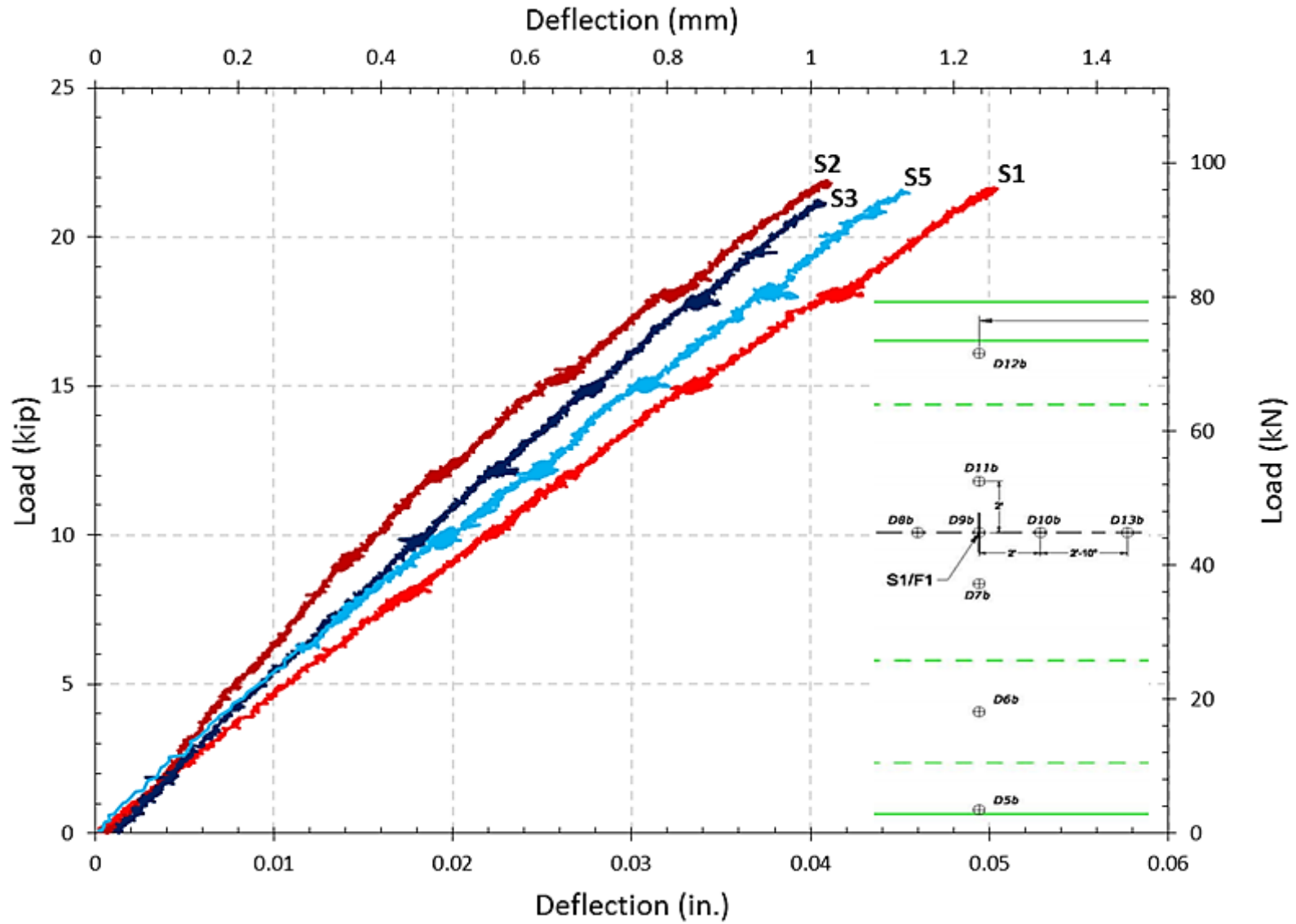


Figure 5.8: Service test load deflection D10b

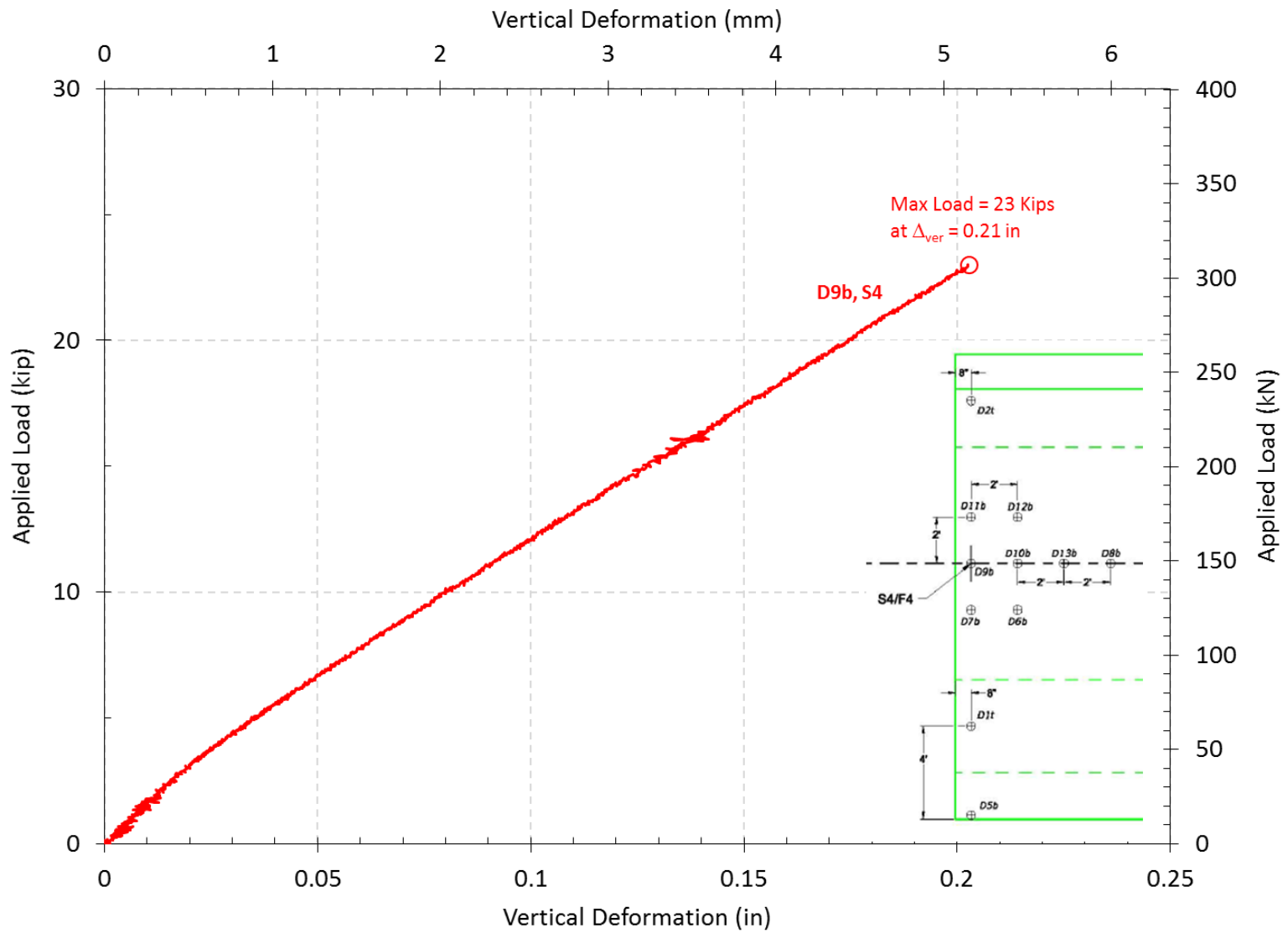


Figure 5.9: S4 Laser deflection gauge for D9b, midspan

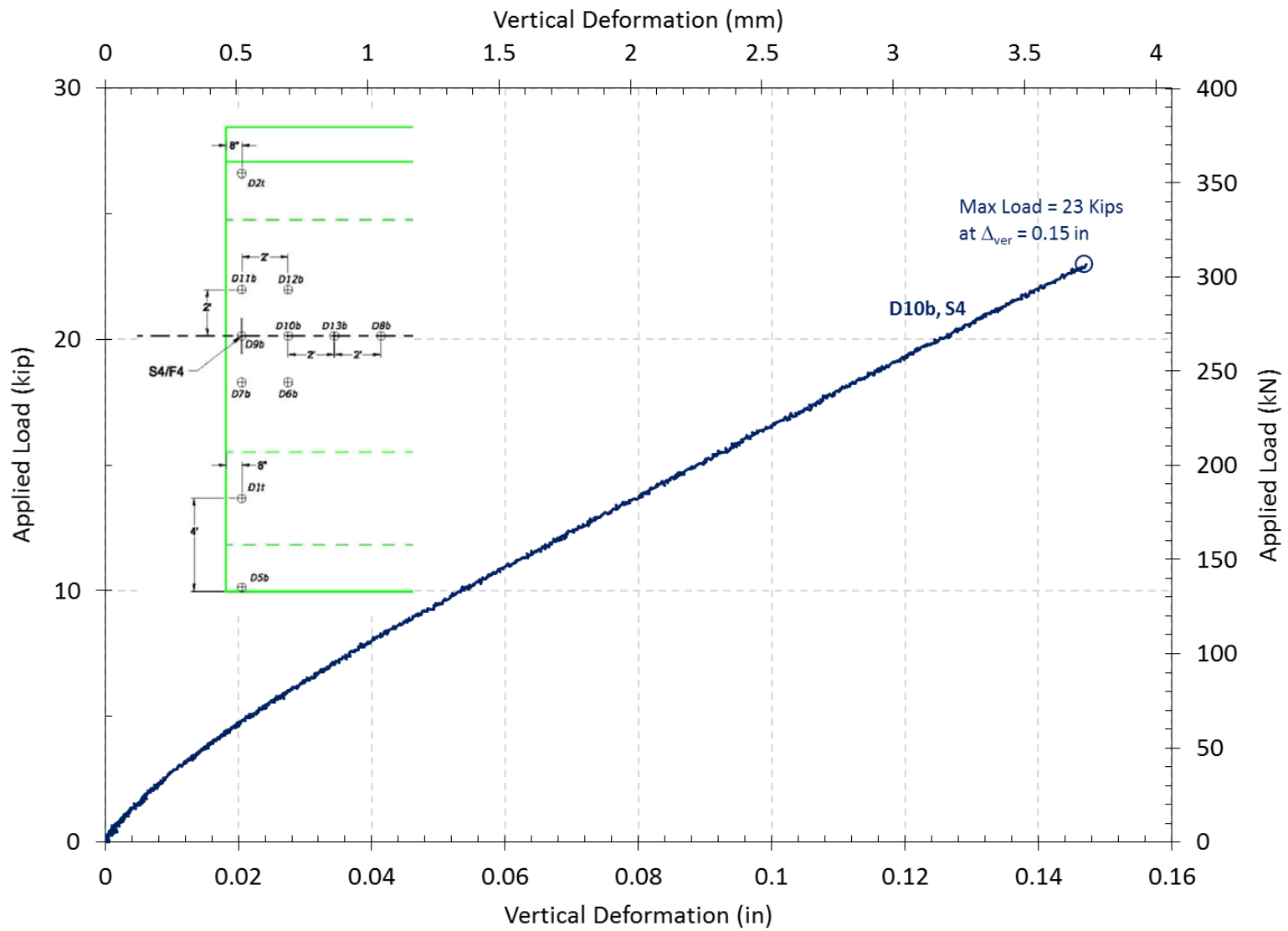


Figure 5.10: S4 Laser deflection gauge for D10b, midspan

The overhang deflection due to the applied load under service conditions can be seen in Figure 5.11. Upward movement readings were recorded during the tests, and the negative sign of the readings in this plot should be disregarded. The magnitudes of these upward movements were minimal (maximum 0.017 in. (0.43 mm) for all interior cases). Case S4 is an exception where a higher upward movement was observed 0.54 in. (13.7 mm). The difference between the different cases can be attributed to the girder stiffness at these locations, which differs based on proximity to the girder supports (see Figure 4.48). The applied load in Case S4 is almost positioned perfectly in line with the girders supports, thus the girders provided an almost rigid support to the deck. Hence, the load distribution is lesser than at midspan in addition to being at the edge as stated before. While these deflections easily meet any deflection limits, they are an indication of negative moment development under service conditions, which may require special attention to reinforcement detailing at these critical edges.

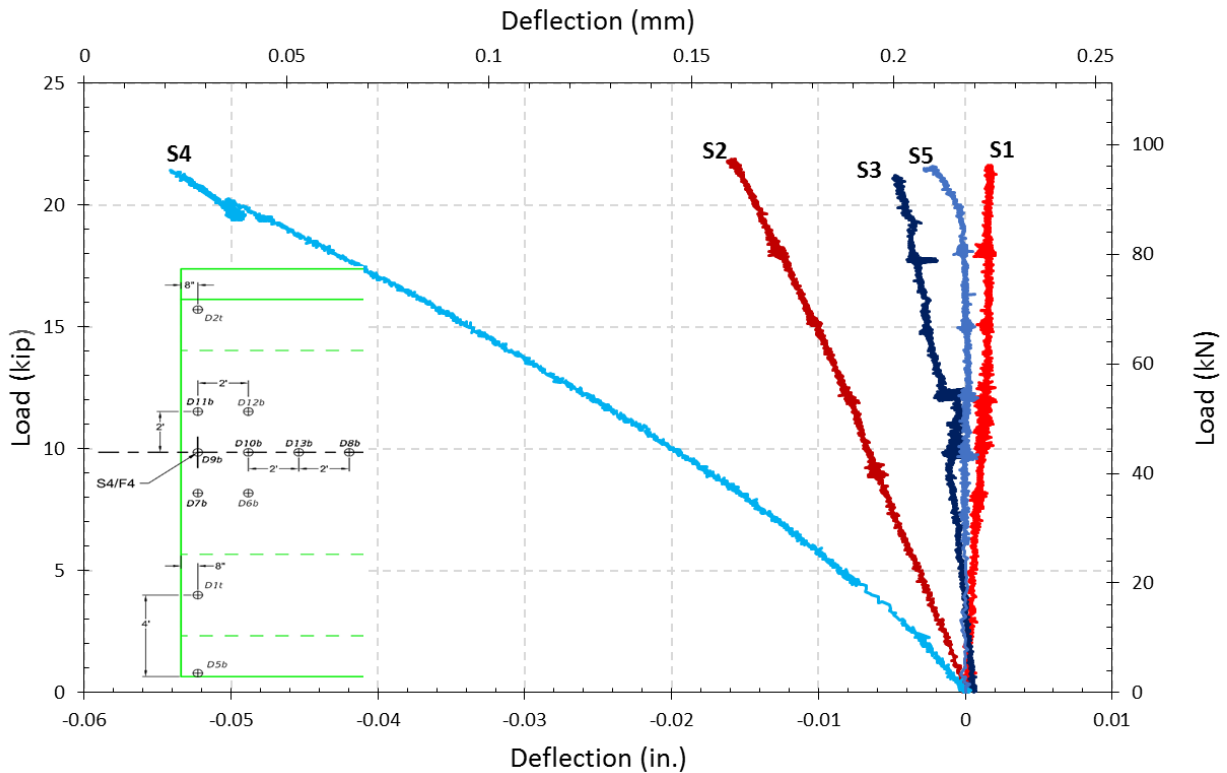


Figure 5.11: Load-deflection plots for D5b under service load levels

### 5.1.2 Strain Readings

Strain readings under service conditions are an indication of how stressed the deck is. In this section, strain readings from strain gauges on embedded reinforcement in the transverse and longitudinal directions will first be discussed. Concrete surface strain levels in both directions will then be presented and discussed. Figure 5.12 through Figure 5.15 show the evolution of strain levels with applied load. The shown plots are for strains in the main bottom rebar in the transverse direction for service test cases, S1, S2, S3, and S4. Each figure shows seven plots for gauges along the critical line exactly under the applied load; i.e. gauges TB10, TB11, TB12,

TB13, TB14, TB15, and TB16. For all cases, the gauge directly under the applied load, TB13, recorded the largest positive strains. The subsequent gauges on both sides, TB12 and TB14, also recorded positive strains but at a lower level. Gauges TB11 and TB15 can be considered as inflection points. Strains at these locations were low; staying close to 10 microstrain. The last gauges in this line of gauges, TB10 and TB16, were located at the edge of the top girder flanges. These gauges recorded small negative strains indicating the existence of small continuity moments. The maximum strain levels recorded by TB13 were 225, 95, 52, and 102 microstrain for S1, S2, S3, and S4, respectively. Comparing these strain levels to concrete cracking strain,  $\epsilon_{cr}$ , sheds a light on whether cracking is to be expected under the applied service load. Concrete cracking strain can be estimated to be equal to  $f_r/E_c$ , where  $f_r$  is the modulus of rupture and  $E_c$  is the modulus of elasticity of the concrete, Equation 45. Using AASHTO LRFD estimates for both quantities:

$$\epsilon_{cr} = \frac{f_r}{E_c} = \frac{0.24\sqrt{f'_c}}{1,820\sqrt{f'_c}} = 132 \text{ microstrain} \quad \text{Eq. 45}$$

It should be noted that this estimate can be considered a lower limit as higher estimates of the modulus of rupture,  $f_r$ , can be found in the literature, especially for higher strength concrete mixes. With the exception of S1, all the recorded strains fall below the level that induces concrete cracking (Figure 5.30). Even though TB13 for Case S1 recorded strain readings that exceeded the concrete cracking strain, cracks were not observed during the test under this load level. Therefore, this gauge may have been faulty as the other two internal cases, S2 and S3, did not exceed the estimated concrete cracking strain. Another explanation for the high strains recorded by TB13 for Case S1 is that it is possible that a crack preexisted at this location, resulting in higher strain levels from the cracked section. These hypotheses will be revisited later when surface concrete strain readings will be discussed. It should also be noted that recorded strains (from the available gauges embedded for Case S3) for the most critical case, S4, for which the load was applied on the edge of the deck and after conducting the S3 test, were also lower than the rupture strain.

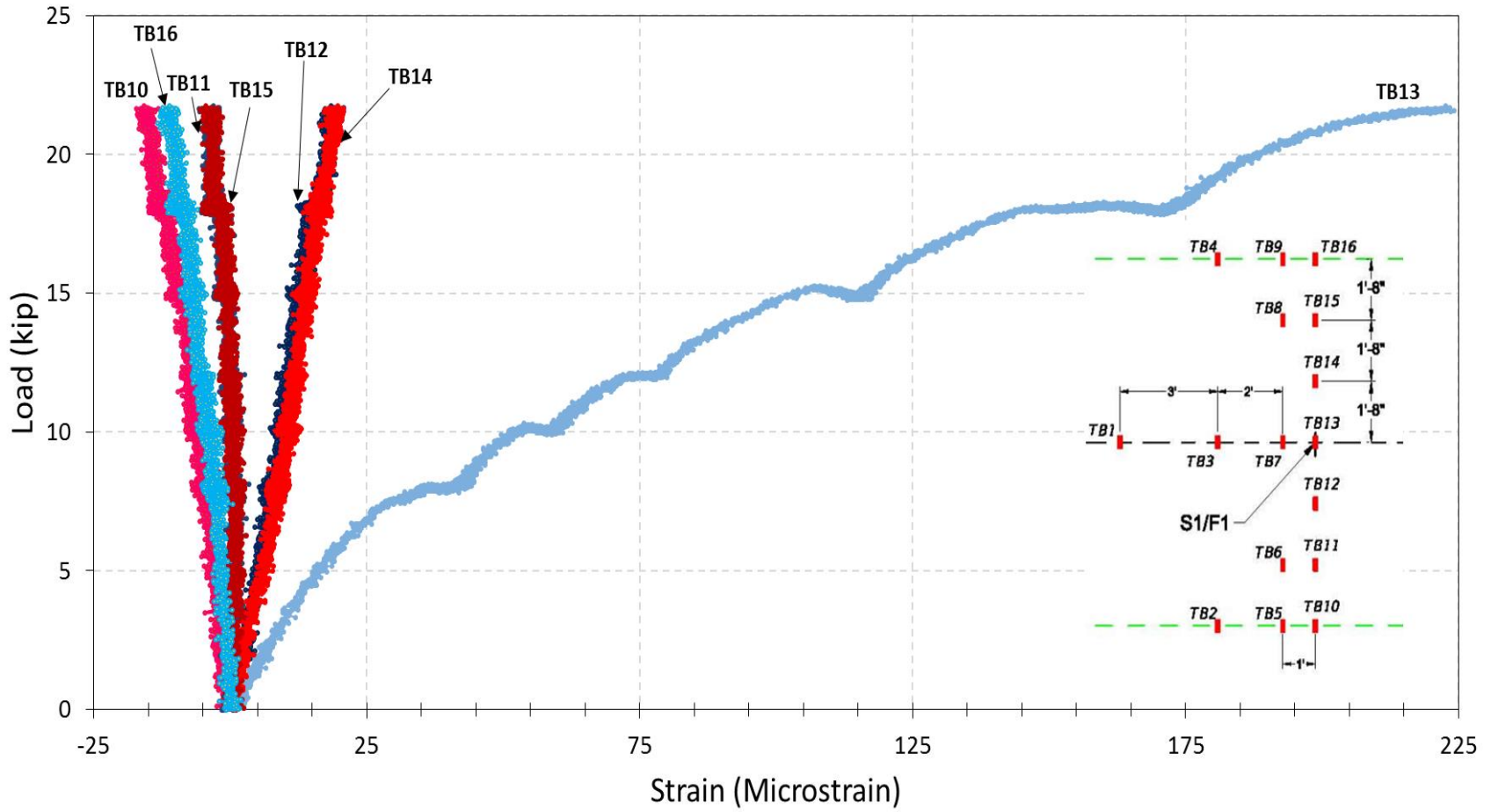


Figure 5.12: Service test S1 load strain for TB10-TB16

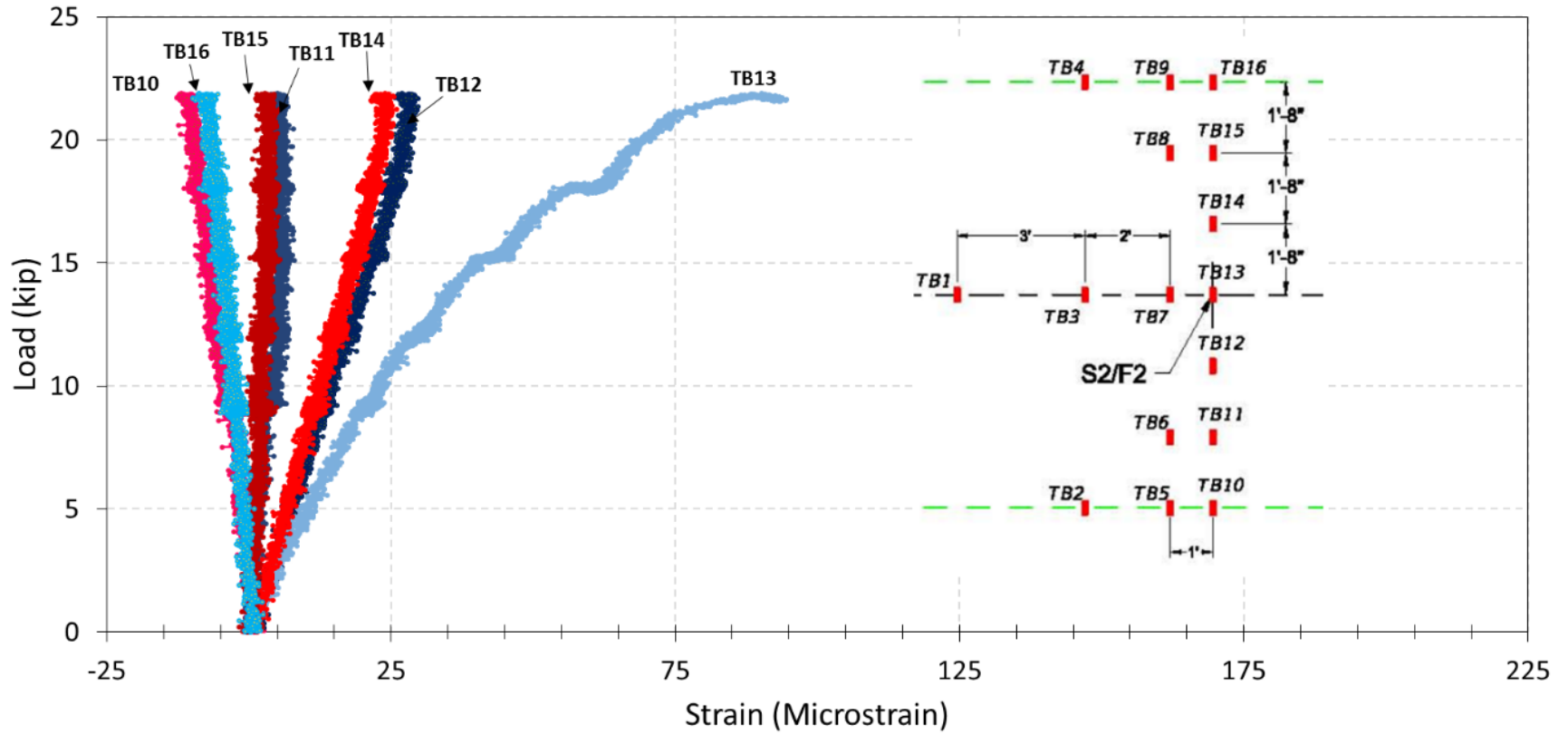


Figure 5.13: Service test S2 load strain for TB10-TB16

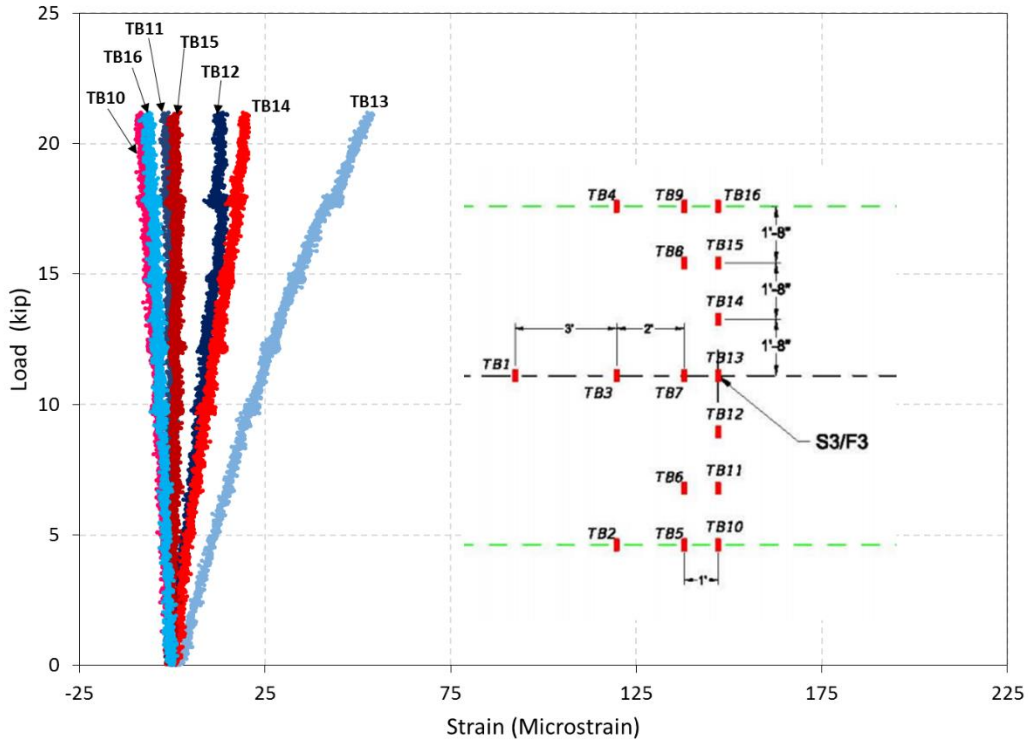


Figure 5.14: Service test S3 load strain for TB10-TB16

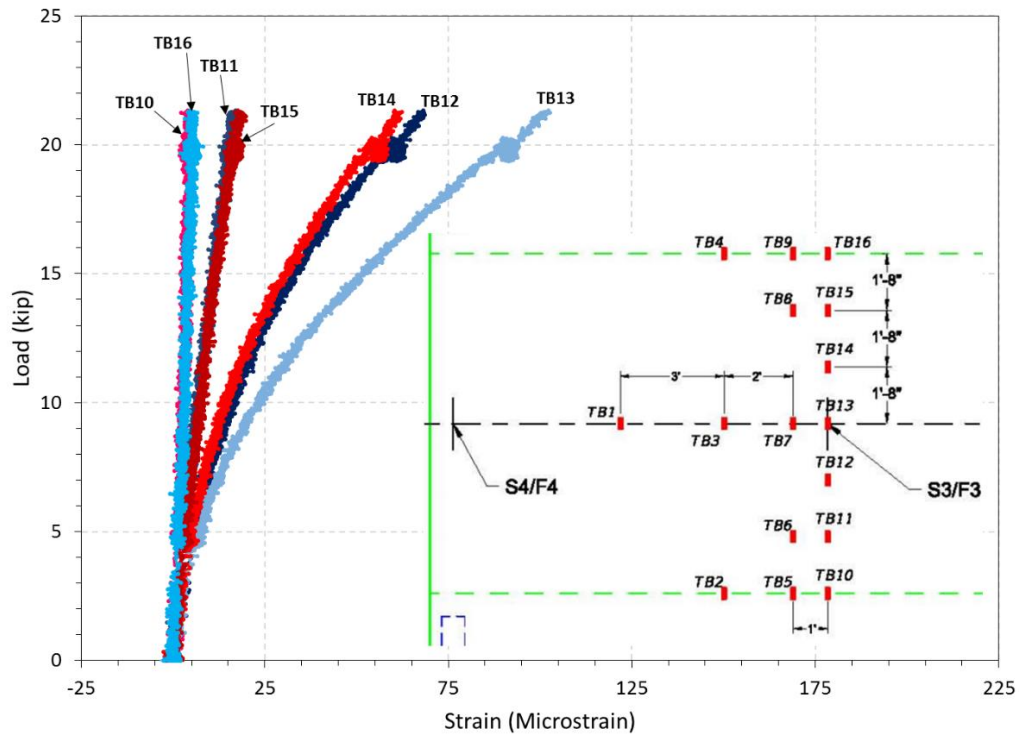


Figure 5.15: Service test S4 load strain for TB10-TB16 (S3 gauges read)

In the longitudinal direction, strains from gauges installed on the distribution reinforcement were also recorded. Five gauges, LB1, LB2, LB3, LB4, and LB5, were selected for presentation. They are all located on a rebar at midspan of the deck. As expected the gauge directly under the applied load, LB3, recorded the highest strain level. The other gauges recorded smaller positive strain levels, while the farthest gauges, LB1 and LB5, mostly recorded small negative strains indicating the end of the influence area under the applied load. All recorded strains under service load levels were below concrete cracking strain except for S1 under which LB3 recorded 160 microstrain, which coincides with TB13. Despite indicating a similar behavior to that discussed earlier for TB13, it is unlikely that gauges installed 18 in. away (LB2 and LB4) would record the observed lower strain levels if a crack had existed. Therefore, LB3 may also be an unreliable gauge. Figure 5.16 through Figure 5.19 show plots of the relationship between the applied load and strain reading from the gauges on the bottom longitudinal steel reinforcement. LB3 is shown to be the highest for most cases as it is directly under the load. It should be noted that the plotted strains for load case S4 were obtained from the gauges installed for load case S3 since S4 was not in the original testing plan, hence, no embedded gauges were installed at the edge of the deck.

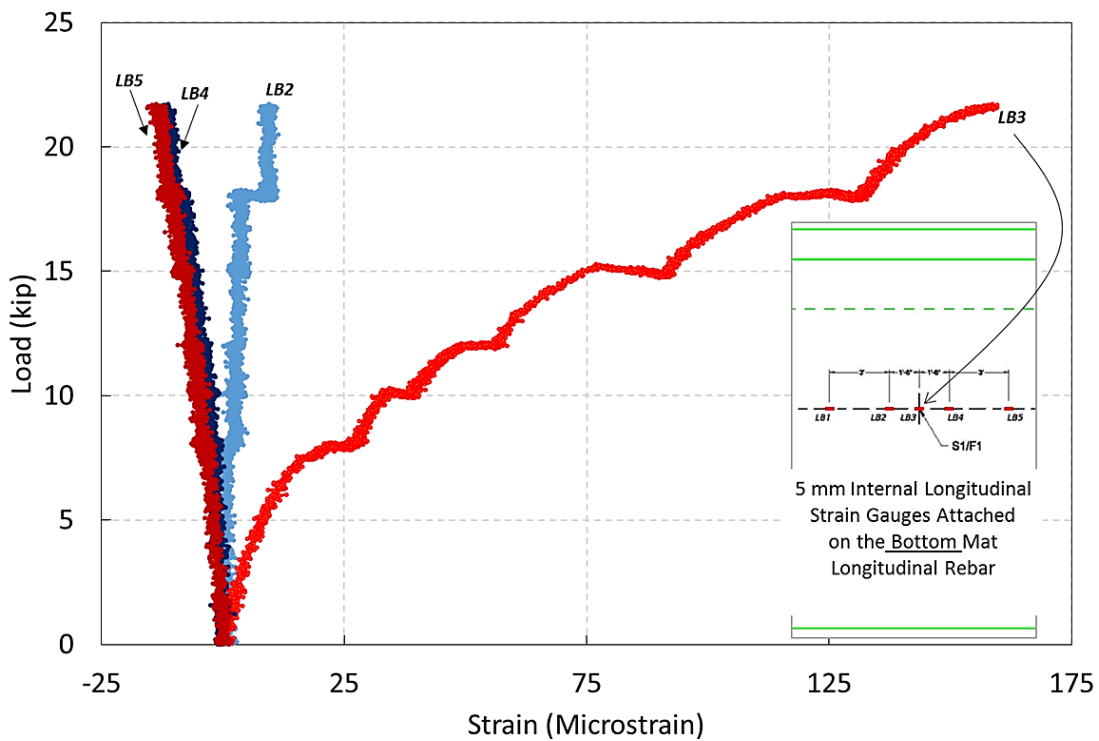


Figure 5.16: Service test S1 longitudinal rebar strains for LB2-LB5

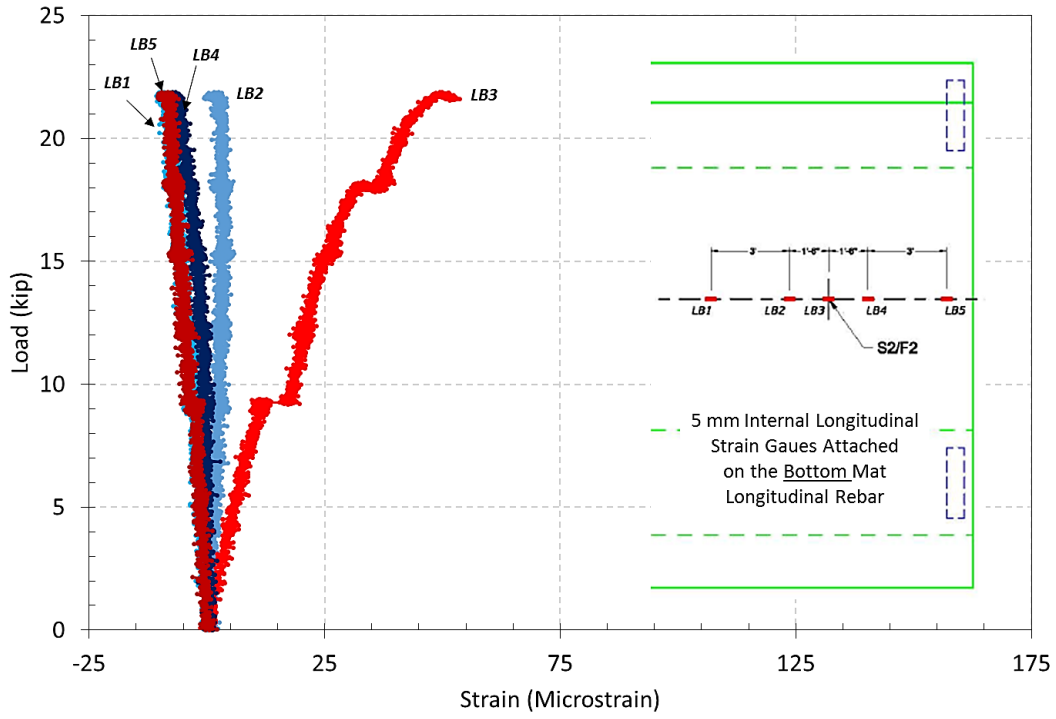


Figure 5.17: Service test S2 longitudinal rebar strains for LB1-LB5

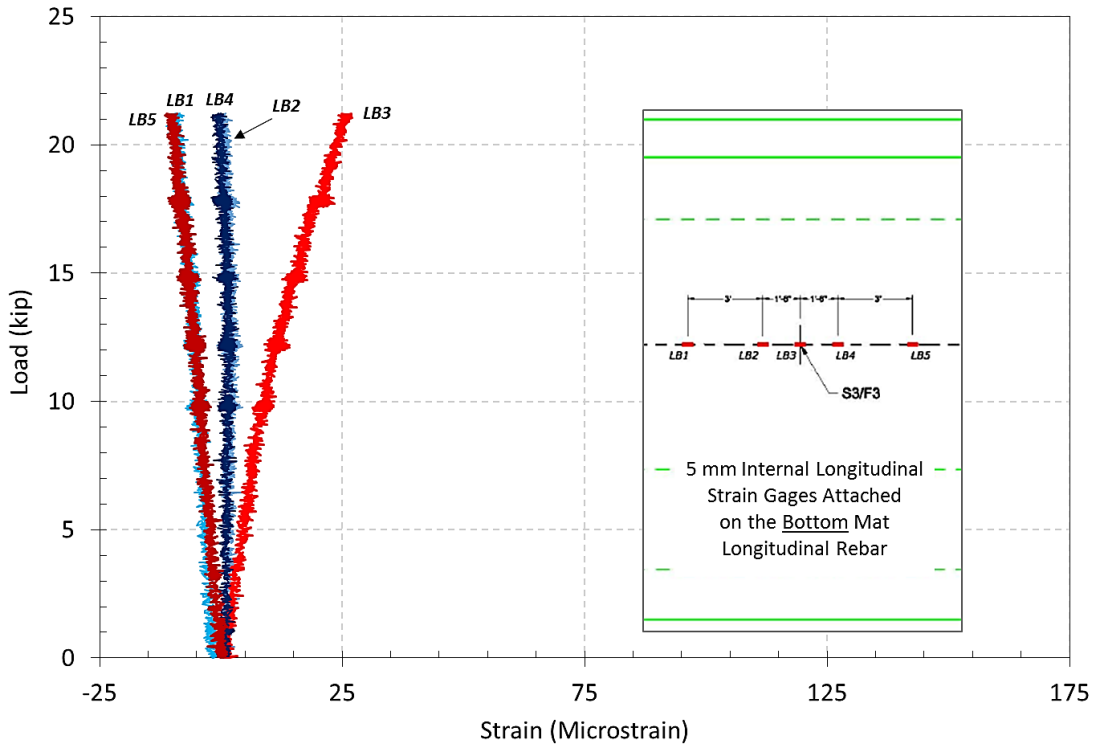


Figure 5.18: Service test S3 longitudinal rebar strains for LB1-LB5

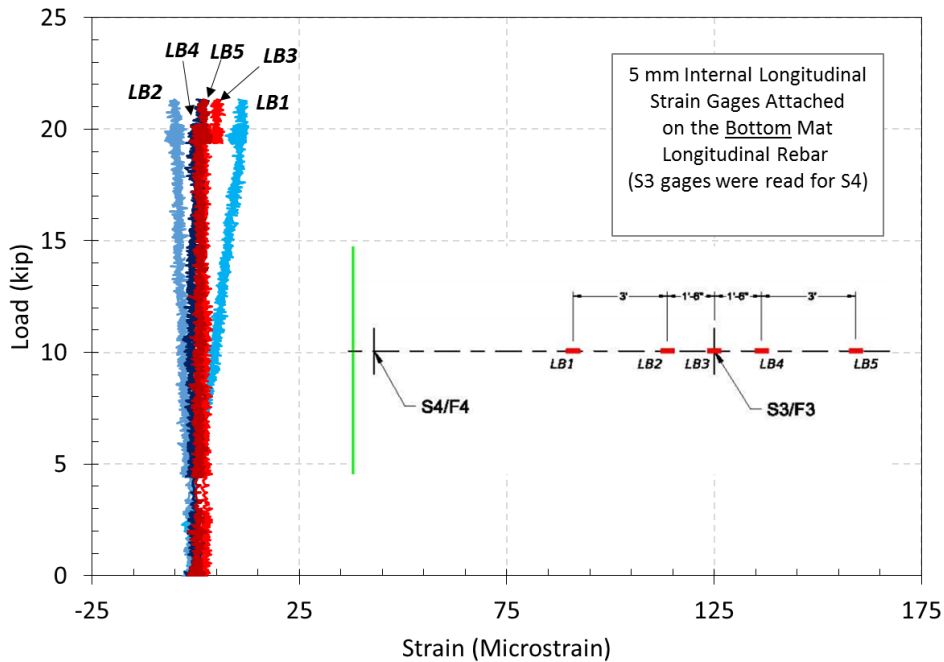


Figure 5.19: Service test S4 longitudinal rebar strains for LB1-LB5 (S3 gauges read)

The concrete surface strains were measured using 60 mm foil gauges at different locations in addition to 200 mm full bridge crack gauges. Results from the foil gauges are presented in Figure 5.20 through Figure 5.26 for top and bottom slab gauges. It was not possible to place a gauge on the deck top surface exactly where the load was applied because of the bearing pad size. Therefore, the closest gauges on the top surface, S3t and S4t, were placed 20 inches away from the point of load in the transverse direction. Figure 5.20 and Figure 5.21 show the recorded strains from S3t and S4t, respectively. As expected, all recorded top strains close to the deck's midspan recorded negative strain values (indicating compression). The magnitude of the recorded compressive strains was limited to 60 microstrain for all service test cases except for S4, for which strains reached 120-130 microstrain. These compressive strain levels are considered low as they are about 6% of the typical concrete strain at peak resistance (0.002) and 4% of the ultimate concrete strain (0.003). The linearity of the shown plots up to service load levels indicate that events such as cracking did not take place.

Additional strain gauges were placed 2 ft and 4 ft away from the load point in the longitudinal direction on top deck surface. Figure 5.22 displays the relationship between the applied load and the strain readings from the first gauge 2 ft away from the applied load. Figure 5.23 displays the relationship between the applied load and the 2 ft further away, also placed along the same line. Both gauges recorded positive strains, but the magnitude of the recorded strains dropped for S14t compared to S11t for most load cases. Nevertheless, the fact that positive strains are recorded at 4 ft away from the load is an indication that the influence area of the load extends beyond that point.

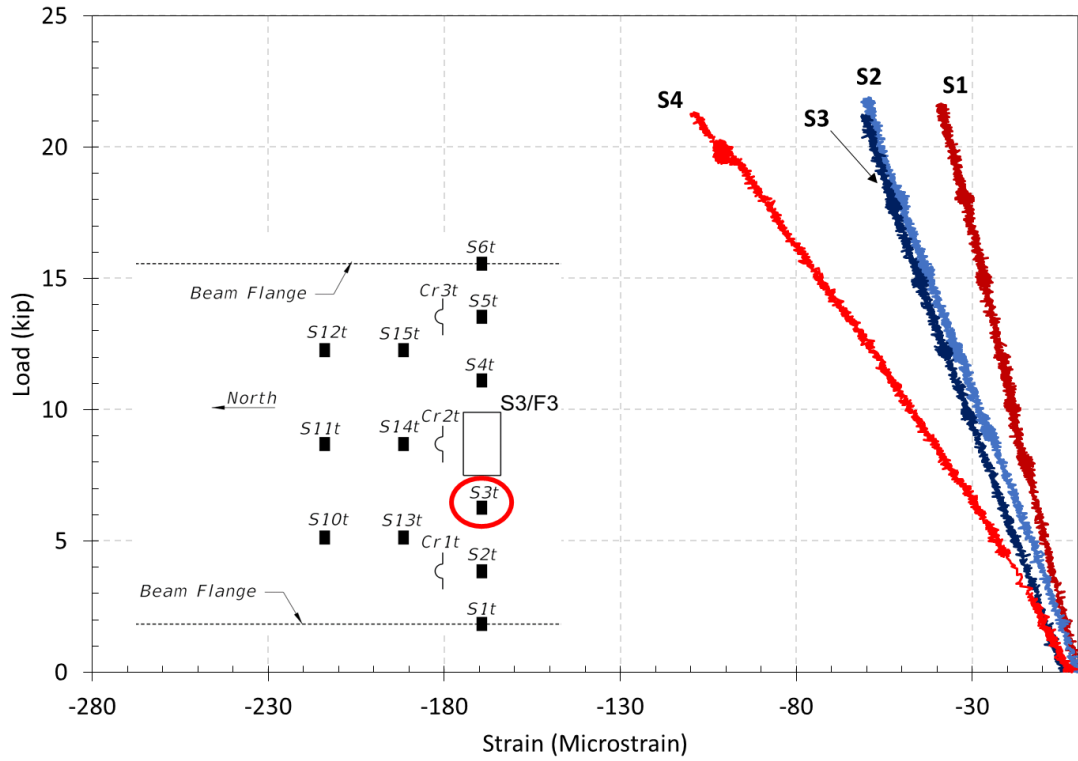


Figure 5.20: Service tests top deck strains - Gauge S3t

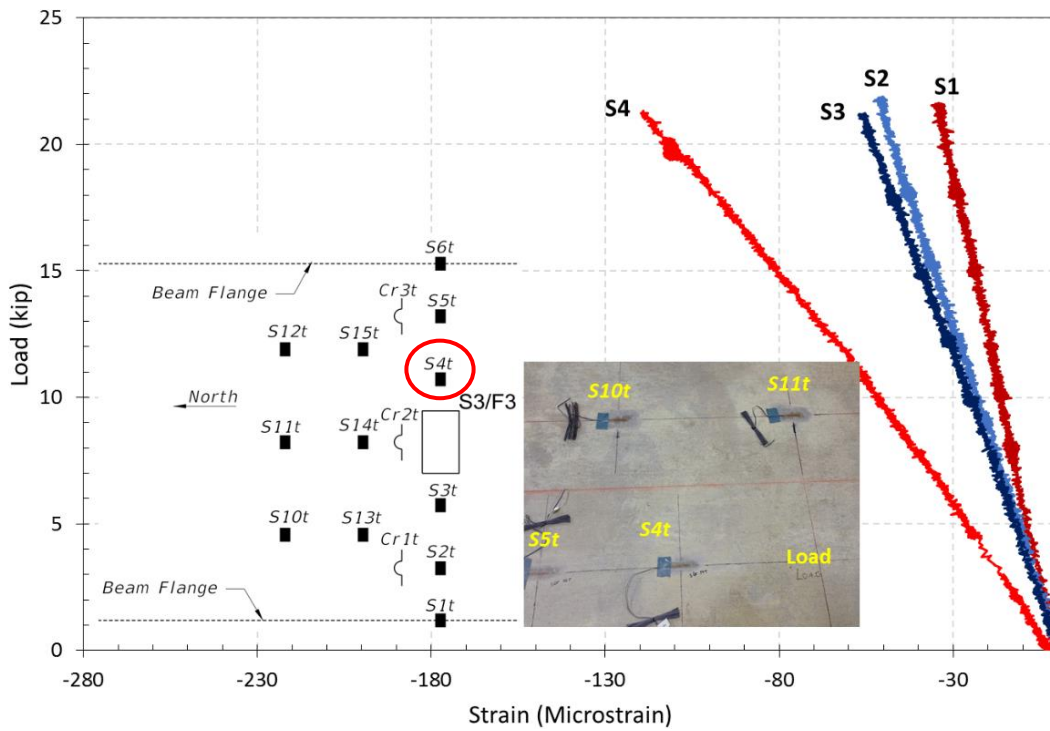


Figure 5.21: Service tests top deck strains - Gauge S4t

On the bottom side of the deck, three gauges (S7b, S8b, and S9b) were installed to measure strains in the transverse direction. The recorded strains from these three locations are plotted in Figure 5.24 through Figure 5.26. The gauge that was placed exactly under the applied load, S8b, recorded positive; i.e. tensile, strains as can be seen in Figure 5.25. The maximum recorded strain level did not exceed 75 microstrain for any of the service test cases, which is below the concrete cracking strain. Readings from S8b deviate from a linear trend for two load cases, S1 and S3, but an abrupt change was not observed. The lack of an abrupt change reduces the possibility of crack initiation. The other two gauges, S7b and S9b, were placed on the bottom deck surface at the edge of the girders' top flange. For these locations, negative strains were recorded. The magnitude of the strains did not exceed 30 microstrain corroborating the previous observation that small negative continuity moments develop in the deck over the girder flanges.

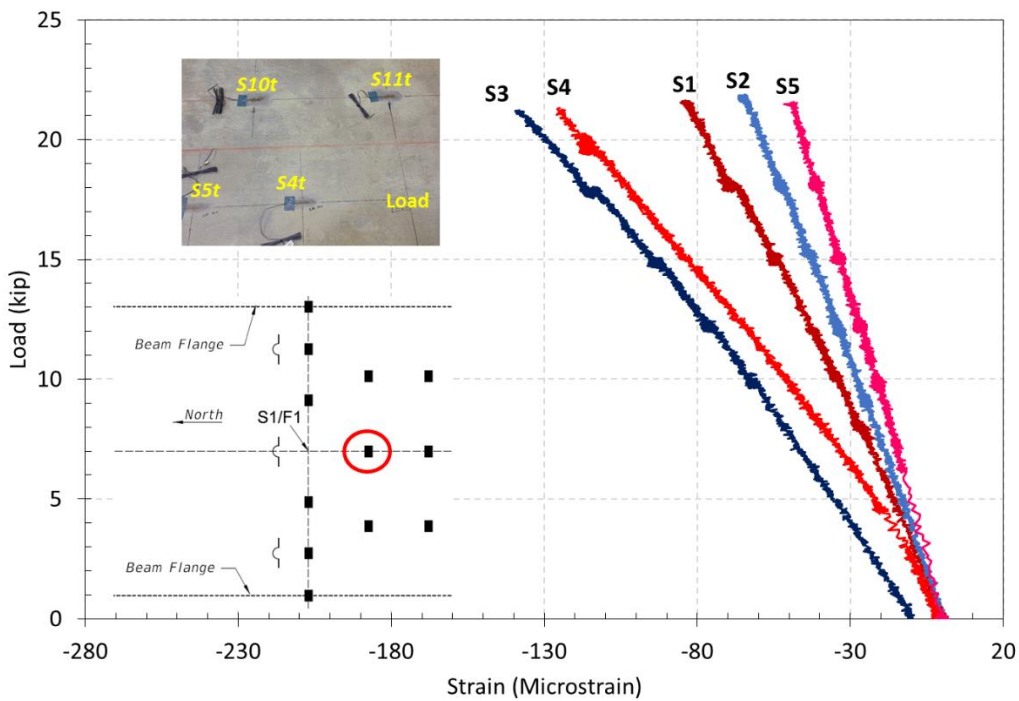


Figure 5.22: Service tests top strains - Gauge S11t (S14t for S3)

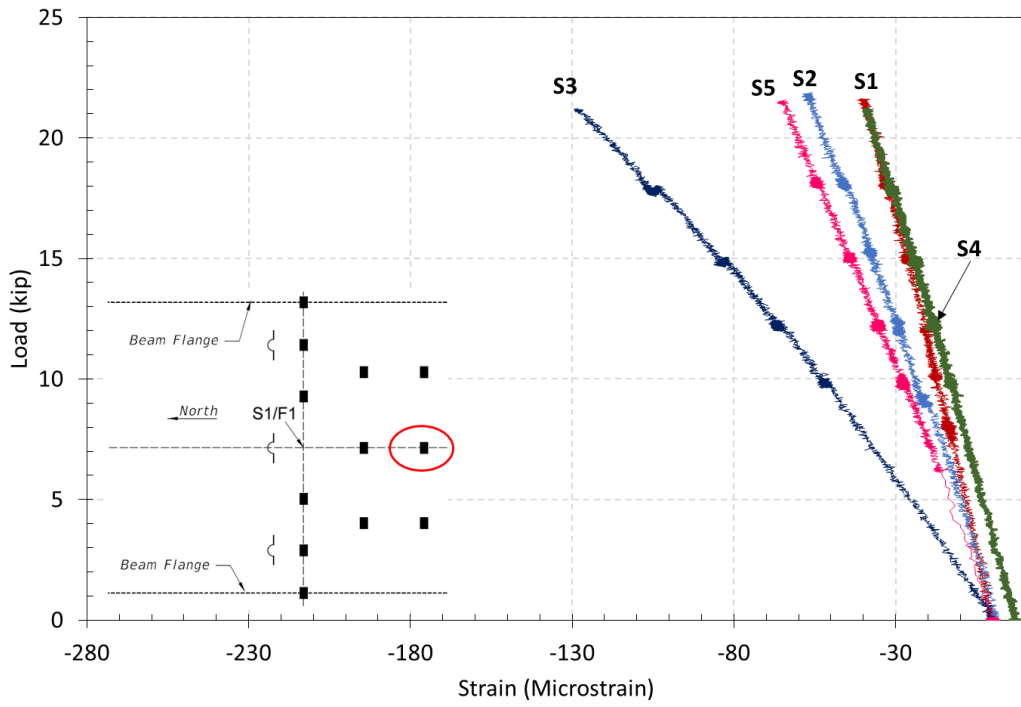


Figure 5.23: Service tests top strain gauge S14t (S11t for S3)

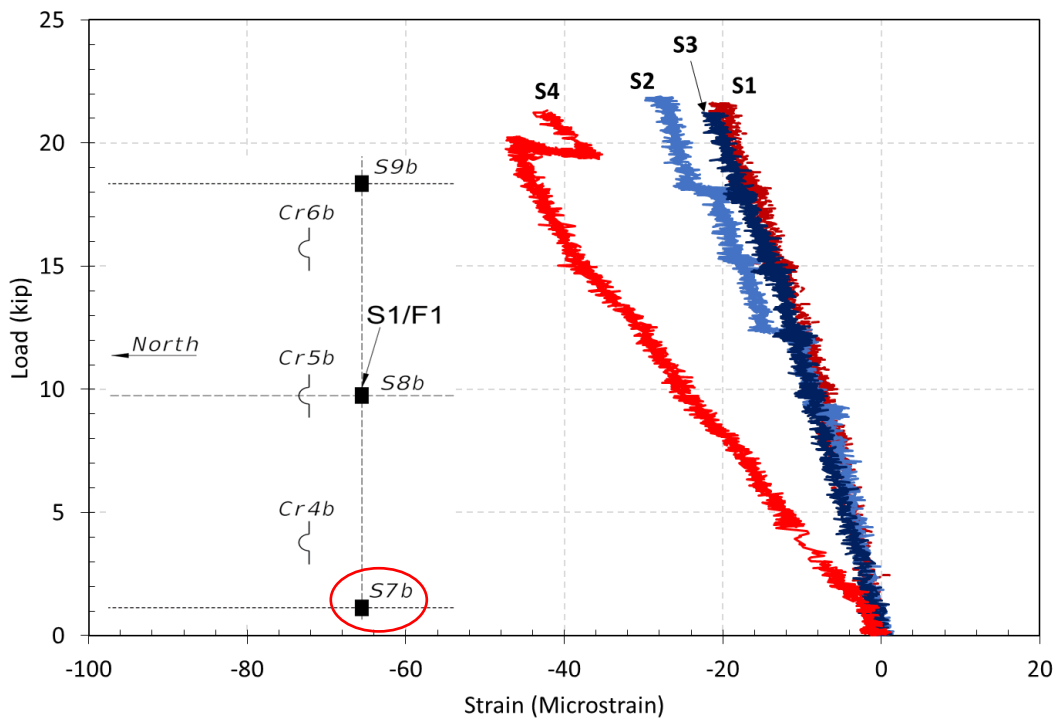


Figure 5.24: Service tests bottom strain gauge S7b

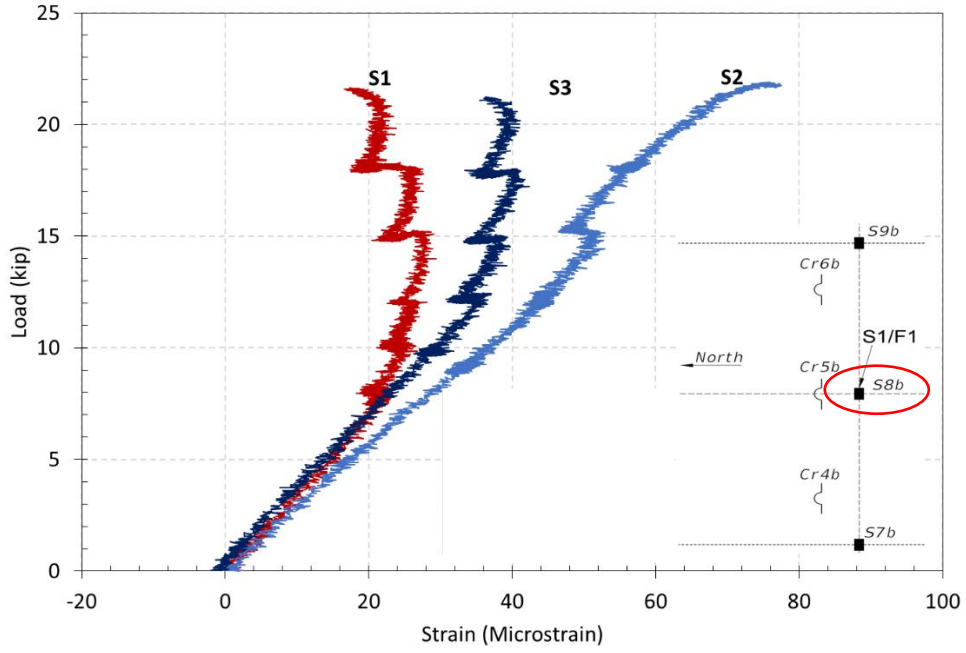


Figure 5.25: Service tests bottom strain gauge S8b

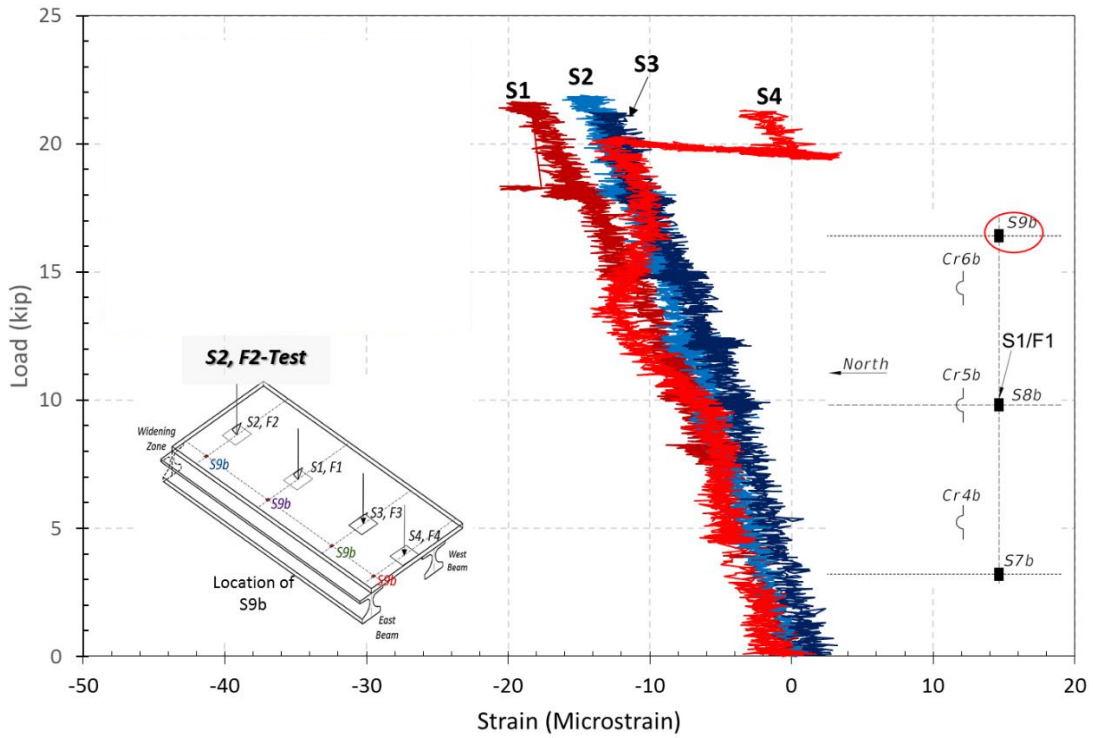


Figure 5.26: Service tests bottom strain gauge S9b

### 5.1.3 Crack Gauges and Widths

In addition to the strain gauges, 200 mm full bridge crack gauges were also installed on the top and bottom surfaces of the concrete deck in an attempt to continuously capture strain once the deck cracks. In this section, we select two service test cases, S1 and S2, to present the results from these gauges. As stated earlier, we did not observe any cracking visually under service load levels. Without cracking, these gauges should indicate very small changes in readings, which can be converted into equivalent strains using their corresponding gauge length. If cracks do take place but do not pass within the gauge length, a drop in the crack gauge readings should be expected. The crack gauge plots can be seen in Figure 5.27 through Figure 5.30. It should be noted that these gauges had to be shifted 1 ft from the transverse line passing through the applied load because of the loading pad and other installed gauges.

In all cases, only the gauges that are directly aligned with the applied load (Cr2t and Cr5b) recorded changes in the range of 0.02-0.03 mm. The crack gauges that were not directly under the load (Cr1t, Cr3t, Cr4b, and Cr6b) recorded minimal changes, albeit of the same sign as the readings from the gauges directly aligned with the applied load. None of the gauges showed any abrupt changes as an indication of crack initiation. This further corroborates the previous observations that no cracking took place in the conducted service test cases.

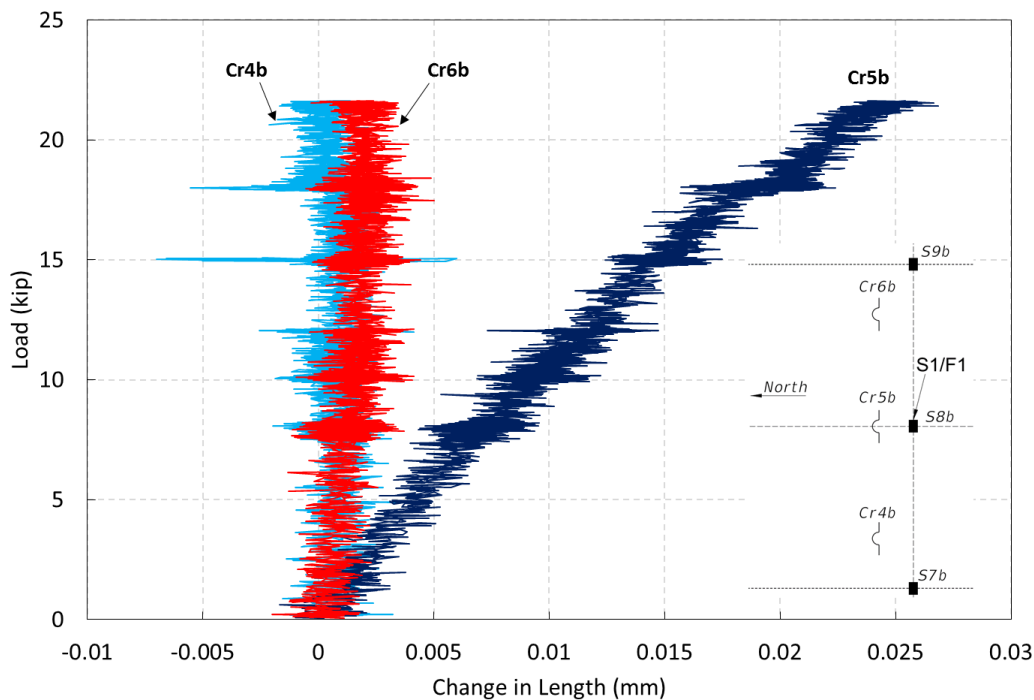


Figure 5.27: Service test S1 bottom crack gauges

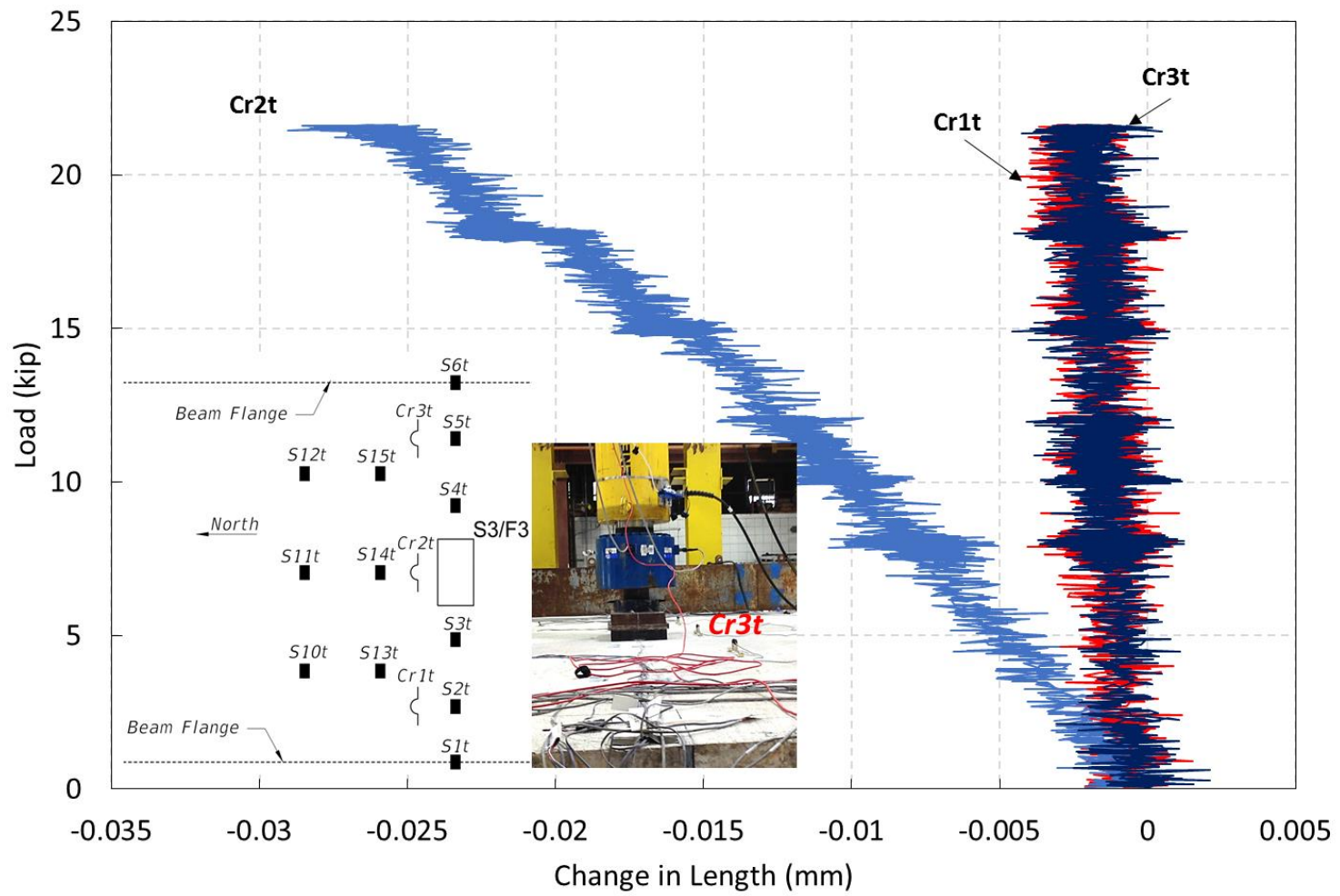


Figure 5.28: Service test S1 top crack gauges

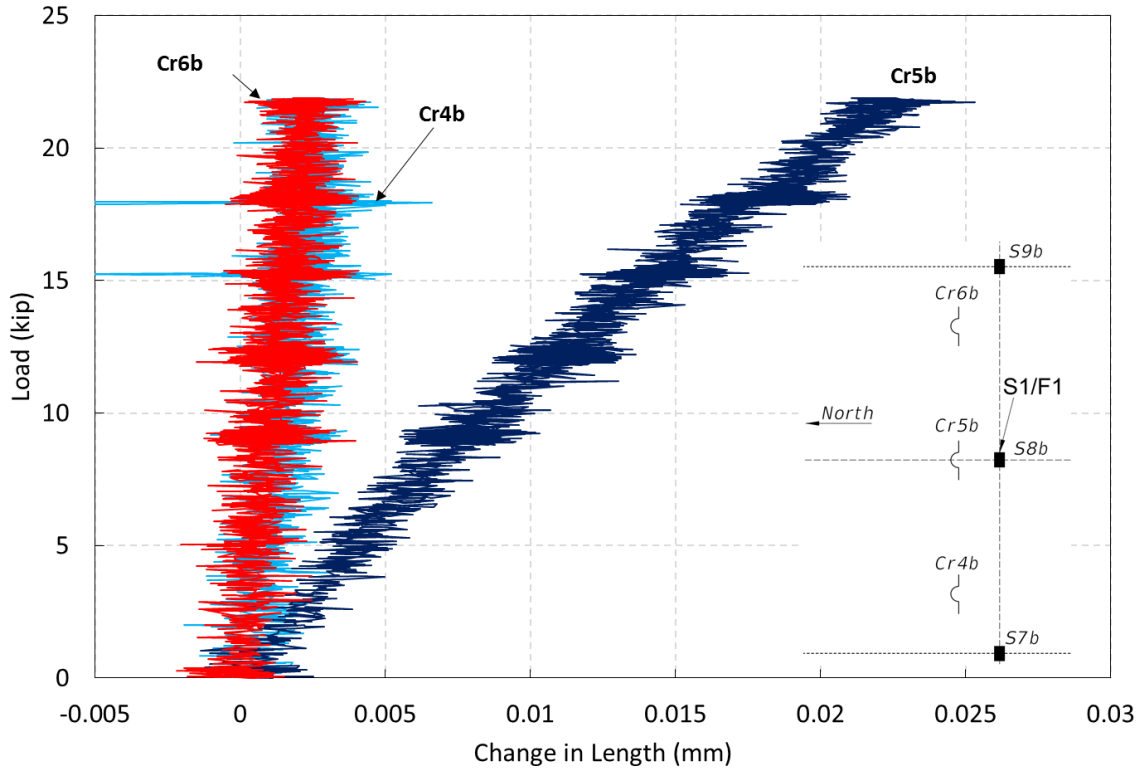


Figure 5.28: Service test S2 bottom crack gauges

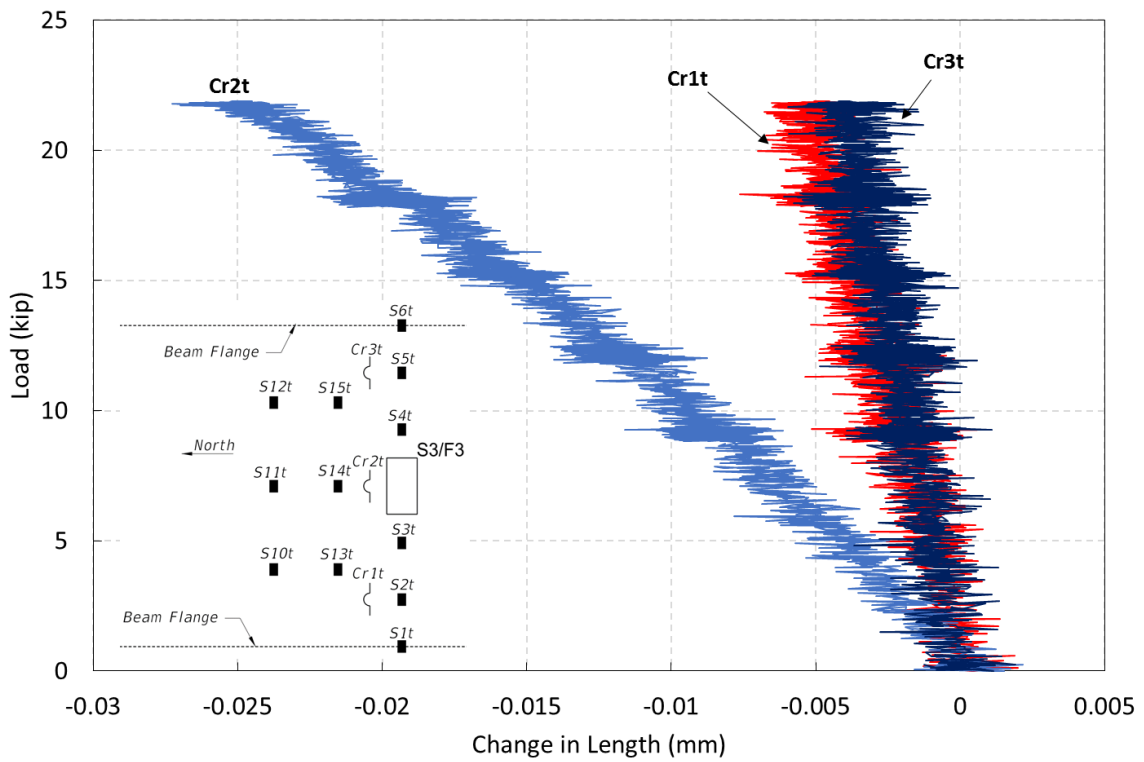


Figure 5.29: Service test S2 top crack gauges

To further test this hypothesis, Figure 5.30 was plotted for S1 to show a comparison between a crack gauge reading after converting it to strains and a rebar strain gauge at the same location, namely Cr5b and TB7. As can be seen, the plots are almost identical and the strain levels are below the estimated concrete cracking strain. Based on this comparison, the readings for TB13 in Figure 5.12 appear to be out of line from all other readings and visual inspection that did not indicate the existence of cracks in any of the service load test cases. Cracks were monitored during the strength load cases for load levels beyond the service load limit. All crack patterns from the failure tests were mapped and plotted, which can be found in Appendix VII.

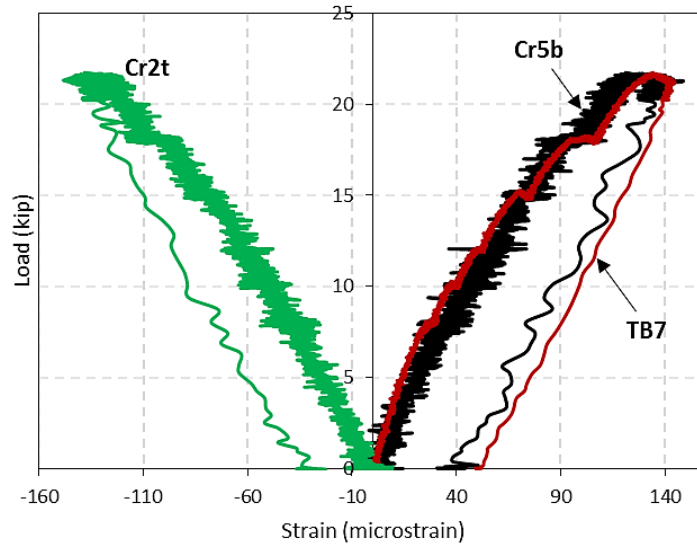


Figure 5.30: S1 crack gauge vs. transverse gauge

The specimen was visually examined for structural crack development during loading at intermittent intervals. As soon as cracking commenced or became visually apparent, a small handheld microscope was used to determine the crack width opening, and each observed crack was marked along its length and denoted by the magnitude of the applied load at the time it was measured. To protect the equipment, the laser gauges were removed from underneath the slab when the vertical applied load reached 100 kip for the F1 load case. At that load level, some structural cracks had already started to develop at the bottom of the slab. At higher load levels, horizontal hairline cracks were noticed on the outer web of east beam; i.e., the widening side at midspan.

Figure 5.31 shows a sketch of the crack pattern taken during the F1 load test. In the figure, the main cracks are identified by numeric values (① through ⑥). Table 5.2 provides more details about each of the identified main cracks. Table 5.3 lists the crack width data for S1/F1 test cases, measured during retesting. It should be noted that the listed results were obtained during the retesting of load case F1; i.e., crack initiation had already happened during the first F1 loading that reached 100 kip. It can be seen that crack widths up to the identified service load level, 22 kip (97.8 kN), are considered acceptable. This is based on the on the limit most manuals used in practice consider as not in need for action to repair. The 2015 FDOT Standard Specs, Section

400-21, lists, lists the actions to be taken based on exposure type, cracking significance range, elevation range, and crack width. It can be seen that for a typical bridge over land or with 12 ft Above Mean High Water (AMHW), that no treatment is needed (NT) up to crack widths of 0.01 in. (0.254 mm) for isolated cracking under all exposure conditions. The recorded crack widths under the identified service load level were in the range of 0.006 in. and 0.0085 in. (0.0152 mm to 0.216 mm) for Cracks ② and ⑤, respectively. For this maximum observed crack width under service conditions, the 400-21 specification calls for no treatment (NT) under normal conditions of exposure and significance and calls for the use of Methacrylate (M) or Epoxy injection (EI) if exposed to moderately aggressive conditions with high significance. It should be noted that most newly constructed decks are built using stay-in-place (SIP) forms, therefore, the cracks may be considered to be isolated from exposure to the environment or at least the level of aggressiveness will be reduced because of the existence of the SIP forms.

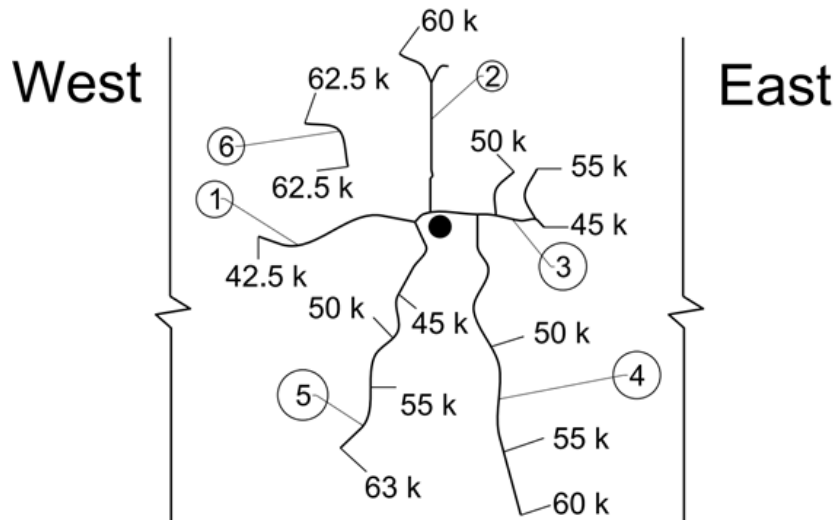


Figure 5.31: Crack pattern underneath the F1 test (dark circle represents load center)

Table 5.2: Crack Location and Orientation for the bottom surface of the F1 Test

Location #	Distance from Load Point (in)	West of Centerline (in)	East of Centerline (in)	Crack Orientation
①	2.5	13	---	Transverse
②	7	1	---	Longitudinal
③	3	---	4	Transverse
④	7	---	4	Longitudinal
⑤	4	7	---	Long/Diagonal (NW)
⑥	11	16	---	Diagonal (SW)

Table 5.3: Crack Widths for the bottom surface of the F1 Test

Load (kip)	Crack Width Measurements (in)					
	Crack ①	Crack ②	Crack ③	Crack ④	Crack ⑤	Crack ⑥
0	0.002	0.0002	0.003	0.002	0.004	0.0002
20	0.003	0.0002	0.005	0.004	0.008	0.003
25	0.005	0.001	0.005	0.006	0.009	0.004
30	0.009	0.001	0.007	0.007	0.010	0.004

Table 5.4 and Table 5.5 show crack width information for the F4 test. All the observed cracks in the bottom surface of this test case were longitudinal cracks and were present at the start of testing F4 due to the previous tests. It can be seen that under service conditions that the crack widths are in the same range as what has been discussed for the S1/F1 case. Therefore, a similar conclusion may be drawn.

Table 5.4: Crack Location and Orientation for the bottom surface of the F4 Test

Location #	South of Slab Edge (in)	West of Centerline (in)	East of Centerline (in)
1	21.75	---	---
2	9.75	---	6
3	14.00	7.5	---
4	7.75	18.5	---
5	13.00	---	22

Table 5.5: Crack Widths for the bottom surface of the F4 Test

Load (kip)	Crack Width Measurements (in)				
	1	2	3	4	5
0	0.001	0.001	0.002	0.002	0.001
20	0.005	0.005	0.005	0.002	0.001
25	0.005	0.008	0.008	0.004	0.003
30	0.009	0.010	0.010	0.005	0.003
35	0.010	0.013	0.013	0.003	0.0045
40	0.012	0.020	0.014	0.004	0.004

## 5.2 Failure Test Results

In this section, results obtained from the failure tests F1, F2, F3, and F4 are presented. Figure 5.32 shows the failure load for the five different failure load cases.

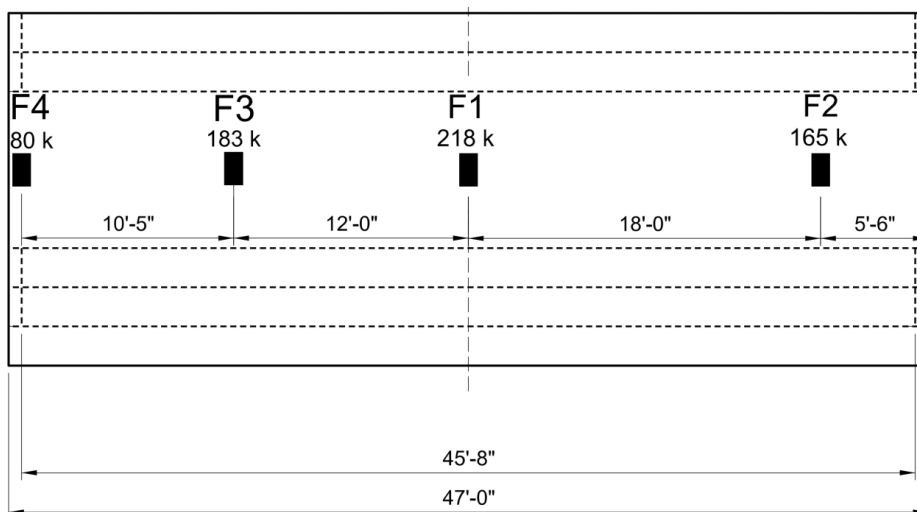


Figure 5.32: Failure test ultimate loads

The maximum load that was recorded for F1 was 218.1 kip and the deflection under the point load reached 3.23 in. (including pad and jacking beam deformations). Adjusted deflection results gave a deflection of approximately 2 in. at failure. In addition, it was noticed during testing that the FIB girders experienced lateral deformation as the vertical load increased. The pattern of failure of the slab observed during failure tests was of typical compressive membrane action (CMA) followed by a punching shear failure.

The size of the failure zone at the top surface of F1 was slightly larger than the size of the loading pad, which is taken to be 10 inches x 20 inches simulating the size of the wheel contact area, per current AASHTO LRFD standard. The damage at the bottom surface of the slab exhibited an elliptical shape with diameters of roughly 95-in. x 80-in in the transverse and longitudinal directions.

The second failure test of the deck slab, F2, failed at a load of 165 kip in a similar manner to the observed failure mode for the F1 test; i.e., CMA with a punching shear. The damage at the bottom surface of the slab has an elliptical shape with diameters of approximately 98 inches transversely by 105 inches longitudinally.

A close comparison between the failure loads for cases F1, F2, F3 and F4 has confirmed the effect of the ability of the deck to distribute the load longitudinally, i.e. equivalent strip width, on the strength of the deck slab. The higher strength of the deck slab in load case F1 is a result of its location, which allows for a wider area of load distribution as a result of being supported on the most flexible portion of the girder (midspan) and being away from the limiting influence of the deck edge. In other words, it can be said that the failure load for load cases F1 (218 kip), F3 (183 kip), F2 (165 kip), and F4 (80 kip) correlate to the distance from the deck edge in the longitudinal direction. The size of the failure zone at the top surface of F1 was slightly larger exceeded the expected failure loads calculated from flexural capacity, punching shear capacity, and the factored AASHTO wheel load with appropriate equivalent strip width. The expected failure capacity was approximately 108 kip, for concrete compressive strength of 8,500 psi, using the method by Taylor (Taylor et al., 2007). Another predicted capacity of 101.96 kip (Table 3.2) was based on  $f'_c$  of 5,000 psi. The calculated flexural capacity assuming pure bending behavior was estimated to be 26.5 kip, the expected punching shear was calculated according to AASHTO and ACI as 175 kip for all load cases except for F4.

The AASHTO LRFD factored wheel load was 37.2 kip. It can be seen from the test results that the concrete deck resisted high failure loads of up to 4 to 6 times the factored load that would be used in design of such a deck. The aforementioned design wheel load includes the effect of dynamic impact magnification factor (IM) and Strength I load factor ( $1.75 \times 1.33 \times 16 = 37.24$  kip). The only exception for this conclusion is Case F4 as a result of being right at the edge of the deck, however it still resisted more than twice the design wheel load. Based on these results, it can be said that decks designed using the empirical method exceed strength requirements in a widening scenario. It should be noted that even though the actual concrete strength was higher than the design value of 4,500 psi, the reduction in deck resistance will not be to the extent that it would drop below the required strength. This is based on the mode of failure that was observed from the tests and is discussed next.

For equivalent strip width (AASHTO LRFD section 4.6.2.1) is given in Equation 46,

$$E = 26.0 + 6.6 S \quad \text{Eq. 46}$$

The flexural capacity was calculated using Equation 47.

$$M_n = A_s f_y \left( d - \frac{a}{2} \right) \quad \text{Eq. 47}$$

The corresponding failure load was found to be 24.4 kip assuming a simply supported slab of an equivalent strip width equal to 9ft-10in. (3.01 m). However, if the continuity is accounted for, the flexural capacity will be increased to approximately 26.5 kip. The test results indicate that the failure mode was not purely flexure since the failure load exceeded the estimated the pure flexure failure capacity by about 6 to 8 times for load cases F1, F2, and F3. This is an indication that the deck behavior does not follow the classical bending theory. The higher failure loads

happened when the deck suddenly failed around the applied load in a manner similar to classical punching shear.

Punching shear was estimated by using AASHTO LRFD equation 5.13.2.5.4-1 and 5.13.3.6.3 (Equation 48 and 49), which is essentially the same equation that is given by ACI equation 11-5 with the slight difference being that the AASHTO equation is expressed in kip while ACI expresses the punching shear capacity in lbf. Equation 48 is more applicable to two way shear such as the non-edge load tests and Equation 49 more suitable towards edge loads such as the F4 load case. The constant and square root of the compressive strength of concrete remains the same.

$$V_n = \left(0.063 + \frac{0.126}{\beta_c}\right) \sqrt{f'_c} b_o d_v \leq 0.126 \sqrt{f'_c} b_o d_v \quad \text{Eq. 48}$$

$$V_n = 0.125 \sqrt{f'_c} (W + 2L + 2d_e) d_e \quad \text{Eq. 49}$$

where  $W$  is width of loading pad (inch),  $L$  is length of loading pad (inch),  $d_e$  is effective depth from extreme compression fiber to centroid of tensile force (in.),  $\beta_c$  is the ratio of long side to short side of the rectangle through which the concentrated load is transmitted,  $b_o$  is the perimeter of the critical section in inches,  $d_v$  is the effective shear depth in inches ( $d_e$ ).

According to the AASHTO LRFD Bridge Design Specifications, it is estimated that the punching failure load is 175 kip for load case F1 through F3, and 120 kip for F4. The average of the experimentally observed load levels, excluding load case F4, was 188.9 kip which is close to estimated punching shear failure load. The variations of these loads (218 kip for F1 and 165 kip for F2) may be attributed to the location of the applied load as a result of proximity to the deck's edge and the girder stiffness which varies from one location to the other. It is known that the punching shear resistance is a function of  $\sqrt{f'_c}$ . As such, the effect of the higher concrete strength used in pouring the lab specimen can be estimated to be a function of the ratios of  $\sqrt{f'_c}$ . In other words, the resistance of a similar deck designed using the design concrete strength of 4500 psi could be estimated by taking the tested results and multiply by 0.73 ( $\sqrt{4,500}/\sqrt{8,500}$ ). This would translate into specimen resistance of approximately 4.44 to 5.86 times (approximately 4 to 6 times) the factored design wheel load.

However, using the method by Taylor (S. Taylor, et al. 2007) described earlier in Section 2.4.4, the controlling failure load was calculated as 108 kip. Deflection at ultimate load was about 2 inches at failure. Comparing the behavior of the tested specimens under different load cases indicated higher deflection when the load was closest to the span edge as seen from the F4 load case. This can be attributed to the smaller equivalent strip width at that location (half of the width available in comparison with interior cases such as F1).

### 5.2.1 Overall Comparison

In this section, an overall comparison between all tested load cases is first presented before a detailed description of the performance of each load case is given. A load vs. strain plot for the failure tests is presented in Figure 5.33. It should be noted that all the shown strains are below the elongations report on the mill test report for the #5 bars used in the specimen's fabrication (see Table 4.4). As stated earlier, load case F4 did not have any direct steel reinforcement strain

gauges in the immediate vicinity of the applied load. Instead, gauges from the F3 test were read and TB1 (closest gauge to F4) is reflected in the plot. It would be expected that the strain in the area directly beneath the load point of F4 would be higher than what is shown Figure 5.33. During testing, it was noticed that data from some of the embedded gauges were not consistent which indicated either the gauges were damaged or failure occurred at the contact surface between the gauges and the steel reinforcement. It is known that strain gauges attached to the reinforcement are prone to experience adhesive mobility at extreme strain values. Therefore, readings from these gauges were either smoothed on the plots to a point before the adhesive failure occurred or taken out and not included within this report.

Table 5.6 shows the maximum test deflection,  $\delta_{max}$ , results at failure. Two values are given for each failure test, namely the raw readings directly recorded from the gauge installed on the hydraulic actuator, and the corrected readings produced by the extrapolation method depicted in Figure 5.1. It should be noted that the listed deflections are not the net deck deflections, but rather include girder deflections as well.

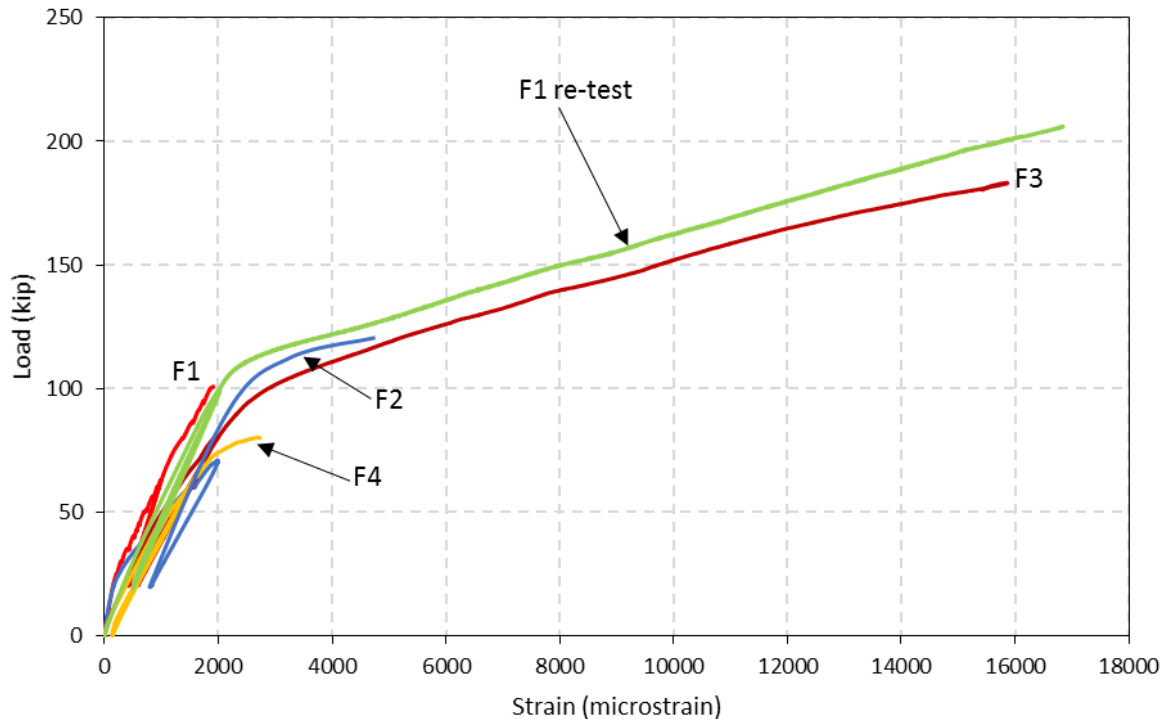


Figure 5.33: Failure tests load vs. strain, displaying TB13

Table 5.6: Failure Test Deflection Results

Failure Test	Maximum Vertical Load ( $P_{max}$ ) (Kip)	Maximum Vertical Deflection $\delta_{max}$ (in)	
		Raw Readings	Corrected Readings
F1	218.12	3.23	2.00
F2	165.45	2.75	1.88
F3	183.29	2.84	1.73
F4	80.25	2.30	2.00

Figure 5.34 through Figure 5.37 show load deflection relationships for all failure load cases at select gauges up to a load level when the test was stopped to remove the laser gauges for protection. Figure 5.34 shows load vs. deflection for gauge D7b for all failure load cases. As expected, the magnitude of the recorded deflections at any given load level was highest for load case F4 as a result of the limited load distribution at the deck's edge.

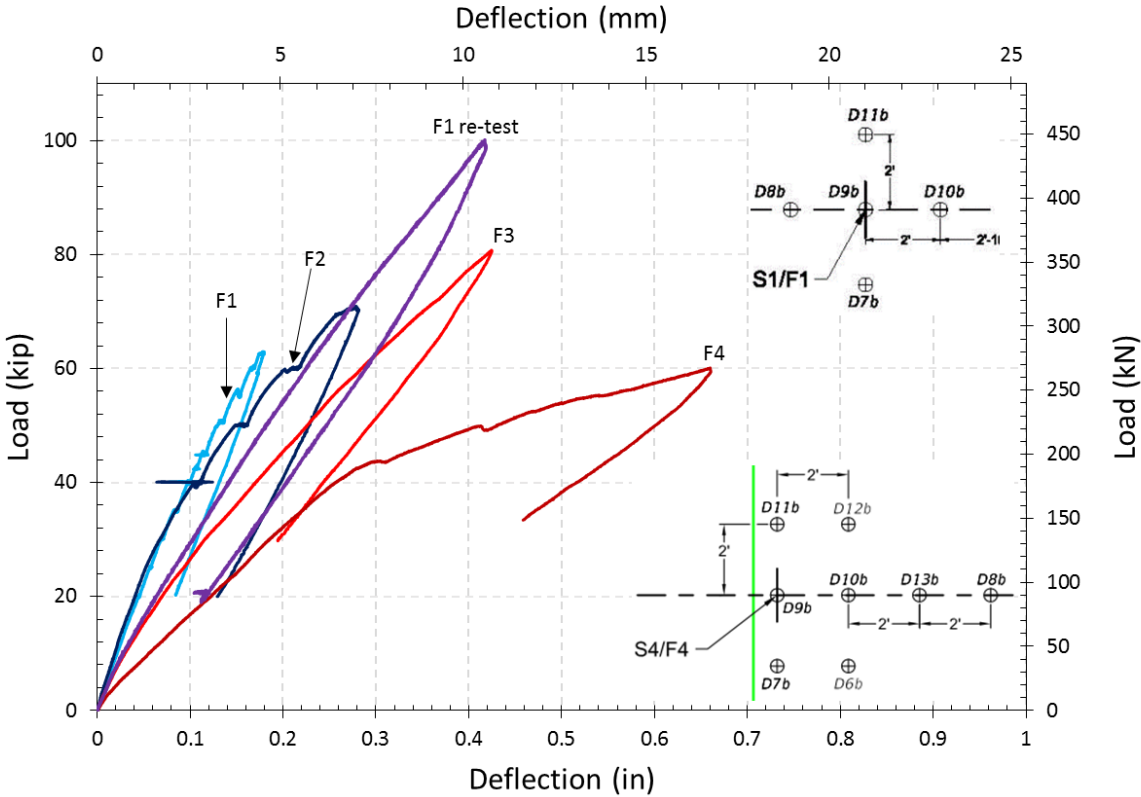


Figure 5.34: Load vs. deflection from failure tests for D7b

It can be seen in Figure 5.35 that deflections from load case F4 were less than deflections recorded during load case F3, which is due to D8b being moved 6 feet away from the center of the load as shown in the lower right corner of Figure 5.35. Figure 5.36 shows deflections for D9b are higher with the F4 case as that load case was at the edge of the slab which has less resistance due to the decreased amount of surrounding concrete slab. Figure 5.38 shows the load deflection relationships up to failure for all load cases. The plotted curves in Figure 5.38 were obtained using the actuator gauge, and later by the extrapolation method depicted in Figure 5.1. Just like Table 5.6, these deflection measurements also include girder deflection.

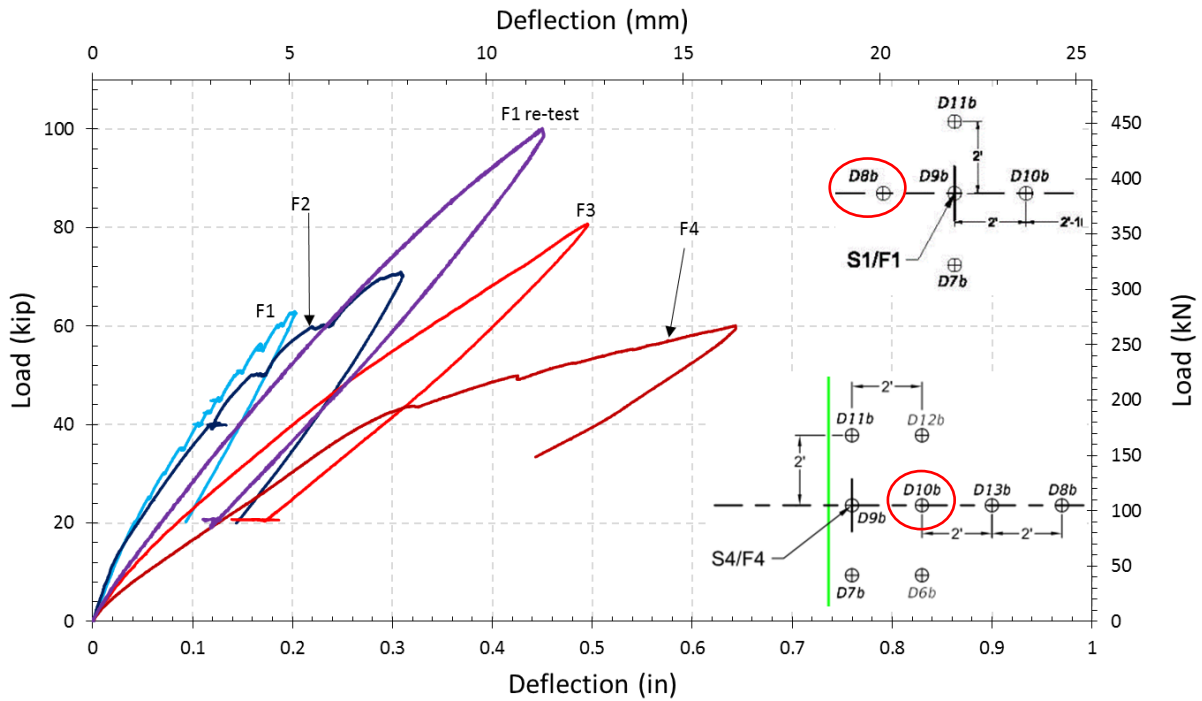


Figure 5.35: Load vs. deflection from failure tests for D8b (load cases F1, F2, and F3) & D10b (load case F4)

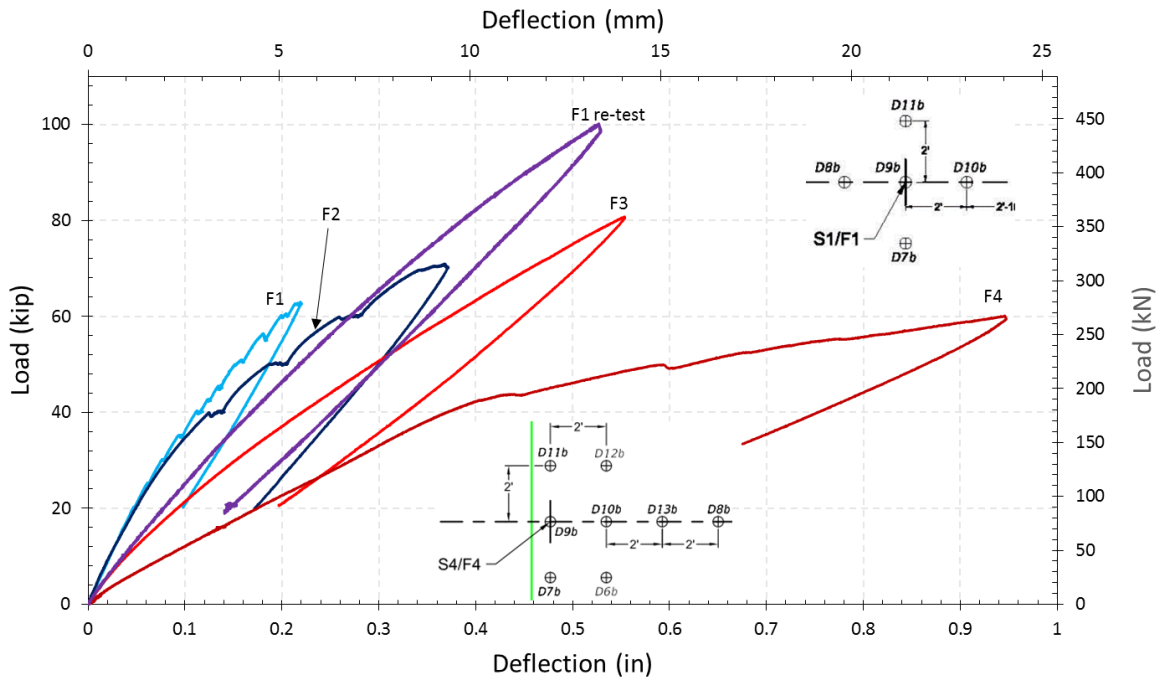


Figure 5.36: Load vs. deflection from failure tests for D9b

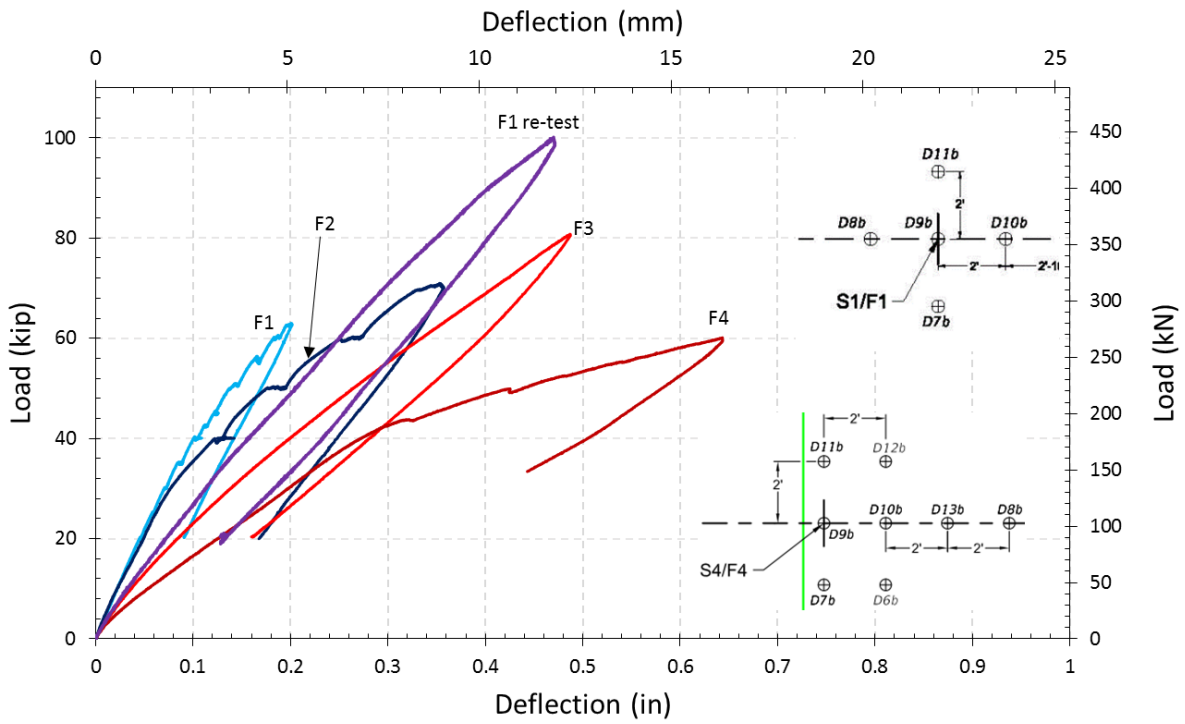


Figure 5.37: Load vs. deflection from failure tests for D10b

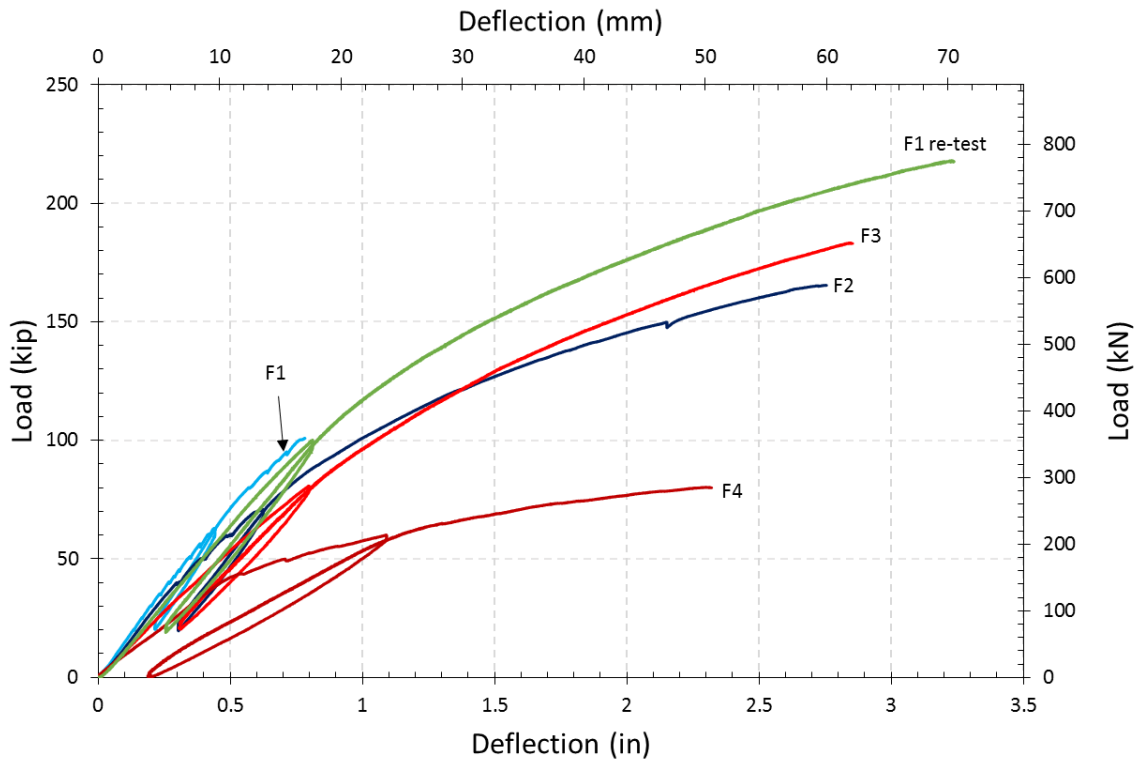


Figure 5.38: Load vs. deflection relations up to failure (raw readings from actuator displacement gauge before corrections)

## 5.2.2 Deck Performance under Load Case F1

### 5.2.2.1 Strain Cross-Sections

Figure 5.39 to Figure 5.42 show the transverse strains along three bottom steel reinforcing bars; namely, one directly under the load and two others at 1 ft and 3 ft from the applied load. It can be seen from Figure 5.39 that the tensile strains reach a peak value under the applied load, which is expected. The extent to which these tensile strains spread is about 3.5 feet in the initial stages of loading (up to 50 kip). As the applied load increased, strain gauges TB12 and TB14 started experiencing higher tensile strains. Beyond these two gauges, the other gauges (TB10, TB11, TB15, and TB16) recorded much lower strain levels that were mainly small compressive strains. This implies that a small level of continuity existed in the deck over the prestressed concrete girder's top flanges. However, these negative moments can be ignored in the design. Nevertheless, top mat reinforcement was installed per the empirical design method which aids the integrity of the connection between the deck and top flange of the girder. In Figure 5.40 and Figure 5.42, a similar behavior is observed confirming that the compressive stresses at the deck ends close to the girder top flanges are extremely small compared to the tensile stresses that take place at midpoint of the deck.

The plotted results show that the maximum recorded strain for the first failure test was about 1900 microstrain for a 100 kip load. This strain level is still below the yield strain of the steel reinforcement (about 0.00207 for Grade 60).

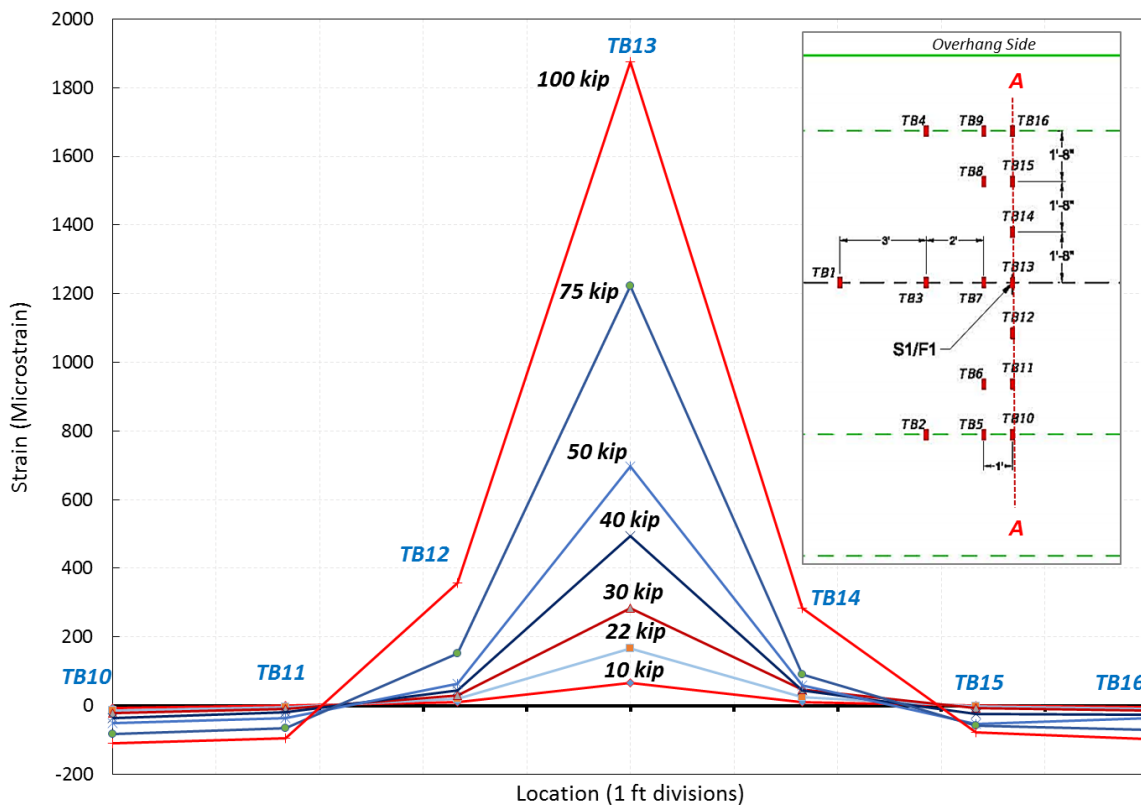


Figure 5.39: F1 Transverse cross-section of bottom transverse strain TB10-TB16

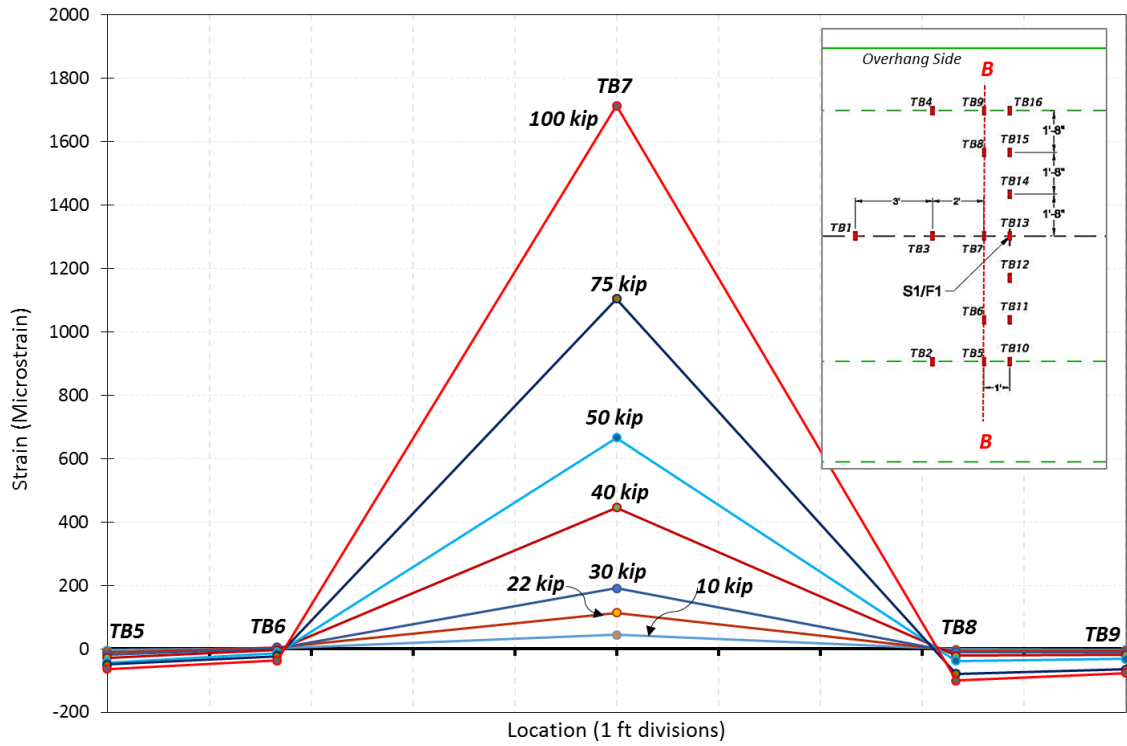


Figure 5.40: F1 Transverse cross-section of bottom transverse strain TB5-TB9

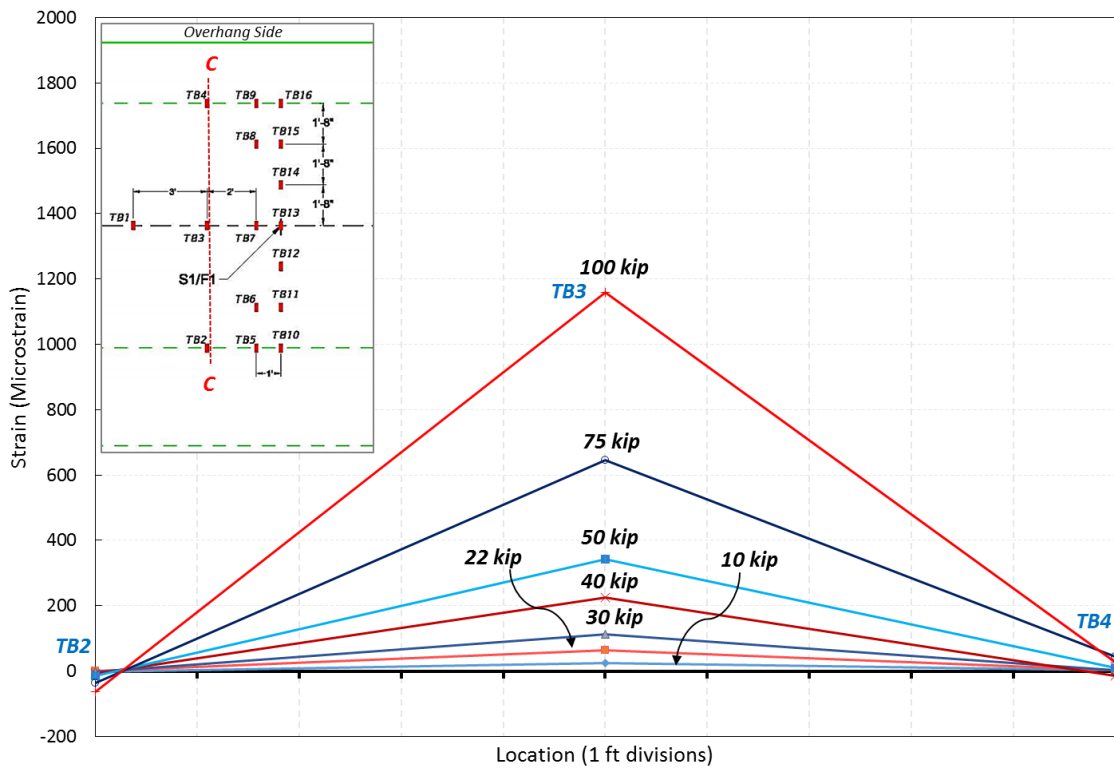


Figure 5.41: F1 Transverse cross-section of bottom transverse strains TB2-TB4

Figure 5.42 is a plot of the same strain data in a longitudinal section of the deck showing that the maximum recorded strains took place under the applied load. Transverse strains away from the applied load drop as the distance from the load increased. However, it can be seen that even the farthest gauge (TB1), which is installed 6 ft away from the applied load still recorded positive strains, which is an indication that the area or distance influenced by the applied load is at least equal to 12 ft (2 x 6 ft).

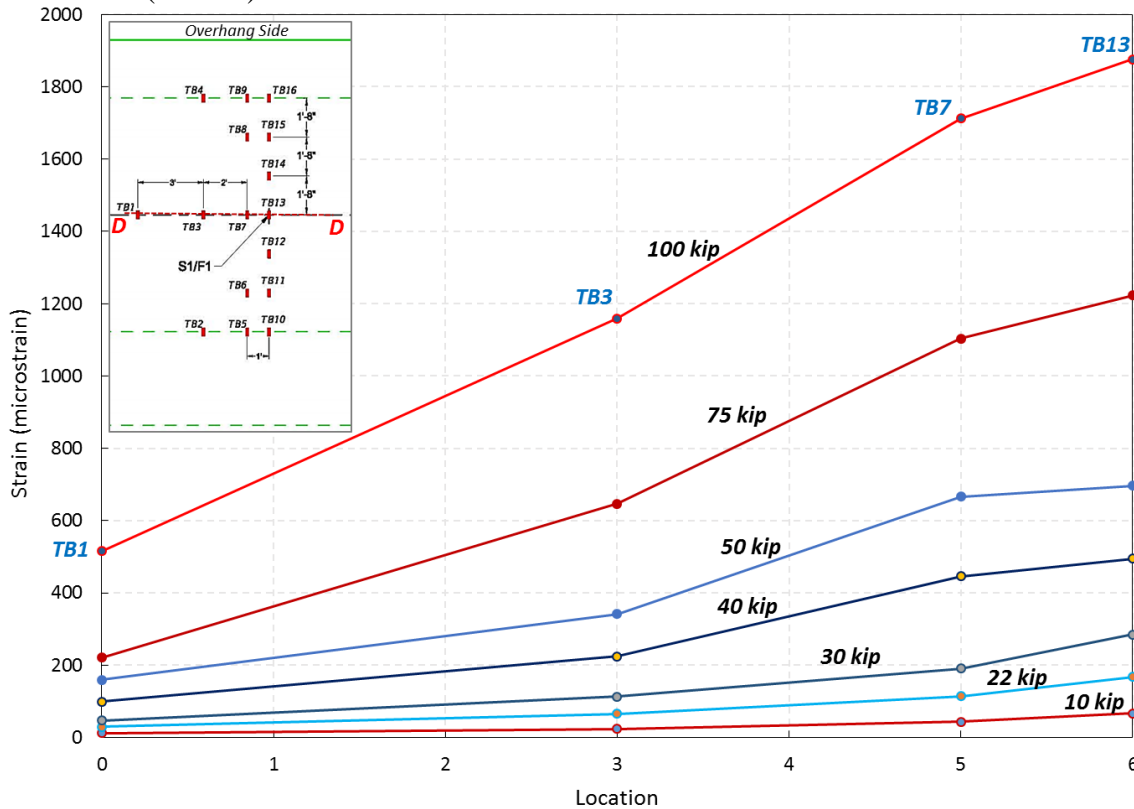


Figure 5.42: F1 Longitudinal cross-section view of bottom transverse strains (TB1, TB3, TB7, and TB13)

Figure 5.43 to Figure 5.45 show bottom steel strain readings in transverse cross sections as obtained from the F1 re-test, which failed at 218 kip. In these figures, the strain plots are shown up to a load near 100 kip. Beyond this level, which far exceeds the required strength load level, several strains started recording erratic readings. For example, Figure 5.46 shows that some gauges experience strain reduction perhaps due to adhesive failure/breakdown at high load levels, e.g. 125 kip. It can be seen that the trends of these plots compared well with the plots discussed previously (Figure 5.39 through Figure 5.41). The recorded strain readings were much higher during the F1-retest than what was observed in the initial loading; i.e. F1. This is mainly attributed to the fact that the slab was uncracked at these load levels during the initial load test (F1). Conversely, the F1-retest started with a precracked slab as a result of reaching a high load level that exceeded the cracking load during F1. This is another observation indicating that cracking did not take place under service load levels.

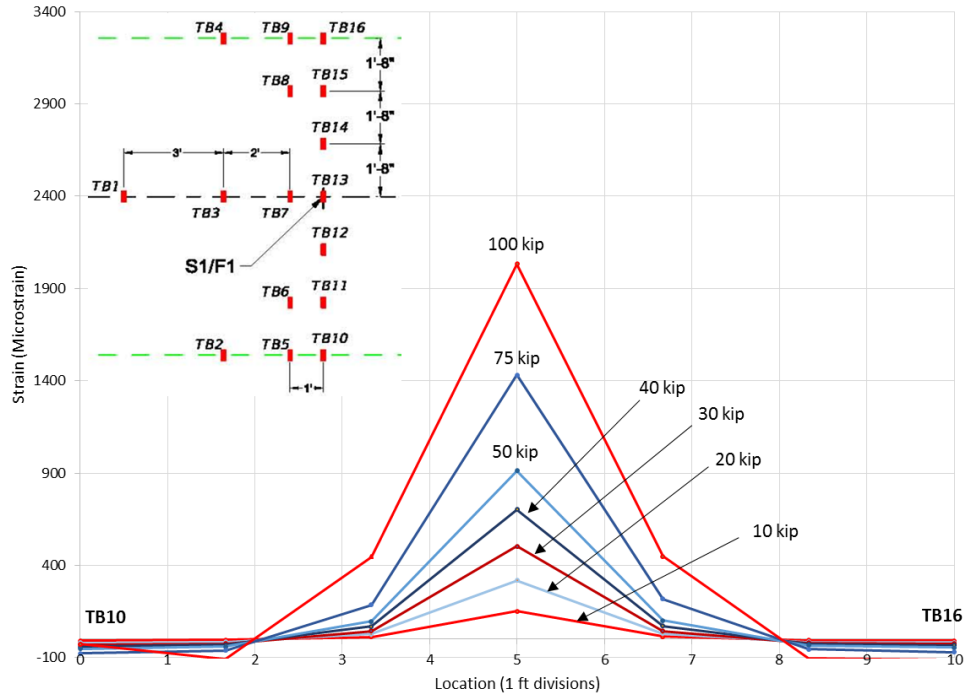


Figure 5.43: F1-retest transverse cross-section view of bottom transverse strains (TB10-TB16)

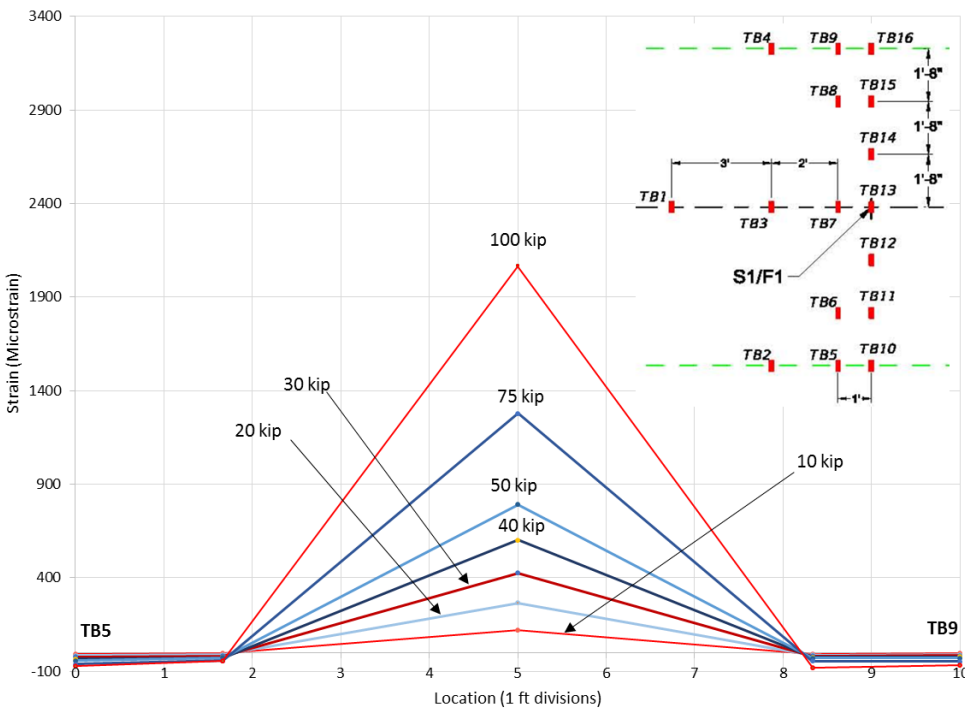


Figure 5.44: F1-retest transverse cross-section view of bottom transverse strains (TB5-TB9)

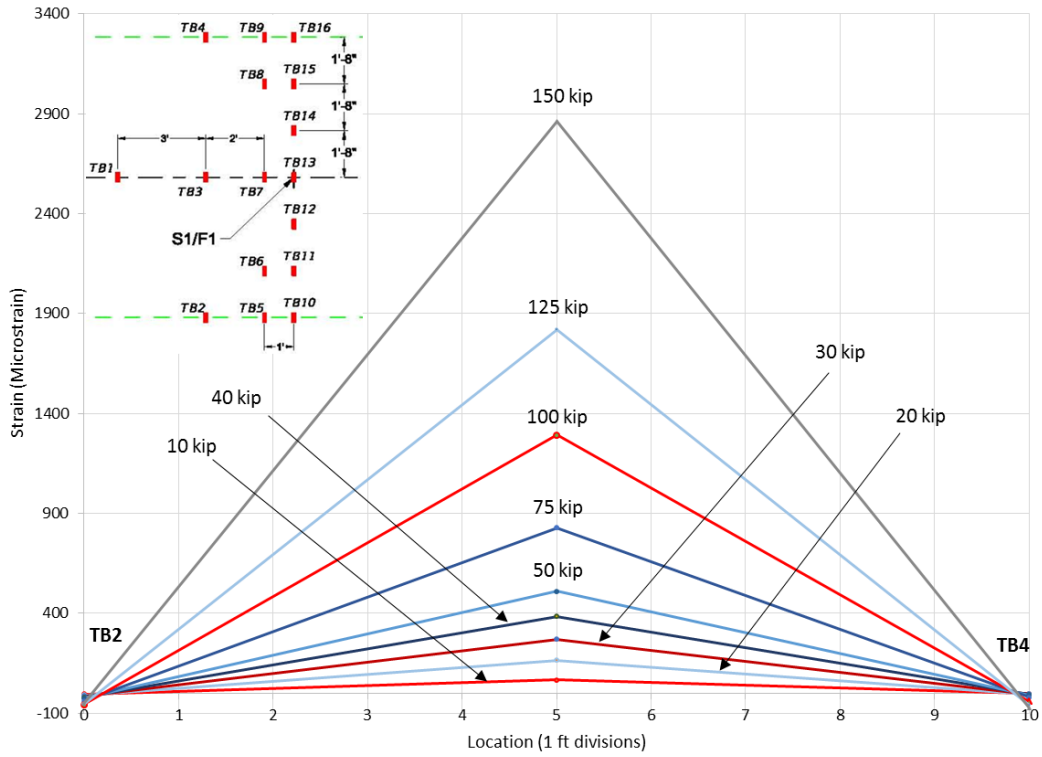


Figure 5.45: F1-retest transverse cross-section view of bottom transverse strains (TB2-TB4)

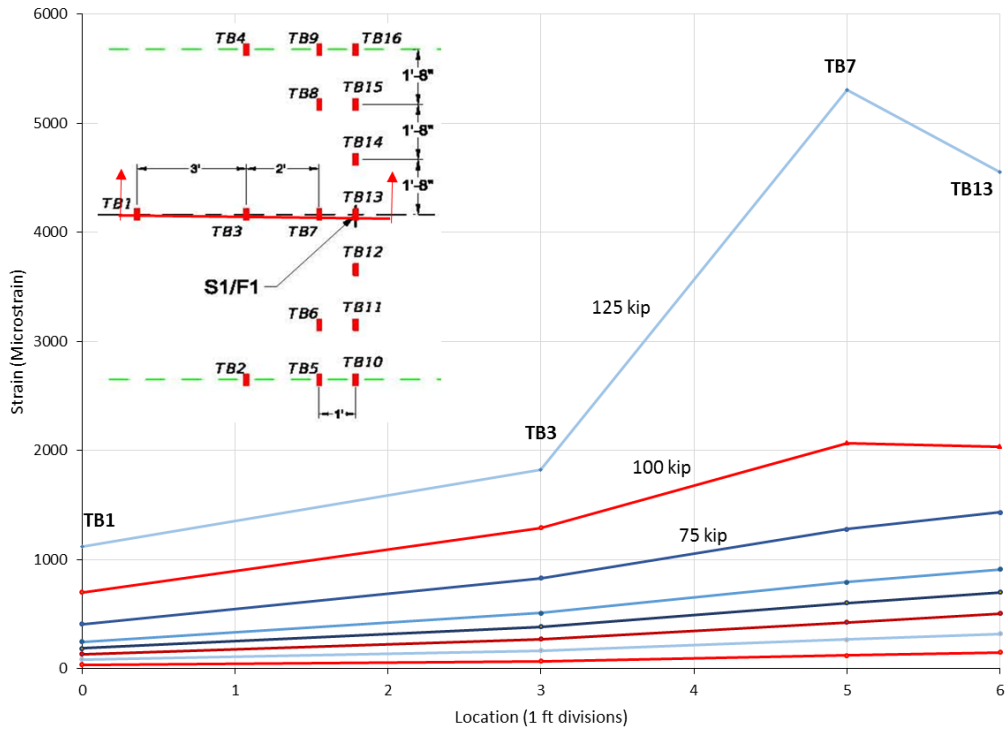


Figure 5.46: F1 re-test longitudinal cross-section view of bottom transverse strains (TB1, TB3, TB7, and TB13)

### 5.2.2.2 Load Deflection

Figure 5.47 is a plot of the load deflection relationship for F1. Two curves are provided in the figure. The one on the right represents the uncorrected reading from the gauge installed on the load actuator, while the other curve is for the same relationship after deducting system flexibility using an extrapolated relationship. At failure, the maximum adjusted deflection was 2 in. compared to the raw deflection including system flexibility of 3.23 in. Even though punching shear is typically considered to be a brittle failure, the recorded deflections at failure are substantial and would be noticed during a field inspection. Figure 5.48 represents the deflection profile at 100 kip for case F1.

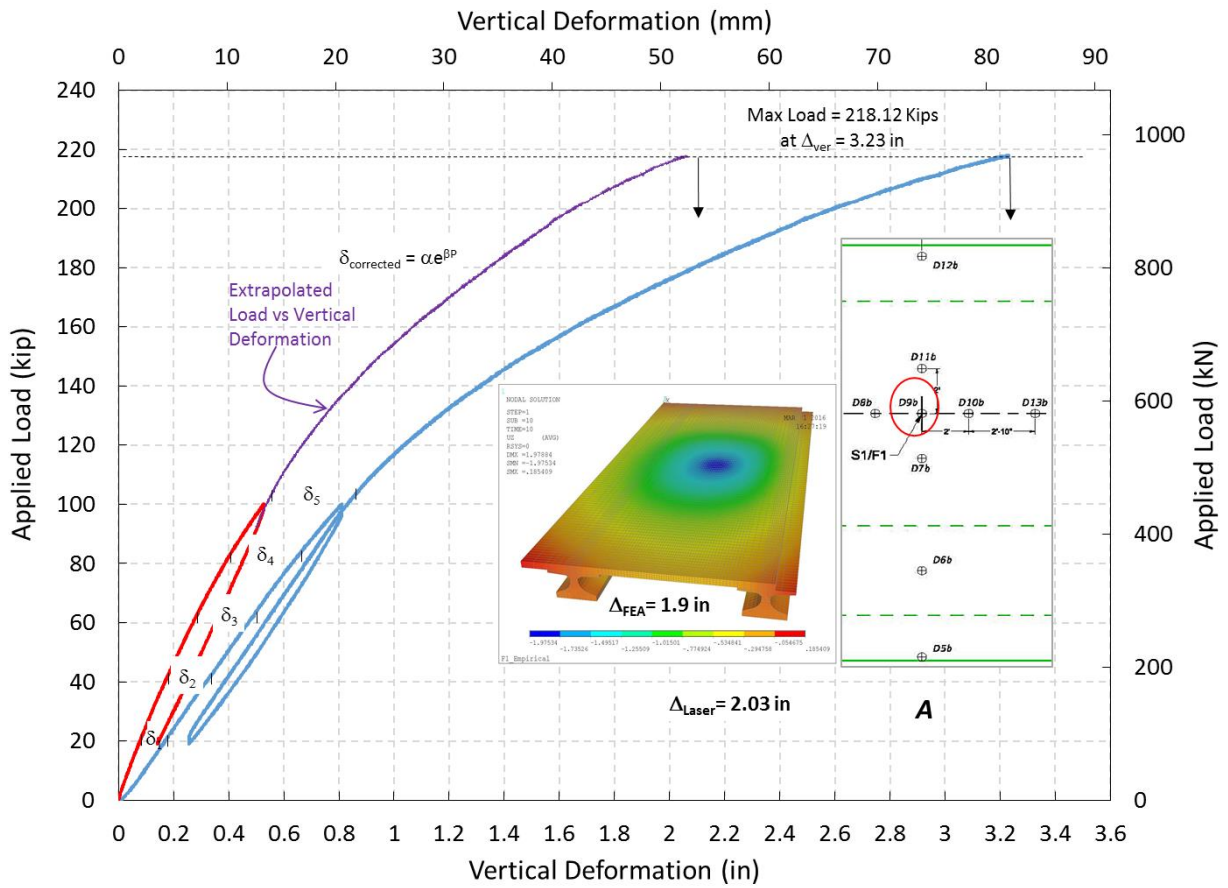


Figure 5.47: F1 Load vs. deflection with extrapolated curve

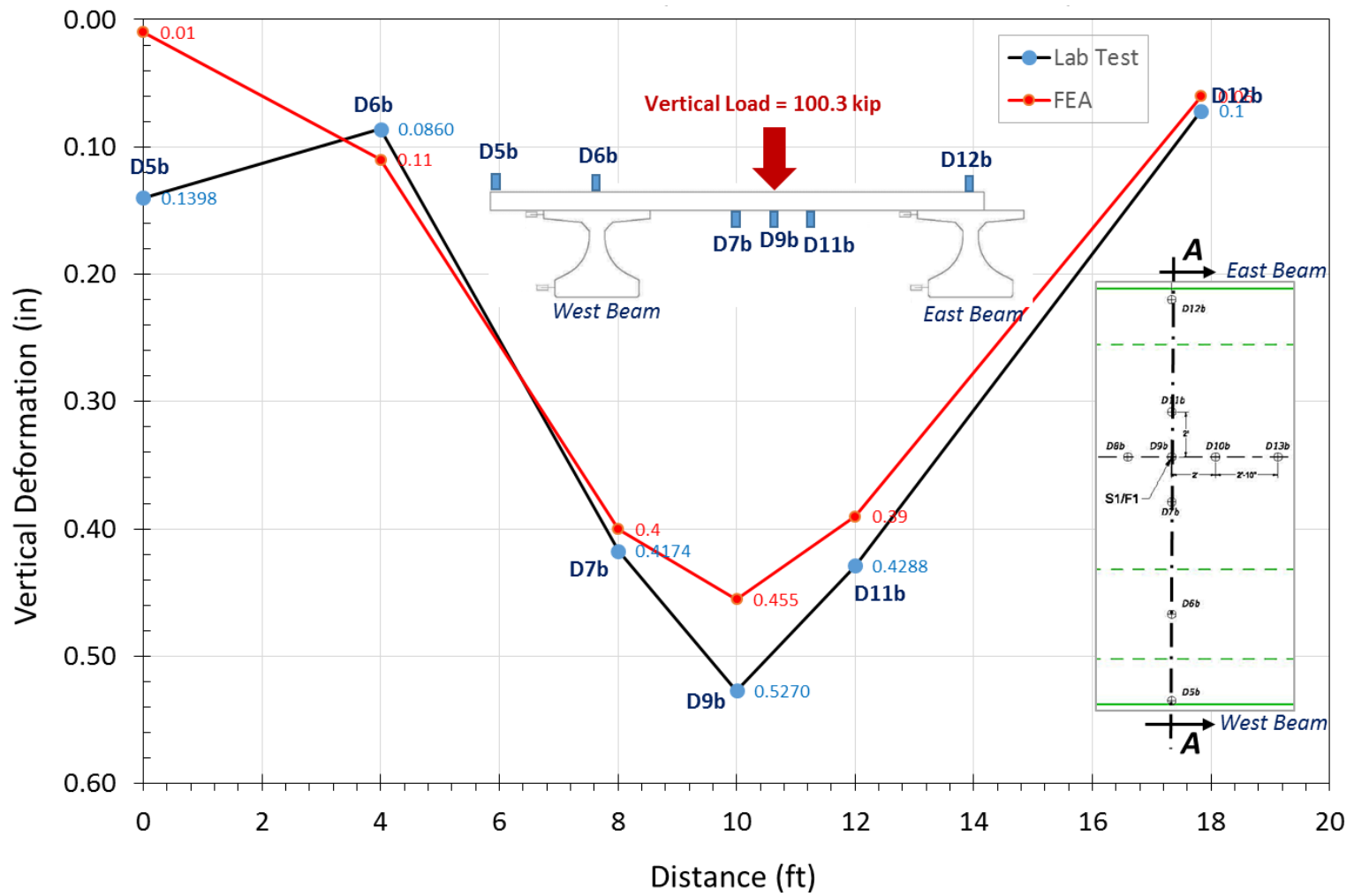


Figure 5.48: F1 deflection profile at 100 kip

### 5.2.2.3 Horizontal Displacements

Figure 5.49 represents load vs. horizontal displacement of girder flanges for load case F1. The plot shows that the displacements increase considerably after a load level of 100 kip. The plot also confirms that recorded displacements at the top and bottom flanges for each girder are different; an indication that the girder undergo a rotational movement due to the applied load. Contrary to the behavior observed for F2 and F3 tests, the D15 gauge recorded a positive displacement; i.e., the bottom flange moved to the inside towards the center of the specimen. This is an unexpected behavior and may be caused by an incorrect wiring connection that reversed sensor polarity or a misinterpretation of the sign convention for that particular gauge. The expected behavior is what has been observed during the F2 and F3 tests, which is also confirmed by the finite element models.

It can be seen in Figure 5.49 that laser gauge D16 readings were not recorded after the second cycle of loading up to failure as it started acting erratically.

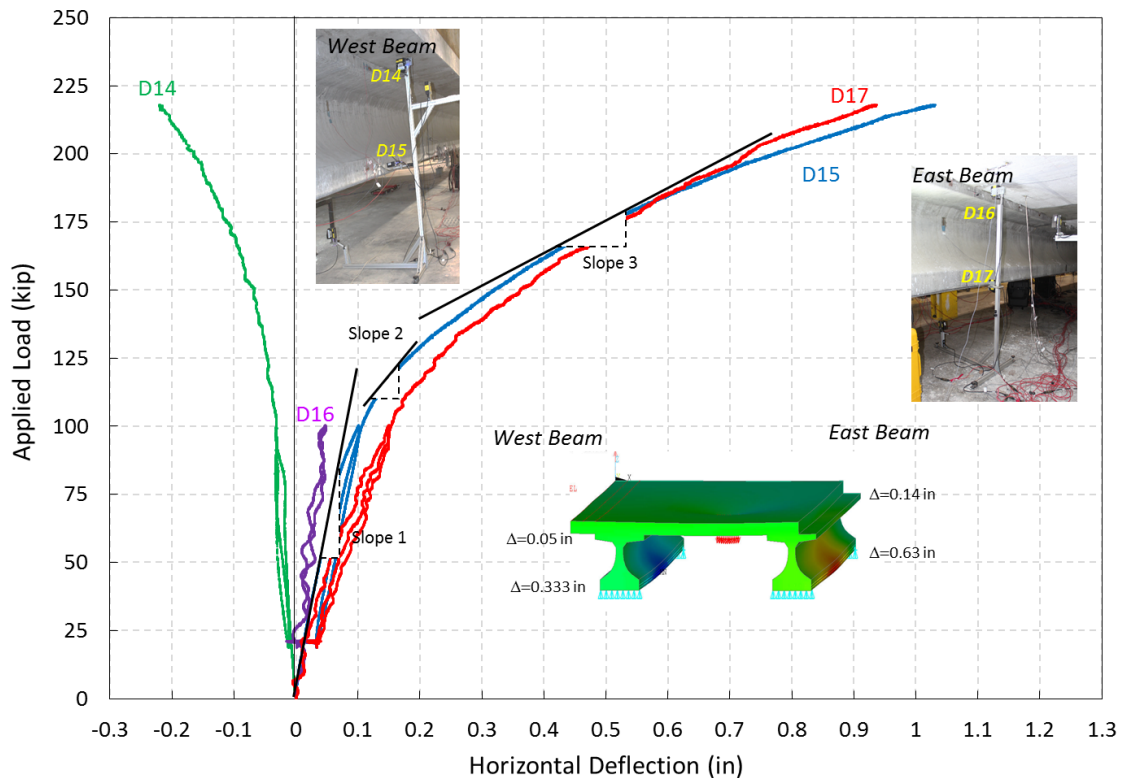


Figure 5.49: F1 Load vs. horizontal displacement of girder flanges

### 5.2.3 Deck Performance under Load Case F2

#### 5.2.3.1 Strain Cross-Sections

Figure 5.50 through Figure 5.52 show strain cross-sections for various load levels, note the yield strain at TB13 being reached between 75 and 100 kip. Figure 5.53 confirms what has been observed for load case F1 with respect to the area influenced by the applied load. It can be seen that at failure, gauge TB1 recorded strains in excess of the yield strain; i.e. the area or distance influenced by the applied load is at least equal to 12 ft (2 x 6 ft). As expected, the recorded strains under the applied load were higher than at other locations with TB13 dropping after reaching 5000 microstrain indicating a malfunction such as failure of the strain gauge / steel bar interface. Figure 5.53 to Figure 5.56 show strain across the transverse and longitudinal bars for both top and bottom mats. Figure 5.57 shows load deflection relationships for load case F2.

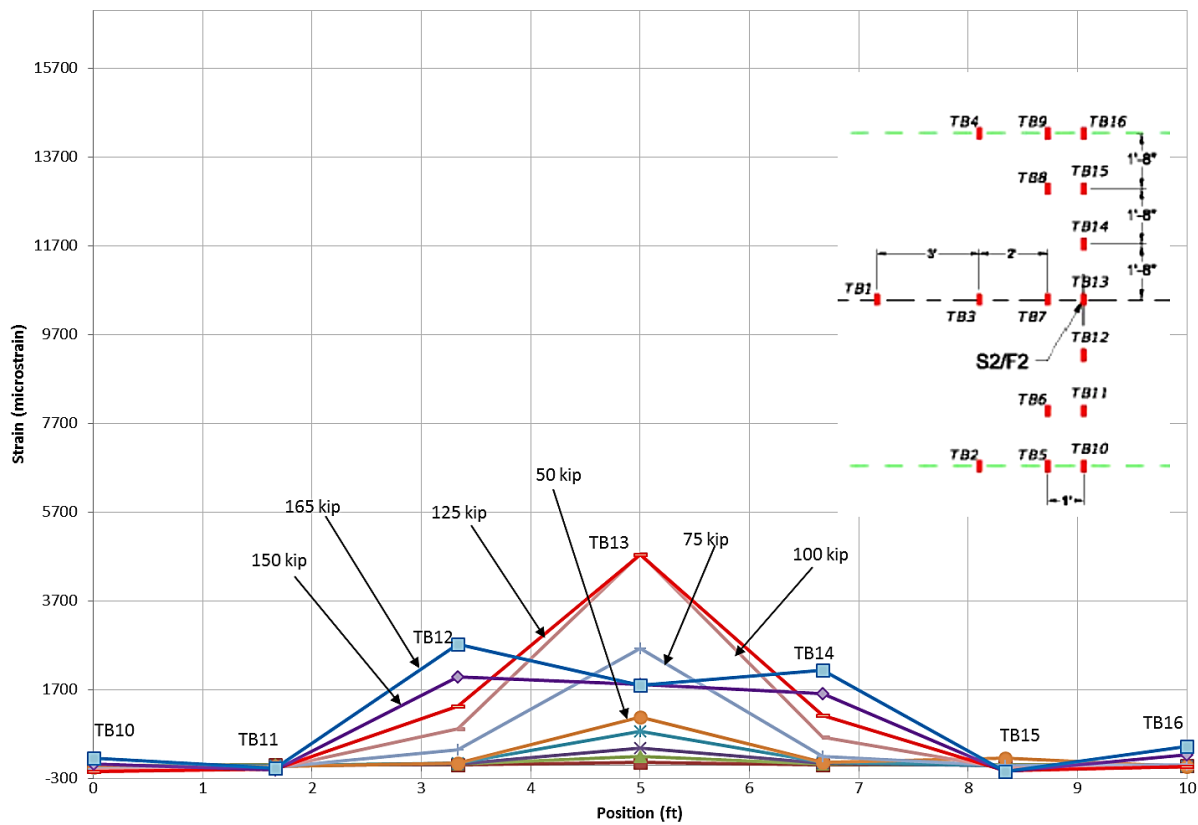


Figure 5.50: F2 Transverse cross-section view of bottom transverse strains (TB10-TB16)

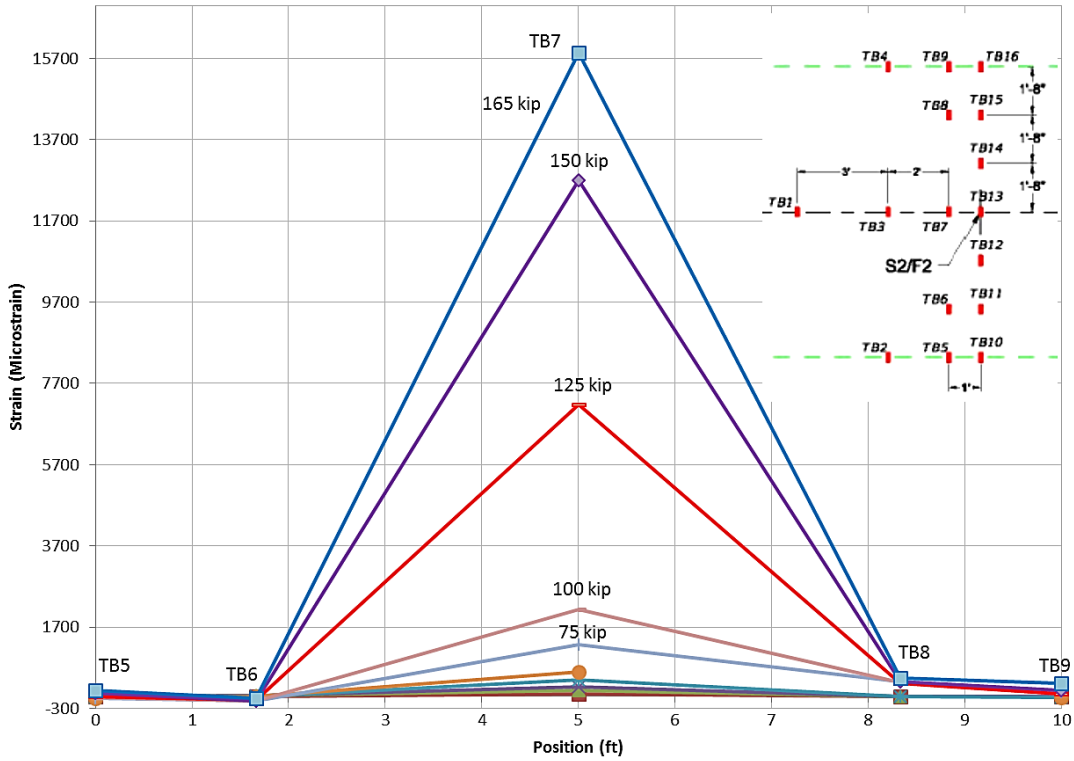


Figure 5.51: F2 Transverse cross-section view of bottom transverse strains (TB5-TB9)

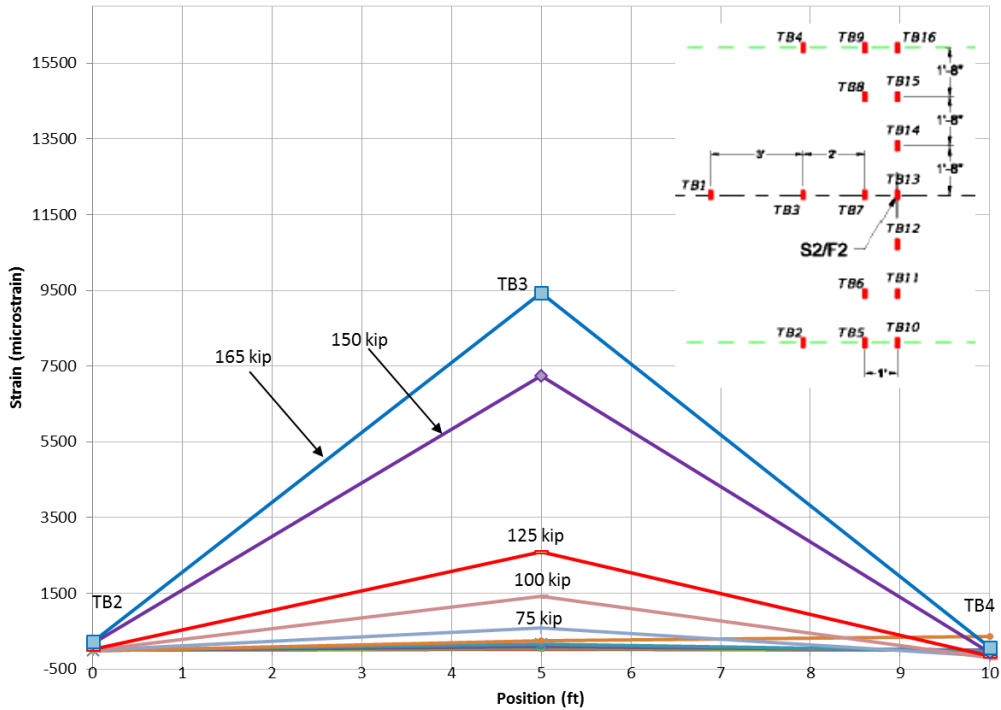


Figure 5.52: F2 Transverse cross-section view of bottom transverse strains (TB2-TB4)

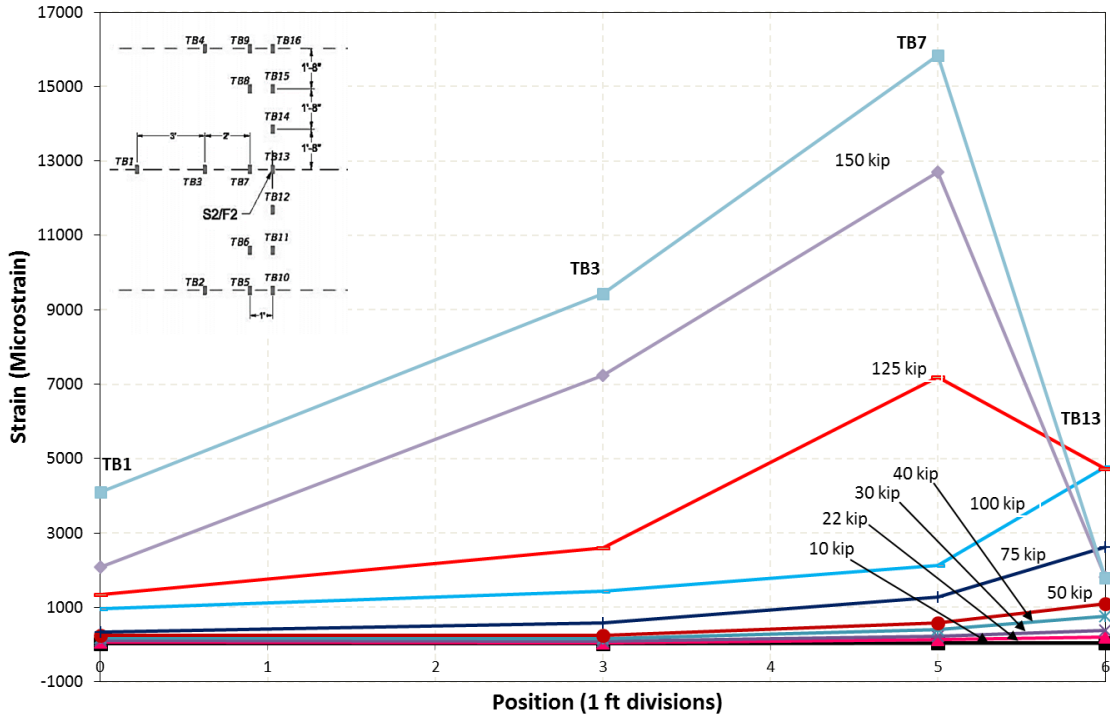


Figure 5.53: F2 Longitudinal cross-section view of bottom transverse strains

Figure 5.54 and Figure 5.55 show plots of the strains recorded from the top embedded transverse rebar gauges. It can be seen that the strains are extremely localized on this side of the slab to the area in the vicinity of the loading pad. For example, both TT6 and TT8 that are at a distance of 1-ft 8-in from the center of the applied load in the transverse directions barely recorded any strains compared to TT7. This is an indication that these gauges (TT6 and TT8 as well as TT3 and TT5) appear to be beyond the direct influence of the loading pad, which can be explained in light of the wheel load transfer dome presented in Figure 2.1. The strain gauges on the top side of the slab beyond the dome's influence area show minimal strain levels compared to the gauges closer to the center of the dome. It should be noted that the positive strain readings recorded at 165 kip, right before failure, by TT3 in Figure 5.54 and TT8 in Figure 5.55, are an exception to the observed trend. This may be attributed to severe dislocation of the failure surface before complete punching takes place. Such strains were not observed at slightly lower loads; e.g. 150 kip.

At the girder's top flange edge, readings from gauges TT1 and TT2 show that positive strains take place in this area. This is due to the aforementioned negative moments that develop as a result of slab continuity over the girders. The magnitude of the strains recorded by TT1 exceed cracking strain levels, which explains the cause of the cracks observed in this area as will discussed later in Section 5.3.

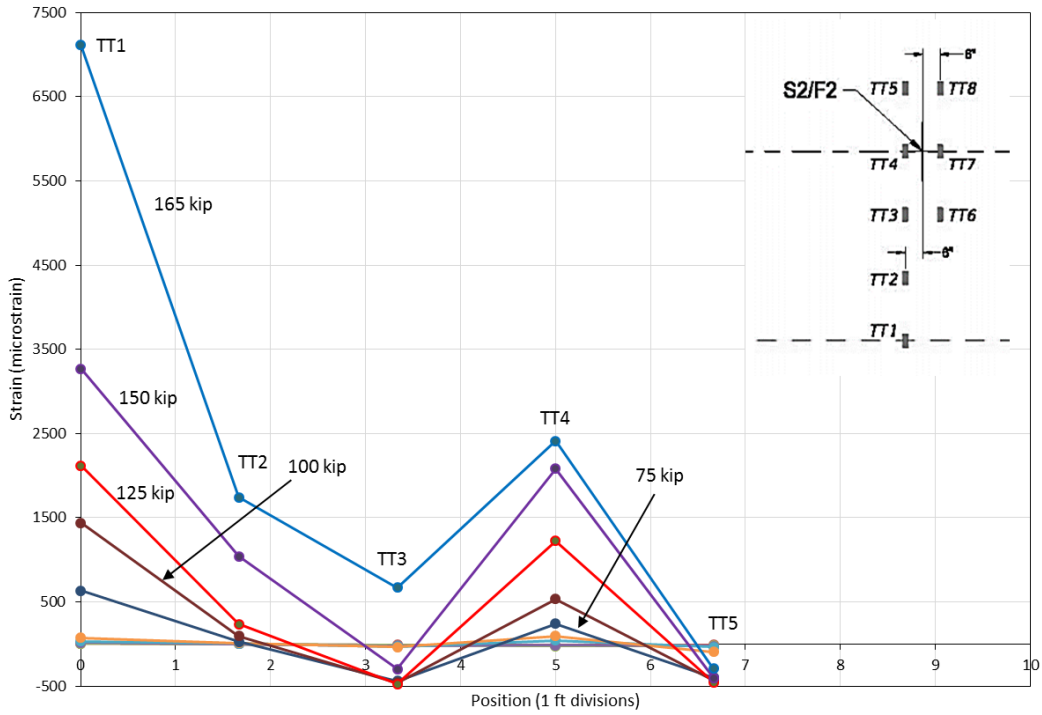


Figure 5.54: F2 Transverse cross-section view of top transverse strains (TT1-TT5)

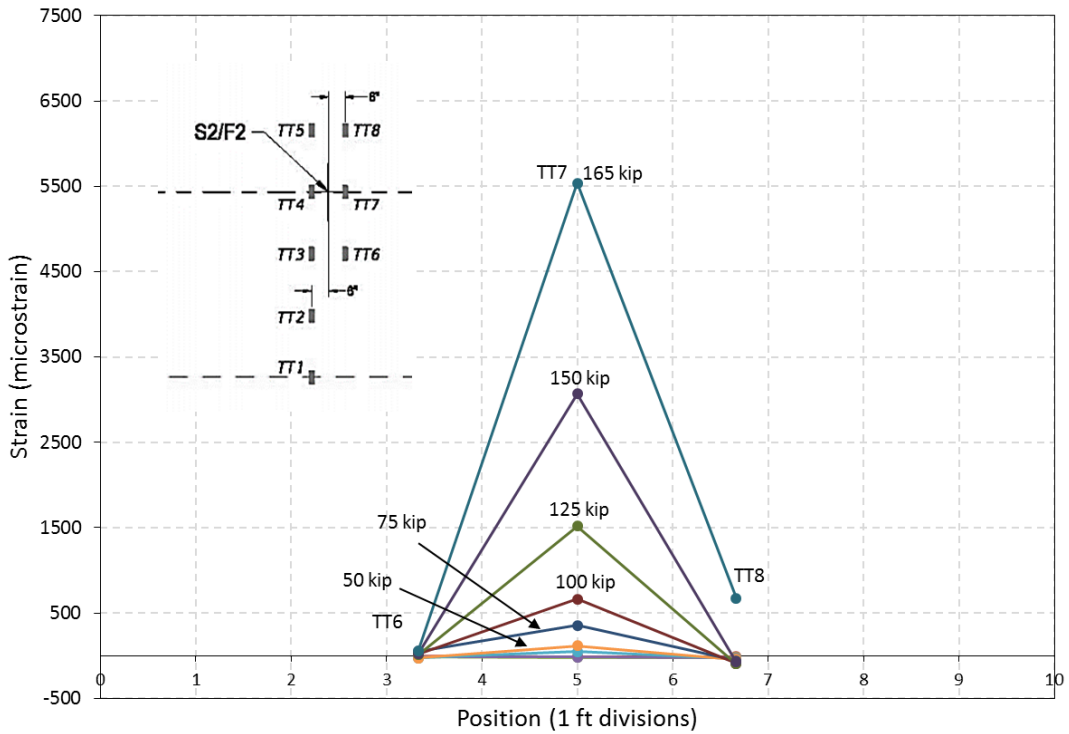


Figure 5.55: F2 Transverse cross-section view of top transverse strains (TT6-TT8)

Figure 5.56 is a plot of strain levels in the distribution reinforcement (longitudinal bottom bar). As the test progressed and the applied load exceeded 100 kip, gauges LB2 and LB4 indicated that the load started getting distributed over a wider influence area with gauges LB1 and LB5 also being strained, however, at a smaller level of strain. It is possible that this behavior is an indication of the size of the arching action dome (see Figure 2.1), which appears to increase in size as the load increases. It can be said that the influence area of the applied load at failure does not extend beyond the locations of gauges LB1 and LB5 by much. The failure pattern for F2 load case showed crack propagation at the bottom surface of the deck with diameters of 98-in x 105-in in the transverse and longitudinal directions.

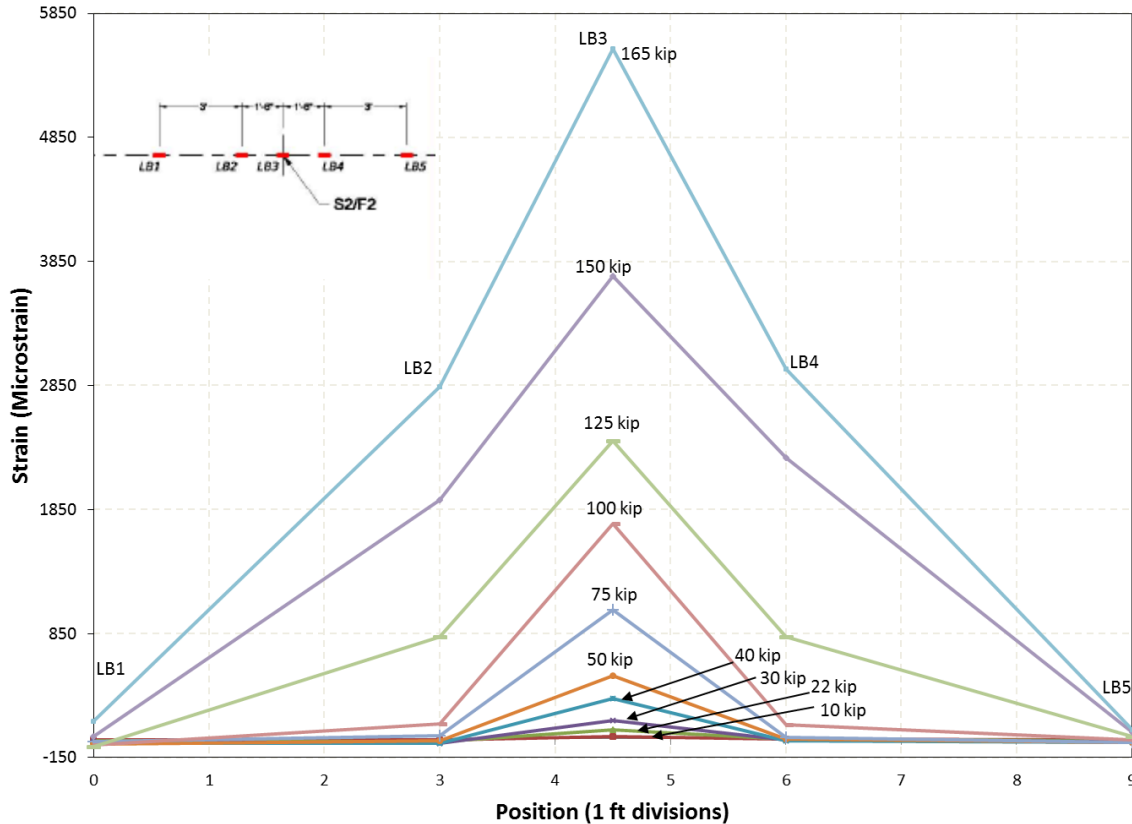


Figure 5.56: F2 Longitudinal cross-section view of bottom longitudinal strains

### 5.2.3.2 Load Deflection

In Figure 5.57, the two curves representing the deflection of the specimen for load case F2 are plotted. It can be seen that the raw recorded deflection at failure was 2.75 in., which translated into 1.875 in after taking the loading system flexibility out of the reading based on the initial laser gauge readings. Again, this level of deflection would be noticeable during field inspection despite the fact that the mode failure is relatively brittle. Despite including girder deflections in the presented results, under service load levels, the observed deflections were minimal and fall below the allowable limits.

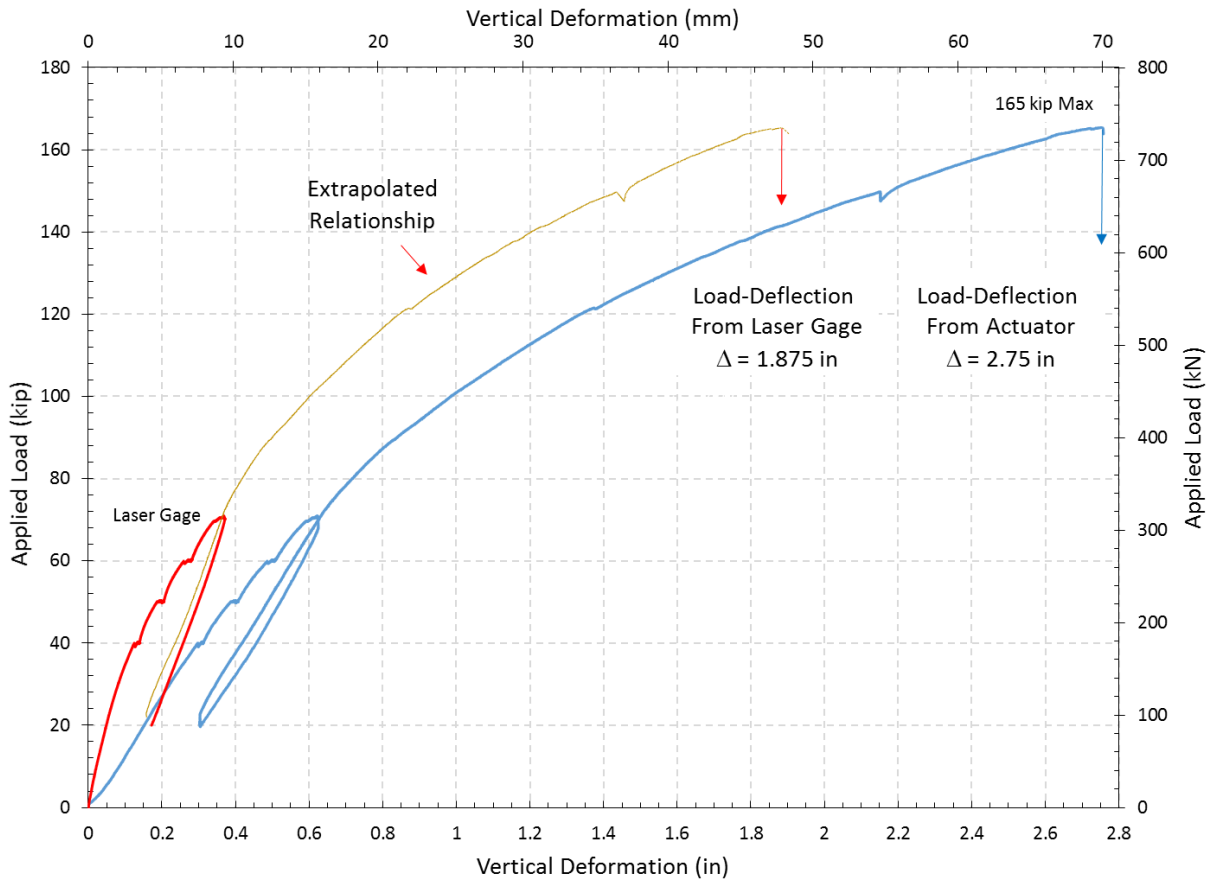


Figure 5.57: F2 Load-deflection

### 5.2.3.3 Horizontal Displacement

Reading from the laser displacement gauges measuring the girders' horizontal movement are shown in Figure 5.58. As is indicated on the figure, the gauges measuring the east girder's horizontal movement were removed for protection at a load equal to about 68 kip since they were positioned under the slab between the girders, whereas the west girder's gauges were positioned on the outside; i.e., not vulnerable to damage due to slab failure. The behavior was linear up to this load level and indicated that the bottom flanges moved to the outside more than the top flanges did, which is expected because of the restraining action the deck imposes on the top movement of the girder. The behavior started deviating from the linear trend up to failure, which happened at an applied load equal to 165.4 kip.

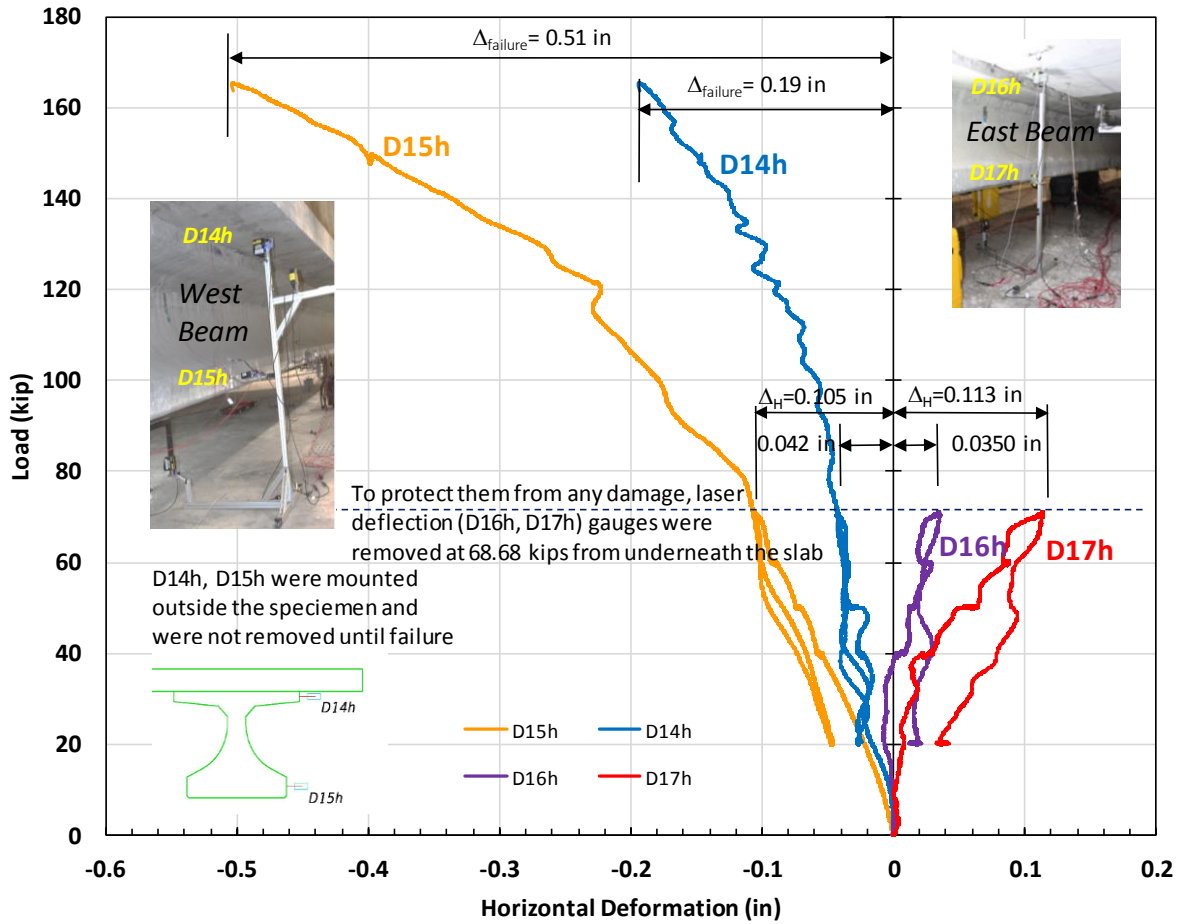


Figure 5.58: F2 Load vs. horizontal displacement of girders flanges

## 5.2.4 Deck Performance under Load Case F3

### 5.2.4.1 Strain Cross-Sections

Figure 5.59 through Figure 5.61 show results from the failure test at the F3 location. The same trends observed for load cases F1 and F2 are also observed for F3. This is true for the localization of bottom transverse strains under the applied loads with minimal development of negative continuity moments. The strain levels in the middle of the deck exceeded yield strain levels for all plotted gauges (TB13, TB7, and TB3) at failure.

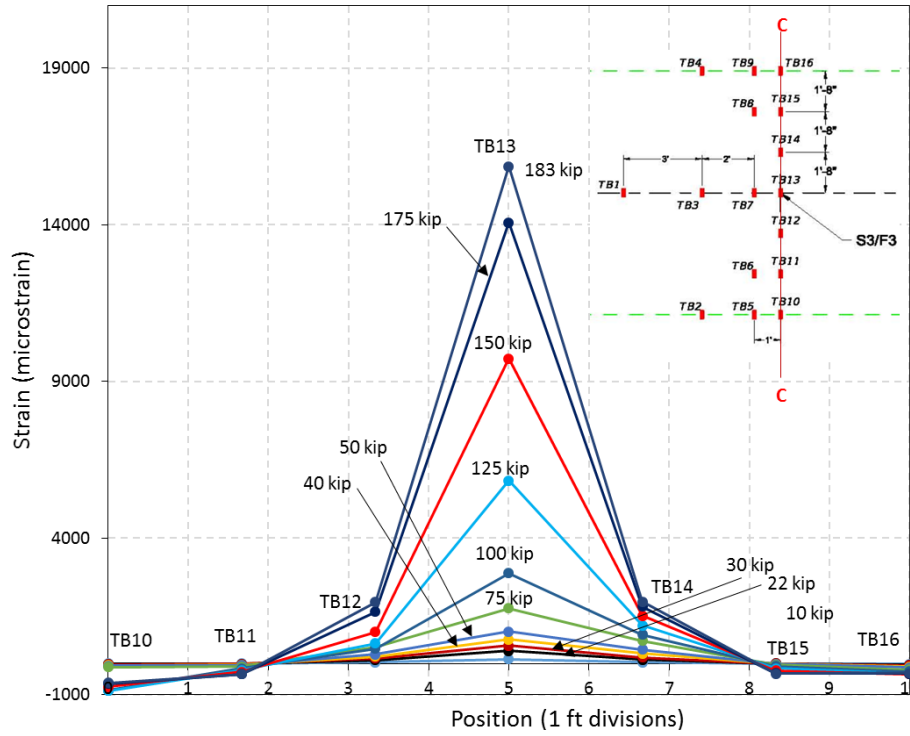


Figure 5.59: F3 Transverse cross-section view of bottom transverse strains TB10-TB16

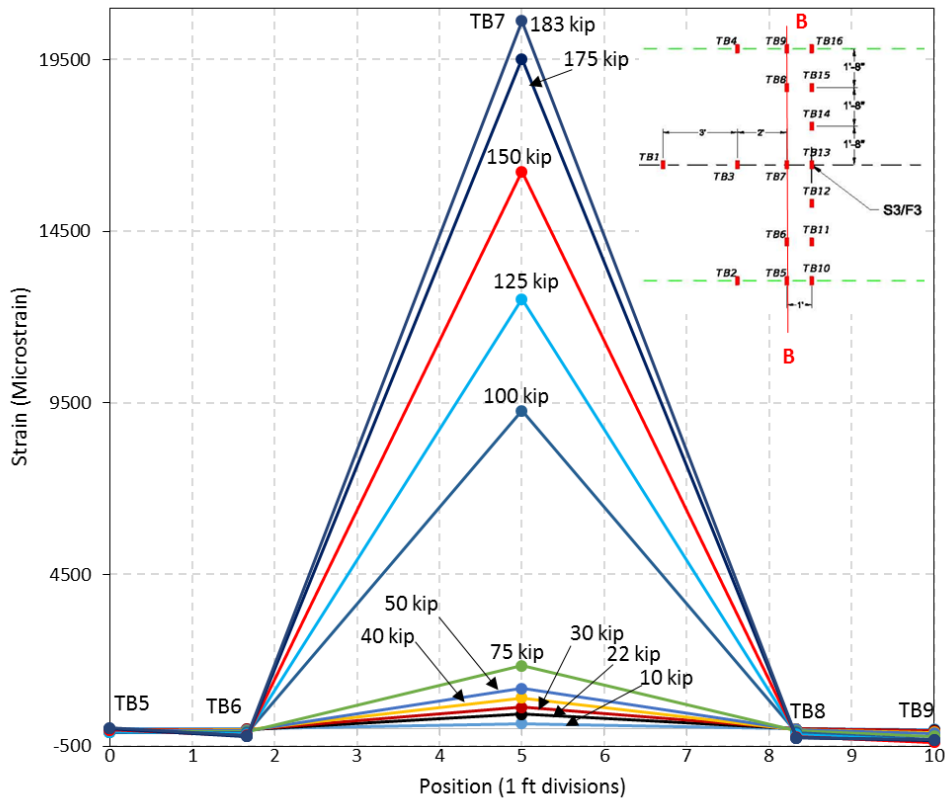


Figure 5.60: F3 Transverse cross-section view of bottom transverse strains TB5-TB9

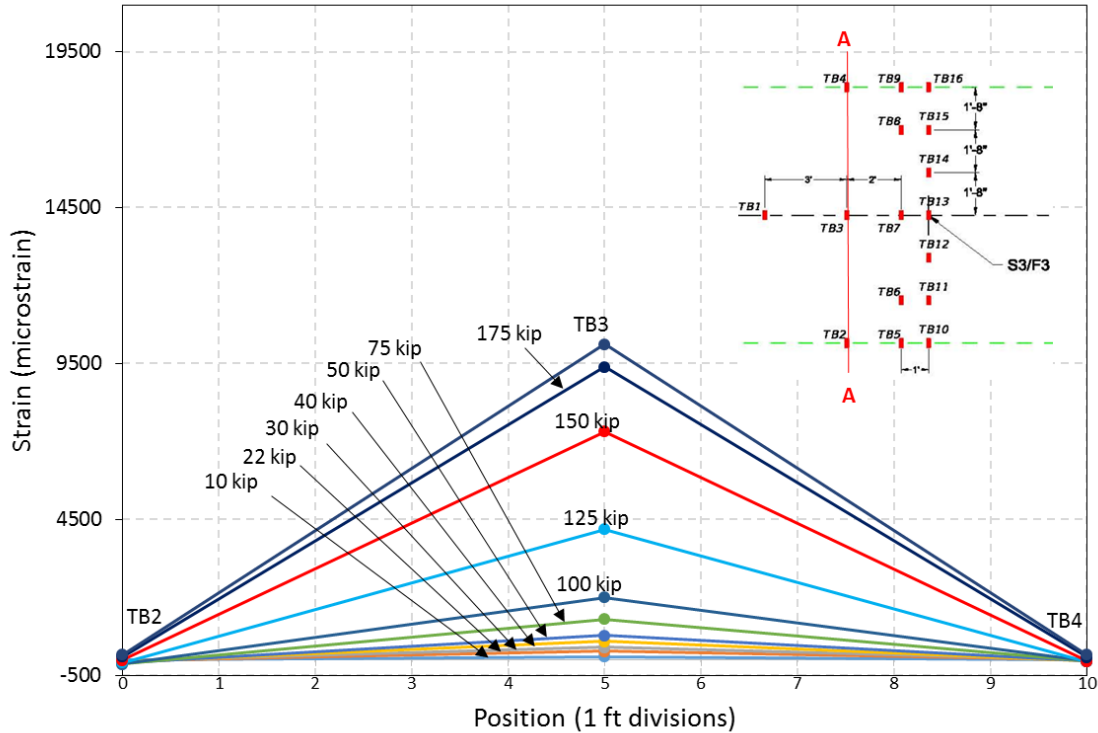


Figure 5.61: F3 Transverse cross-section view of bottom transverse strains TB2-TB4

In the longitudinal direction, a similar trend to what was observed for the other load cases is also true for Load Case F3. Larger strains were recorded under the applied load that decreased with the increase of the distance of the gauge location from the load position. An interesting observation is that the recorded strains directly under the load (TB13) were lower than the strains recorded by the subsequent gage (TB7). This behavior was consistent for three tests (F1-re-test, F2, and F3), which can be explained by a redistribution of forces due to failure zone dislocation or gage detachment at high strain levels. Regardless, all recorded strains, including that measured using TB1, exceeded the yield strain of the reinforcement. Hence, it can be said that a clear tie for the arching action behavior is developing for a distance equal to at least 12 ft as observed in the previously discussed load cases.

Figure 5.63 shows a plot of the strain distribution in the longitudinal direction. Unlike the observed behavior for Load Case F2 (Figure 5.56), a more localized load effect was observed based on the strain readings even at higher load levels. This difference in behavior makes it hard to evaluate the importance of the distribution reinforcement structurally. However, it is definitely needed to resist temperature and shrinkage effects, and since the slab achieved, and exceeded the required load capacity, it can be said that the used distribution reinforcement is sufficient for achieving the required load resistance for a bridge deck.

The top transverse cross-sectional plots for Load Case F3 are shown in Figure 5.64 and Figure 5.65. The very localized effect around the loading pad is clear in these plots. The abrupt changes of TT5 to negative strains may be caused by the dislocations that develop into the failure surface at the top of the failure dome discussed later in Section 5.3. For the gauges placed at the edge of the girder's top flange (TT1), a clear and increasing positive strain as the applied load increased.

The development of these positive strains happened at a faster rate starting at a load level equal to 125 kip. This is probably associated with the development of a crack in the slab at the girder's top flange edge as will be discussed later in Section 5.3 (see Figure 5.74).

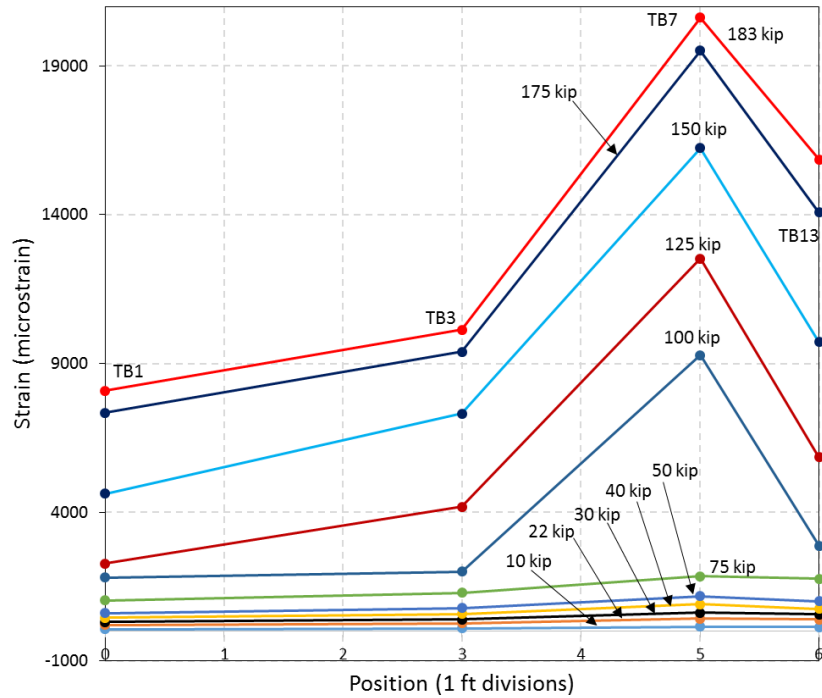


Figure 5.62: F3 Longitudinal cross-section view of bottom transverse strains (TB1-TB13)

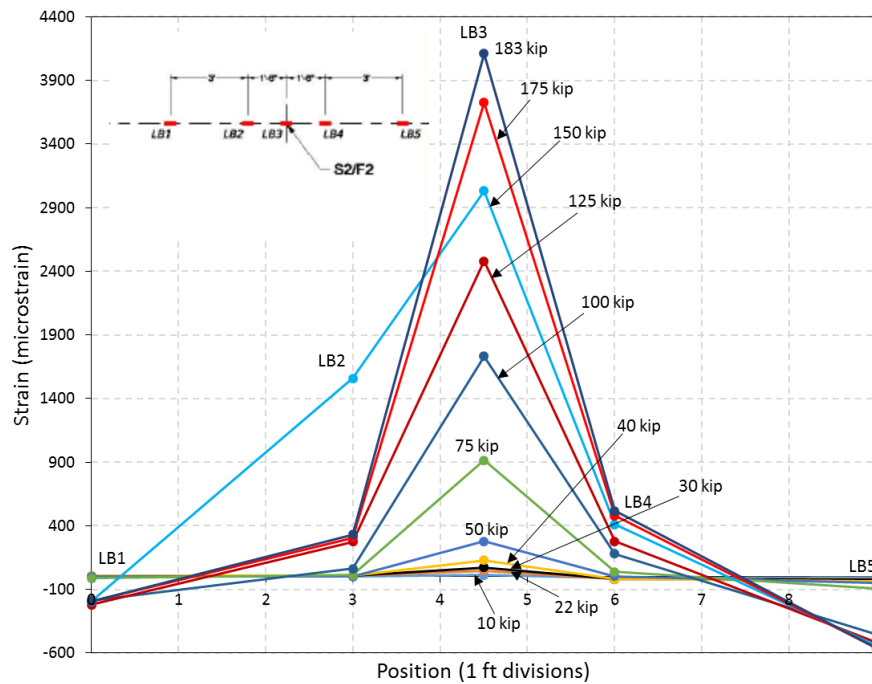


Figure 5.63: F3 Longitudinal cross-section view of longitudinal bottom strains (LB1-LB5)

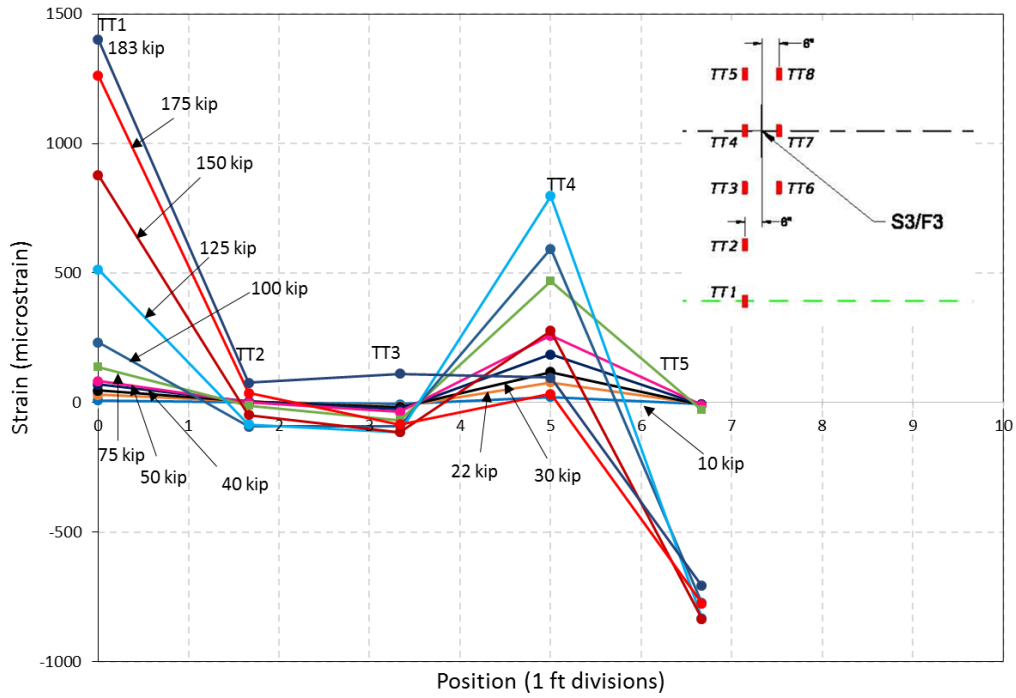


Figure 5.64: F3 Transverse cross-section view of top transverse strains (TT1-TT5)

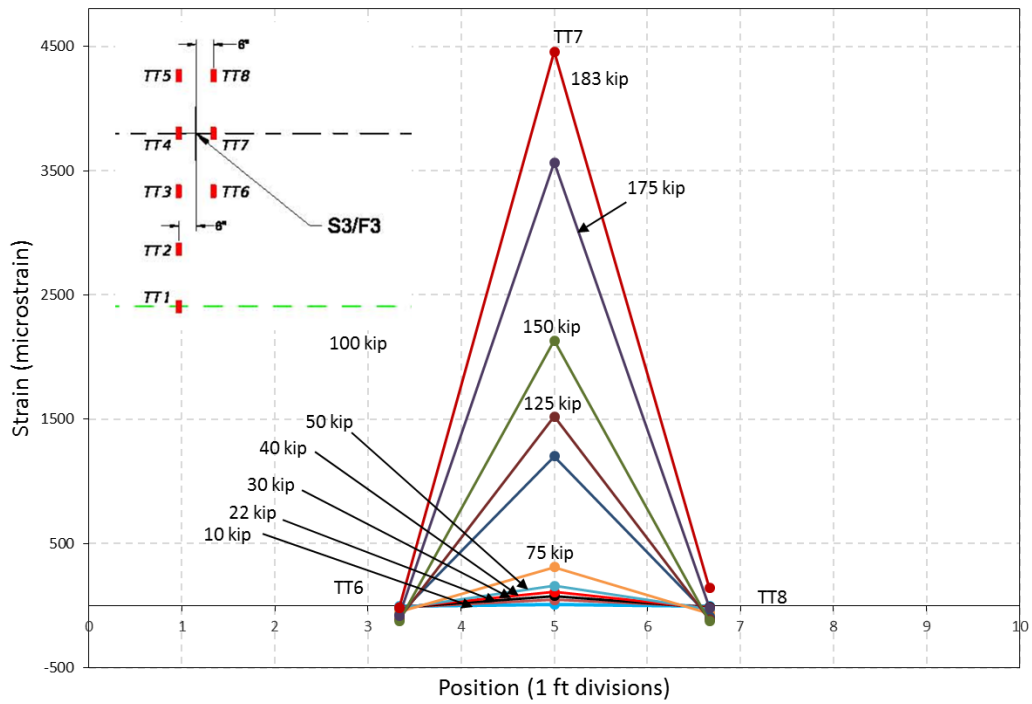


Figure 5.65: F3 Transverse cross-section view of top transverse strains (TT6-TT8)

### 5.2.4.2 Load Deflection

The recorded deflections for load case F3 at failure were 2.8 in. and 1.9 in. based on the raw and extrapolated data, respectively. These values are very similar to the recorded values from the previous two cases (F1 and F2). Under service load levels, the deflections are minimal and fall below the allowable limits.

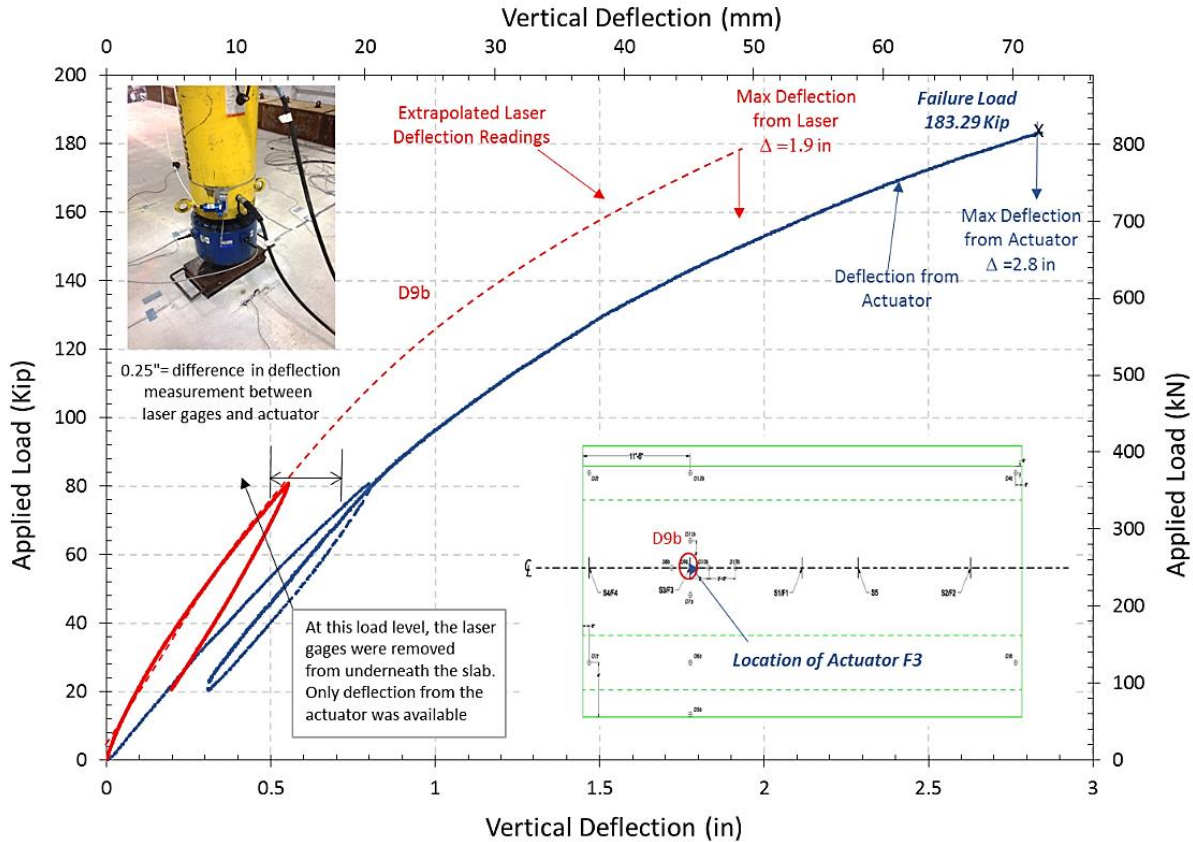


Figure 5.66: F3 Load-deflection

### 5.2.4.3 Horizontal Displacement

Reading from the laser displacement gauges measuring the girders' horizontal movement are shown in Figure 5.67. As is indicated on the figure, the gauges measuring the east girder's horizontal movement were removed for protection since they were positioned under the slab between the girders, whereas the west girder's gauges were position on the outside; i.e., not vulnerable to damage due to slab failure. Up to the point when the gauges on both sides were recording deformations (80 kip), there was minimal difference between the girders' behavior. The behavior was linear up to this level. The behavior started deviating from the linear trend up to failure, which happened at an applied load equal to 183.3 kip.

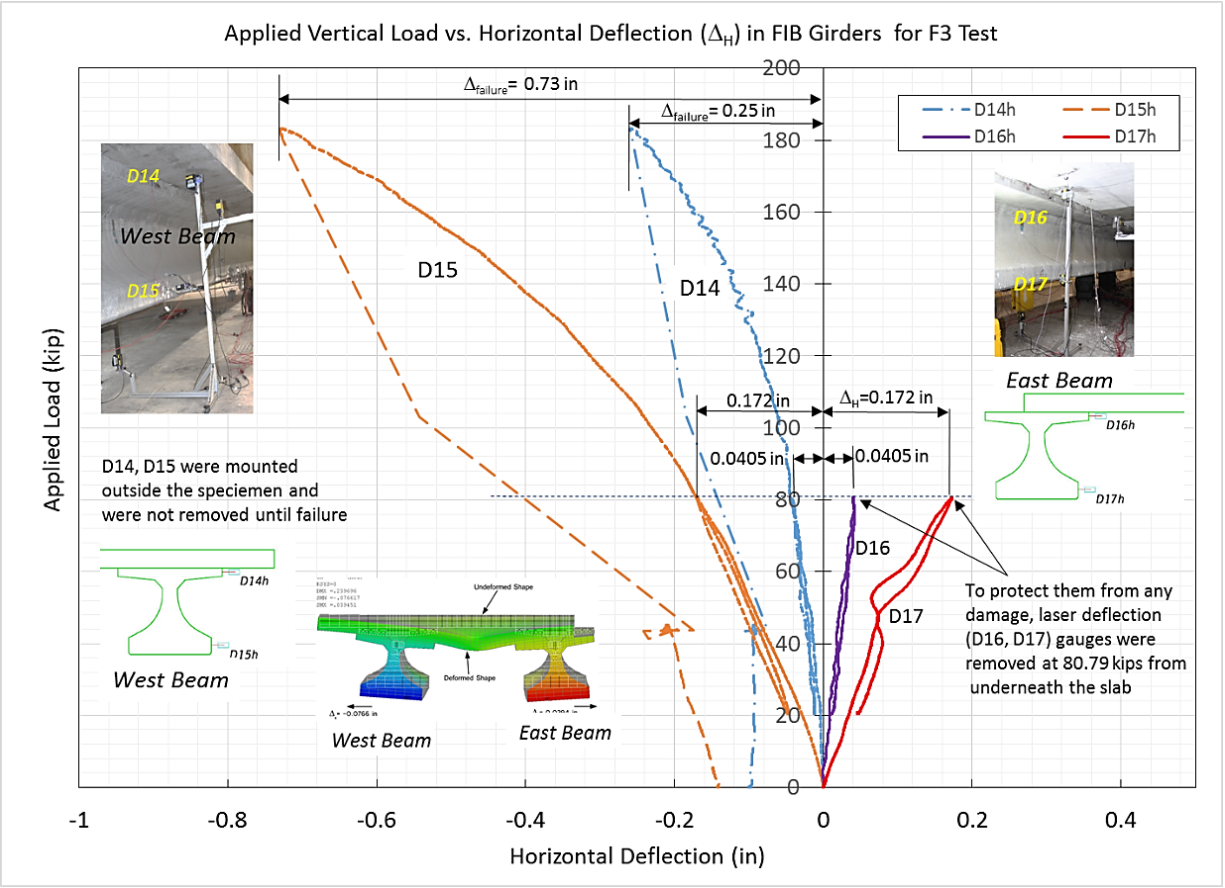


Figure 5.67: F3 Load vs. horizontal displacement of girders flanges

5.2.5 Deck Performance under Load Case F4

As stated earlier, Load Case F4 was not in the original testing program, and hence, the instrumentation plan did not include embedded gauges at its location, i.e. edge of the deck. Therefore, the closest embedded gauges; i.e. installed for Load Case S3/F3, will be used instead. Other gauge types, e.g. laser deflection gauges and surface mounted gauges, were installed with a slightly different configuration to accommodate the deck limits as described earlier. Therefore, the plots for Load Case F4 will be slightly different than what was described in the previous sections for the other load cases.

5.2.5.1 Strain Cross-Sections (readings from S3/F3 gauges)

Figure 5.68 through Figure 5.70 show plots of cross-sectional strains in the transverse direction. The plot shown in Figure 5.68 is the closest to the slab’s edge; i.e., applied load position. In this plot, it can be seen that high positive strain values were recorded close to failure (75 kip) all across the slab including close to the girder’s edge. A similar behavior was also observed for the following transverse cross sections where the TB5-TB9 (Figure 5.69) and TB10-TB16 (Figure 5.70) were installed, respectively. However, the magnitude of the strains at the girder’s edge become smaller as the distance from the applied load increases. These positive strains are different than what was observed for the other load cases as a result of the different failure surface shape for F4 (discussed later in Section 5.3.4). That is because the plotted cross-sectional

strains are closer to the edges of the semi-elliptical failure surface than to its center as is the case for the other load cases.

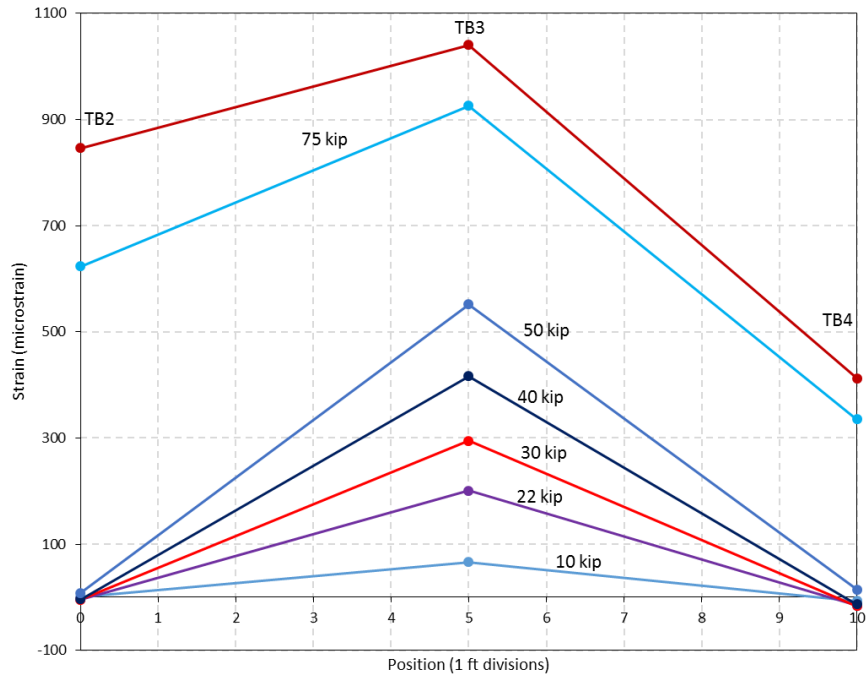


Figure 5.68: F4 Strain cross-section (TB2-TB4)

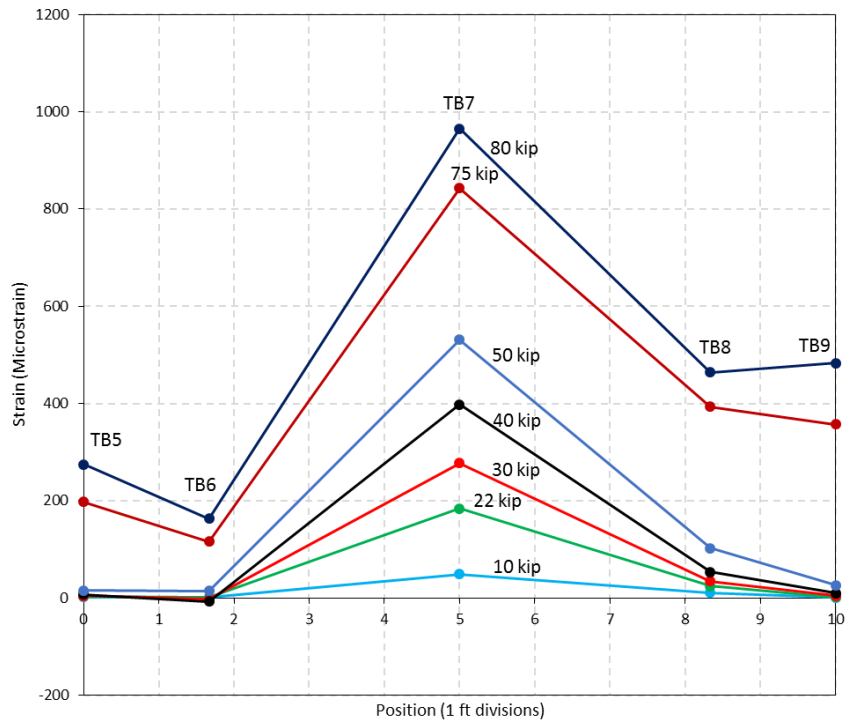


Figure 5.69: F4 Strain cross-section (TB5-TB9)

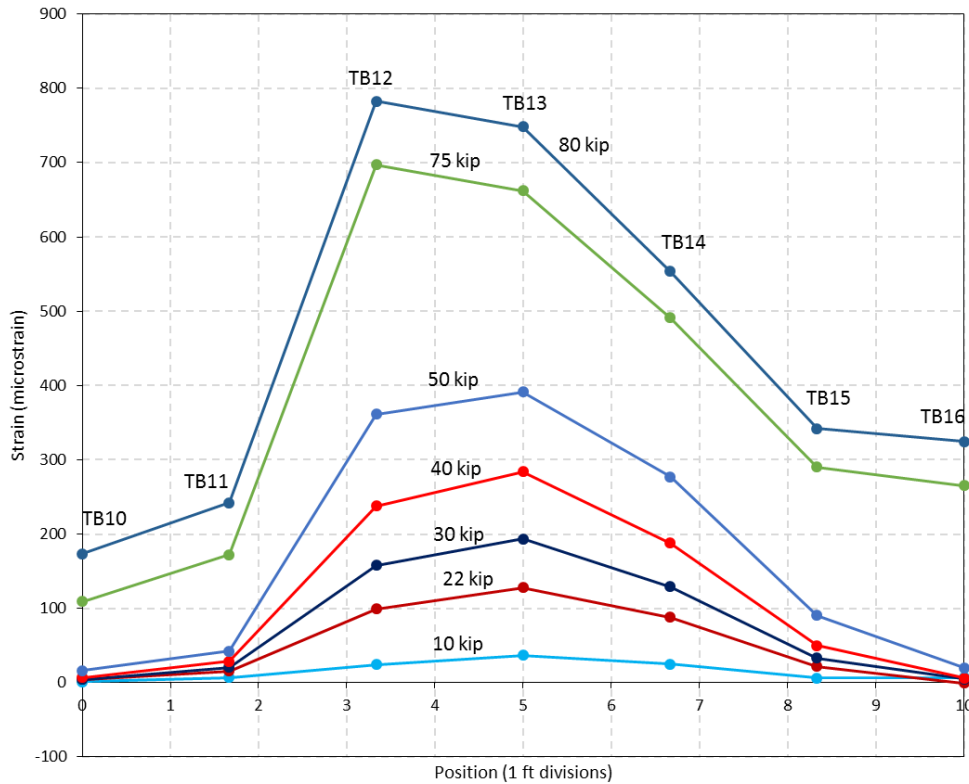


Figure 5.70: F4 Transverse cross-section view of bottom transverse strains (TB10-TB16)

In the longitudinal direction, the transverse strains followed the expected trend of decreasing strain values as the distance from the applied load increased, as shown in Figure 5.71. It should be noted that the first gauge (TB1) is at a distance equal to 4ft-10in. from the applied load. Nevertheless, it experience large strains exceeding the yield strain at failure.

A similar trend was also observed for the distribution reinforcement. Figure 5.72 shows a plot of the longitudinal strain values along the middle of the slab. As expected, readings from gauge LB1, i.e. closest to the applied load, recorded the largest readings, with other gauges recording decreasing values as the distance from the applied load increased. The magnitudes of the strains in the distribution reinforcement were much smaller than what was recorded for the other cases. This due to the fact that these embedded gauges were farther away from the applied load compared to gauges for the other load cases. It can be said that, except for LB1, the other gauges are beyond the edge of the failure surface, and hence the lower strain readings.

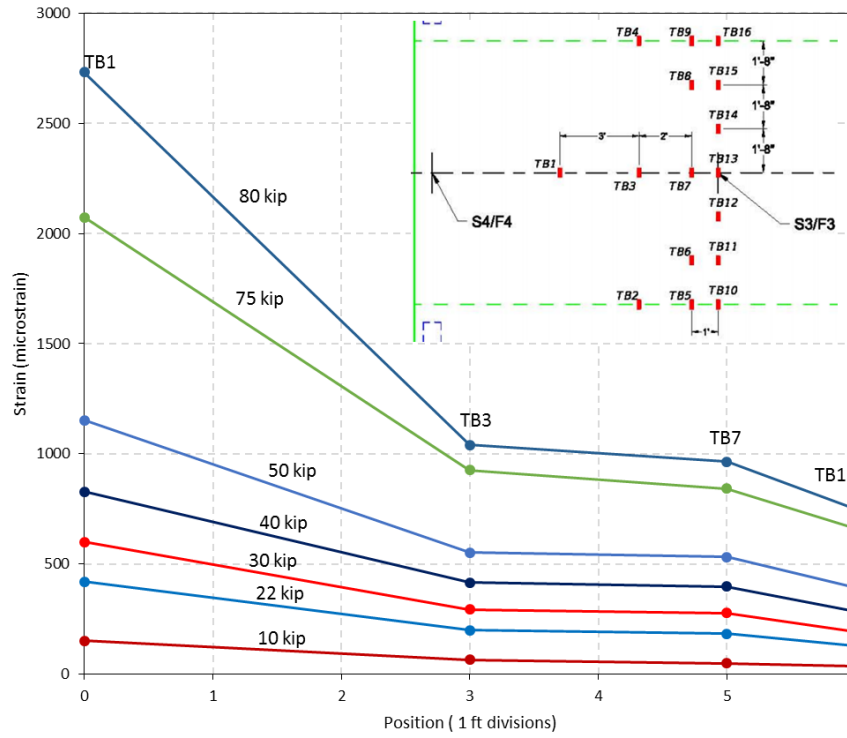


Figure 5.71: F4 Longitudinal cross-section view of bottom transverse strains (TB1, TB3, TB7, TB13)

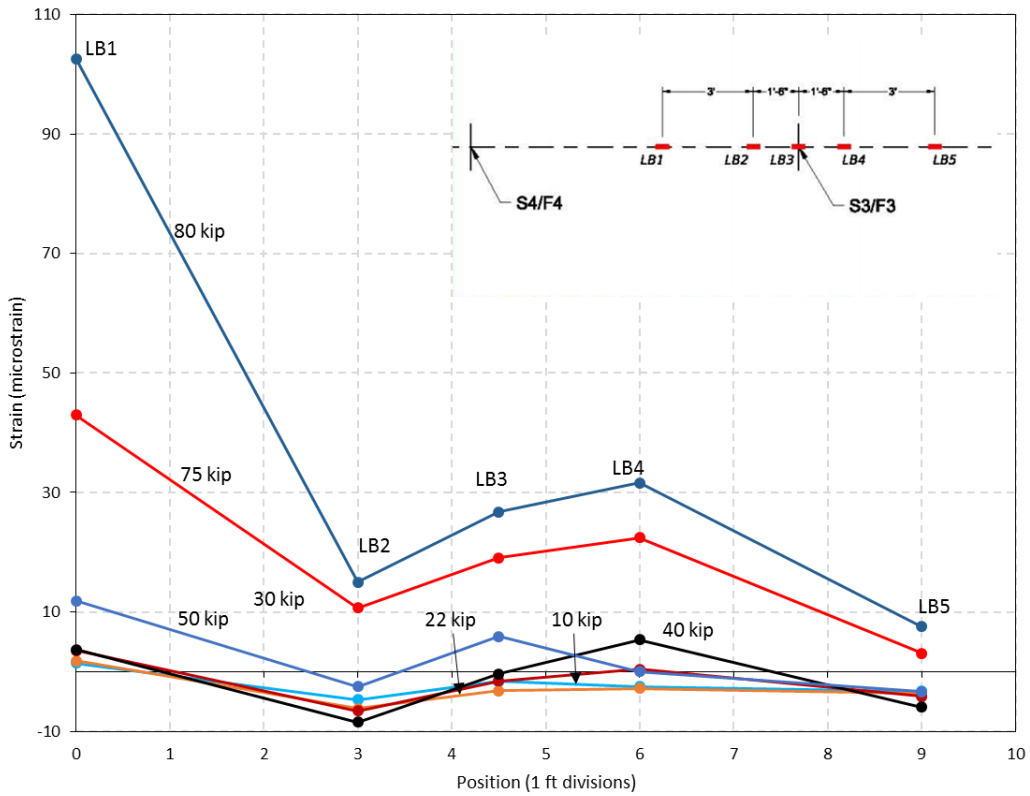


Figure 5.72: F4 Longitudinal cross-section view of bottom longitudinal strains (LB1-LB5)

### 5.2.5.2 Load Deflection

The load deflection relationship from the laser displacement gauge positioned exactly under the applied load is plotted in Figure 5.73. The figure shows the relationship starts with a linear behavior up to a load level of about 42 kip. Despite being the weakest part of the slab for resisting wheel loads; i.e., the edge of the slab, this load level is about twice the service load level for one wheel load (21 kip) and more than the factored design load (37.2 kip). A hardening nonlinear behavior followed this initial linear trend all the way up to failure at 80.3 kip. There was no softening behavior observed, and the failure was a sudden drop in load resistance as a result of punching.

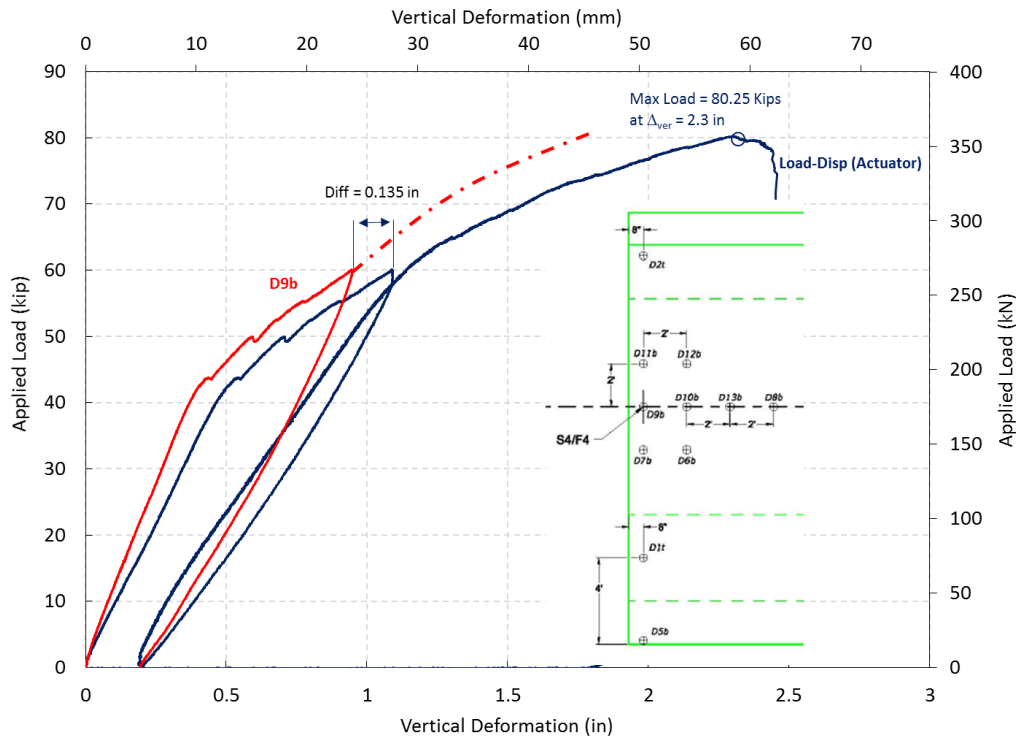


Figure 5.73: F4 Load vs. deflection (D9b)

### 5.3 Mode of Failure

As shown in the figures presented in this section and based on the test results, it is clear that the failure mode was not purely flexure. A pure flexure failure of the deck would happen at an applied load equal to 26.5 kip, which was exceeded experimentally by 5 to 7 times (reaching 6 to 8 times) for failure load cases F1, F2, and F3. This is an indication that the deck behavior does not follow the classical bending theory. The failure loads also exceeded the factored design wheel load of 37.24 kip, reaching levels of 4 to 6 times that factored load.

The mode of failure was a hybrid flexural/punching shear mode where compressive membrane arching action was developed showing a big elliptical-shaped damage at the bottom surface of the slab followed by a sudden punching shear failure that caused damage slightly larger than the size around the loading pad shown clearly at the top of deck. The high failure loads happened

when the deck suddenly failed around the applied load in a manner similar to classical punching shear. Figure 5.75 through Figure 5.97 show the failure mode and crack patterns. For each load case, several figures are provided showing the load position, the extents of the failure surface at the top and bottom of the slab, and additional cracking observations at the top of the slab. Figure 5.74 shows a schematic of the typically observed cracks and failure cone.

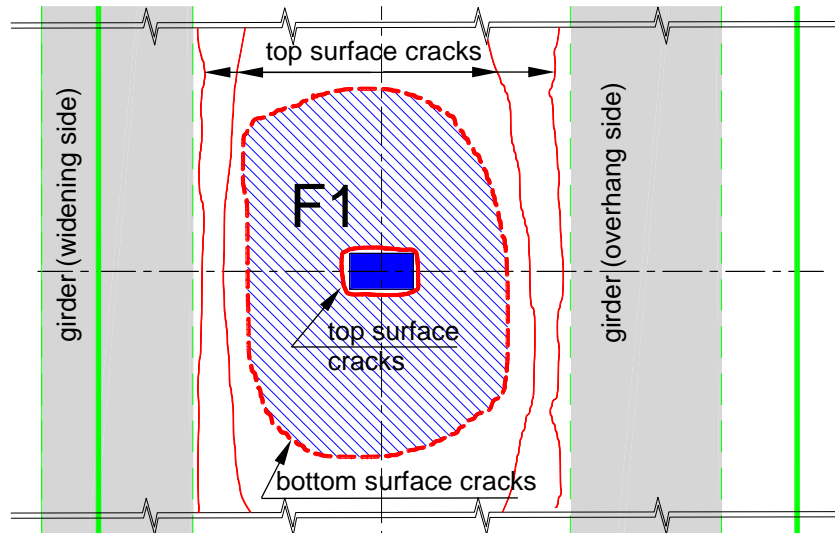


Figure 5.74: Typically observed cracks at failure

### 5.3.1 Load Case F1

Load Case F1 is positioned right in the middle of the specimen longitudinally (see Figure 5.76). As such, load distribution is the more than it is for other cases due to proximity of the deck's edge or stiffer girder support. The bottom and top of the failure surface can be seen in Figure 5.78 and Figure 5.77, respectively. It can be seen that the failure surface size is smaller at the top of the slab than it is at the bottom. At the top of the slab, the failure surface closely follows the extents of the applied load pad. The dimensions of the failure surface are much larger at the bottom of the slab. This indicates that the failure surface is cone-shaped, which is consistent with a punching shear behavior. In addition to the main failure surface cracks, other cracks were also observed. Figure 5.79 shows top surface longitudinal cracks in the slab along the girder's top flange edge on the continuous side with the loaded overhang. Such cracks are caused by the presence of tensile stresses at the top of the slab indicating the development of negative moments along the edge of the supporting wide flange beam. The fact that loading blocks were put on the overhang stiffened this side of the slab and helped in the development of the negative moments. However, it is clear that this negative moment was not the controlling mode of failure, which would have resulted in these longitudinal top slab cracks to be wider as a result of yielding in addition to crushing at the slab's bottom side by the supporting girders' top flange edge.



Figure 5.75: Load Case F1 – Test location close-up



Figure 5.76: Load Case F1 – Test location



Figure 5.77: Load Case F1 – Failure ellipse area from bottom slab: 87 in. (7.25 ft) x 96 in. (8 ft)



Figure 5.78: Load Case F1 – Failure at load point from top of slab

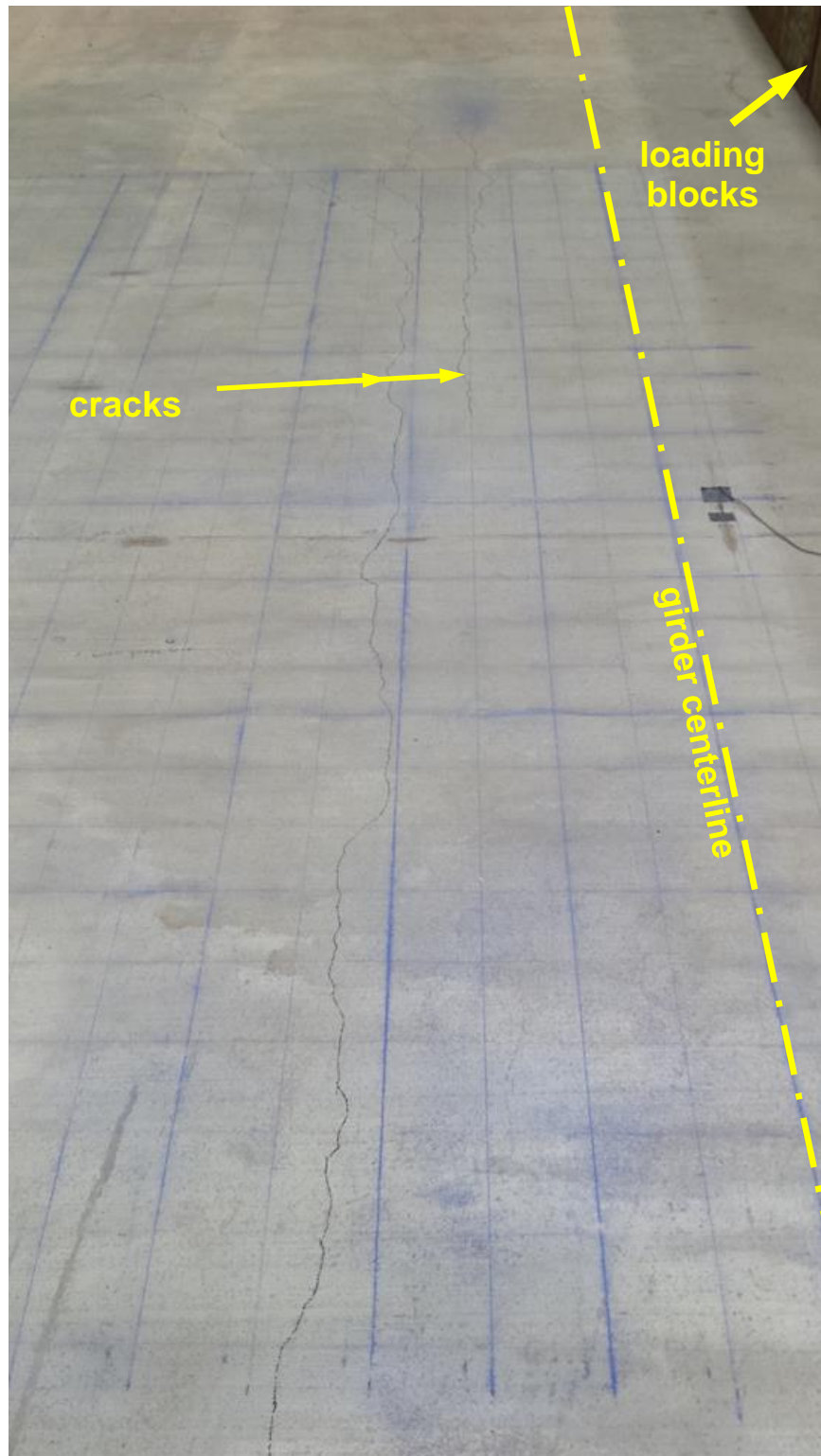


Figure 5.79: Load Case F1 – Longitudinal cracking on top of slab near overhang

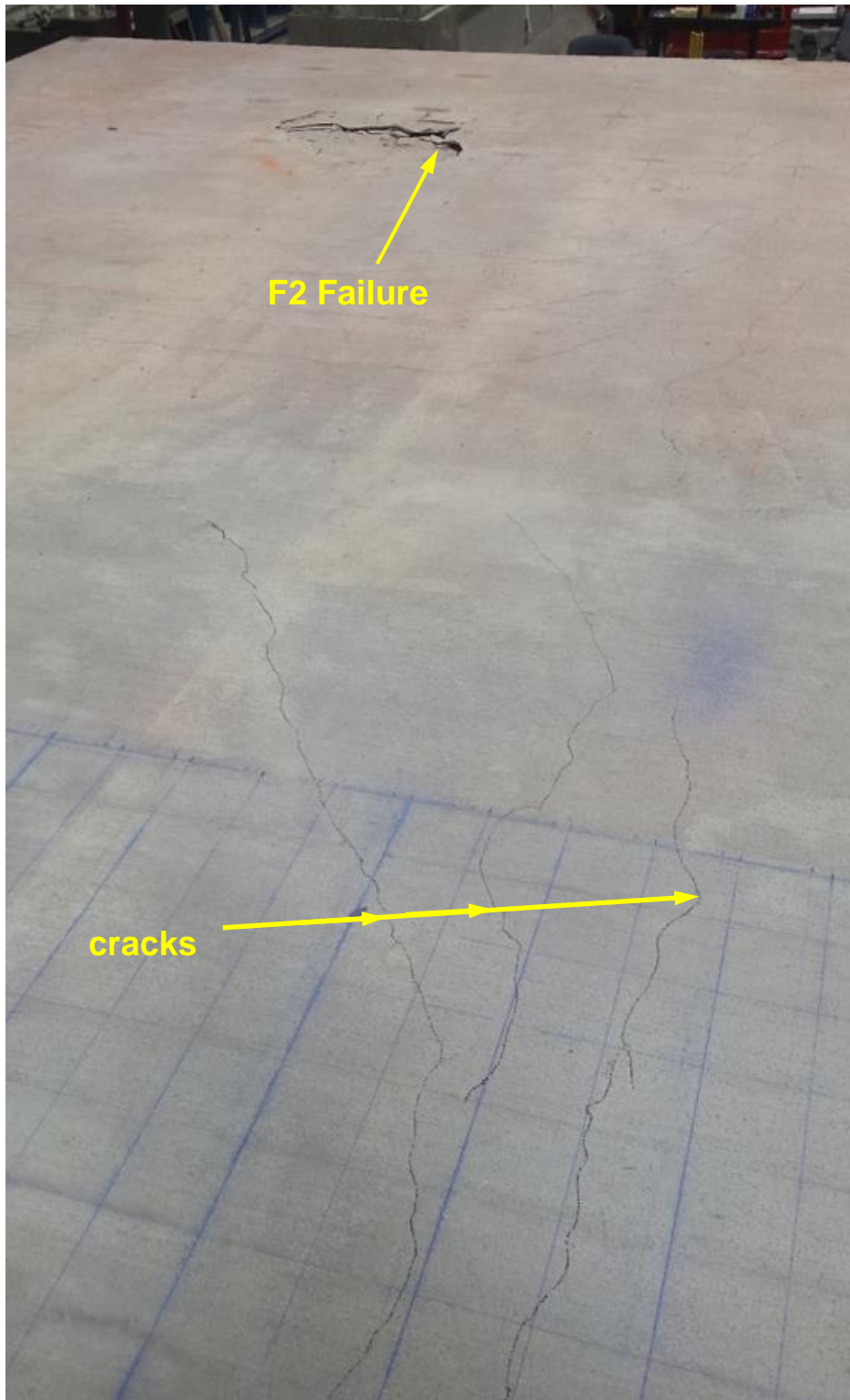


Figure 5.80: Load Case F1 – Longitudinal crack extending roughly 80 inches from center line of load to farthest visible crack towards F2 location

### 5.3.2 Load Case F2

The position of the applied load for Load Case F2 is closer to the edge of the deck than for other cases, except for Load Case F4. Figure 5.83 shows the extent of the failure surface at the top of the slab, which did not extend much beyond the footprint of the applied load pad. After the test was completed, the load pad was removed and the extents of the failure surface at the top of the slab were measured as can be seen in Figure 5.87 and Figure 5.88. The extents of the failure surface at the bottom of the slab can be seen in Figure 5.89. Similar to the observation made for Load Case F1, it is clear that the failure surface is cone-shaped, which is consistent with a punching shear behavior. Figure 5.85 and Figure 5.86 show longitudinal top slab cracking at the edges along the supporting prestressed concrete girders on the widening and overhang sides, respectively. These top cracks are an indication of the development of negative moments at these locations. However, the magnitude of these negative moments did not control the failure mode, which would have been indicated by concrete crushing at the bottom of the slab near the girders.



Figure 5.81: Load test Load Case F2 – Test location

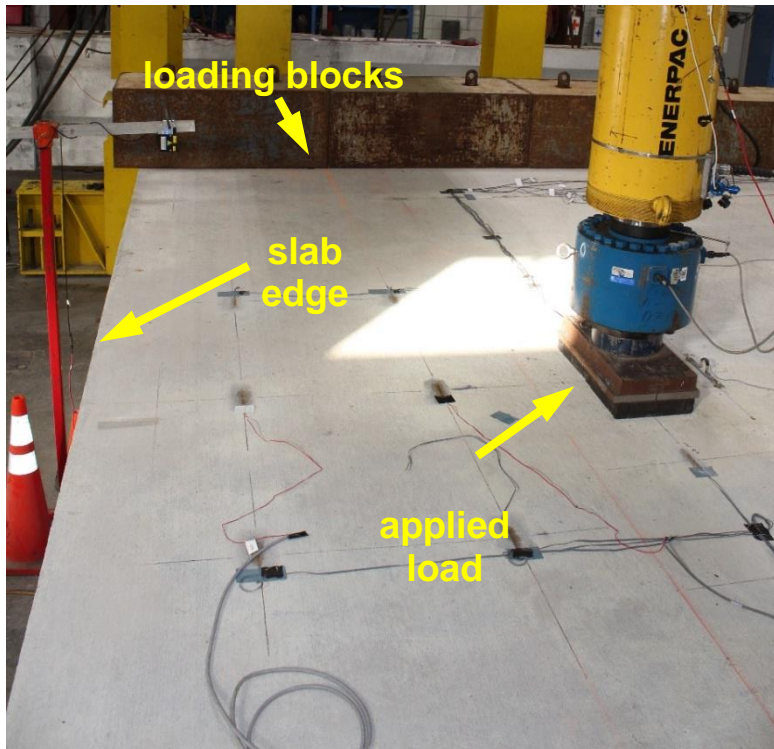


Figure 5.82: Load Case F2 – Test location close-up



Figure 5.83: Load Case F2 – Failure at the top of slab

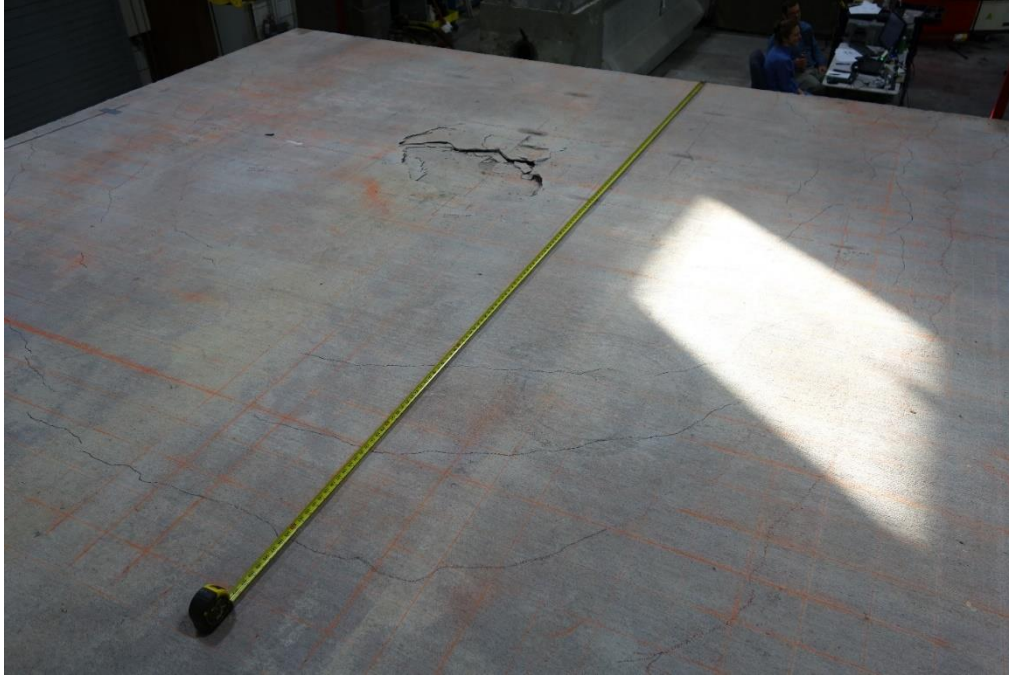


Figure 5.84: Load Case F2 – Tracing cracks at top of slab

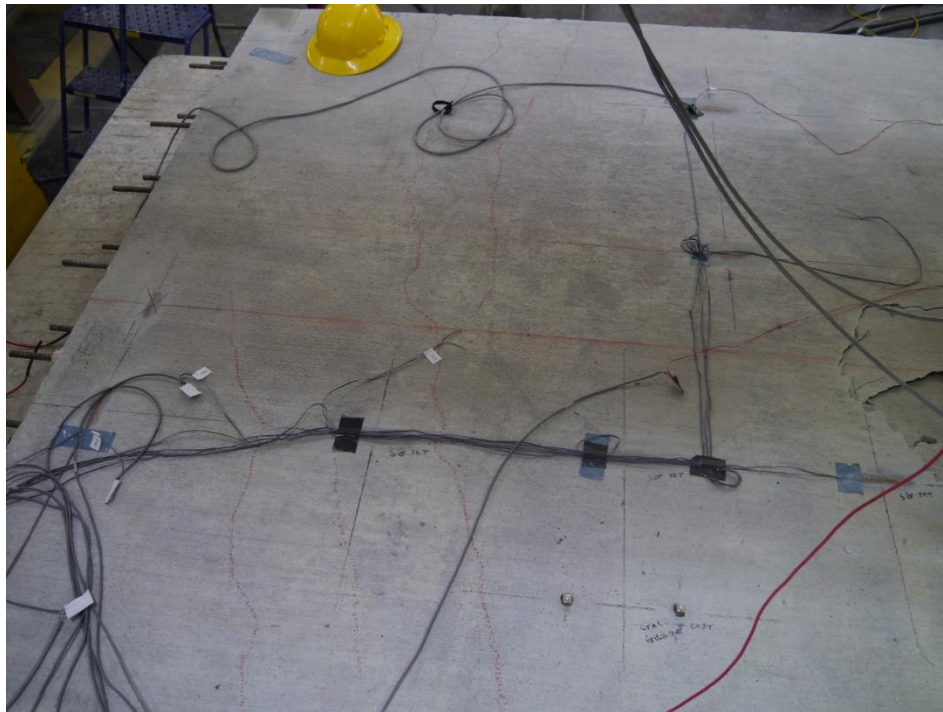


Figure 5.85: Load Case F2 – Top slab cracking near widening side.

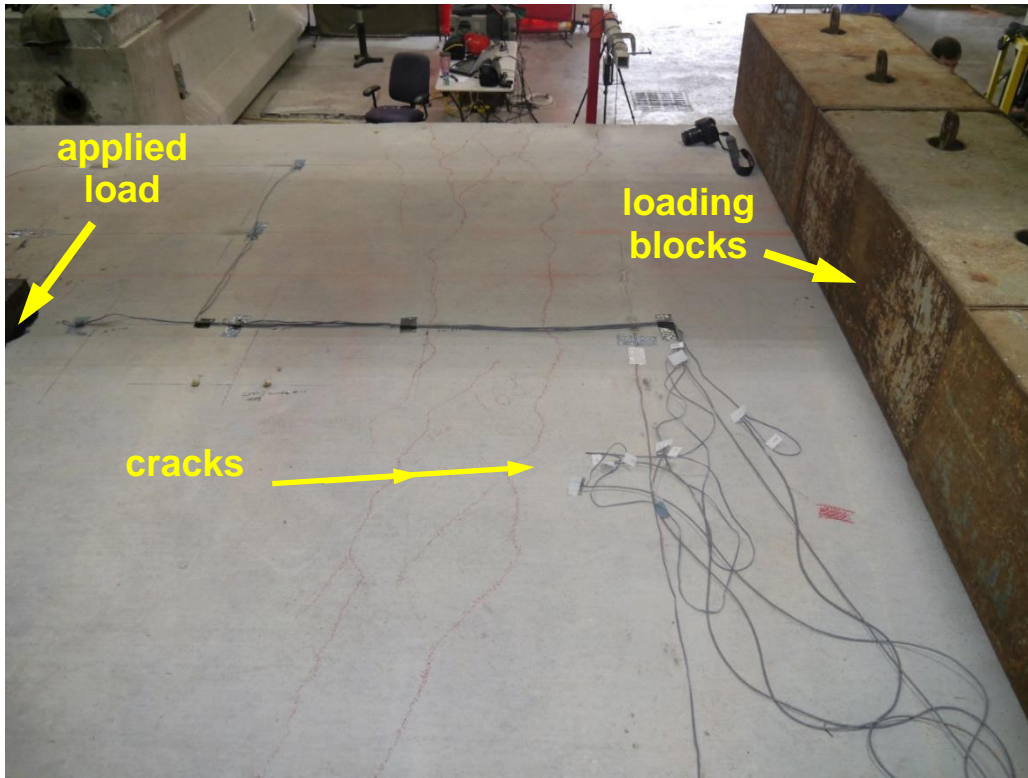


Figure 5.86: Load Case F2 – Longitudinal cracking near overhang

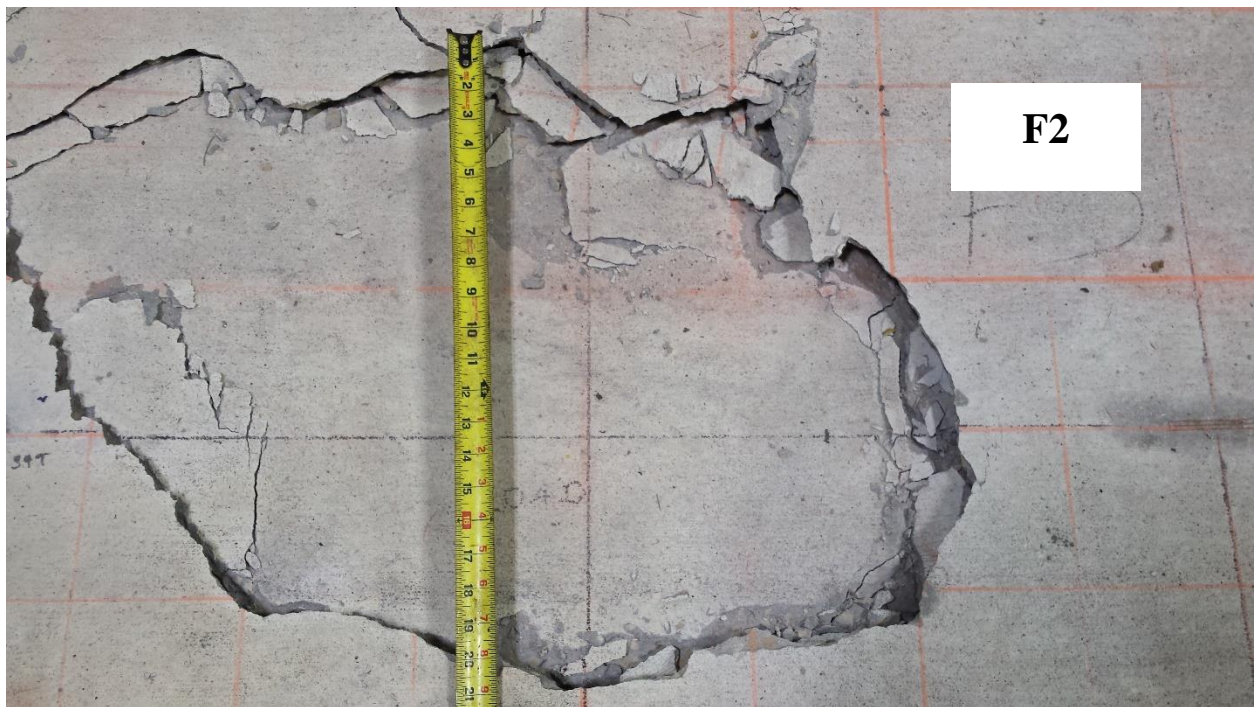


Figure 5.87: Load Case F2 – Close-up of failure at top of slab under load point



Figure 5.88: Load Case F2 – Close-up of failure at top of slab under load point



Figure 5.89: Load Case F2 – Failure at bottom of slab

### 5.3.3 Load Case F3

A similar pattern was observed for the failure mode in load case F3. Figure 5.91 shows the extent of the failure surface from the top of the slab, which almost followed the extents of the applied

load pad. From the bottom of the slab (see Figure 5.92), it can be seen that the failure surface extended a lot further than the footprint of the applied load pad.

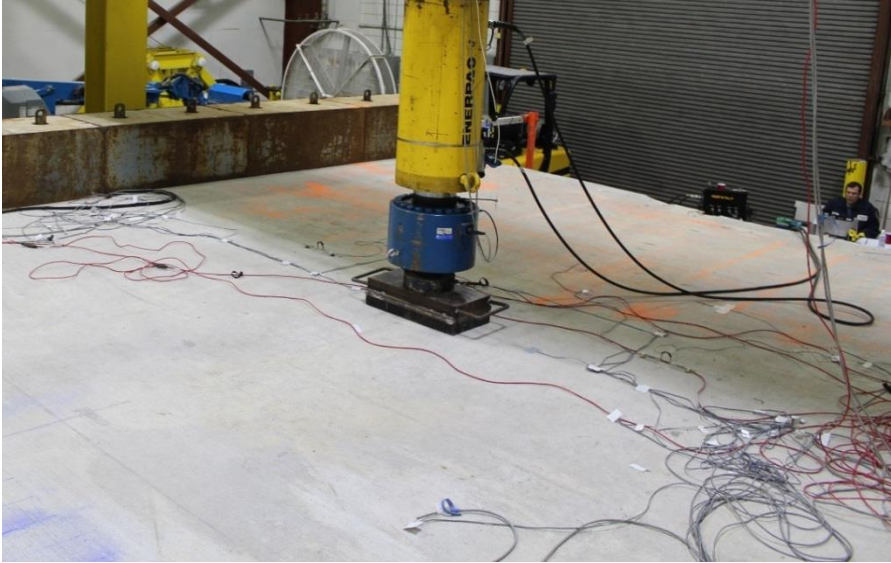


Figure 5.90: Load Case F3 – Test location



Figure 5.91: Load Case F3 – Failure at load point



Figure 5.92: Load Case F3 – Extent of failure surface at bottom of slab

#### 5.3.4 Load Case F4

As with all other test locations, Load Case F4 also failed by punching shear, albeit at a lower load level due to being at the edge of the deck. As with the other cases, the main failure surface at the top of the slab was close to the footprint of the applied load, as can be seen in Figure 5.95. At the bottom of the slab, the failure surface extended beyond the extents observed at the top of the slab (see Figure 5.96). The unique location for this case allowed a better view of the failure mode from a side view in addition to the top and bottom views. Figure 5.94 shows a side view of the slab at failure. It can be seen that the failure surface is cone-shaped, which is consistent with a punching shear failure mode rather than flexure, for which the main crack would have been vertical and concrete crushing would have been evident. It is noted that the cone was not exactly symmetrical about the point of load application. This may be attributed to the effect of the overhang and the loads applied on it that, unlike on the widening side, restrains deck rotation. Figure 5.97 shows that in addition to the main failure surface, elliptically-shaped top slab cracks extended in an increasing spacing away from the applied load.



Figure 5.93: Load Case F4 – Test location

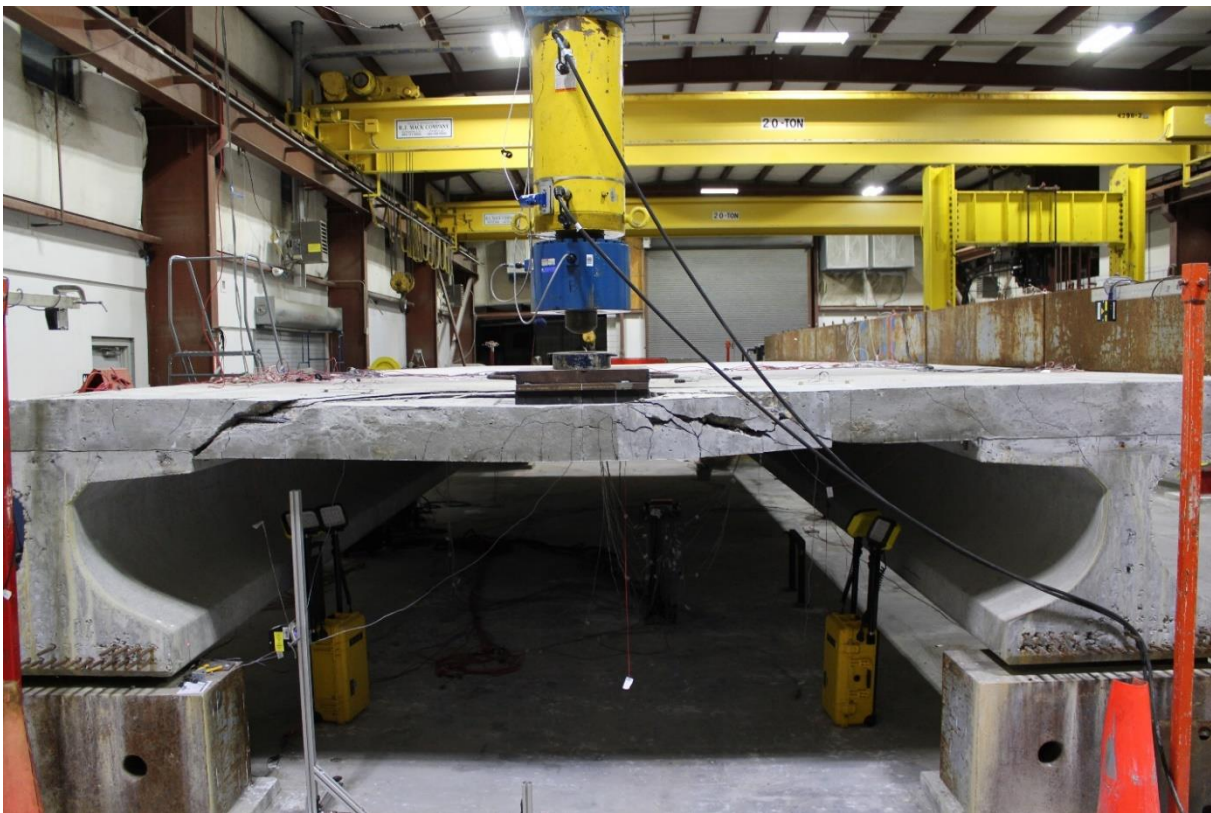


Figure 5.94: Load Case F4 – Failure

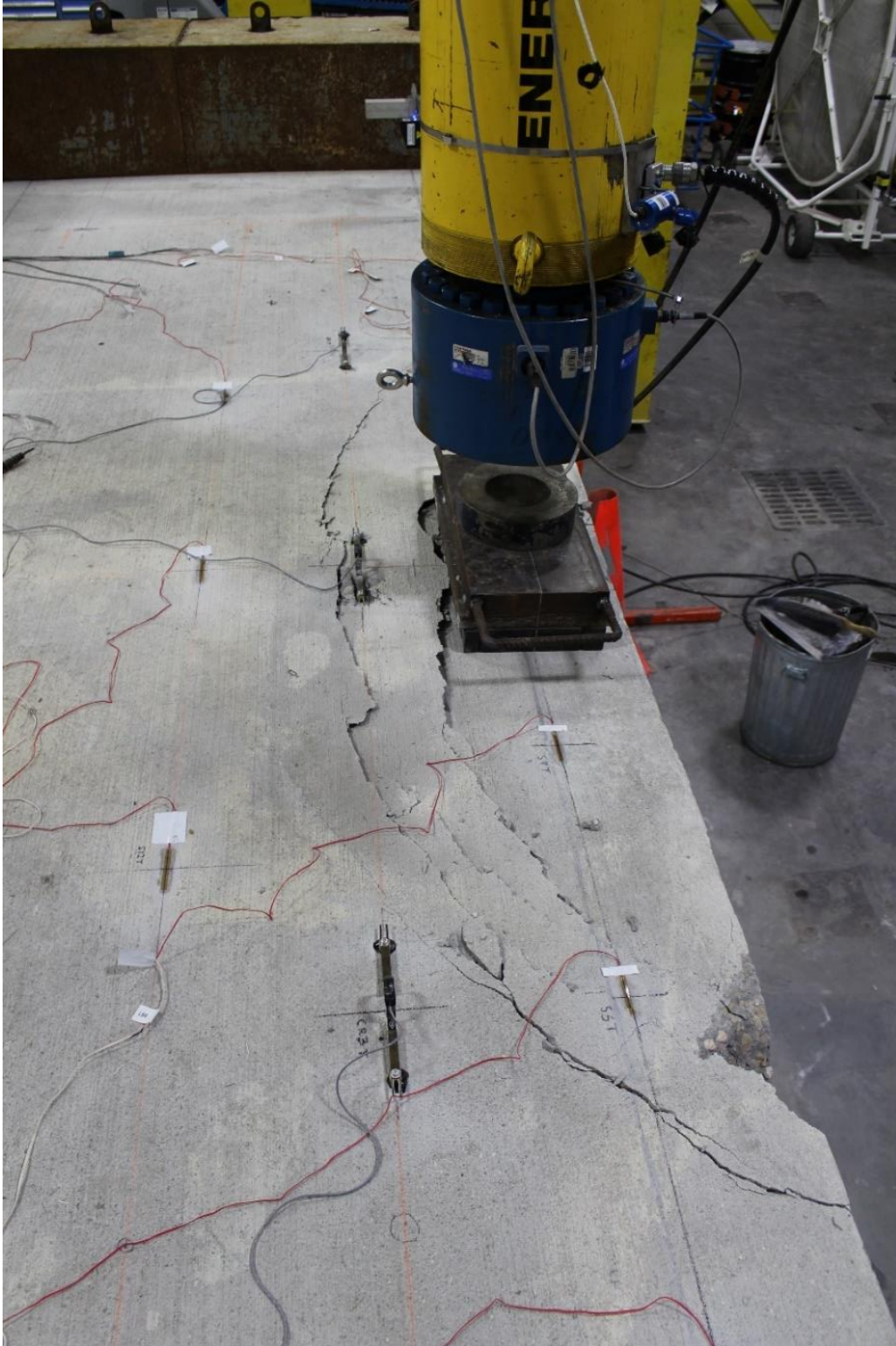


Figure 5.95: Load Case F4 – Failure at top of slab



Figure 5.96: Load Case F4 – Extent of failure surface at bottom of slab

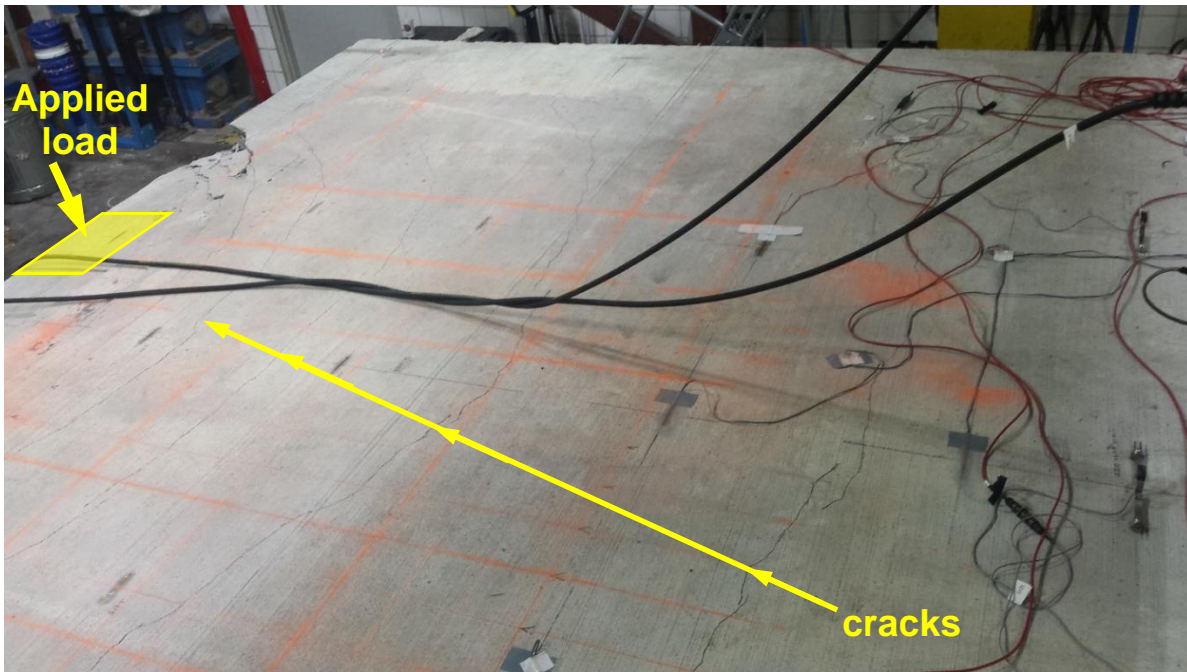


Figure 5.97: Load Case F4 – Extent of top deck cracking

## 5.4 Results

Results from both the failure tests and the service tests (for both deflection and crack width) came out favorable. Table 5.7 shows a summary of test results for deflection and crack width under service loads. Failure load results are shown in Figure 5.32. The serviceability requirements of deflection and crack width under service loads were satisfied. Under service load, the deflections were minimal satisfying the maximum deflection limit for concrete decks with no pedestrian traffic which is  $L/800$  in AASHTO LRFD (9.5.2), where  $L$  is the span length. This limit translates into 0.21 inch (5.33 mm). By comparing the presented results to this limit, it can be stated that the design wheel load including dynamic magnification meet the AASHTO LRFD requirements for all interior service load cases, namely S1, S2, S3, and S5, with a huge margin. The critical edge case, S4, also meets AASHTO LRFD deflection limit, however, the margin is much smaller. If a higher margin against deflection is desired, thickening of the deck may be needed as is currently required by the FDOT SDG.

Cracking was not noticed during initial service loads. After exceeding the crack load and unloading of the specimen to remove the laser gauges, the measurements obtained during reloading revealed that crack widths up to the identified service load level, 22 kip, are considered acceptable. This is based on the limit most practice manuals consider as not in need for action to repair the crack. The recorded crack widths under the identified service load level were in the range of 0.006-in and 0.0085-in (0.0152 to 0.216 mm).

In addition, all recorded strains under initial service load levels, except for TB13 and LB5 during the S1 test, which have been discussed earlier, were below concrete cracking strain of 132 microstrain. No cracking took place in the conducted service test cases. Except for S1, all the recorded strains fall below the level that induces concrete cracking. Even though TB13 for Case S1 recorded strain readings that exceeded the concrete cracking strain, cracks were not observed during the test under this load level. Therefore, this gauge may have been faulty as the other two internal cases, S2 and S3, did not exceed the estimated concrete cracking strain. It should also be noted that recorded strains (from the available gauges embedded for Case S3) for the most critical case, S4, for which the load was applied on the edge of the deck and after conducting the S3 test, were also lower than the rupture strain. Another explanation for the high strains recorded by TB13 for Case S1 is that it is possible that a crack preexisted at this location, resulting in higher strain levels from the cracked section.

In failure load cases F1, F2, and F3, the test failure load was 6 to 8 times the estimated pure flexure capacity and was 4 to 6 times the calculated factored design wheel load of 37.24 kip (165.7 kN). The test results showed clearly that the failure mode was not of pure flexure. The failure loads happened at a higher load level when the deck suddenly failed around the applied load in a manner similar to classical punching shear.

Table 5.7: Testing Summary under service loads

Testing Summary			
Location	Deflection at Service (in)	Max Service Load (kip)	Crack Width (in)
S1/F1	0.053	21.46	0.008
S2/F2	0.045	21.84	--
S3/F3	0.047	21.21	--
S4/F4	--	--	0.005
S5	0.050	21.53	--

## Chapter 6 Comparison of Analytical, Finite Element, and Test Results

### 6.1 Comparison of the Finite Element Results and the Failure Test Results

Results from the ANSYS finite element analyses described in Chapter 3 were compared to the service and failure test results presented in Chapter 5. These finite element analyses were conducted after the completion of the laboratory testing to validate the previously developed finite element models. Refined models of the deck designed with empirical method were calibrated using the actual behavior of the empirical deck specimen since it was the only tested specimen. By validating the results of the FEA for the empirical slab models with the actual behavior of the actual lab specimen, it was possible to reconstruct another set of FEA models for an almost identical bridge deck specimen whose deck reinforcement was designed using the traditional method. Steel reinforcement in the bridge deck using ANSYS finite element program was simulated using the smeared concrete element SOLID 65. The element allows for concrete cracking and crushing as well as steel reinforcement yielding. Several finite element models were established and analyzed to investigate the slab behavior with steel reinforcement modeled as link elements and as smeared elements.

Transverse and longitudinal reinforcement ratios for both the traditional and the empirical deck designed with different girder spacing were conducted using a developed MathCAD sheet, Appendix III. The locations of the applied vertical loads in the FEA models for the mid span analyses were selected to match the locations used in the testing program (Figure 6.1).

In the overhang FEA models, the applied loads were shifted closer to the exposed top flange at the widening section at a distance equal to the 36 inch from the center of the exposed FIB (Figure 6.2). The purpose of these models was to investigate whether the proximity of the vertical load affects the horizontal deformation of the FIB beams the same way the mid-span vertical deformation affected the horizontal deformation of the beam.

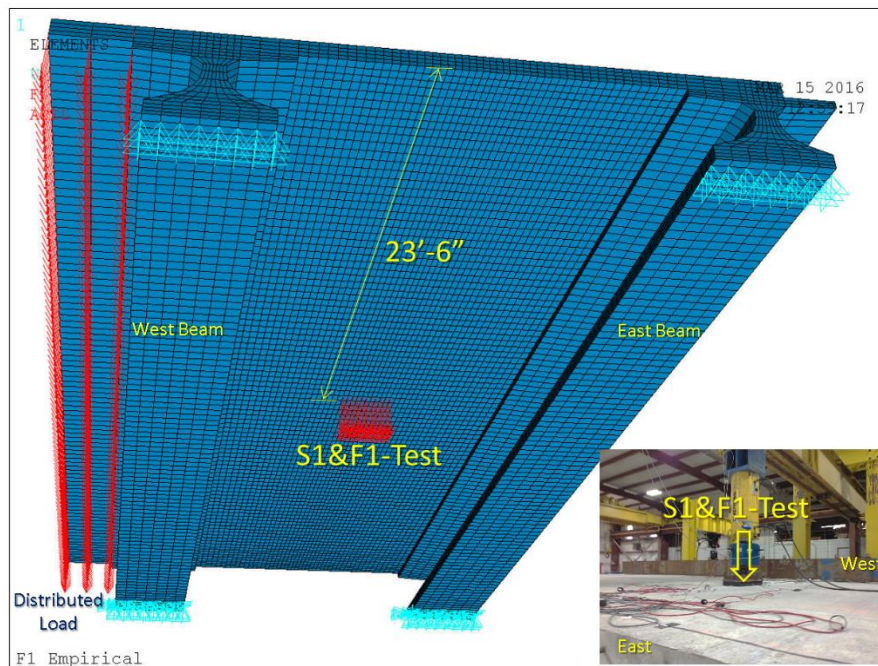


Figure 6.1: Empirical and traditional FEA model for S1 and F1-test, loading at mid span

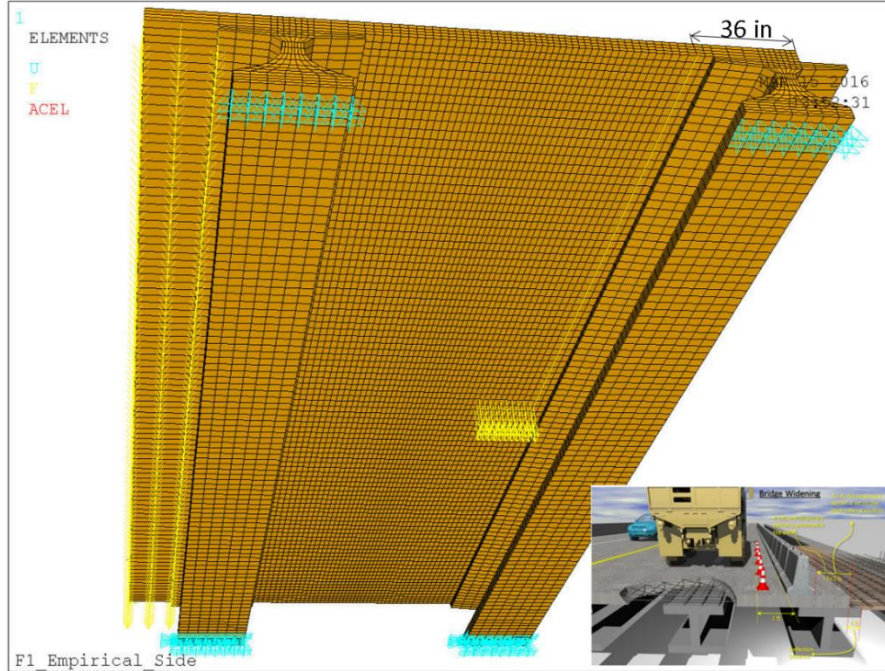


Figure 6.2: Empirical and traditional FEA model for S1 and F1-test, loading near the overhang

The relationships between the load and deformation for all the FEA service and failure tests using both empirical and traditional methods will be presented next including the condition of moving the loads from the testing locations at the mid span closer to the overhang side. Test results for F1 load case are presented. Figure 6.3 and Figure 6.4 show the maximum deflections for the FEA of decks designed with both empirical and traditional methods for the mid-span loading condition. The deflection was found to be equal to 2.02 inch for empirical slab and about 1.78 inch for the traditional slab at ultimate load. This is an indication that the additional steel reinforcement in the traditional slab has reduced the deflection by about 13%.

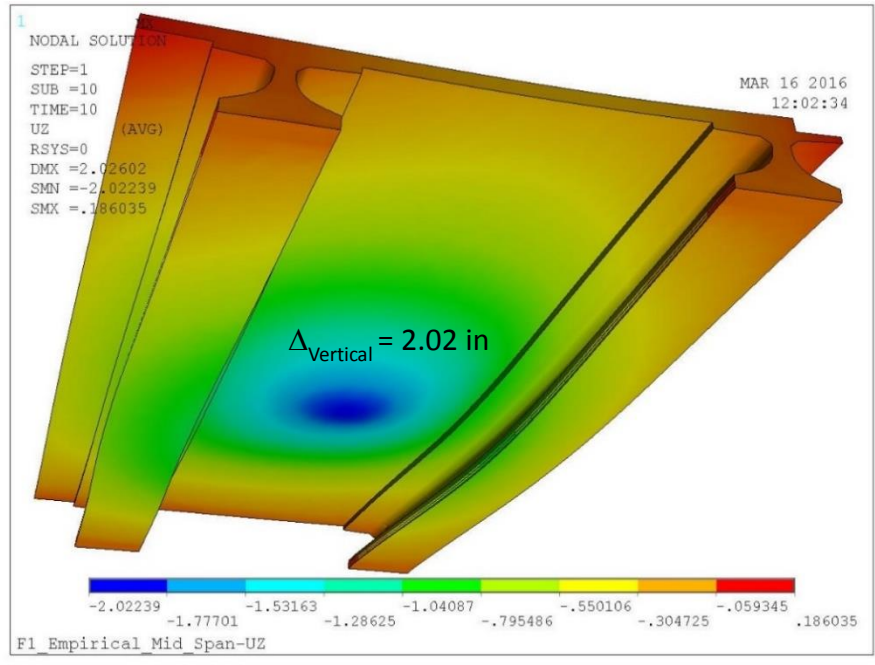


Figure 6.3: Deformation of the empirical slab

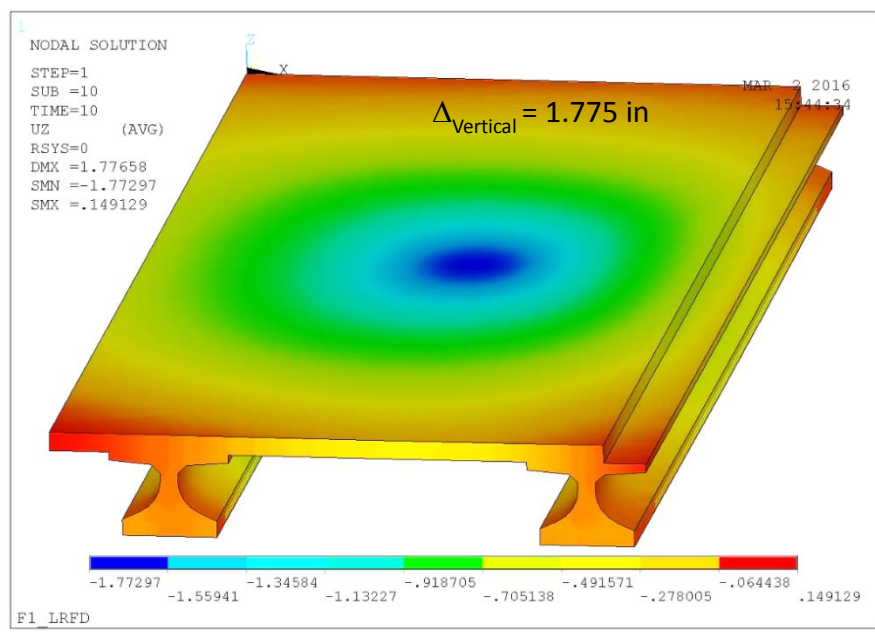


Figure 6.4: Deformation of the traditionally designed slab

The results from FEA for the empirical slab were comparable to that laboratory test results, as shown in Figure 6.5. It should be noted that the results presented in Figure 6.5 show the extrapolated curve from test data to obtain a more realistic value for the experienced deflection; since deformation of the load system and bearings were included in the overall deformation as discussed earlier (see Ch. 5). The finite element model results predicted that the deflection was

2.02 inch. Figure 6.6 shows a comparison of the deformations from laboratory and FEA models for the F1 case.

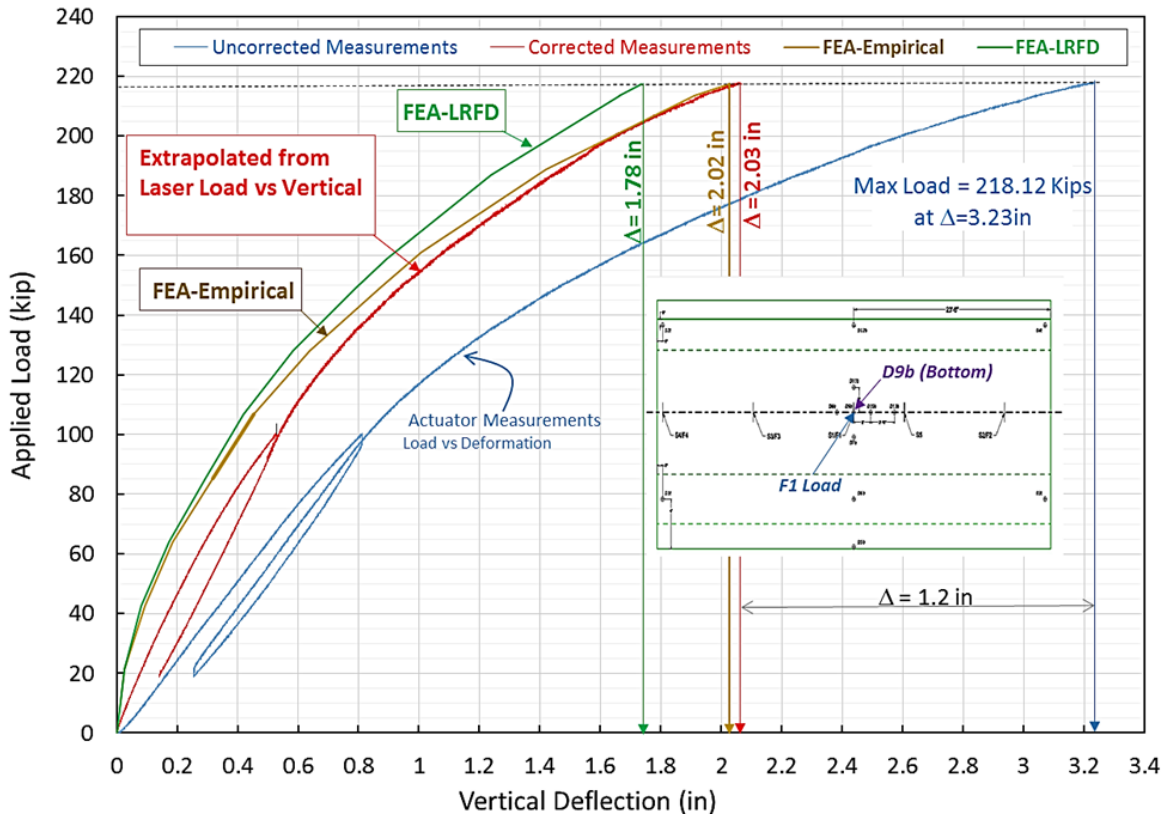


Figure 6.5: Laboratory test results and FEA results of F1-Test

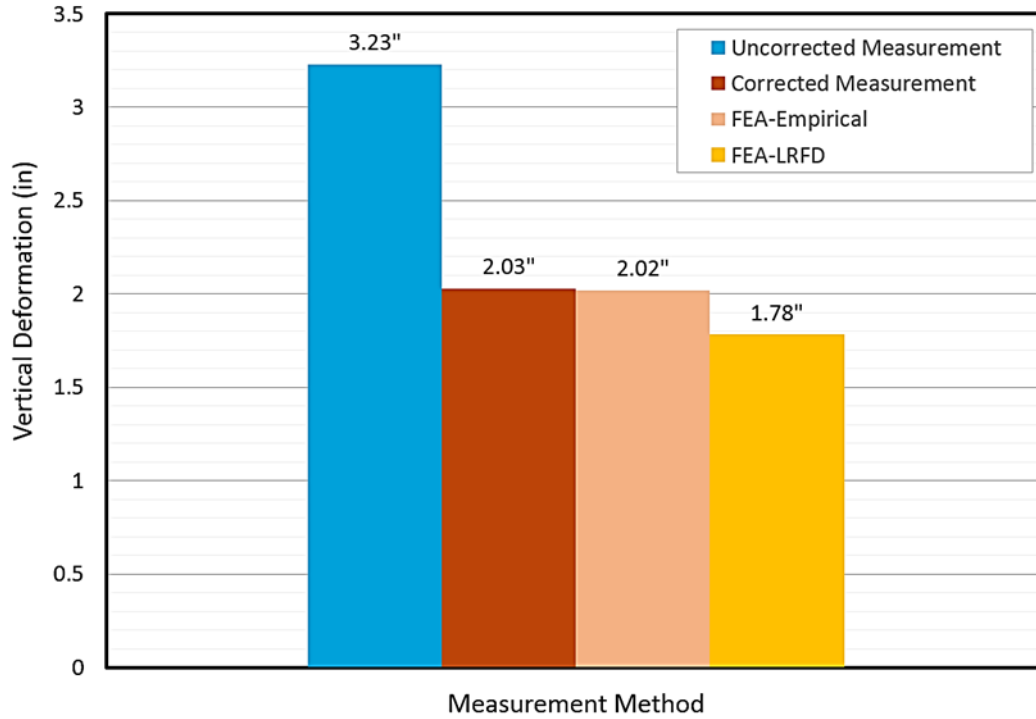


Figure 6.6: Vertical deformations from laboratory and FEA models for F1-Test

A comparison of the crack patterns in the actual test specimen and in the finite element model were shown in Figure 6.7 and Figure 6.8. It shows a good prediction by the finite element model for the crack distribution. The crack propagation and extent in transverse and longitudinal directions of the tested deck specimen in failure load case F1 were approximately 87 to 96 inch. The FEA predicted a similar range of 80 x 102 inch. Figure 6.8 show the finite element crack distribution.



Figure 6.7: Top and bottom slab crack distribution and failure (F1-test)

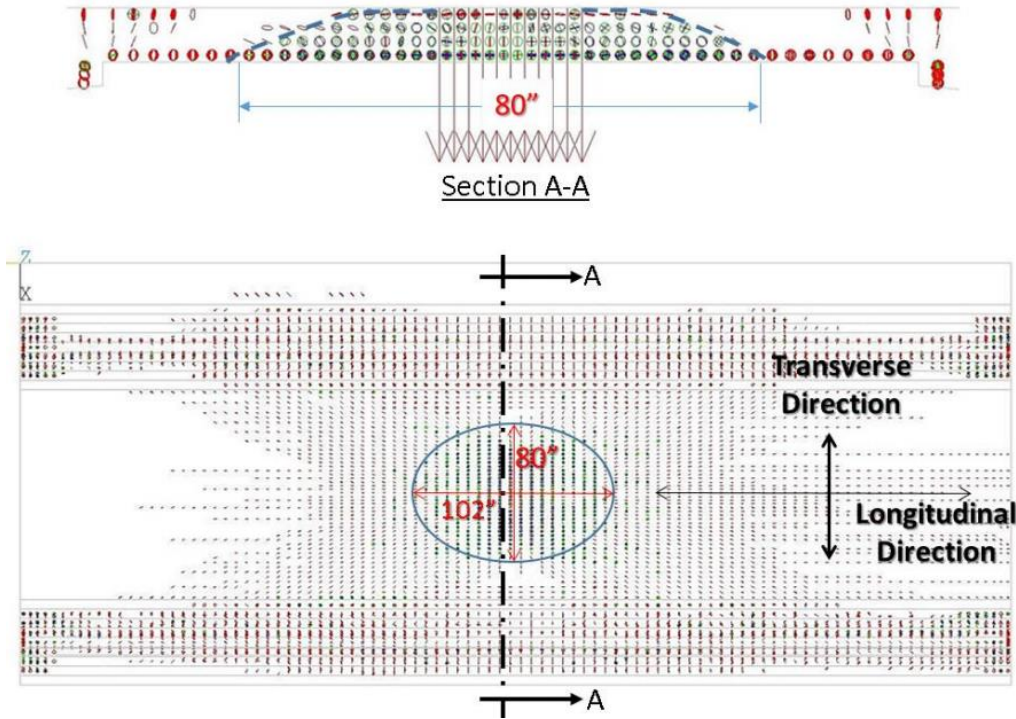


Figure 6.8: Crack distribution from FEA-empirical slab

## 6.2 Comparison of Analytical Results and the Failure Test Results

In addition to the FEA methods, three analytical methods were used in this study to predict the failure load for the tested specimens. Those methods were: flexural analysis, punching shear, and Taylor et al.'s approach. These methods were used to compare the failure load only as they cannot predict the entire behavior; i.e., under different load levels such as service.

Failure load predictions obtained from all of these methods underestimated the capacity of the tested deck specimen. Experimentally, the specimen's highest failure load was 218 kip. Flexural analysis of the deck specimen resulted in a predicted failure load of 26.5 kip, which is only 12.2% of the actual recorded capacity of the tested specimen. Taylor et al.'s approach predicted a failure load of 108 kip, which is a combination of ultimate flexure capacity and ultimate arching capacity. Although Taylor et al.'s approach produced a higher failure load than the one predicted using flexural analysis, it is still much lower than the experimentally recorded capacity of the test specimen. Failure load predicted using the punching shear method was the closest to the experimentally recorded failure load. A failure load of 171.6 kip was predicted using the AASHTO LRFD punching shear provisions, which is still 21.3% lower than the experimentally obtained deck capacity.

## Chapter 7                      Conclusions and Recommendations

In this chapter, the results from this study are summarized and proposed changes to current specifications and details for the construction of bridge decks that would be subjected to future widening are recommended. These recommendations are based on observations and test results of the empirical deck specimen.

### 7.1      Summary

Based on the extensive research in literature investigating the behavior of concrete deck slabs, findings from this research confirmed that the primary structural action by which reinforced concrete bridge deck slabs resist concentrated wheel loads is not flexure, but rather a complex internal membrane stress state referred to as internal arching (AASHTO LRFD, C9.7.2.1). This action is sustained by in-plane membrane forces that develop as a result of lateral confinement provided by the surrounding concrete slab and supporting girders or other components that may restrain the slab's lateral deformation. The empirical design method is based on the assumption that the deck behaves more like a "membrane" than a series of continuous beams. The arching creates an internal compressive dome. The arching action is complemented by a flexural component in resisting the full wheel load. The bottom transverse steel reinforcement acts as ties providing the lateral confinement required to develop such arching effect; in addition to providing flexural resistance for positive moments. It is well known that the traditional design method typically results in a higher ratio of steel reinforcement than the empirical method, hence the continued interest in the empirical design method (cost savings, ease of construction, and reduced design time).

AASHTO LRFD requires that four layers of isotropic reinforcement shall be provided in slabs designed according to the empirical method. It also requires that reinforcement shall be provided in each face of the slab with the outermost layers placed in the direction of the effective length; i.e., transversally for typical slab on girder bridges. Although 0.2% steel reinforcement in each of four layers based on the effective depth ( $d_e$ ) satisfies strength requirements, the minimum amount of reinforcement for better crack control in the positive moment area shall be 0.3% of the gross area. This corresponds to about 0.27 in.<sup>2</sup>/ft of steel (in a 7.5-in. slab) and 0.288 in.<sup>2</sup>/ft of steel (in an 8.0-in. slab) for each bottom layer. AASHTO LRFD also requires about 0.2% reinforcement steel or 0.18 in.<sup>2</sup>/ft for each top layer. Spacing of steel bars shall not exceed 18.0 in. Reinforcing steel shall be Grade 60 or better.

The scope of this research did not address arching action in the cantilevered overhang of the deck. However, literature included some work related to this topic. For example, AASHTO LRFD states in the commentary for provision 9.7.2.2 that although tests in the literature indicated that arching action may exist in the cantilevered overhang of the slab, the available evidence is not sufficient to formulate code provisions for it. Consequently, the provisions of this article are not allowed to be applied to overhangs. The overhang should be designed for: (1) Wheel loads for decks with discontinuous railings and barriers using the equivalent strip method, (2) Equivalent line load for decks with continuous barriers, and (3) Collision loads.

The challenge this research addresses, is whether or not the FDOT SDG should change its stance on the empirical design method for deck slabs and allow its use per AASHTO LRFD, 9.7.2.4. Currently, all deck slabs are required to be designed according to the Traditional Design Method (AASHTO LRFD, 9.7.3). According to the FDOT SDG the empirical design method is not permitted because of the potential for future widening or phased construction and associated traffic control impact in order to comply with AASHTO LRFD, 9.7.2.4. Another challenge is that some of the conditions for using the empirical design method are not met for a considerable range of bridge configurations, e.g. exceeding the maximum effective length or effective length to design depth ratio limits.

Chapter 7 of the FDOT Structures Design Guidelines (SDG) discusses widening and rehabilitation. This chapter includes considerations such as load rating, analysis, and design. The widening and rehabilitation of the bridge should take aesthetics into consideration. The overall purpose is to avoid having the new girders and slab seem as an obvious “add-on” to the bridge. The FDOT SDG, 7.1.2 also has the following requirements for bridge decks: (a) Evaluate existing beam and girder supported decks for the temporary partially demolished condition; (b) For existing decks designed using the empirical deck design method, and where the distance from the centerline of the exterior girder web to the saw-cut line of the overhang is less than 5.0 times the existing deck thickness per AASHTO LRFD, 9.7.2.4, restricts traffic from the first outer bay for I beam superstructures. In addition, the FDOT SDG, 7.3.4 requires that: (a) Design all widenings and rehabilitations in accordance with AASHTO LRFD; (b) Review stresses in the main exterior member of the existing structure for construction conditions and the final condition; i.e., after attachment of the widened portion of the structure. When computations indicate overstresses in the exterior member of the existing structure, request a Design Variation from the appropriate FDOT Structures Design Office. The FDOT SDG, 7.4.4 also lists some connection details pertaining to superstructure widening. Figure 7.1 is a copy of Figure 7.4.4-3 of the FDOT SDG, and shows deck connection recommendations for prestressed concrete girder bridges being widened.

### Figure 7.4.4-3 AASHTO Beam Superstructure Widening

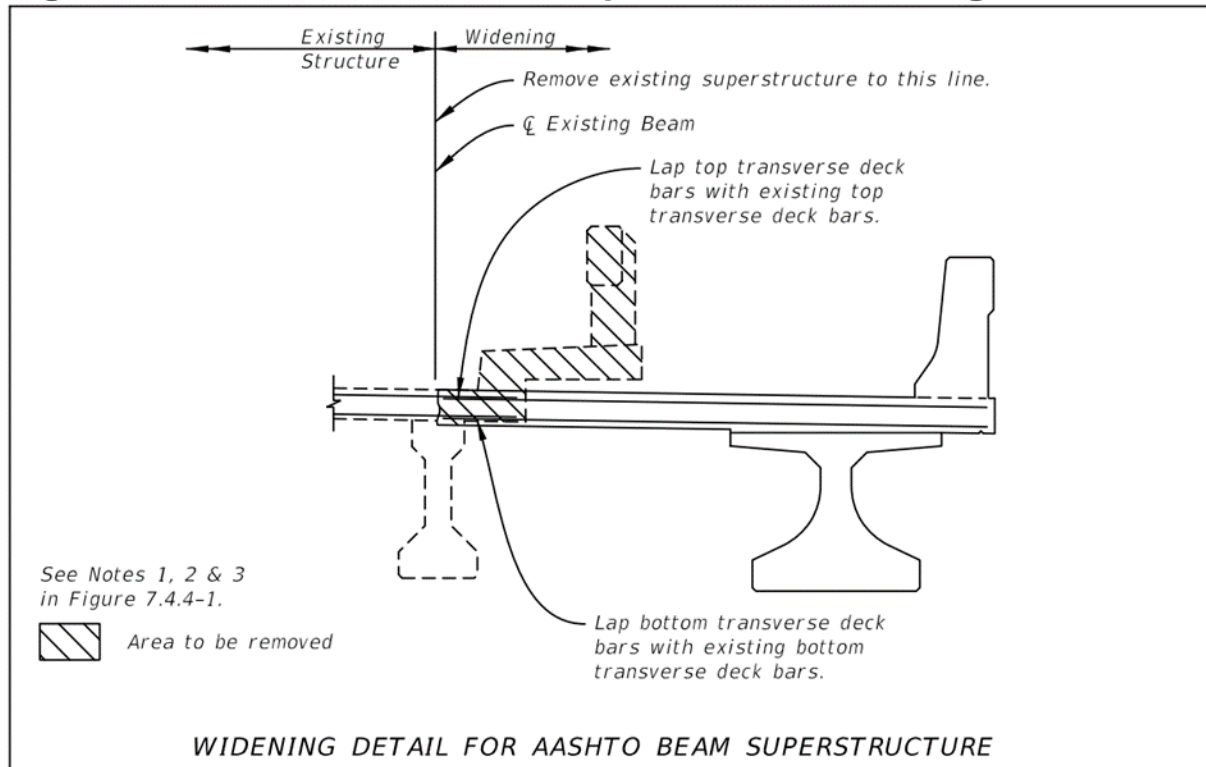


Figure 7.1: Typical widening taken from FDOT SDG

To explore whether the empirical design method could be extended beyond AASHTO’s existing limitations, the test specimen used in this study was designed to cover an extreme case. For example, it was decided to use the maximum allowable beam spacing of 14 feet, with 8-inch thickness for the tested deck specimen. These dimensions were close to AASHTO LRFD’s maximum limit pertaining to the ratio of the effective span length as determined by girder spacing to the slab design depth; should be less than, or equal to, 18.0. Other conditions that the Canadian code specified for allowing the use of the empirical method is that the spacing of the supporting beams shall be limited such that the effective length does not exceed 13.12 ft (4.0 m). Also, it is required that the slab shall extend sufficiently beyond the external beams to provide full development length for the bottom transverse reinforcement. According to AASHTO LRFD, the effective length limit is 13.5 ft. The tested specimen, with 14 ft beam spacing, had an effective length of 11 ft-8.5 inch. However, the deck at the widening side did not have any overhang as it was cut close to the centerline of the exterior beam. The results of the testing are summarized in the following section.

## 7.2 Conclusions

The tested specimen in this research confirmed that the failure occurred as a result of overstraining around the perimeter of the wheel footprint. The peak failure loads happened when the deck suddenly failed around the loading pad in a manner similar to classical punching shear. The deck failure started with a hybrid flexural/punching shear mode where compressive

membrane action led to a large elliptical-shaped damage at the bottom surface of the slab followed by a sudden punching shear failure at the top surface that was slightly larger than the loading pad. The cracks at the bottom surface of the deck extended to distances ranging from 6.6 ft to more than 8.8 ft (see Appendix VII).

The test results turned out to be favorable meeting the requirements set by AASHTO LRFD. Strength and serviceability requirements were satisfied for all load cases and locations. Load case F1, at midspan of the longitudinal direction had the highest load capacity of 218 kip. Under service loads, the design wheel load including dynamic magnification resulted in deflections that meet the AASHTO LRFD, 9.5.2 requirements ( $L/800$ ) for service load cases, namely S1, S2, S3, and S5, with a huge margin. The critical edge case, S4, also meets the AASHTO LRFD deflection limit with a smaller margin. If a higher margin against deflection is desired for slab end loading case, thickening of the deck may be needed, as the FDOT requires.

Cracking was not visually noticeable during initial service load tests up to service load levels, and crack widths under repeated service loads of 22 kip (97.8 kN) were considered acceptable. The cracks present, induced from higher loads, did not open wide enough to be a problem when service loads were repeated and put back on the bridge. The acceptance of crack width is based on the limit most practice manuals consider as not in need for action to repair the crack. In failure load cases F1, F2, and F3, the test failure load exceeded the estimated pure flexure capacity multiple times reaching 6 to 8 times the estimated flexural load capacity. The failure loads also exceeded the calculated factored design wheel load of 37.24 kip (165.7 kN), reaching 4 to 6 times that factored load. That indicated that the deck behavior does not follow the classical bending theory. According to AASHTO LRFD, C9.7.2.1, the empirical method is conservative with a significant factor of safety of 8, thus providing a considerable reserve strength. This factor of safety comes from working stress design from the 16th edition of AASHTO Standard Specifications.

### 7.3 Recommendations for Construction and Design

In this study, load tests were conducted on a bridge deck specimen that had 0.3% orthotropic reinforcement (top and bottom) of the gross concrete area, supported on wide flanged Florida I-beams. From static test results and analyses, the following recommendations were made. It should be noted that cyclic, thermal, and dynamic loads were not part of the scope of this study.

1. In comparison to AASHTO beams, the wider top flanges of FIB precast prestressed concrete sections (4 ft) allow extending the distance at which existing deck concrete removal starts beyond the centerline of the beam, thus keeping both legs of girder stirrups embedded in old deck concrete. It is recommended that the extent of existing deck demolition (for widening projects) or cold joint location (for phased construction projects) be set at a distance equal to 6 in. beyond the centerline of the exterior girder as shown below in Figure 7.2.

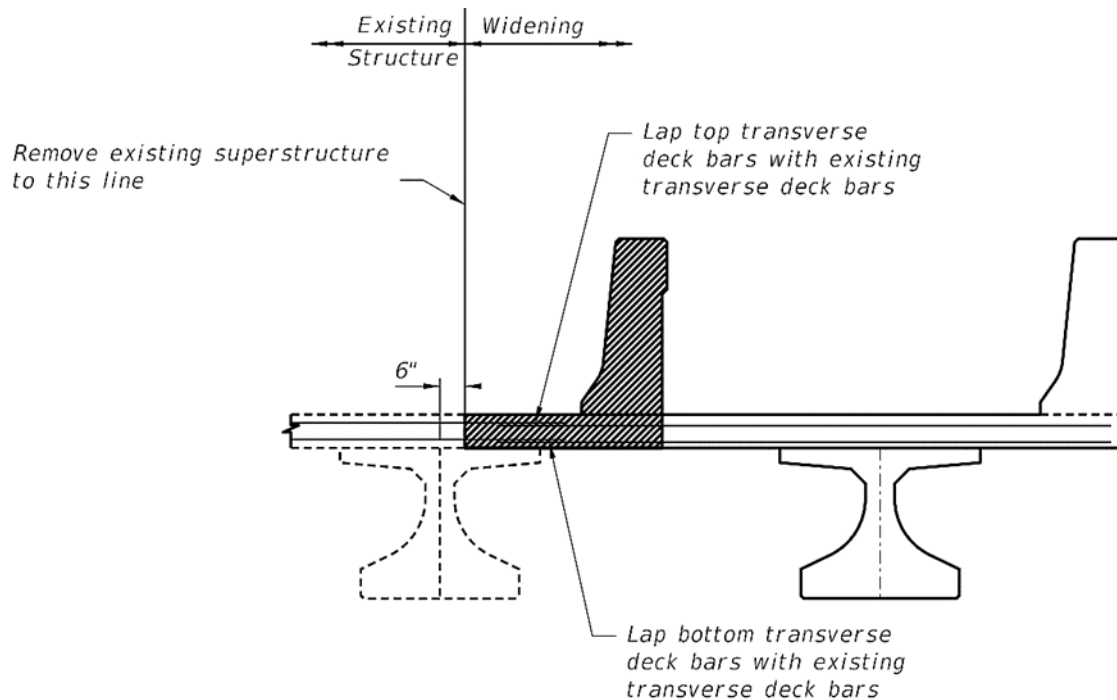


Figure 7.2: Proposed widening detail

2. It is recommended to stagger the steel reinforcement in both transverse and longitudinal direction in the concrete deck to enhance distribution and for ease of construction.
3. It is recommended to use a minimum deck thickness of 8 inches excluding any sacrificial thickness.
4. As per FDOT Structures Design Guidelines, 4.2.4, it is required to provide thickened deck ends at locations of deck discontinuity that are not supported by full depth diaphragms. Reference should be made to the FDOT Structures Detailing Manual, Chapter 15 for thickened deck end details for use with Florida-I Beams.
5. The tested specimen performed satisfactorily with the deck reinforced using two meshes of #5 bars at 12 in. It is recommended to use steel reinforcement of either #5 bars at 12 inches or #4 at 8 inches in both transverse and longitudinal directions for both top and bottom steel layers to further improve crack control under service conditions. The extreme layers of steel (top and bottom) should be placed transversely for enhanced effectiveness in the transverse direction. In addition, proper curing as per FDOT Standard Specifications is important to minimize early age cracking.
6. Using Florida I-Beams with a beam spacing of 14 feet proved to be acceptable to support an 8-inch-thick deck designed with the empirical method. The deck fulfilled both serviceability and strength requirements.
7. It is recommended that future research should investigate the skew effects on bridge deck behavior.

## References

- AASHTO. 2012. *AASHTO LRFD Bridge Design Specifications 6th Edition*. Washington, D.C.: American Association of State Highway and Transportation Officials.
- . 2002. *AASHTO Standard Specifications for Highway Bridges*. Washington, D.C: American Association of State Highway and Transportation Officials.
- . 1996. *AASHTO Standard Specifications for Highway Bridges*. Washington, D.C: American Association of State Highway and Transportation Officials.
- Alabama Department of Transportation. 2008. "Structures Design and Detailing Manual." *ALDOT Bridge Bureau*. January 1.  
<https://www.dot.state.al.us/brweb/doc/ALDOTStructuresDesignDetailManual.pdf>.
- American Concrete Institute. 2014. *ACI Committee 318. Building Code Requirements for Structural Concrete (ACI 318-14) and Commentary (318R-14)*. Farmington Hills, Michigan: American Concrete Institute.
- Arizona Department of Transportation. 2012. "Bridge Design Guidelines." *Arizona DOT*.  
<http://www.azdot.gov/docs/default-source/bridge-group/section9-decksanddecksystems.pdf>.
- Bakht, Baidar. 1993. *Less Steel in Bridge Decks Saves \$1 Million a Year, No.1*. Ontario, Canada: Ministry of Transportation and Communications.
- Bakht, Baidar, and L G Jaeger. 1992. "Ultimate Load Test of Slab-on-Girder Bridge." *American Society of Civil Engineers, Structural Engineering* 1608-1624.
- Bakht, Baidar, and R P Csagoly. 1972. *Bridge Testing, SRR-79-10*. Ontario, Canada: Ontario Ministry of Transportation and Communicatons.
- Barth, F, and R Frosch. 2001. *Control of Cracking in Concrete Structures*, 224. Farmington Hills, Michigan: American Concrete Institute Committee, 12-16.
- Batchelor, B D. 1990. *Membrane Enhancement in Top Slabs of Concrete Bridges*. Kingston, Ontario, Canada: Elsevier Applied Science Publishers Ltd.
- Batchelor, B V, and B E Hewitt. 1976. "Tests of Model Composite Bridge Decks." *American Concrete Institute Journal* 73 340-343.
- British Standards Institute. 1990. *Part 2 & 4, British Standards for the Design of Steel, Concrete and Composite Bridges*. London: British Standards Insitution.
- California Department of Transportation. 2011. "Bridge Manuals." *CALTRANS*.  
[http://www.dot.ca.gov/hq/esc/techpubs/manual/bridgemanuals/bridge-designpractice/pdf/bdp\\_10.pdf](http://www.dot.ca.gov/hq/esc/techpubs/manual/bridgemanuals/bridge-designpractice/pdf/bdp_10.pdf).
- Canadian Standards Association. 2006. *Canadian Highway Bridge Design Code* . Mississauga, Ontario, Canada: Canadian Standards Association.

- Christiansen , K P, and V T Frederiksen . 1983. "Experimental Investigation of Rectangular Concrete Slabs with Horizontal Restraints, Vol. 16, Issue 3." *Materiaux et Construction* 179-192.
- Christiansen , K P. 1963. "The Effect of Membrane Stresses on the Ultimate Strength of the Interior Panel in a Reinforced Concrete Slab, Archive, Volume 41, Issue 8." *The Structural Engineer, The institute of Structural Engineers*.
- Colorado Department of Transportation . 1989. "Bridge Design Manual." *Colorado DOT*.  
[http://www.coloradodot.info/library/bridge/bridge-manuals/bridge-designmanual/dm\\_s08.pdf](http://www.coloradodot.info/library/bridge/bridge-manuals/bridge-designmanual/dm_s08.pdf).
- Connecticut Department of Transportation . 2011. "Bridge Design Manual." *Connecticut DOT* .  
<http://www.ct.gov/dot/lib/dot/documents/dpublications/bridge/bdm.pdf>.
- Delaware Department of Transportation. 2005. "Bridge Design Manual." *Delaware DOT*.  
[http://deltrac.org/information/pubs\\_forms/manuals/bridge\\_design/pdf/bdm-05-](http://deltrac.org/information/pubs_forms/manuals/bridge_design/pdf/bdm-05-)
- Fang, I K. 1985. *Behavior of Ontario-type Bridge Deck on Steel Girders*. Austin, Texas: University of Texas.
- Fang, I K, J H Lee, and C R Chen. 1994. "Behavior of Partially Restrained Slabs Under Concentrated Load." *American Concrete Institute Structural Journal*, 91(2) 133-139.
- Fang, I K, J Worley, N H Burns, and R E Klinger. 1990. "Behavior of Isotropic Concrete Bridge Decks on Steel Girders." *American Society of Civil Engineers Journal of Structural Engineering* 116(3) 659-678.
- FDOT. 2012. *Bridge Load Rating Manual*. Tallahassee, FL: Florida Department of Transportation.
- . 2014. *Structures Design Guidelines*. Tallahassee: Florida Department of Transportation.
- Florida Department of Transportation. 2016. *FDOT Standard Specifications for Road and Bridge Construction*. Tallahassee: Florida Department of Transportation.
- Frosch, R J, D T Blackman, and R D Radabaugh. 2003. *Investigation of Bridge Deck Cracking in Various Bridge Superstructure Systems (Publication No. FHWA/IN/JTRP-2002/25)*. Indiana Department of Transportation and Purdue University .
- Fu, G, S Alampalli, and F Pezze . 1992. *Long-Term Serviceability of Isotropically Reinforced Bridge Deck Slabs*. New York: Transportation Research Board.
- Georgia Department of Transportation . 2012. "Bridge and Structure." *Georgia DOT*.  
<http://www.dot.ga.gov/doingbusiness/PoliciesManuals/roads/>.
- Gvozdev, A A. 1939. *Comments on Clause 33 of the Russian Code for Reinforced Concrete*. Russia: Stroitel'naya Promyshlennost, Vol 17, No. 3.

- Hewitt, B E, and B V Batchelor . 1975. "Punching Shear Strength of Restrained Slabs." *American Society of Civil Engineers Journal of Structural Engineering 101(ST9)* 1837-1853.
- Hung , T Y, and E G Nawy. 1971. "Limit Strength and Serviceability Factors in Uniformly Loaded, Isotropically Reinforced Two-Way Slabs, Paper 30-14." *American Concrete Institute Publication SP-30*.
- Idaho Department of Transportation . 2005. "Bridge Manual." *Idaho DOT*.  
<http://itd.idaho.gov/bridge/manual/09%20Decks%20and%20Deck%20System/A9.1%20Minimum%20deck%20thickness.pdf>.
- Illinois Department of Transportation. 2012. "Bridge Manual Design Guides." *Illinois DOT*.  
[http://www.dot.il.gov/bridges/Design%20Guides/Design\\_Guides\\_Web.pdf](http://www.dot.il.gov/bridges/Design%20Guides/Design_Guides_Web.pdf).
- Indiana Department of Transportation. 2012. "Design Manual." *Indiana DOT* . [http://www.in.gov/indot/design\\_manual/files/Ch404\\_2013.pdf](http://www.in.gov/indot/design_manual/files/Ch404_2013.pdf) .
- Iowa Department of Transportation. 2012. "LRFD Bridge Design Manual." *Iowa DOT*.  
<http://www.iowadot.gov/bridge/policy/52DecklrfdJa14.pdf>.
- Kansas Department of Transportation . 2010. "LRFD Bridge Design Manual." *Kansas DOT*.  
[http://www.ksdot.org/burdesign/bridge/lrfd/Chapter3\\_9.pdf](http://www.ksdot.org/burdesign/bridge/lrfd/Chapter3_9.pdf).
- Kirkpatrick, J, G I Rankin, and A E Long. 1984. "Strength Evaluation of M-beam Bridge Deck Slabs." *Structural Engineer 62b(3)* 60-68.
- Kirkpatrick, J, G I Rankin, and A E Long. 1986. "The Influence of Compressive Membrane Action on Serviceability of Beam and Slab Bridge Decks." *Structural Engineering 64b(1)* 6-9,12.
- Long , A E, and G I Rankin . 1989. "Real Strength and Robustness of Reinforced Concrete Structures ." *Conservation of Engineering Structures, Thomas Telford* 47-58.
- Long , A E, J Kirkpatrick, and G I.B Rankin . 1995. "Enhancing Influence of Compressive Membrane Action in Bridge Decks ." *Bridge Modification Conference Proceedings* 217-227.
- Louisiana Department of Transportation and Development. 2008. *LRFD Bridge Design Manual*. Baton Rouge, LA. : Lousiana Department of Transportation and Development .
- Maine Department of Transportation. 2003. "Bridge Design Guide ." *Maine DOT*. <http://www.maine.gov/mdot/technicalpubs/documents/pdf/brgdg/chapter6concretefinal.pdf>.
- Majumdar, P, J Lesko, T Cousins , and Z Liu. 2009. "Conformable Tire Patch Loading for FRP Composite Bridge Deck." *J. Compos. Constr. 10.1061/(ASCE)CC.1943-5614.0000033* 575-581.
- Massachusetts Department of Transportation. 2009. "LRFD Bridge Manual." *Massachusetts DOT*.

- [http://www.mhd.state.ma.us/downloads/bridge/manual\\_lfrd/part1/CHAP3\\_LRFD\\_MassDOT\\_September13.pdf](http://www.mhd.state.ma.us/downloads/bridge/manual_lfrd/part1/CHAP3_LRFD_MassDOT_September13.pdf).
- Materson, D M, and A E Long . 1974. "The Punching Strength of Slabs, A Flexural Approach using Finite Elements ." *American Concrete Institute 2(SP 42, Part 4)* 747-768.
- McDowell, E L, K E McKee, and E Sevin . 1956. "Arching Action Theory of Masonry Walls." *American Society of Civil Engineers Journal of Structural Engineering* 82(ST2) 915-1 to 915-18.
- Michigan Department of Transportation. 2012. "Design Manual - Bridge Design ." *Michigan DOT*. <http://mdotcf.state.mi.us/public/design/englishbridgemanual/>.
- Minnesota Department of Transportation. 2013. "LRFD Bridge Design Manual." *Minnesota DOT*. <http://www.dot.state.mn.us/bridge/pdf/lrfdmanual/section09.pdf>.
- Missouri Department of Transportation. 2013. "LRFD Bridge Design Guidelines ." *Missouri DOT*. [http://epg.modot.org/index.php?title=751.10\\_General\\_Superstructure](http://epg.modot.org/index.php?title=751.10_General_Superstructure).
- Montana Department of Transportation . 2002. *Structures Manual*. Helena, MT: Montana Department of Transportation.
- Mufti , A A, L G Jaeger , B Bahkt , and L D Wegner. 1993. "Experimental Investigation of Fiber Reinforced Concrete Deck Slabs Without Internal Steel Reinforcement ." *Canadian Journal of Civil Engineering* 20 (3) 398-406.
- Nebraska Department of Roads . 2013. "Bridge Office Policies and Procedures Manual." *Nebraska DOT*. <http://www.transportation.nebraska.gov/design/bridge/bopp/BOPPMannual.pdf>.
- Nevada Department of Transportation. 2008. "Structures Manual." *Nevada DOT*. [http://www.nevadadot.com/uploadedFiles/NDOT/About\\_NDOT/NDOT\\_Divisions/Engineering/Structures/Structures\\_manual.pdf](http://www.nevadadot.com/uploadedFiles/NDOT/About_NDOT/NDOT_Divisions/Engineering/Structures/Structures_manual.pdf).
- New Jersey Department of Transportation . 2009. *Design Manual for Bridges and Structures* . Trenton, NJ: New Jersey Department of Transportation .
- New Mexico Department of Transportation. 2013. "Bridge Procedures and Design Guide ." *New Mexico DOT*. [http://dot.state.nm.us/content/dam/nmdot/Bridge/BRIDGE\\_](http://dot.state.nm.us/content/dam/nmdot/Bridge/BRIDGE_).
- New York Department of Transportation . 2011. *Bridge Manual 4th Ed*. Albany, NY: New York Department of Transportation.
- Nielsen, R, E R Schmeckpeper, C Shiner , and M Blandford . 2010. *The Effect of the Bridge Deck Design Methodology on Cracking Control, Research Paper RP184*. NIATT-University of Idaho.
- North Carolina Department of Transportation. 2013. "Structures Design Manual ." *North Carolina DOT*. February. <https://connect.ncdot.gov/resources/Structures/StructureResources/LRFDManual>.

- North Dakota Department of Transportation . 2004 . "LRFD Bridge Design Specifications ." *North Dakota DOT* .  
[https://www.dot.nd.gov/manuals/design/designmanual/chapter4/DM-4-04\\_tag.pdf](https://www.dot.nd.gov/manuals/design/designmanual/chapter4/DM-4-04_tag.pdf).
- Ockleston , A J. 1955. "Load Test in a 3-Storey RC Building in Johannesburg." *Structural Engineer* (33) 304-322.
- Ohio Department of Transportation. 2012. "Bridge Design Manual." *Ohio DOT*.  
<http://www.dot.state.oh.us/Divisions/Engineering/Structures/standard/Bridges/BDM/BD>.
- Ontario Ministry of Transportation. 1979. *Ontario Highway Bridge Design Code (OHBDC) 1st Ed.* . Ontario, Canada : Ontario Ministry of Transportation.
- Oregon Department of Transportation. 2012. "Bridge Engineering ." *Oregon DOT*.  
<http://www.oregon.gov/ODOT/HWY/BRIDGE/Pages/index.aspx>.
- Park , R. 1965. "The Lateral Stiffness and Strength Required to Ensure Membrane Action at Ultimate Load." *Magazine of Concrete Research*, V.17, No. 50 29-38.
- Park , R, and W L Gamble . 1980. "Reinforced Concrete Slabs." *Wiley Interscience* (Wiley Interscience) 562-612.
- Pennsylvania Department of Transportation . 2012. "Design Manual- (Publication No. 15M)." *Pennsylvania DOT*. <ftp://ftp.dot.state.pa.us/public/PubsForms/>.
- Pucher , A. 1964. *Influence Surfaces of Elastic Plates*. Wein, New York: Springer-Verlag.
- Rankin , G I, and A E Long . 1997. "Arching Action Strength Enhancement in Laterally Restrained Slab Strips ." *Proceedings of the Institution of Civil Engineers, Structures and Buildings No. 122* 461-467.
- Rankin, G I.B. 1982. *Punching Failure and Compressive Membrane Action in Reinforced Slabs, PhD Thesis*. Dept. of Civil Engineering Queen's University of Belfast.
- Rhode Island Department of Transportation. 2007. "LRFD Bridge Design Manual ." *Rhode Island DOT*.  
<http://www.dot.ri.gov/documents/engineering/br/RILRFDBridgeManual.pdf>.
- South Carolina Department of Transportation . 2006. "Bridge Design Manual." *South Carolina DOT*. <http://www.scdot.org/doing/technicalPDFs/structuralDesign/Files/Foreword.pdf>.
- Taylor, R, and B Hayes. 1965. "Some Tests on the Effect of Edge Restraint on Punching Shear in Reinforced Concrete Slabs." *Magazine of Concrete Research Volume 17, Issue 50*, March: 39-44.
- Taylor, S E. 2000. *Compressive Membrane Action in High Strength Concrete Bridge Deck Slab (doctoral dissertation)*. Belfast Northern Ireland, UK: Queen's University.

- Taylor, S E, G I Rankin, and D J Cleland. 2003. "High Performance Concrete Bridge Deck Slabs 156(BE2)." *Proceedings of Institution of Civil Engineers, Structures and Buildings* 81-90.
- Taylor, S E, G I.B Rankin, and D J Cleland. 2002. *Guide to Compressive Membrane Action in Concrete Bridge Decks, Technical Paper 3*. Camberley, Surrey: Concrete Bridge Development Group.
- Taylor, S, G Rankin, D J Cleland, and J Krikpatrick. 2007. "Serviceability of Bridge 179 Deck Slabs with Arching Action." *American Concrete Institute Structural Journal No.104-S05* 39-48.
- Texas Department of Transportation. 2015. *Bridge Design Manual*. Austin, Texas: Texas Department of Transportation.
- Tsui, C K, N H Burns, and R E Klinger . 1986. *Behavior of Ontario-Type Bridge Decks on Steel Girders: Negative Moment Region and Load Capacity*. Austin, Texas.
- Turner , C. 1980. "Concrete Steel Construction." *Michigan: Buildings ACI Special Publication SP-52, American Concrete Institute (ACI)*.
- UK Highway Agencies. 2002. "Use of Compressive Membrane Action in Bridge Decks (BD81/02)." *Design Manual of Roads and Bridges* 20.
- Vermont Agency of Transportation. 2010. *Structures Design Manual*. Montpelier, Vermont: Vermont Agency of Transportation.
- Virginia Department of Transportation. 2012. "Structures and Bridge Manuals." *Virginia DOT*. <http://www.extranet.vdot.state.va.us/locdes/electronic%20pubs/Bridge%20Manuals/Volu>
- Washington State Department of Transportation . 2011. "Bridge Design Manual LRFD." *Washington State DOT*. <http://www.wsdot.wa.gov/publications/manuals/fulltext/M23->
- West Virginia Department of Transportation. 2006. *Bridge Design Manual*. Charleston, West Virginia: West Virginia Department of Transportation.
- Wisconsin Department of Transportation. 2011. "LRFD Bridge Manual." *Wisconsin DOT*. [http://on.dot.wi.gov/dtid\\_bos/extranet/structures/LRFD/BridgeManual/Ch-17.pdf](http://on.dot.wi.gov/dtid_bos/extranet/structures/LRFD/BridgeManual/Ch-17.pdf).
- Wyoming Department of Transportation . 2012. "Bridge Design Manual." *Wyoming DOT*. [http://www.dot.state.wy.us/files/live/sites/wydot/files/shared/Bridge/Bridge%20Design%](http://www.dot.state.wy.us/files/live/sites/wydot/files/shared/Bridge/Bridge%20Design%20Manual.pdf)

APPENDICES

APPENDIX I: FORMWORK PICTURES









# APPENDIX II: MIX DESIGN

## CONCRETE MIX DESIGN

Class: **II DECK**

Mix Design Number: **03-1905-01**

Minimum Strength: **4500 psi**

FDOT Approval Date: **02/07/2015**

Hot Weather? **Yes** Issuer's Name: \_\_\_\_\_

Status: **APPROVED**

Slip Form? **No** Project #: \_\_\_\_\_

Producer: **Argos**

Plant #: \_\_\_\_\_

### Source of Materials

Product Product Name	Quantity	Producer Plant #	QPL # Spec:	SSD	FM	Geological Type
Cement: Type II Cement MH	511 LB	ARGOS CEMENT-NEWBERRY CMT09	AASHTO M85 II LS (MH)	3.15		
Fly Ash: Class F Fly Ash	132 LB	SEPARATION TECHNOLOGIES-CRYSTAL RIVER FA01	ASTM C 618 - Class F	2.40		
Coarse Aggregate: # 57 Stone	1750 LB	MARTIN MARIETTA MATERIALS 38228		2.56		Limestone
Fine Aggregate: Silica Sand	1191 LB	ROBERTS SAND COMPANY, LLLP 50382		2.63	2.38	Silica Sand
Air Ent Admixture: Darex AEA	1.6 OZ	W R GRACE CO	924-000-002 AASHTO M 154 - AEA			
Type D Admixture: WRDA 64	35.5 OZ	W R GRACE CO	924-003-020 AASHTO M 194 - Type D			
Water: Water for Concrete	33.5 GA					
Water: Water for Concrete	279 LB					

	Specification Limits		Producer Data		
ROLL-A-METER Air Content	<u>1.00 to 6.00</u>	percent	W/cm Ratio	0.43	LB per LB
Compressive Strength	<u>greater than or equal to 4500</u>	avgpsi	Theoretical Yield	26.98	CF
Heat of Hydration	<u>Less than or equal to 88</u>	cal/g	Temperature	94	degree F
Slump	<u>1.50 to 4.50</u>	inches	Slump		inches
Temperature	<u>Less than or equal to 100</u>	degree F	Heat of Hydration	79	cal/g
W/CM Ratio	<u>Less than or equal to 0.43</u>	LB per LB	Unit Weight (Wet)	143.1	LBperCF
			Chloride Content	0.236	LB per CY
			Air Content		percent
			Aggregate Correction Factor		

Aggregate Correction Factor:

### Comments:

Fine Aggregate Substitution: 50-382 for GA-668

### APPENDIX III: FEA AND DESIGN CALCULATIONS

The following present calculations performed using MATHCAD to determine the steel reinforcement requirements in both traditional and empirical methods of all iterations used in FEM analyses. Slab thickness of 8 inch, 9 inch and 10 inch were considered in the calculations of the steel distribution including vertical steel reinforcement in supporting girders. The steel/concrete ratios were used in the smeared reinforcement of concrete elements.

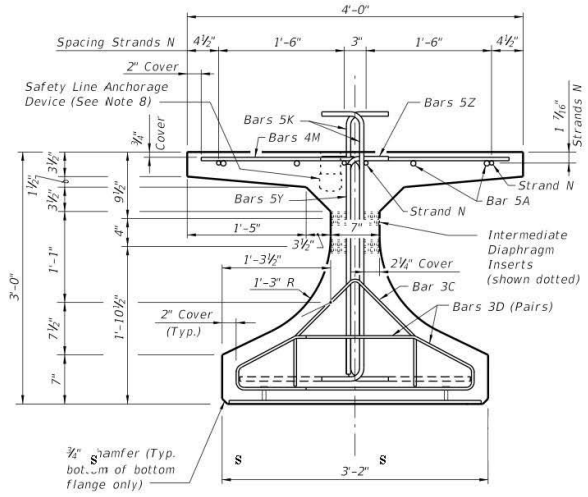
Span := 90ft

**ZONE 2 CALCULATIONS**

Span Calculations

Space<sub>1</sub> := 12.3in

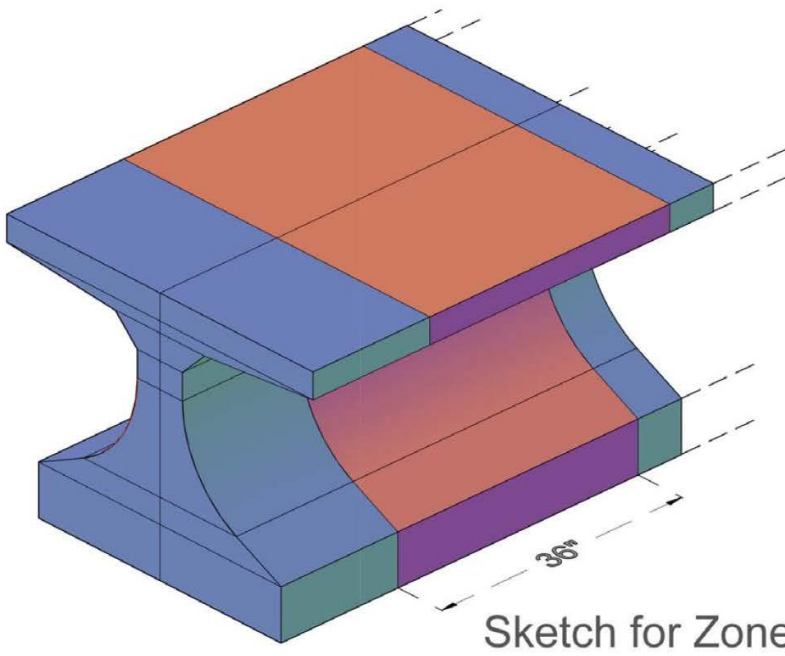
Space<sub>2</sub> := 6.6in



END VIEW

$Z2_{Span} := \max(\text{Space}_1, \text{Space}_2)$

$Z2_{Span} = 36\text{-in}$



Sketch for Zone 2

Reinforcement Details

**5k Bars**

Total Number of Bars

Y - Direction

$$\text{Length} := 36\text{in} - \frac{3}{4}\text{in} - \frac{1}{4}\text{in} = 35\text{in}$$

$$\text{Area} := \frac{\pi \cdot d_b^2}{4}$$

$$\text{Volume} := \text{Area} \cdot \text{Length}$$

$$Y_{\text{total}_1} := \text{Volume} \cdot n$$

X - Direction

$$\text{Length} := 6\text{in}$$

$$\text{Area} := \frac{\pi \cdot d_b^2}{4}$$

$$\text{Volume} := \text{Area} \cdot \text{Length}$$

$$X_{\text{total}_1} := \text{Volume} \cdot n$$

$$n := 22$$

$$d_b := \frac{5}{8}\text{in}$$

$$\text{Area} = 0.31 \cdot \text{in}^2$$

$$\text{Volume} = 10.74 \cdot \text{in}^3$$

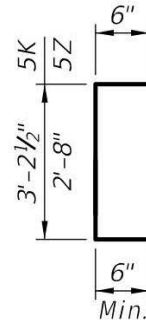
$$Y_{\text{total}_1} = 236.23 \cdot \text{in}^3$$

$$d_b := \frac{5}{8}\text{in}$$

$$\text{Area} = 0.31 \cdot \text{in}^2$$

$$\text{Volume} = 1.84 \cdot \text{in}^3$$

$$X_{\text{total}_1} = 40.5 \cdot \text{in}^3$$



**BARS 5K & 5Z**

**5z Bars**

Total Number of Bars

Y - Direction

$$\text{Length} := 36\text{in} - \frac{3}{4}\text{in} - \frac{1}{4}\text{in} = 35\text{in}$$

$$\text{Area} := \frac{\pi \cdot d_b^2}{4}$$

$$\text{Volume} := \text{Area} \cdot \text{Length}$$

$$Y_{\text{total}_2} := \text{Volume} \cdot n$$

X - Direction

$$\text{Length} := 6\text{in}$$

$$\text{Area} := \frac{\pi \cdot d_b^2}{4}$$

$$\text{Volume} := \text{Area} \cdot \text{Length}$$

$$X_{\text{total}_2} := \text{Volume} \cdot n$$

$$n := 22$$

$$d_b := \frac{5}{8}\text{in}$$

$$\text{Area} = 0.31 \cdot \text{in}^2$$

$$\text{Volume} = 10.74 \cdot \text{in}^3$$

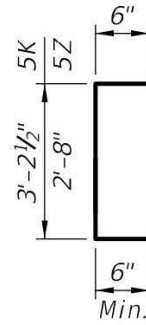
$$Y_{\text{total}_2} = 236.23 \cdot \text{in}^3$$

$$d_b := \frac{5}{8}\text{in}$$

$$\text{Area} = 0.31 \cdot \text{in}^2$$

$$\text{Volume} = 1.84 \cdot \text{in}^3$$

$$X_{\text{total}_2} = 40.5 \cdot \text{in}^3$$



**BARS 5K & 5Z**

**4M Bars**

Total Number of Bars

Z - Direction

Length := 36in

$$\text{Area} := \frac{\pi \cdot d_b^2}{4}$$

Volume := Area·Length

Z<sub>total\_1</sub> := Volume·n

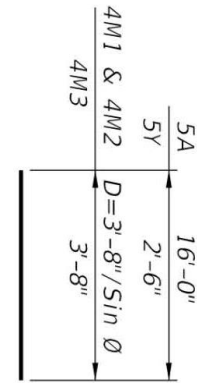
n := 8

$$d_b := \frac{4}{8} \text{ in}$$

Area = 0.2·in<sup>2</sup>

Volume = 7.07·in<sup>3</sup>

Z<sub>total\_1</sub> = 56.55·in<sup>3</sup>



**BARS 5A, 4M1, 4M2, 4M3 & 5Y**

**3D Bars**

Total Number of Bars

Y - Direction

Length<sub>1</sub> := 4.5in      Length<sub>2</sub> := 3.25in

$$\text{Area} := \frac{\pi \cdot d_b^2}{4}$$

Volume :=  $\frac{\text{Area} \cdot \text{Length}_1}{2} + \text{Area} \cdot \text{Length}_2$

Y<sub>total\_3</sub> := Volume·n

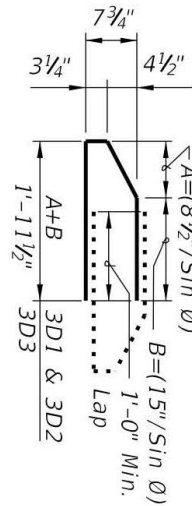
n := 12

$$d_b := \frac{3}{8} \text{ in}$$

Area = 0.11·in<sup>2</sup>

Volume = 0.61·in<sup>3</sup>

Y<sub>total\_3</sub> = 7.29·in<sup>3</sup>



**BARS 3D1, 3D2 & 3D3**

X - Direction

Length<sub>1</sub> := 8.5in      Length<sub>2</sub> := 15in

$$\text{Area} := \frac{\pi \cdot d_b^2}{4}$$

Volume :=  $\frac{\text{Area} \cdot \text{Length}_1}{2} + \text{Area} \cdot \text{Length}_2$

X<sub>total\_3</sub> := Volume·n

$$d_b := \frac{3}{8} \text{ in}$$

Area = 0.11·in<sup>2</sup>

Volume = 2.13·in<sup>3</sup>

X<sub>total\_3</sub> = 25.51·in<sup>3</sup>

### 3C Bars

Total Number of Bars

Y - Direction

$$\text{Length}_1 := 6.75\text{in} \quad \text{Length}_2 := 9\text{in}$$

$$\text{Area} := \frac{\pi \cdot d_b^2}{4}$$

$$\text{Volume} := \frac{\text{Area} \cdot \text{Length}_1}{2} + \text{Area} \cdot \text{Length}_2$$

$$Y_{\text{total}_4} := \text{Volume} \cdot n$$

X - Direction

$$\text{Length}_1 := 8.75\text{in} \quad \text{Length}_2 := 8.75\text{in}$$

$$\text{Area} := \frac{\pi \cdot d_b^2}{4}$$

$$\text{Volume} := \frac{\text{Area} \cdot \text{Length}_1}{2} + \frac{\text{Area} \cdot \text{Length}_2}{2}$$

$$X_{\text{total}_4} := \text{Volume} \cdot n$$

$$n := 6$$

$$d_b := \frac{3}{8}\text{in}$$

$$\text{Area} = 0.11 \cdot \text{in}^2$$

$$\text{Volume} = 1.37 \cdot \text{in}^3$$

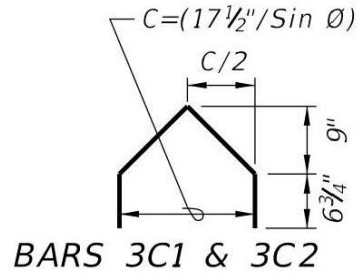
$$Y_{\text{total}_4} = 8.2 \cdot \text{in}^3$$

$$d_b := \frac{3}{8}\text{in}$$

$$\text{Area} = 0.11 \cdot \text{in}^2$$

$$\text{Volume} = 0.97 \cdot \text{in}^3$$

$$X_{\text{total}_4} = 5.8 \cdot \text{in}^3$$



### N Strands

Total Number of Bars

Z - Direction

$$\text{Length} := 36\text{in}$$

$$\text{Area} := \frac{\pi \cdot d_b^2}{4}$$

$$\text{Volume} := \text{Area} \cdot \text{Length}$$

$$Z_{\text{total}_2} := \text{Volume} \cdot n$$

$$n := 4$$

$$d_b := \frac{3}{8}\text{in}$$

$$\text{Area} = 0.11 \cdot \text{in}^2$$

$$\text{Volume} = 3.98 \cdot \text{in}^3$$

$$Z_{\text{total}_2} = 15.9 \cdot \text{in}^3$$

**5A Bars**

Total Number of Bars

$n := 4$

Z - Direction

Length := 36in

$d_b := \frac{5}{8} \text{in}$

$\text{Area} := \frac{\pi \cdot d_b^2}{4}$

Area = 0.31·in<sup>2</sup>

Volume := Area·Length

Volume = 11.04·in<sup>3</sup>

$Z_{\text{total}_3} := \text{Volume} \cdot n$

$Z_{\text{total}_3} = 44.18 \cdot \text{in}^3$

**4M Bars**

Total Number of Bars

$n := 5$

Z - Direction

Length := 44in

$d_b := \frac{4}{8} \text{in}$

$\text{Area} := \frac{\pi \cdot d_b^2}{4}$

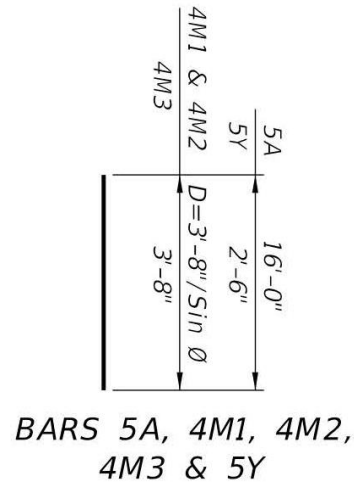
Area = 0.2·in<sup>2</sup>

Volume := Area·Length

Volume = 8.64·in<sup>3</sup>

$X_{\text{total}_5} := \text{Volume} \cdot n$

$X_{\text{total}_5} = 43.2 \cdot \text{in}^3$



FIBS 36 Information

$A_g := 806.6 \text{in}^2$

Volume :=  $A_g \cdot Z2 \text{Span}$

Volume = 29037.6 in<sup>3</sup>

Reinforcement Totals

$X_{\text{direction}} := X_{\text{total}_1} + X_{\text{total}_2} + X_{\text{total}_3} + X_{\text{total}_4} + X_{\text{total}_5}$

$X_{\text{direction}} = 155.5 \text{in}^3$

$Y_{\text{direction}} := Y_{\text{total}_1} + Y_{\text{total}_2} + Y_{\text{total}_3} + Y_{\text{total}_4}$

$Y_{\text{direction}} = 487.96 \text{in}^3$

$Z_{\text{direction}} := Z_{\text{total}_1} + Z_{\text{total}_2} + Z_{\text{total}_3}$

$Z_{\text{direction}} = 116.63 \text{in}^3$

Direction Reinforcement Details for Zone 2

$X_{\text{reinf}} := X_{\text{direction}} \cdot \frac{1}{\text{Volume}}$

$X_{\text{reinf}} = 0.0054$

$Y_{\text{reinf}} := Y_{\text{direction}} \cdot \frac{1}{\text{Volume}}$

$Y_{\text{reinf}} = 0.0168$

$Z_{\text{reinf}} := Z_{\text{direction}} \cdot \frac{1}{\text{Volume}}$

$Z_{\text{reinf}} = 0.0040$

For the rest of the length of girder values obtained for Zone 2 will be assumed to be true. This is due to the fact that the rest of the beam contains less vertical steel per gross volume of cross sectional girder than what is mathematically relevant for the calculations of the project and the Finite Element Analysis. Thus:

**ZONE 3 CALCULATIONS (spans from the end of zone 2 to the CL of the girder)**

Reinforcement Totals

$$X_{\text{direction}} := \frac{1}{Z_{2\text{Span}}} (X_{\text{total}_1} + X_{\text{total}_2} + X_{\text{total}_3} + X_{\text{total}_4} + X_{\text{total}_5})$$

$$X_{\text{direction}} = 51.83 \frac{\text{in}^3}{\text{ft}}$$

$$Y_{\text{direction}} := \frac{1}{Z_{2\text{Span}}} (Y_{\text{total}_1} + Y_{\text{total}_2} + Y_{\text{total}_3} + Y_{\text{total}_4})$$

$$Y_{\text{direction}} = 162.65 \frac{\text{in}^3}{\text{ft}}$$

$$Z_{\text{direction}} := \frac{1}{Z_{2\text{Span}}} (Z_{\text{total}_1} + Z_{\text{total}_2} + Z_{\text{total}_3})$$

$$Z_{\text{direction}} = 38.88 \frac{\text{in}^3}{\text{ft}}$$

Direction Reinforcement Details for Zone 3

$$X_{\text{reinf}} := X_{\text{direction}} \cdot \frac{1}{\text{Volume}}$$

$$X_{\text{reinf}} = 0.0018 \frac{1}{\text{ft}}$$

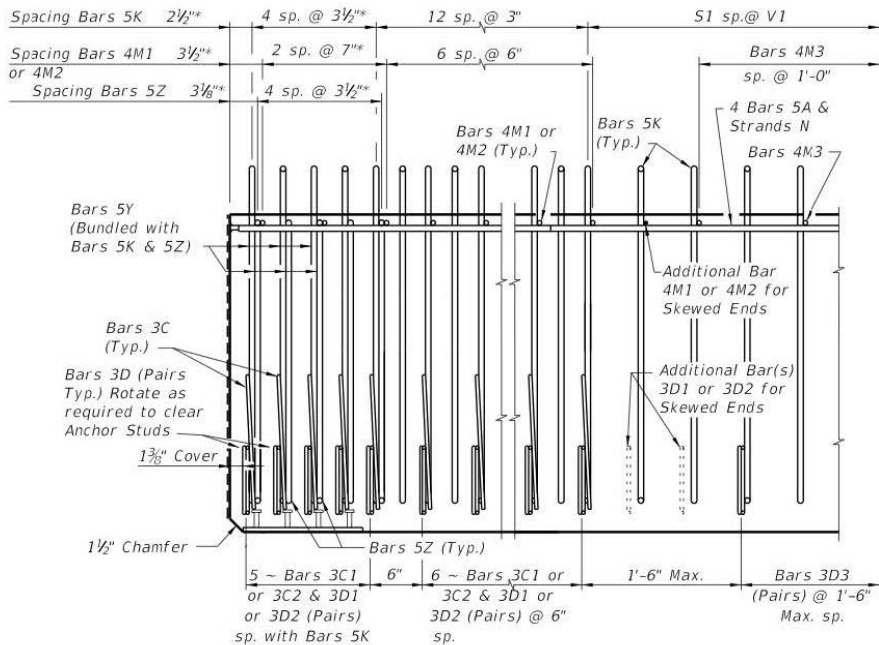
$$Y_{\text{reinf}} := Y_{\text{direction}} \cdot \frac{1}{\text{Volume}}$$

$$Y_{\text{reinf}} = 0.0056 \frac{1}{\text{ft}}$$

$$Z_{\text{reinf}} := Z_{\text{direction}} \cdot \frac{1}{\text{Volume}}$$

$$Z_{\text{reinf}} = 0.0013 \frac{1}{\text{ft}}$$

**VERTICAL REINFORCEMENT PLACEMENT SUMMARY**



ELEVATION AT END OF BEAM  
(Flanges Not Shown For Clarity)

## **TRADITIONAL DECK DESIGN (14ft Girder Spacing)**

### Codes and Specifications Used

- AASHTO - LRFD Bridge Design Specifications - 2007 (AASHTO LRFD)
- Florida Department of Transportation Structural Design Guidelines for LRFD - 2010 (SDG)
- Florida Department of Transportation Design Standards - 2010

### Design Parameters (Deck Reinforcement Properties)

Concrete Strength	$f_c := 4500\text{psi}$	
Concrete Weight	$w_c := 150\text{pcf}$	SDG Table 2.2-1
Aggregate Correction Factor	$K_1 := 0.9$	SDG 1.4.1.A
Yield Strength of Reinforcing Steel	$f_y := 60000\text{psi}$	
Width of Design Section	$b := 12\text{in}$	
Height of Design Section (Deck Thickness)	$h := 10\text{in}$	SDG 4.2.2.B
Reinforcement Minimum Top Cover	$\text{cover}_t := 2\text{in}$	SDG Table 1.4.2-1
Reinforcement Minimum Bottom Cover	$\text{cover}_b := 2\text{in}$	SDG Table 1.4.2-1
Environmental Classification	environment := "normal"	
Beam Spacing	$S_{\text{beam}} := 168\text{in}$	
Traffic Barrier Width	$W_{\text{barr}} := 18\text{in}$	
Traffic Barrier Load	$w_{\text{barr}} := 420\text{plf}$	

### Design Parameters (Girder Properties)

Concrete Weight for Modulus	$\gamma_c := 145\text{pcf}$	SDG 1.4.1.A
Modulus of Elasticity (Deck)	$E_c := 33000 \cdot K_1 \cdot \left( \frac{\gamma_c}{\frac{\text{kip}}{\text{ft}^3}} \right)^{1.5} \cdot \sqrt{\frac{f_c}{\text{ksi}}} \cdot \text{ksi} = 3478.68 \cdot \text{ksi}$	AASHTO 5.4.2.4
Modulus of Elasticity (Steel Reinforcement)	$E_s := 29000\text{ksi}$	AASHTO 5.4.3.2
Modular Ratio	$n := \text{round} \left( \frac{E_s}{E_c} \right) = 8$	AASHTO 5.7.1
Area of Deck Section	$A_c := h \cdot b = 120 \cdot \text{in}^2$	
Crack Control Exposure Factor	$\gamma_e := \begin{cases} 0.75 & \text{if environment} = \text{"extreme"} \\ 1.0 & \text{otherwise} \end{cases} = 1$	AASHTO 5.7.3.4

Design Moment

Top Flange Width	$b_{tf} := 48\text{in}$	
Web Width	$t_w := 7\text{in}$	
Maximum Negative Live Load Location	$Loc_{neg} := \min\left(\frac{1}{3} \cdot b_{tf}, 15\text{in}\right) = 15\text{in}$	AASHTO 4.6.2.1.6
Self-weight of Deck Slab	$w_{slab} := h \cdot b \cdot w_c = 125\text{plf}$	
Weight of Traffic Barriers	$P_{barr} := w_{barr} \cdot b = 420\text{lbft}$	
Maximum Positive Live Load Moment	$M_{LL\_pos} := 9.02\text{kip}\cdot\text{ft}$	AASHTO Table A4-1
Maximum Negative Live Load Moment for Interpolation (Lower Bound)	$Min_{neg\_loc} := 12\text{in}$ $Min_{LL\_neg} := 8.76\text{kip}\cdot\text{ft}$	AASHTO Table A4-1
Maximum Negative Live Load Moment for Interpolation (Upper Bound)	$Max_{neg\_loc} := 18\text{in}$ $Max_{LL\_neg} := 7.18\text{kip}\cdot\text{ft}$	AASHTO Table A4-1
Maximum Negative Live Load Moment by Interpolation	$M_{LL\_neg} := (Loc_{neg} - Min_{neg\_loc}) \cdot \left[ \frac{(Max_{LL\_neg} - Min_{LL\_neg})}{(Max_{neg\_loc} - Min_{neg\_loc})} \right] + Min_{LL\_neg} = 7.97\text{kip}\cdot\text{ft}$	

Loads and Load Factors

Per current FDOT specifications for service and strength design of concrete deck slab, two limit states apply:

Strength<sub>I</sub> := 1.25·DC + 1.5DW + 1.75(LL+IM)<sup>■</sup>

Service<sub>I</sub> := DC + DW + LL + IM<sup>■</sup>

DC = Slab Dead Load	$DC := w_c \cdot b \cdot h = 125\text{plf}$	DC Load on a 1ft strip
DW = 2.5" ACP Overlay	$DW := 140\text{pcf} \cdot 2.5\text{in} \cdot b = 29.17\text{plf}$	DW Load on a 1ft strip
LL + IM = Live Loading and Impact Loading	$LL\_IM_{pos} := M_{LL\_pos} = 9.02\text{kip}\cdot\text{ft}$	AASHTO LRFD Table A4-1 LL + IM Moment on a 1ft strip.
	$LL\_IM_{neg} := M_{LL\_neg} = 7.97\text{kip}\cdot\text{ft}$	
Moment of Inertia (Slab)	$I_{slab} := \frac{b \cdot h^3}{12} = 1000\text{in}^4$	Data parameters needed for max and min moment calculations
Modulus Elasticity (Slab)	$E_c = 3478681.84\text{psi}$	

Max Moments due to DC	$DC\_M_{neg} := 2063.16 \text{ lbf}\cdot\text{ft}$	<i>Data parameters found through the use of computerized beam analysis model (MDSOLIDS), no overhang</i>
	$DC\_M_{pos} := 1527 \text{ lbf}\cdot\text{ft}$	
Max Moments due to DW	$DW\_M_{neg} := 601.82 \text{ lbf}\cdot\text{ft}$	<i>Data parameters found through the use of computerized beam analysis model (MDSOLIDS), no overhang</i>
	$DW\_M_{pos} := 445.43 \text{ lbf}\cdot\text{ft}$	
Maximum Moments Applied	$DC := \max(DC\_M_{neg}, DC\_M_{pos}) = 2063.16 \text{ lbf}\cdot\text{ft}$	
	$DW := \max(DW\_M_{neg}, DW\_M_{pos}) = 601.82 \text{ lbf}\cdot\text{ft}$	
	$LL\_IM := \max(LL\_IM_{neg}, LL\_IM_{pos}) = 9020 \text{ lbf}\cdot\text{ft}$	
Limit State Moments Applied	$Strength_I := 1.25 \cdot DC + 1.50 \cdot DW + 1.25 \cdot LL\_IM$	$Strength_I = 14.76 \text{ kip}\cdot\text{ft}$
	$Service_I := DC + DW + LL\_IM$	$Service_I = 11.68 \text{ kip}\cdot\text{ft}$

Flexure Reinforcement Design

Assume Load Reduction Factor for Moment	$\phi M := 0.9$	
Assume #5 bars @ 8in for Main Reinforcement	$d_b := \frac{5}{8} \text{ in}$	$Spa_{main} := 6 \text{ in}$
		AASHTO 5.7.2
Modulus of Rapture	$f_r := 0.24 \sqrt{\frac{f_c}{\text{ksi}}} \text{ ksi} = 509.12 \text{ psi}$	AASHTO 5.4.2.6
Distance from Extreme Tensile Fiber to Neutral Axis of Composite Section	$y_t := \frac{h}{2} = 5 \text{ in}$	
Cracking Moment	$M_{cr} := \frac{f_r \cdot I_{slab}}{y_t} = 8.49 \text{ kip}\cdot\text{ft}$	
Cracking Moment Limit	$1.2 \cdot M_{cr} = 10.18 \text{ kip}\cdot\text{ft}$	
Design Ultimate Moment	$M_u := \begin{cases} Strength_I & \text{if } Strength_I \geq 1.2M_{cr} \\ \min(1.33 \cdot Strength_I, 1.2M_{cr}) & \text{otherwise} \end{cases} = 14.76 \text{ kip}\cdot\text{ft}$	
Distance from Extreme Compressive Fiber to Centroid of Reinforcing Steel	$d_e := h - cover_b - \frac{d_b}{2} = 7.69 \text{ in}$	

Normal Strength Coefficient of Resistance

$$R_u := \frac{M_u}{\phi M \cdot b \cdot d_e^2} = 277.44 \text{ psi}$$

$$m := \frac{f_y}{0.85 \cdot f_c} = 15.69$$

ACI  $\rho$  Equation

$$\rho := \frac{1}{m} \left( 1 - \sqrt{1 - \frac{2 \cdot R_u}{\text{psi} \cdot m}} \right) = 0.004805$$

$$A_{sreqdpos} := \rho \cdot b \cdot d_e$$

$$A_{sreqdpos} = 0.44 \cdot \text{in}^2$$

Cross-Sectional Area of Reinforcing Bar

$$A_{bar} := \frac{\pi \cdot d_b^2}{4}$$

$$A_{bar} = 0.31 \cdot \text{in}^2$$

Minimum Required  $A_s$  Between Girders

$$A_{s\_minreq} := A_{sreqdpos} = 0.44 \cdot \text{in}^2$$

Area of Reinforcing on a 1ft wide Section

$$A_{s(cc)} := A_{bar} \cdot \frac{12 \text{ in}}{\text{cc}}$$

Area of Main Reinforcing Steel

$$A_{sMain} := A_{s(cc)} \cdot (\text{Spa}_{main}) = 0.61 \cdot \text{in}^2$$

Depth of Equivalent Rectangular Whitney Stress Block

$$a := \frac{A_{sMain} \cdot f_y}{0.85 \cdot f_c \cdot b} = 0.8 \cdot \text{in}$$

Ratio of Reinforcement Provided

$$\rho := \frac{A_{sMain}}{b \cdot d_e} = 0.00665$$

Location of Neutral Axis

$$\beta_1 := \begin{cases} \max \left[ 0.85 - 0.05 \left( \frac{f_c - 4 \text{ ksi}}{\text{ksi}} \right), 0.65 \right] & \text{if } f_c > 4 \text{ ksi} \\ 0.85 & \text{otherwise} \end{cases} = 0.83$$

$$c_{comp} := \frac{a}{\beta_1} = 0.97 \cdot \text{in}$$

AASHTO 5.7.2.1

Tensile Strain in Tension Steel

$$\epsilon_t := 0.003 \cdot \frac{d_e - c_{comp}}{c_{comp}} = 0.02$$

AASHTO Figure C5.7.2.1-1

Comp. and Tension Controlled Section Limits of Net Tensile Strain in the Extreme Tension Steel

$$\epsilon_{T\_Limits} := \begin{pmatrix} 0.002 \\ 0.005 \end{pmatrix}$$

AASHTO 5.5.4.2.1

Comp. and Tension Controlled Reinforced Concrete Section Resistance Factors

$$\phi := \begin{pmatrix} 0.75 \\ 0.9 \end{pmatrix}$$

AASHTO 5.5.4.2.1

Determine Controlling Force

$$\text{Controlling} := \begin{cases} \text{"Compression"} & \text{if } \varepsilon_t \leq \varepsilon_{T\_Limits_0} \\ \text{"Tension"} & \text{if } \varepsilon_t \geq \varepsilon_{T\_Limits_1} \\ \text{"In Transition"} & \text{otherwise} \end{cases} = \text{"Tension"}$$

Determine Controlling Resistance Factor

$$\phi M := \begin{cases} \phi_0 & \text{if Controlling} = \text{"Compression"} \\ \phi_1 & \text{if Controlling} = \text{"Tension"} \\ \text{interp}(\varepsilon_{T\_Limits}, \phi, \varepsilon_t) & \text{otherwise} \end{cases} = 0.9$$

Factored Flexural Resistance

$$\phi M_n := \phi M \cdot A_{sMain} \cdot f_y \cdot \left( d_e - \frac{a}{2} \right) \quad \phi M_n = 20.12 \cdot \text{kip}\cdot\text{ft}$$

Ultimate Moment

$$M_u = 14.76 \cdot \text{kip}\cdot\text{ft}$$

Check Moment Capacity

$$\text{Moment\_Check} := \begin{cases} \text{"PASS"} & \text{if } \phi M_n \geq M_u \\ \text{"FAIL"} & \text{if } \phi M_n < M_u \end{cases} = \text{"PASS"}$$

### Crack Control Check

AASHTO 5.7.3.4

Thickness of Concrete Cover Measured from Extreme Tension Fiber to Center of the Flexural Reinforcement

$$d_c := \text{cover}_b + \frac{d_b}{2} = 2.31 \cdot \text{in}$$

Depth of Neutral Axis

$$f(x) := \frac{b \cdot x^2}{2 \cdot A_{sMain} \cdot n} + x - d_e$$

$$x := \text{root}(f(x), x, 0, d_e) \quad x = 2.13 \cdot \text{in}$$

Tension Stress in Reinforcement at Service Limit State

$$f_{ss} := \frac{\text{Service}_1}{A_{sMain} \cdot \left( d_e - \frac{x}{3} \right)} \quad f_{ss} = 32.75 \cdot \text{ksi}$$

Ratio of Flexural Strain at the Extreme Tension Face to the Strain at the Centroid of the Reinforcement Layer Nearest the Tension Face

$$\beta_s := 1 + \frac{d_c}{0.7 \cdot (h - d_c)} = 1.43 \quad \text{AASHTO 5.7.3.4-1}$$

Maximum Reinforcement Spacing for Crack Control

$$s_{\max} := \left( \frac{700 \cdot \gamma_e}{\beta_s \cdot \frac{f_{ss}}{\text{ksi}}} - 2 \cdot \frac{d_c}{\text{in}} \right) \text{in} = 10.32 \cdot \text{in} \quad \text{AASHTO 5.7.3.4-1}$$

Reinforcement Spacing Provided

$$s_{\text{actual}} := \text{Spa}_{\text{main}} = 6 \cdot \text{in}$$

Check Reinforcement Spacing

$$\text{Spacing\_Check} := \begin{cases} \text{"FAIL"} & \text{if } s_{\text{actual}} \geq s_{\max} \\ \text{"PASS"} & \text{otherwise} \end{cases} = \text{"PASS"}$$

Distribution Reinforcement

AASHTO 9.7.3.2

Primary reinforcing steel for slab perpendicular to traffic

Dist. Between Flanges  $D1 := S_{beam} - b_{tf} = 120 \cdot in$

Flange Overhang  $D2 := b_{tf} - t_w = 41 \cdot in$

Effective Span Length  $s_{p_{eff}} := D1 + D2 = 13.42 \cdot ft$  AASHTO 9.7.2.3

Distribution Reinforcement %  $DR := \min\left(\frac{220}{\sqrt{\frac{s_{p_{eff}}}{ft}}}, 67\right) \cdot \% = 60.06 \cdot \%$

Area of Steel Required  $A_{sDR} := DR \cdot A_{sMain} = 0.37 \cdot in^2$   $Spa_{long} := 8in$

Area of Reinforcing Steel Provided  $A_{sDP} := A_s(s_{p_{long}}) = 0.46 \cdot in^2$

Check Area of Reinforcement Provided  $Reinforcement\_Check := \begin{cases} "PASS" & \text{if } A_{sDP} \geq A_{sDR} \\ "FAIL" & \text{otherwise} \end{cases} = "PASS"$

Temperature & Shrinkage Reinforcement

AASHTO 9.7.3.2

Area of Steel Required for Temp & Shrinkage

$$A_{s_{ts}} := \begin{cases} 0.11 \frac{in^2}{ft} & \text{if } \frac{1.30 \frac{kip}{in \cdot ft} \cdot b \cdot h}{2(b+h) \cdot f_y} \leq 0.11 \frac{in^2}{ft} \\ 0.60 \frac{in^2}{ft} & \text{if } \frac{1.30 \frac{kip}{in \cdot ft} \cdot b \cdot h}{2(b+h) \cdot f_y} \geq 0.60 \frac{in^2}{ft} \\ \frac{1.30 \frac{kip}{in \cdot ft} \cdot b \cdot h}{2(b+h) \cdot f_y} & \text{otherwise} \end{cases} = 0.11 \frac{in^2}{ft}$$

Area of Temp and Shrink Reinforcement  $Spa_{TS} := 8in$

$A_{sTS} := A_s(s_{p_{TS}}) = 0.46 \cdot in^2$

Check Temp and Shrink Reinforcement

$Check_{TS} := \begin{cases} "PASS" & \text{if } A_{sTS} \geq A_{s_{ts}} \cdot ft \wedge A_{sMain} \wedge A_{s_{ts}} \cdot ft \wedge A_{sTS} \geq A_{s_{ts}} \cdot ft \\ "FAIL" & \text{otherwise} \end{cases} = "PASS"$

Maximum Spacing of Temperature and Shrinkage Reinforcement  $s_{TSmax} := \min(3 \cdot h, 18in, 12in) = 12 \cdot in$

Check Temp and Shrink Max Spacing

$Check_{TS\_Spa} := \begin{cases} "PASS" & \text{if } Spa_{long} \leq s_{TSmax} \wedge Spa_{main} \leq s_{TSmax} \wedge Spa_{TS} \leq s_{TSmax} \\ "FAIL" & \text{otherwise} \end{cases} = "PASS"$

Deck Reinforcement Summary

Main Reinforcement, Transverse (Bottom)	Use #5 bars at	Spa <sub>main</sub> = 6-in
Main Reinforcement, Transverse (Top)	Use #5 bars at	Spa <sub>main</sub> = 6-in
Distribution Reinforcement, Longitudinal (Bottom)	Use #5 bars at	Spa <sub>long</sub> = 8-in
Distribution Reinforcement, Longitudinal (Top)	Use #5 bars at	Spa <sub>TS</sub> = 8-in

Overhang Reinforcement Design

SDG 4.2.5

Traffic Railing Type = 32 inch F Shape

$M_c := 15.7 \text{ kip}\cdot\text{ft}$ 
 $T_u := 7.1 \frac{\text{kip}}{\text{ft}}$ 
 $L_d := 7.67 \text{ ft}$ 
SDG Table 4.2.5.A

Nominal Tensile Capacity of the Deck
 
$$P_n := \frac{A_{sMain} \cdot f_y}{ft} = 36.82 \cdot \text{kip}\cdot\text{ft}^{-1}$$
 $\Phi := 1.0$

Total ultimate deck moment from traffic railing impact and factored dead load at the gutter line:

$$M_{u\_Overhang} := M_c + \Phi \cdot M_{DC\_Neg\_Overhang} + \Phi \cdot M_{DW\_Neg\_Overhang}$$

Max Moments at Overhang

Max negative Service DC Moment
 
$$M_{DC\_Neg\_Overhang} := 390.63 \text{ lb}\cdot\text{ft}$$
*Data parameters found through the use of computerized beam analysis model (MDSOLIDS), with overhang*

Max negative Service DW Moment
 
$$M_{DW\_Neg\_Overhang} := 91.16 \text{ lb}\cdot\text{ft}$$

$$M_{u\_Overhang} := M_c + \Phi \cdot M_{DC\_Neg\_Overhang} + \Phi \cdot M_{DW\_Neg\_Overhang} = 16.18 \cdot \text{kip}\cdot\text{ft}$$

Nominal Moment Capacity @ Gutter Line

$$M_{n\_Overhang} := A_{sMain} \cdot f_y \cdot \left( d_e - \frac{a}{2} \right) = 22.35 \cdot \text{kip}\cdot\text{ft}$$

$$\text{Check}_{Overhang\_Reinforcement} := \begin{cases} \text{"PASS"} & \text{if } \left[ \left( \frac{T_u}{\Phi \cdot P_n} \right) + \left( \frac{M_{u\_Overhang}}{\Phi \cdot M_{n\_Overhang}} \right) \right] \leq 1.0 \\ \text{"FAIL"} & \text{otherwise} \end{cases} = \text{"PASS"}$$

Additional Overhang Reinforcement Steel Design

SDG 4.2.4

Reinforcement provided meets criteria for overhang design. No added steel required in this scenario

## **DECK REINFORCEMENT SPECIFICATIONS (SUMMARY)**

### **Codes and Specifications Used**

- AASHTO - LRFD Bridge Design Specifications - 2007 (AASHTO LRFD)
- Florida Department of Transportation Structural Design Guidelines for LRFD - 2010 (SDG)
- Florida Department of Transportation Design Standards - 2010

### **14 ft Spacing Between Girders**

➤ Reference:C:\Users\Javier Muniz\Desktop\Beam Analysis\14ft Spacing\Traditional Deck Design (14ft Girder Spacing).xmcd

### **Deck Reinforcement Summary**

Deck Thickness	h = 10 in
Main Reinforcement, Transverse (Bottom)	Use #5 bars at $Spa_{main} = 6\text{-in}$
Main Reinforcement, Transverse (Top)	Use #5 bars at $Spa_{main} = 6\text{-in}$
Distribution Reinforcement, Longitudinal (Bottom)	Use #5 bars at $Spa_{long} = 8\text{-in}$
Distribution Reinforcement, Longitudinal (Top)	Use #5 bars at $Spa_{TS} = 8\text{-in}$

### **Overhang Reinforcement Summary**

Reinforcement provided meets criteria for overhang design. No added steel required in this scenario

➤ Reference:C:\Users\Javier Muniz\Desktop\Beam Analysis\14ft Spacing\Empirical Deck Design (14ft Girder Spacing).xmcd

### **Deck Reinforcement Summary**

Main Reinforcement, Transverse (Bottom)	Use #5 bars at $Emp_{spacing} = 12\text{-in}$
Main Reinforcement, Transverse (Top)	Use #5 bars at $Emp_{spacing} = 12\text{-in}$
Distribution Reinforcement, Longitudinal (Bottom)	Use #5 bars at $Emp_{spacing} = 12\text{-in}$
Distribution Reinforcement, Longitudinal (Top)	Use #5 bars at $Emp_{spacing} = 12\text{-in}$

### **Overhang Reinforcement Summary**

Additional P Bars Between Main Top Deck Reinforcement	Use #5 bars at $Overhang_{spacing} := 4\text{in}$
---	---

APPENDIX IV: PHOTOS OF SPECIMEN AND TESTING











**APPENDIX V: INSTRUMENTATION**

The total number and types of gauges for S1, S2, S3, F1, F2, and F3 cases were as follows:

**Instrumentation Gauge Count**

Gauge Type	Gauge Count	
Load Cell	2	
Foil Strain	87	
Crack Strain	6	
Deflection	18	
Strand Slip	6	
	119	Total

The total number and types of Gauges for S4 and S5 cases were:

**Gauge Count for S4 & S5**

Gauge Type	Gauge Count	
Load Cell	2	
Foil Strain	50	
Crack Strain	0	
Deflection	18	
Strand Slip	6	
	76	Total

### Strain Gauge Designation, Location, and Label

Meaning	Label
Transverse Rebar, Bottom	TB
Transverse Rebar, Top	TT
Longitudinal Rebar, Bottom	LB
Surface Strain Gauge, Top of Slab	S1t
Surface Strain Gauge, Bottom of Slab	S1b
Crack Strain Gauge, Top of Slab	Cr1t
Crack Strain Gauge, Bottom of Slab	Cr1b
Surface Strain Gauge Top of Slab above East Beam	SE
Surface Strain Gauge Top of Slab above West Beam	SW
East Beam Surface Strain Gauge	BE
West Beam Surface Strain Gauge	BW
East Beam Rosette Longitudinal Direction, exterior	RE3_0e
East Beam Rosette Vertical Direction, exterior	RE3_90e
East Beam Rosette 45° between L & V, exterior	RE3_45e
West Beam Rosette Longitudinal Direction, interior	RW3_0i
West Beam Rosette Vertical Direction, interior	RW3_90i
West Beam Rosette 45° between L & V, interior	RW3_45i
Slip displacement attached to strand or rebar	Slip-
Displacement on Top of Slab	D1t
Displacement on Bottom of Slab	D6b
Displacement on Girder Flanges, Lateral Orientation	D13h
Optional String Pot Crack Monitoring Gauge	DisCr1

\*These Gauges will be read for tests S1, S2, S3, F1, F2, F3

### Channel Names and Gauges

Channel Name		
Load A Load B	<b>Jack</b>	
TB1 TB2 TB3 TB4 TB5 TB6 TB7 TB8	<b>Slab</b>	
TB9 TB10 TB11 TB12 TB13 TB14 TB15 TB16		
TT1 TT2 TT3 TT4 TT5 TT6 TT7 TT8		
LB1 LB2 LB3 LB4 LB5		
S1t S2t S3t S4t S6t		
S7b S8b S9b		
S10t S11t S12t		
S13t S14t S15t		
Cr1t Cr2t Cr3t		<b>Slab</b>
Cr4b Cr5b Cr6b		
SE1 SE2 SE3		<b>Slab</b>
BE1 BE2 BE3 BE4 BE5 BE6 BE7 BE8 BE9	<b>Girder</b>	
RE1_90e RE1_90i		
RE2_90e RE2_90i		
RE3_0e RE3_90e		
RE3_45e RE3_0i		
RE3_90i RE3_45i		
SW1 SW2 SW3		<b>Slab</b>
BW1 BW2 BW3 BW4 BW5 BW6 BW7 BW8 BW9	<b>Girder</b>	
RW1_90e RW1_90i		

continued

RW2_90e RW2_90i	
RW3_0e RW3_90e	
RW3_45e RW3_0i	
RW3_90i RW3_45i	
D1t D2t D3t D4t	Girder
D5t D6b D7b D8b D9b D10b D11b D12b D13b	Slab
DisCr1	
D14h D15h D16h D17h	
Slip-1 Slip-2 Slip-3 Slip-4 Slip-5 Slip-6	Girder

\*Gauges highlighted in orange stay in the same global position and are recorded during all tests.

### Strain Gauge Designation, Location, and Label

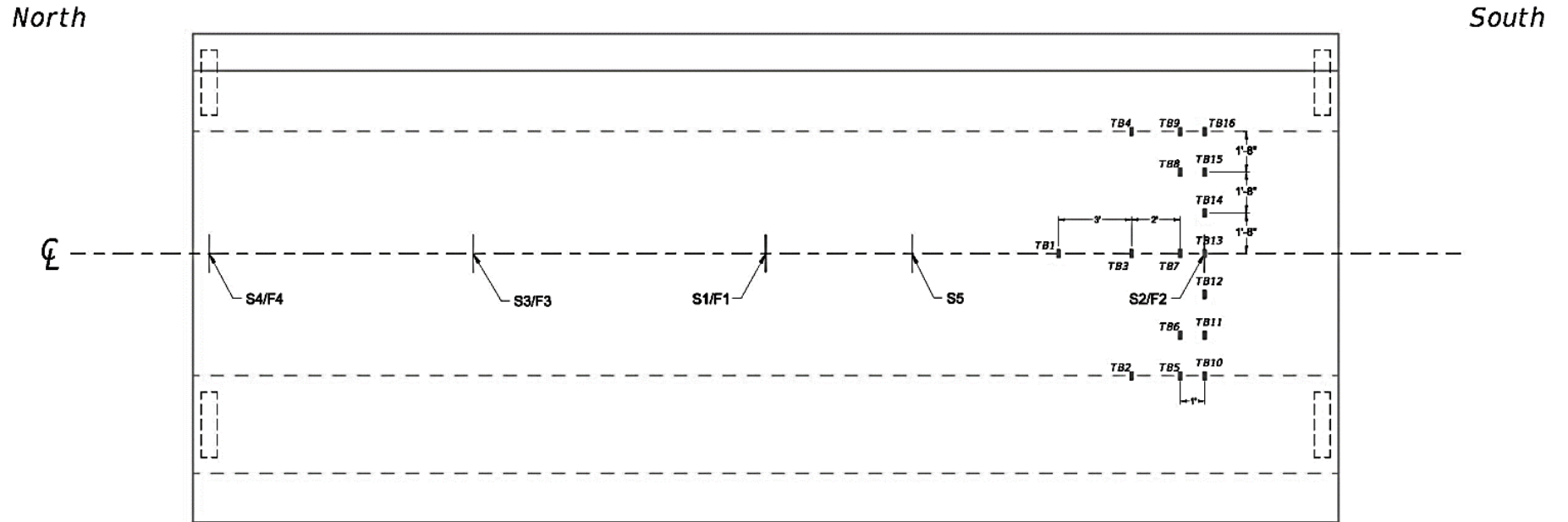
Meaning	Label
Surface Strain Gauge, Top of Slab	S1t
Surface Strain Gauge Top of Slab above East Beam	SE
Surface Strain Gauge Top of Slab above West Beam	SW
East Beam Surface Strain Gauge	BE
West Beam Surface Strain Gauge	BW
East Beam Rosette Longitudinal Direction, exterior	RE3_0e
East Beam Rosette Vertical Direction, exterior	RE3_90e
East Beam Rosette 45° between L & V, exterior	RE3_45e
West Beam Rosette Longitudinal Direction, interior	RW3_0i
West Beam Rosette Vertical Direction, interior	RW3_90i
West Beam Rosette 45° between L & V, interior	RW3_45i
Slip displacement attached to strand or rebar	Slip-
Displacement on Top of Slab	D1t
Displacement on Bottom of Slab	D6b
Displacement on Girder Flanges, Lateral Orientation	D14h
Optional String Pot Crack Monitoring Gauge	DisCr1

\*These Gauges will be read for tests S4, S5

Channel Names and Gauges Read for S4/F4 (excluding S3/F3 Gauges)

Channel Name	
Load A Load B	<b>Jack</b>
S10t S11t S12t S13t S14t S15t	<b>Slab</b>
SE1 SE2 SE3	
BE1 BE2 BE3 BE4 BE5 BE6 BE7 BE8 BE9	<b>Girder</b>
RE1_90e RE1_90i RE2_90e RE2_90i RE3_0e RE3_90e RE3_45e RE3_0i RE3_90i RE3_45i	
SW1 SW2 SW3	
BW1 BW2 BW3 BW4 BW5 BW6 BW7 BW8 BW9	
RW1_90e RW1_90i RW2_90e RW2_90i RW3_0e RW3_90e RW3_45e RW3_0i RW3_90i RW3_45i	<b>Girder</b>
D1t D2t D3t D4t D5t	<b>Girder</b>
D6b D7b D8b D9b D10b D11b D12b D13b	<b>Slab</b>
DisCr1	
D14h D15h D16h D17h	
Slip-1 Slip-2 Slip-3 Slip-4 Slip-5 Slip-6	<b>Girder</b>

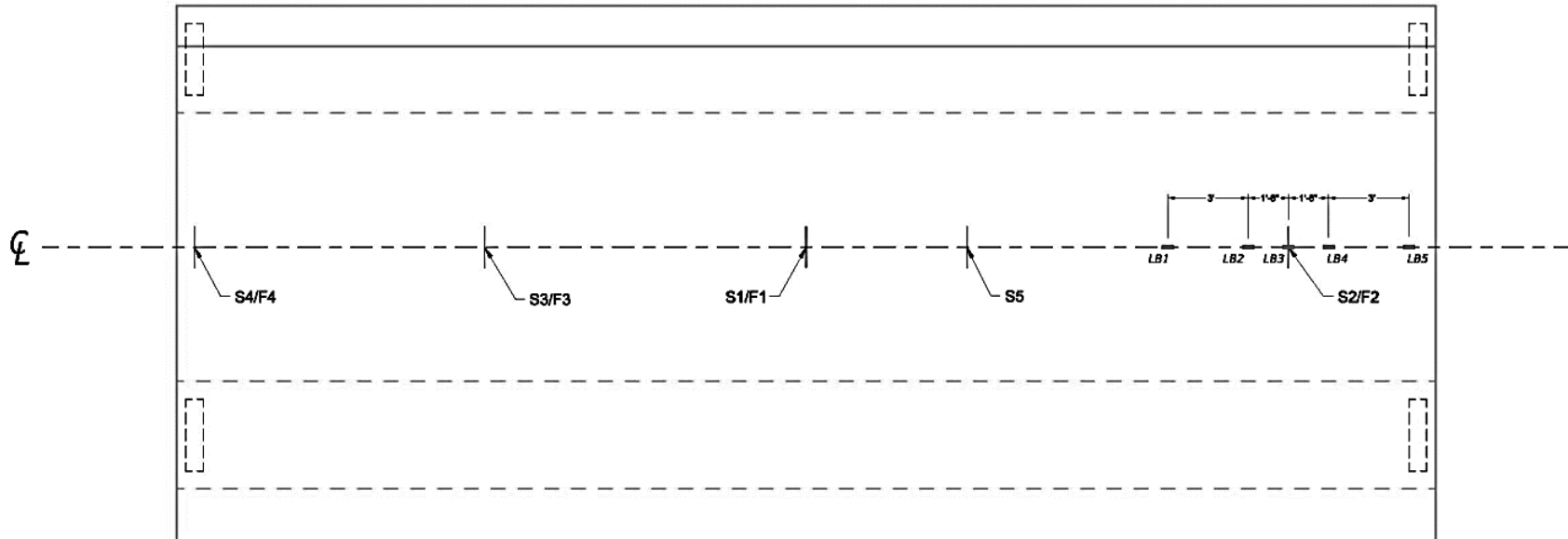
# APPENDIX VI: GAUGE LOCATIONS



Internal Transverse Strain Gauges on Bottom Reinforcement for S2/F2

North

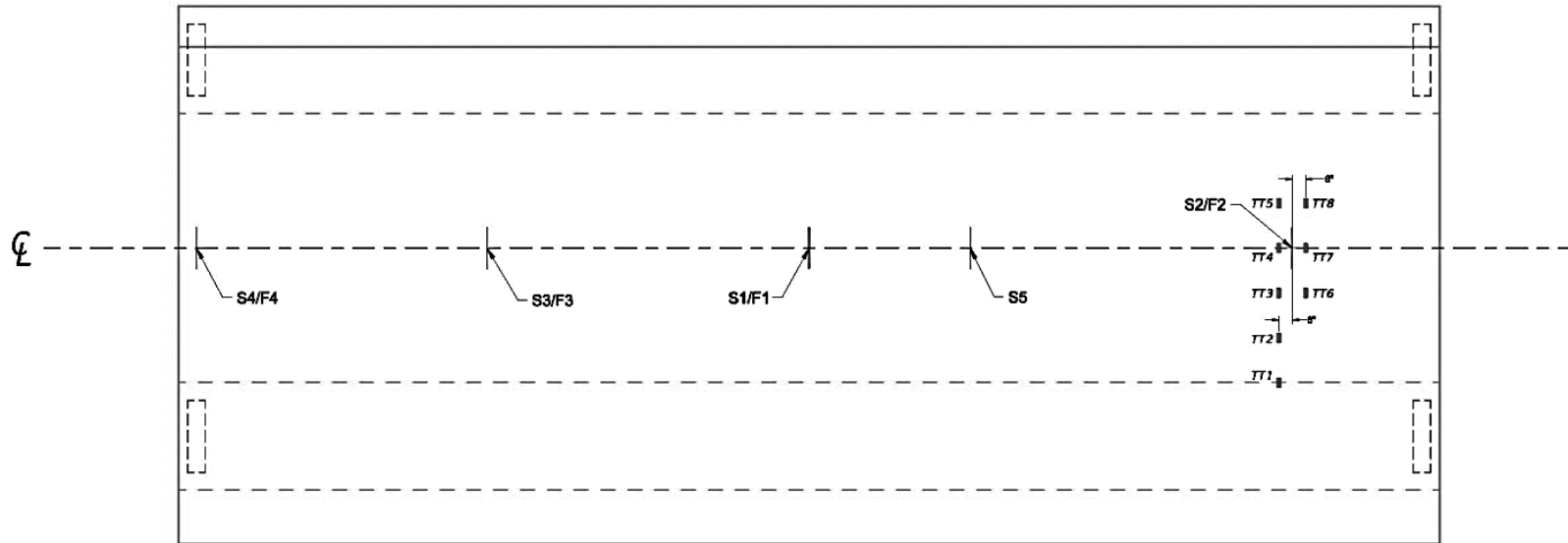
South



*Internal longitudinal strain Gauges for S2/F2*

North

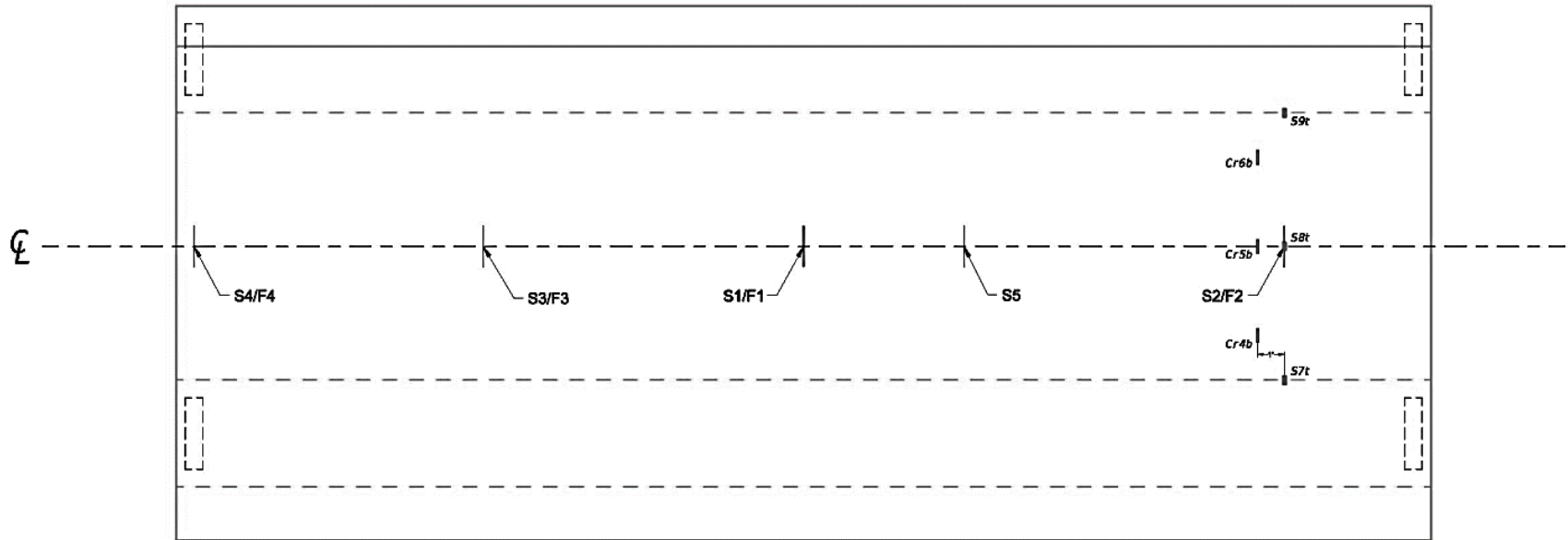
South



*Internal Transverse Strain Gauges on Top Reinforcement for S2/F2*

North

South

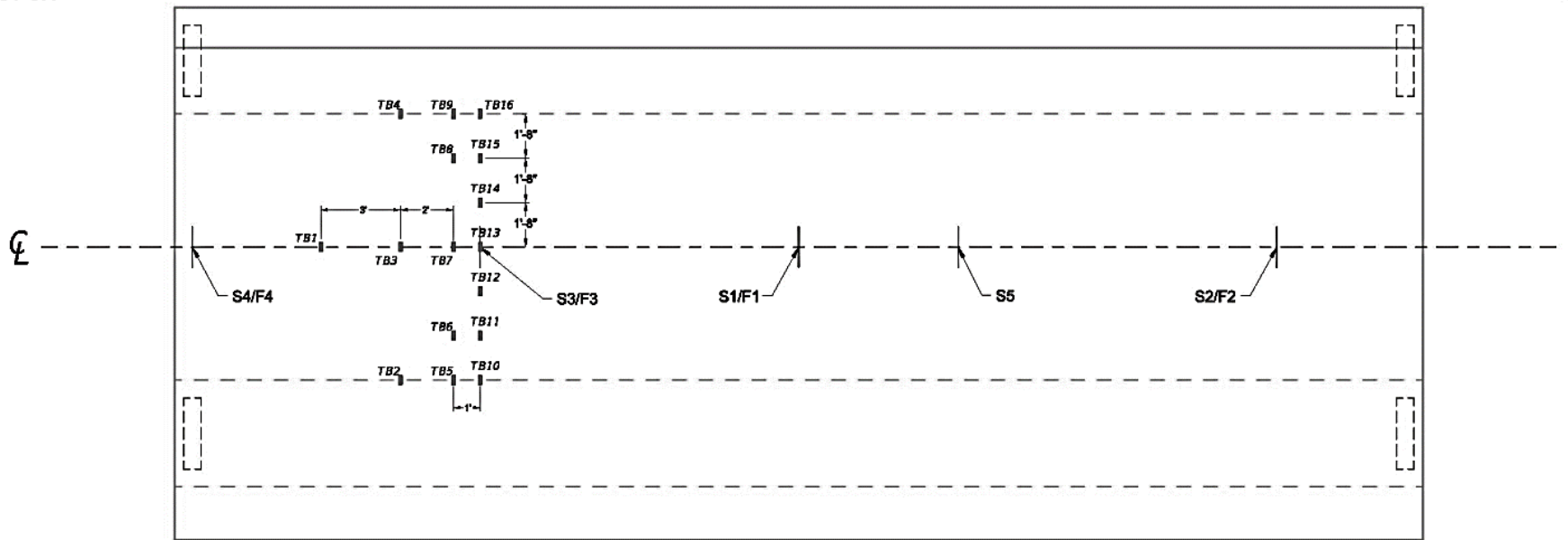


*Bottom deck surface crack and foil Gauges for S2/F2*



North

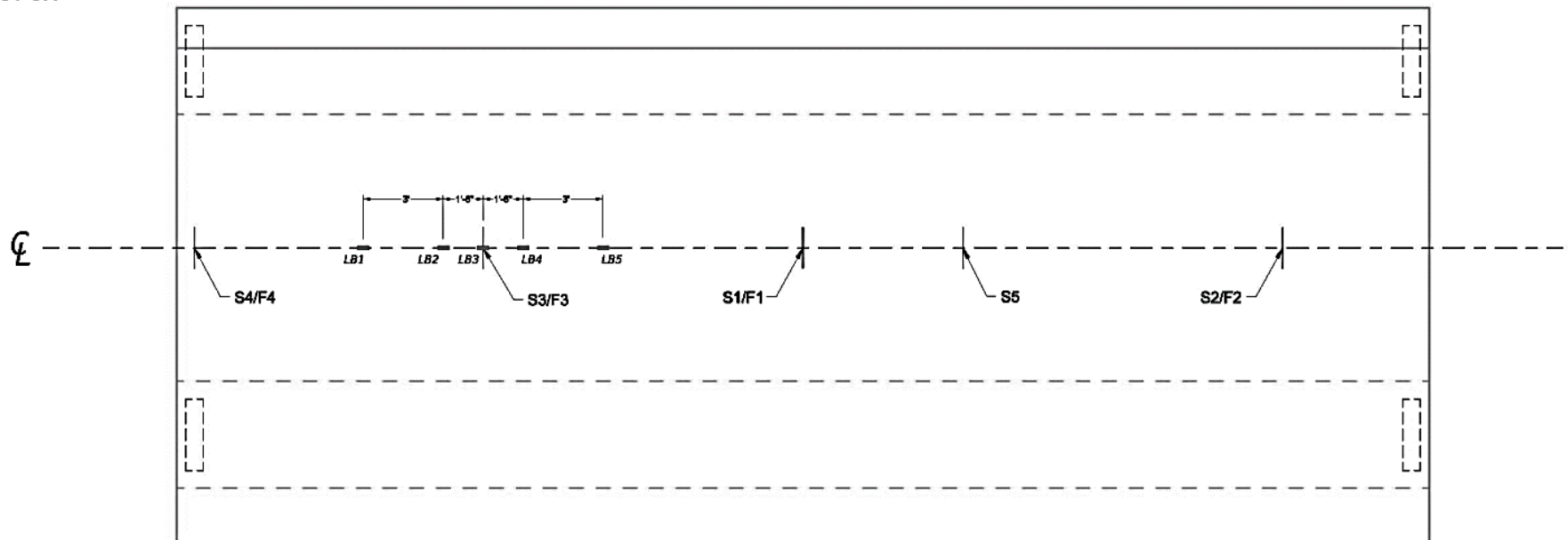
South



Internal Transverse Strain Gauges on Bottom Reinforcement for S3/F3

North

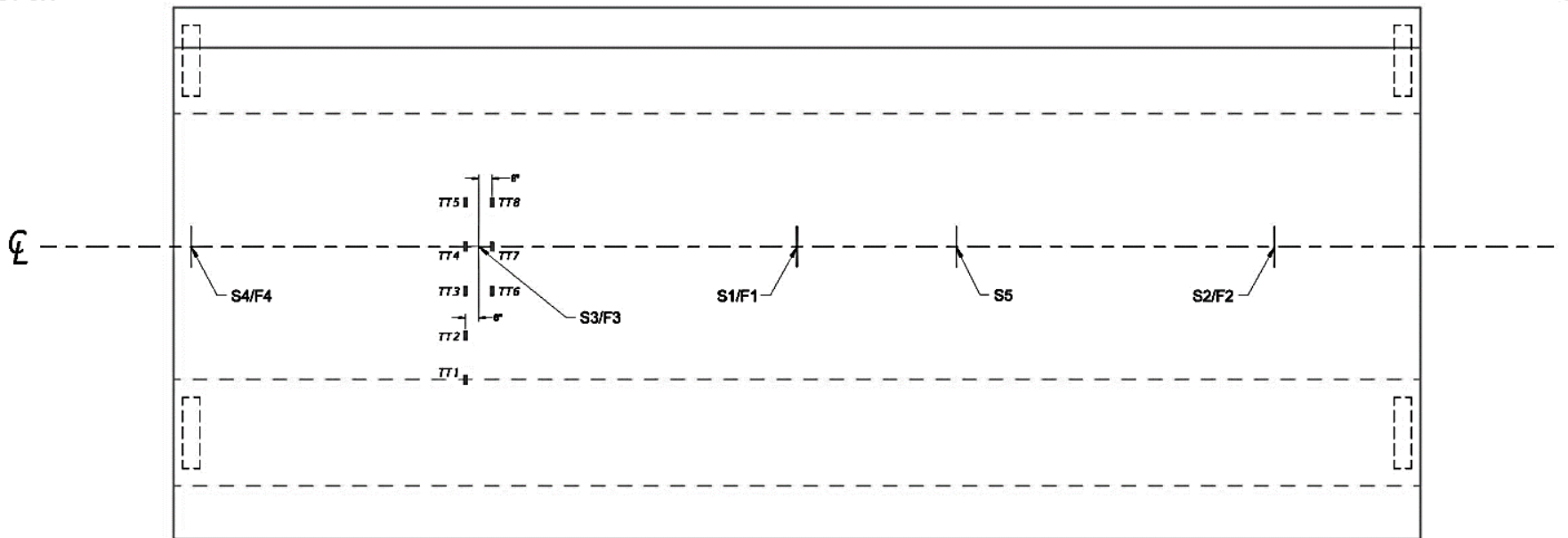
South



*Internal Longitudinal Strain Gauges for S3/F3*

North

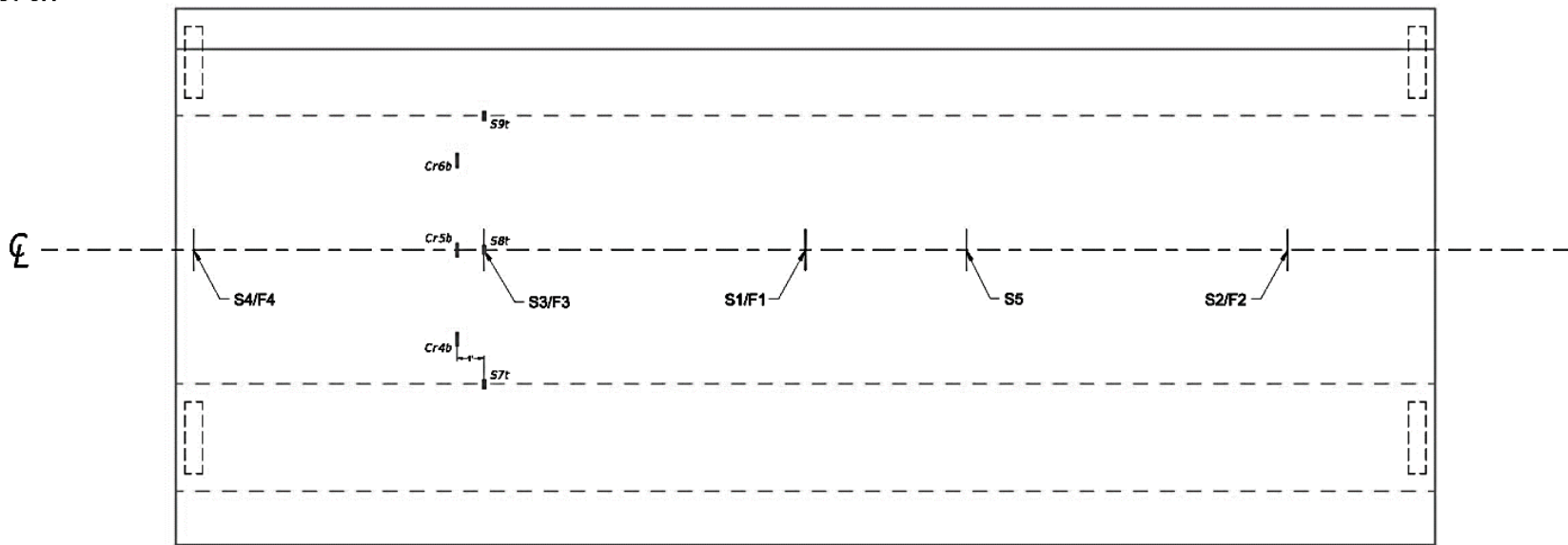
South



Internal Transverse Strain Gauges on Top Reinforcement for S3/F3

North

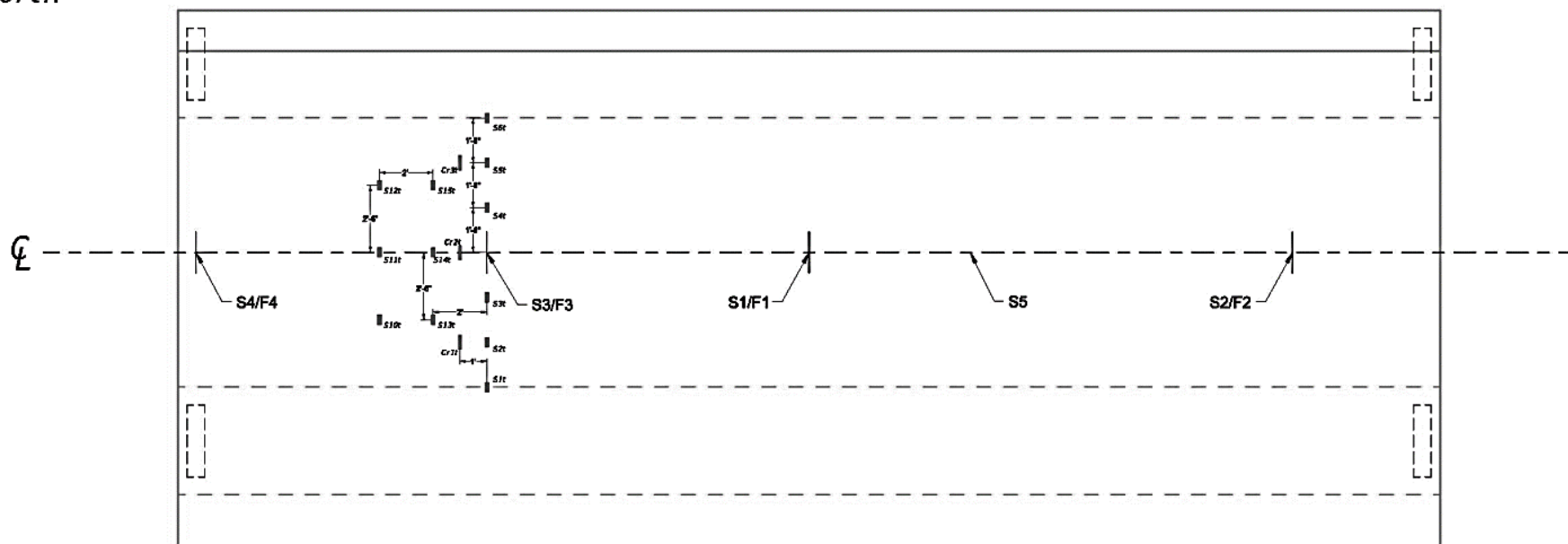
South



*Bottom Deck Surface Crack and Foil Gauges for S3/F3*

North

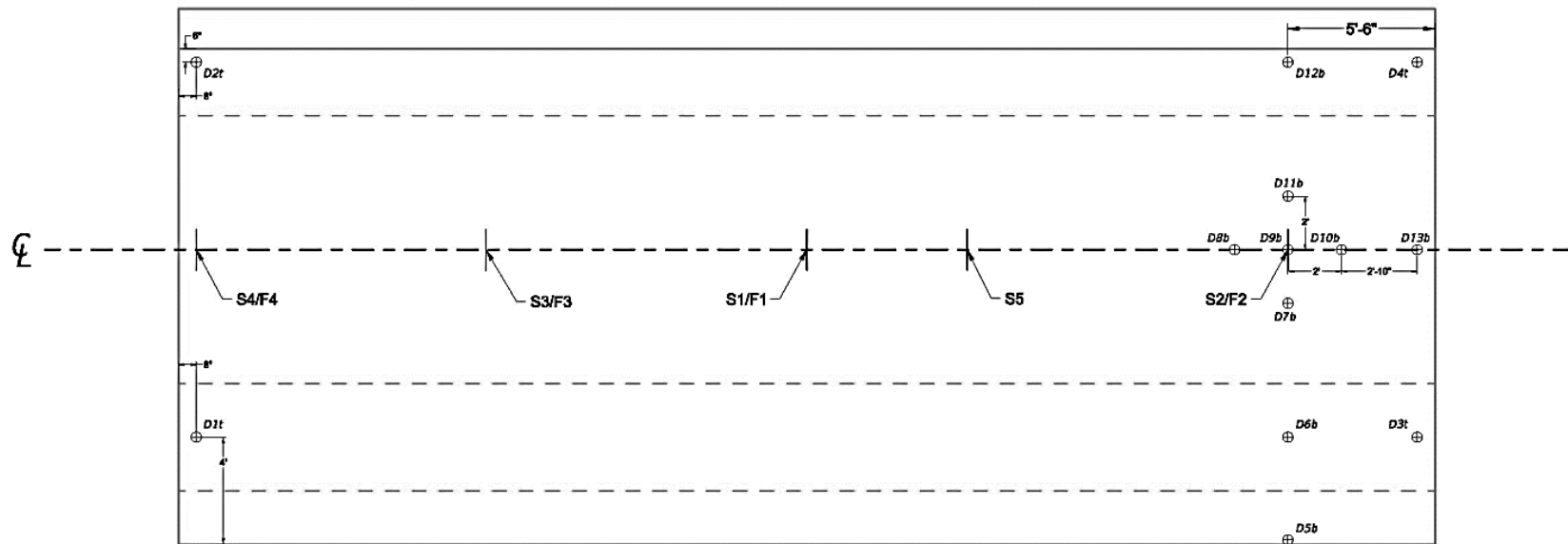
South



Top Deck Surface Crack and Foil Gauges for S3/F3

North

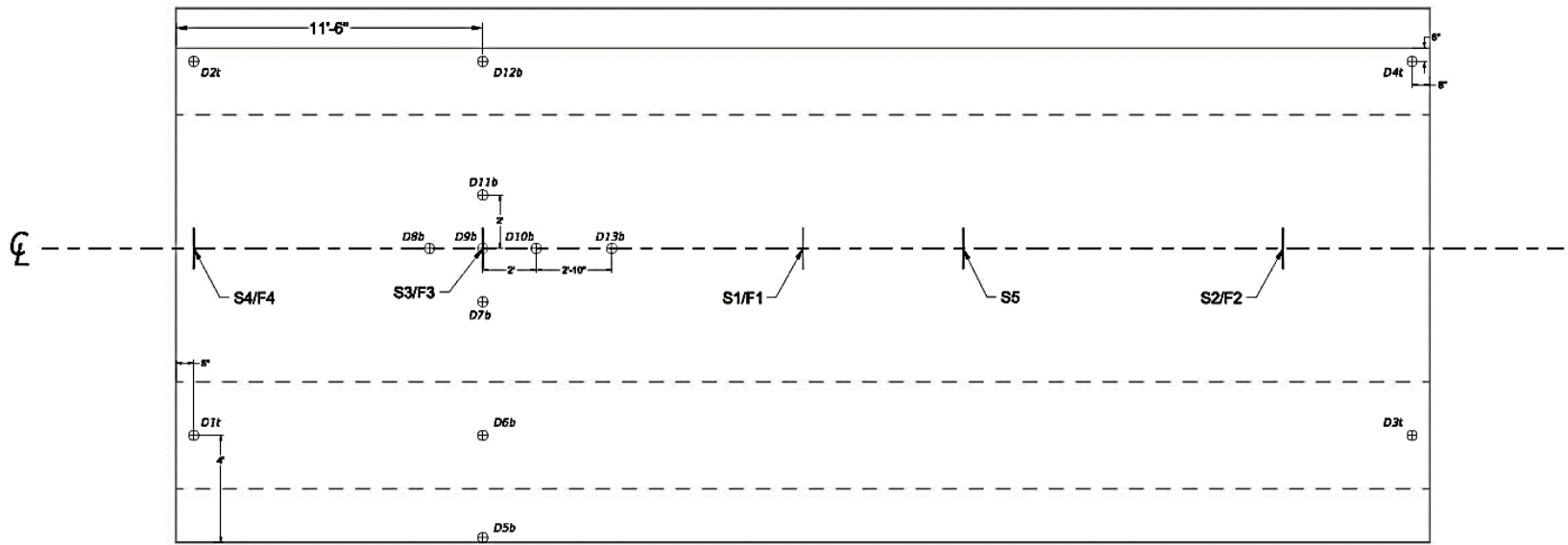
South



: Deflection Gauges for S2/F2

North

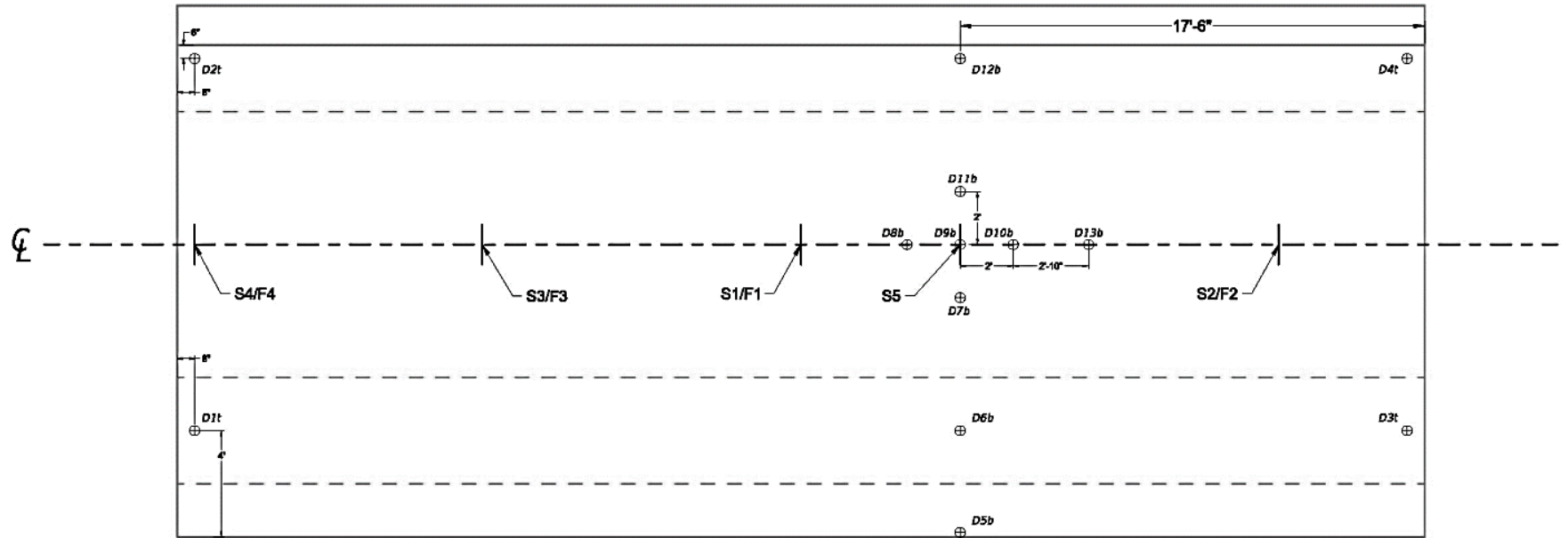
South



*Deflection Gauges for S3/F3*

North

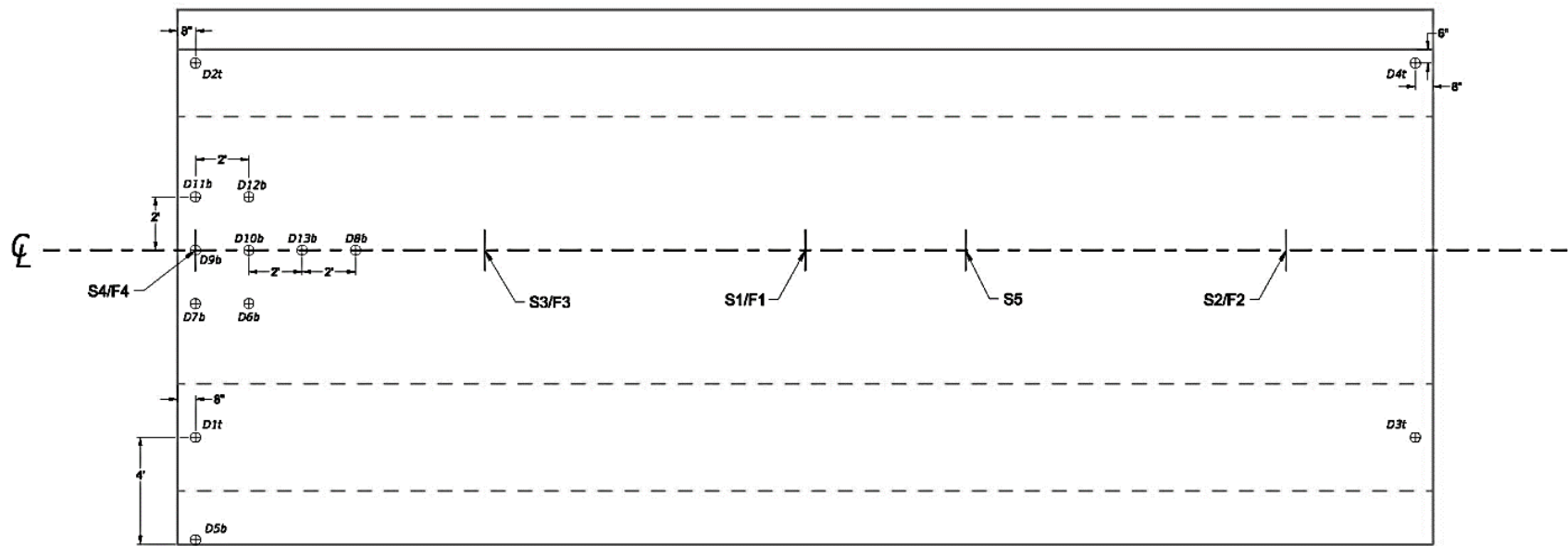
South



Deflection Gauges for S5/F5

North

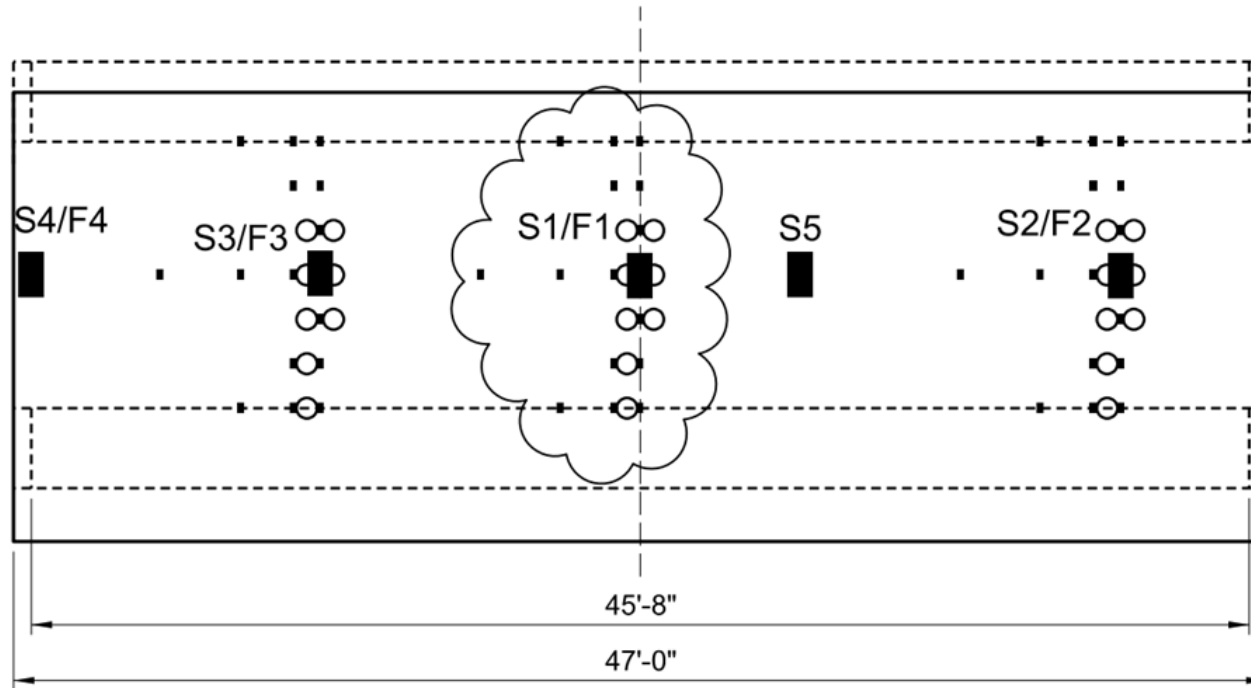
South



Deflection Gauges for S4/F4

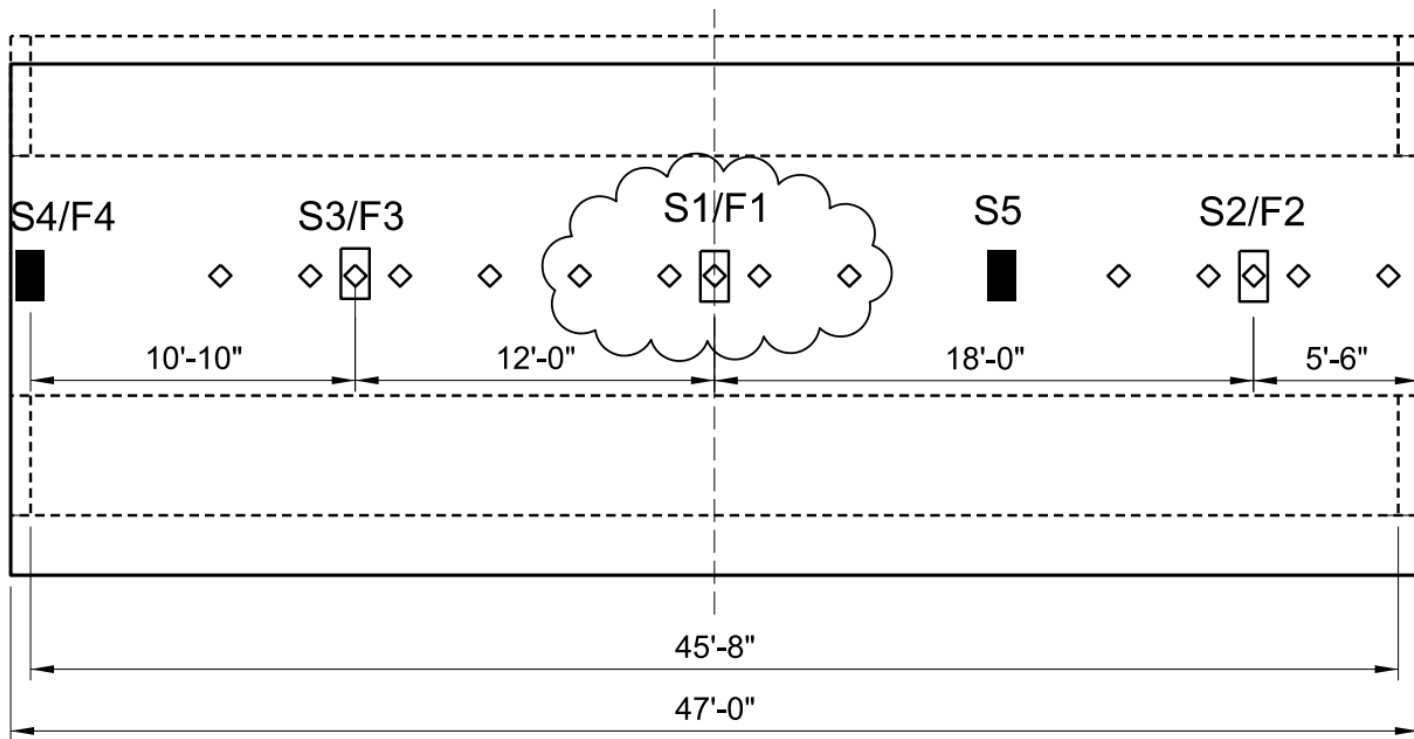
North

South



- Top steel reinforcement strain gauge (Transverse)
- Bottom steel reinforcement strain gauge (Transverse)
- ☁ Cloud Captures The Foil Strain Gauges That Were Read For S1/F1

*Internal Strain Gauges Read for S1/F1*

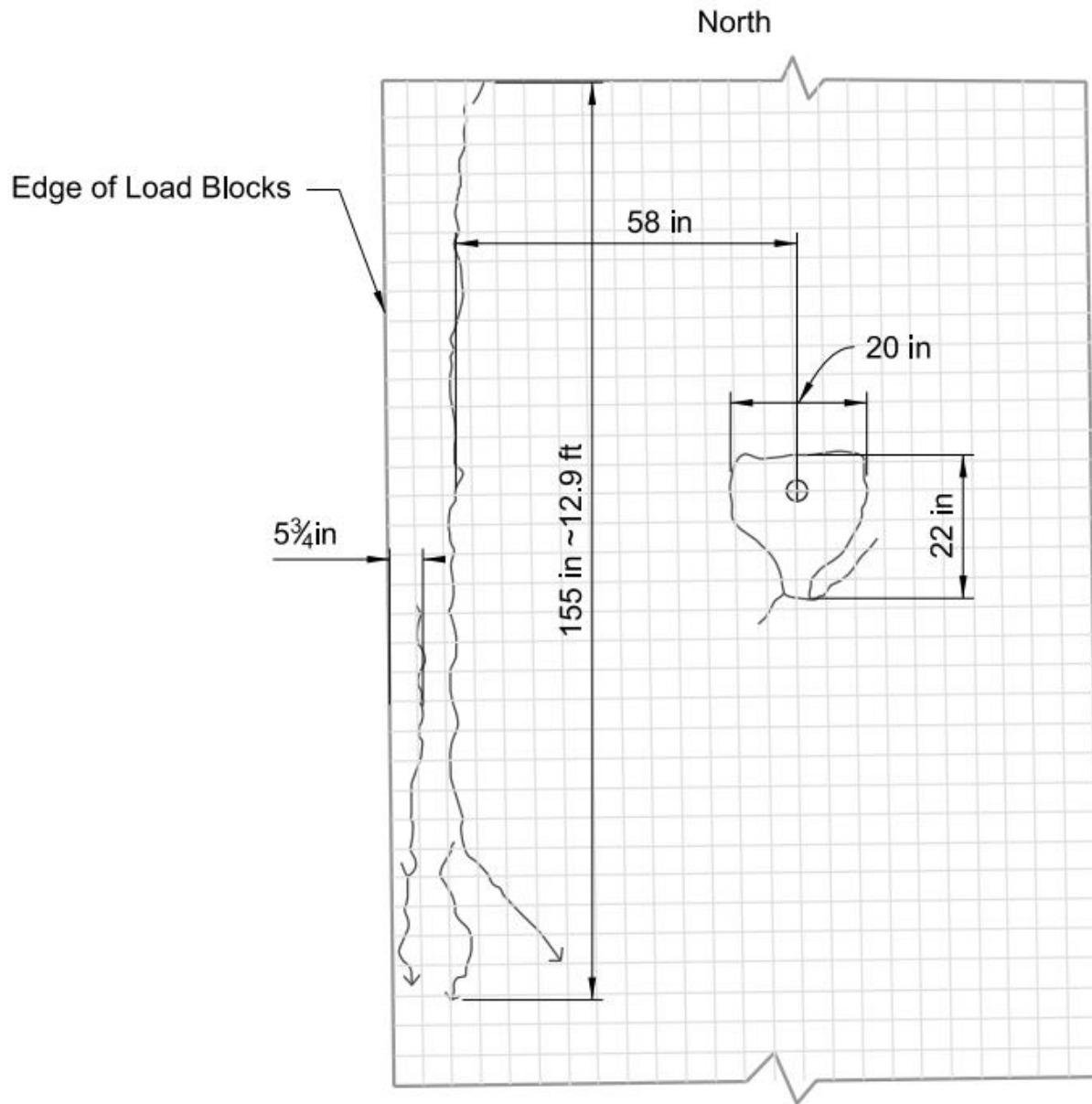


◇ Bottom steel gages(Longitudinal)

☁ Cloud Captures The Strain Gages on the Longitudinal Reinforcement That Were Read For S1/F1

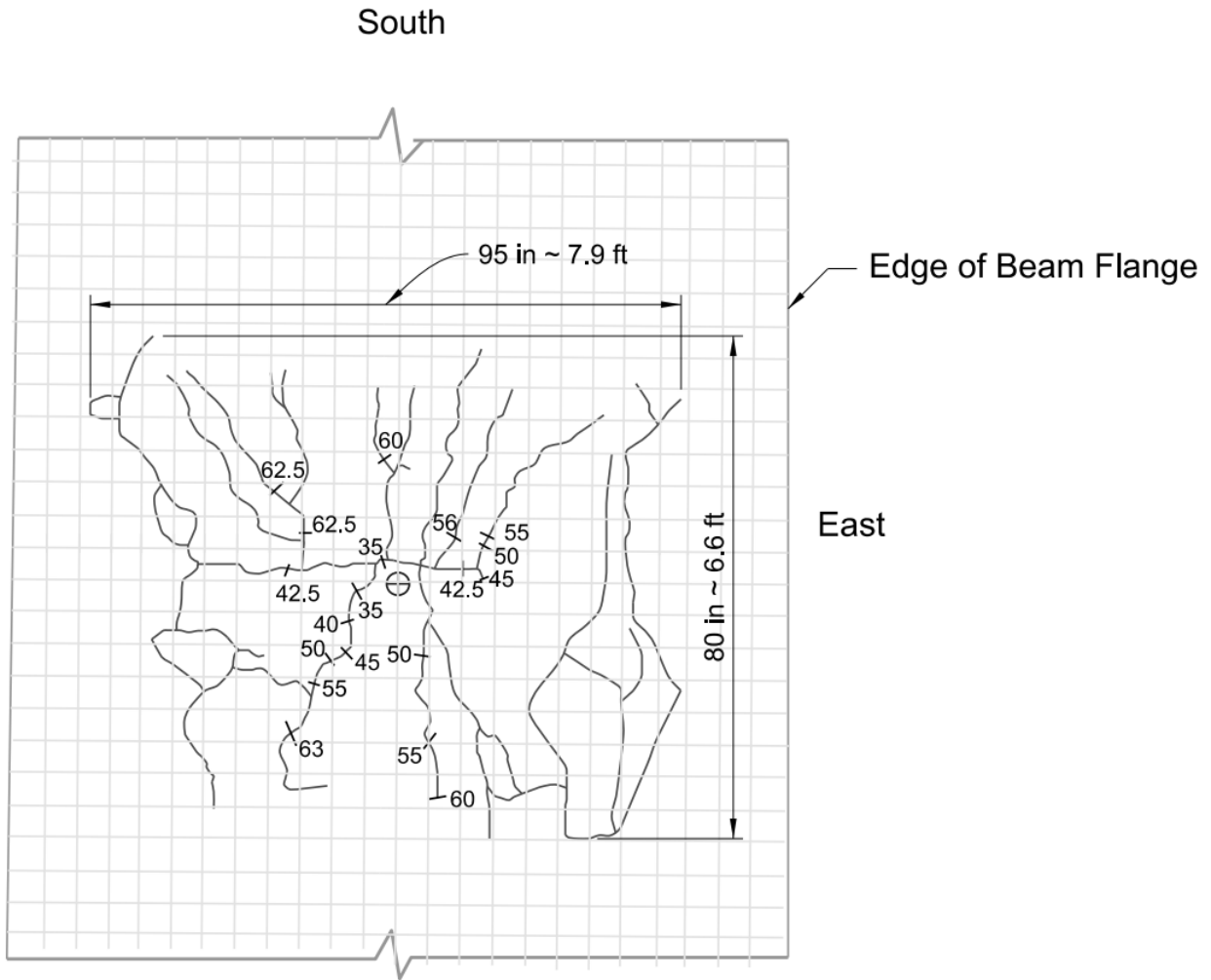
*Bottom Mat Reinforcement Longitudinal Strain Gauges Read for S1/F1*

APPENDIX VII: CRACK MAPPING



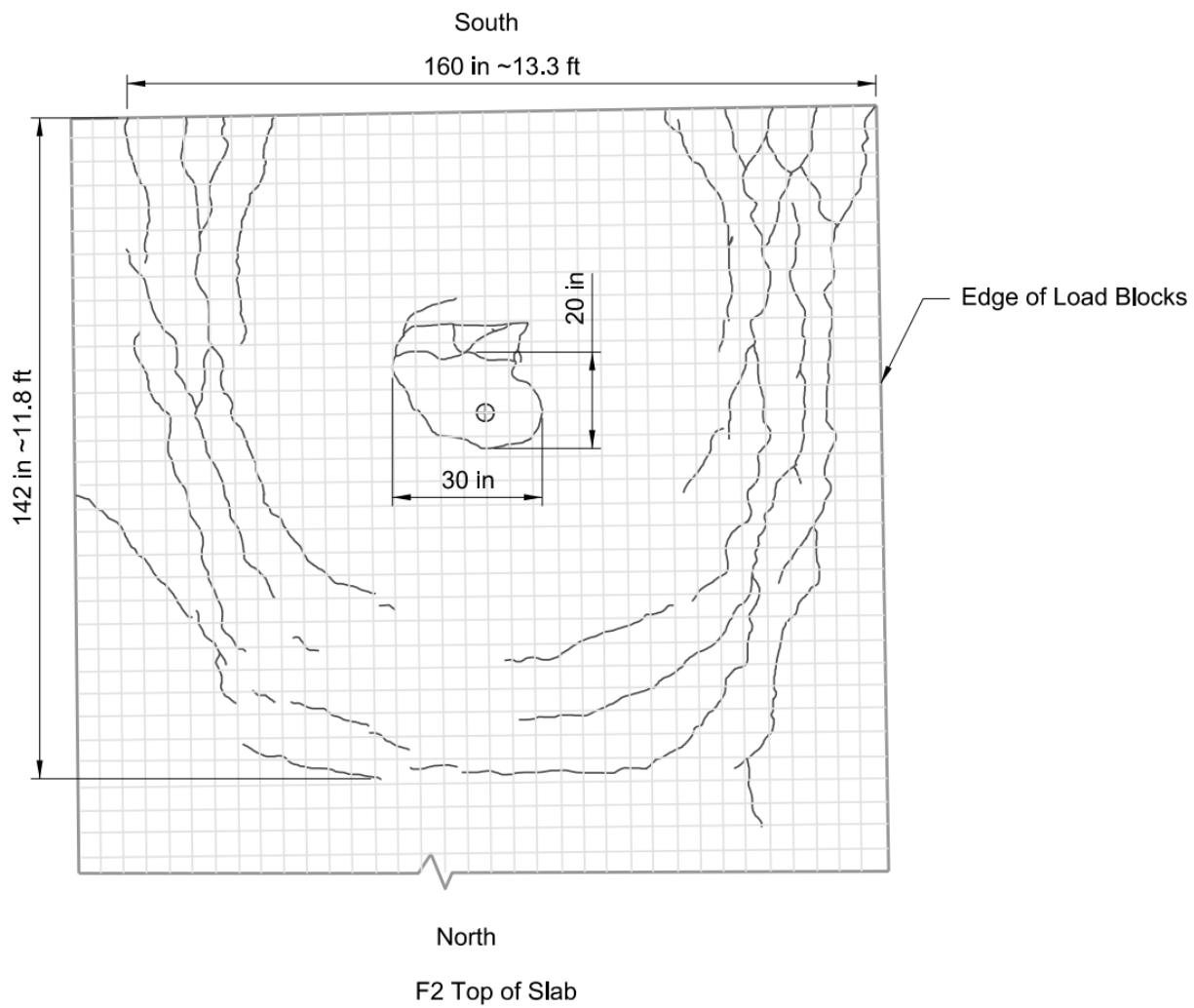
F1 Top of Slab

*Crack Mapping for F1 Top of Slab (5 inch grid)*

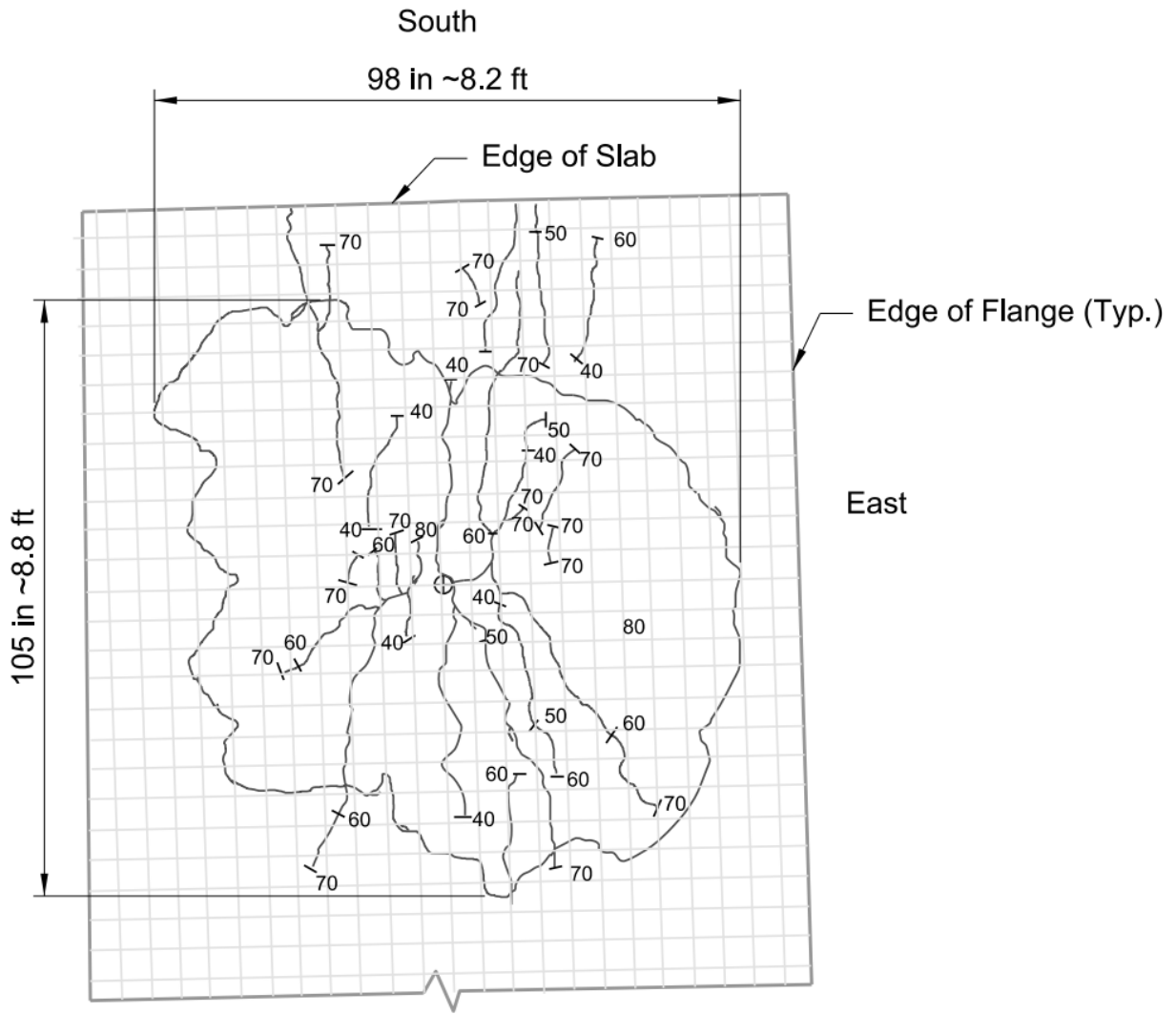


**F1 Bottom of Slab**

*Cracking Mapping for F1 Bottom of Slab (5 inch grid)*

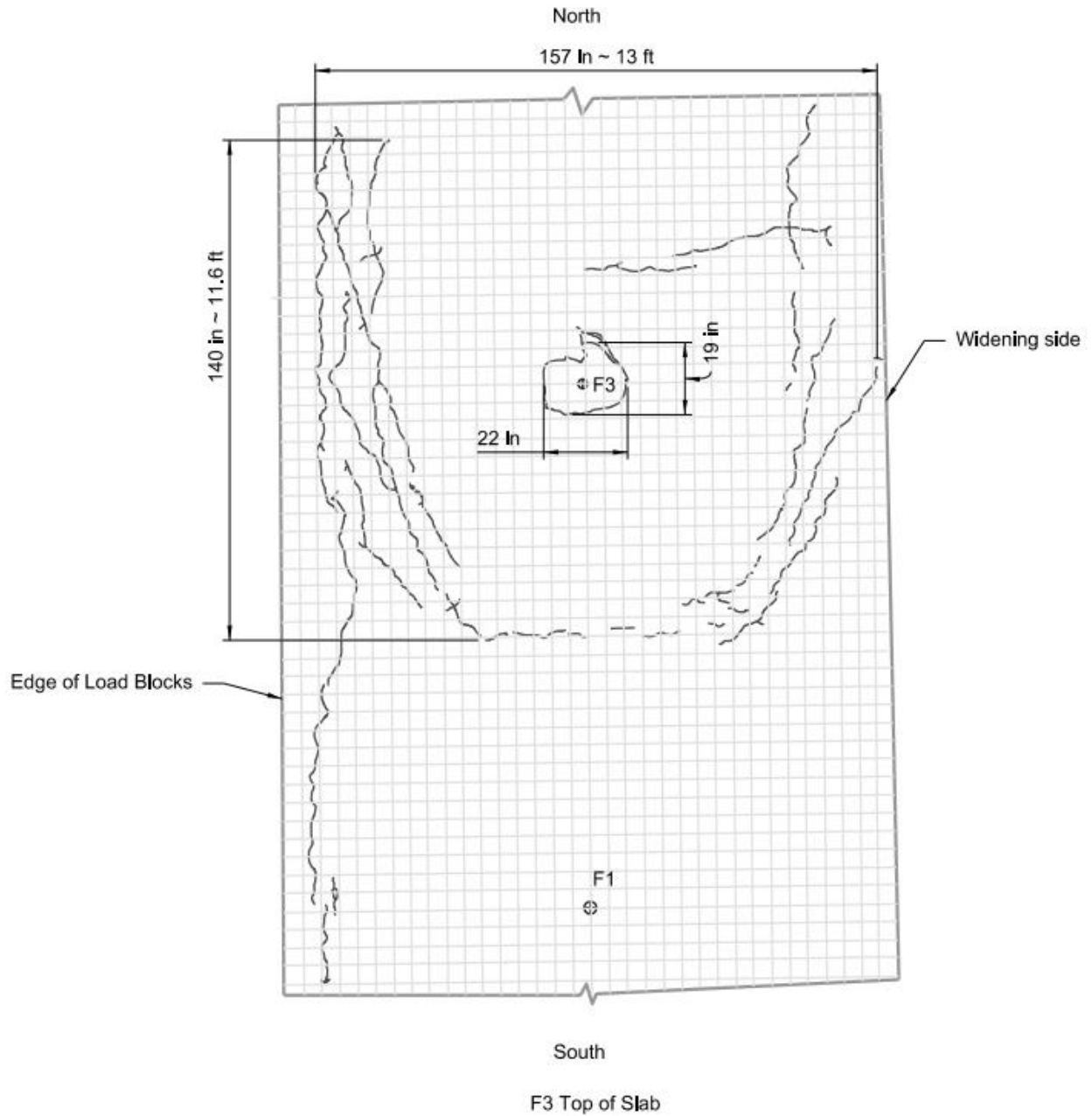


*Crack Mapping for F2 Top of Slab (5 inch grid)*

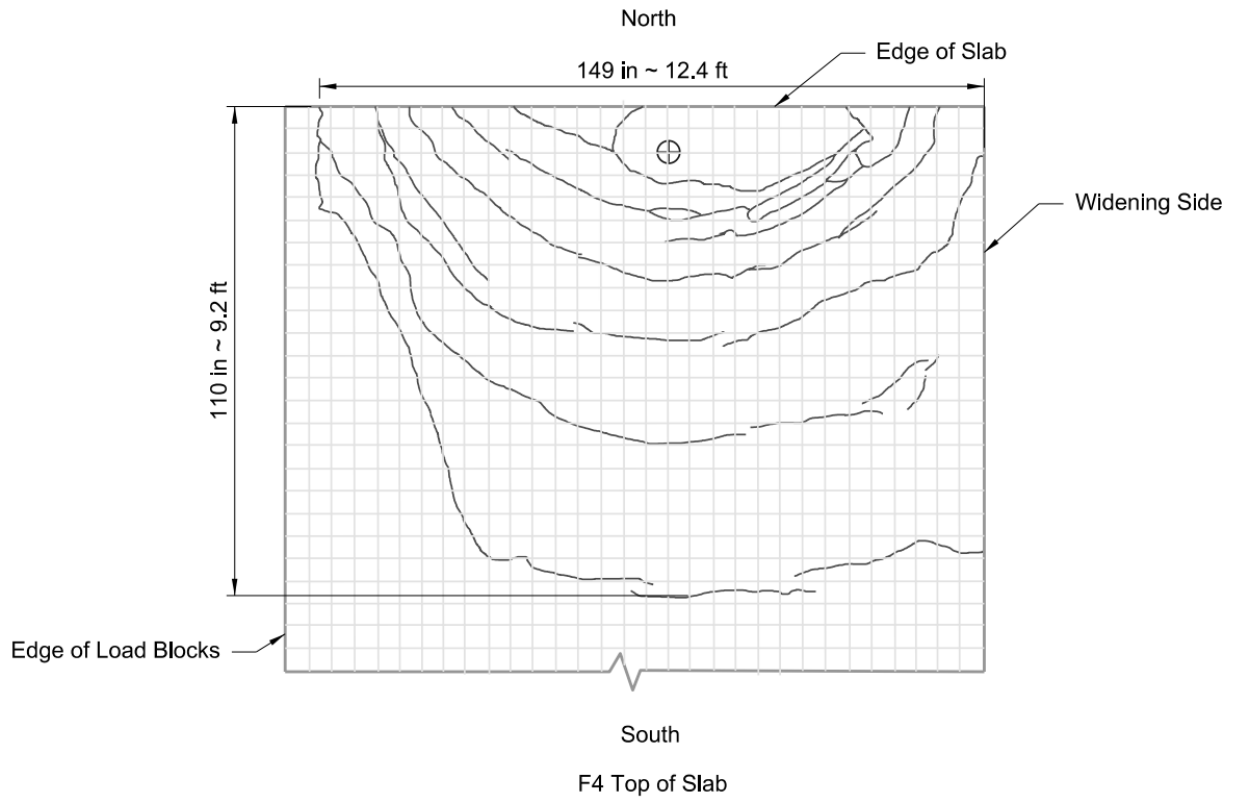


F2 Bottom of Slab

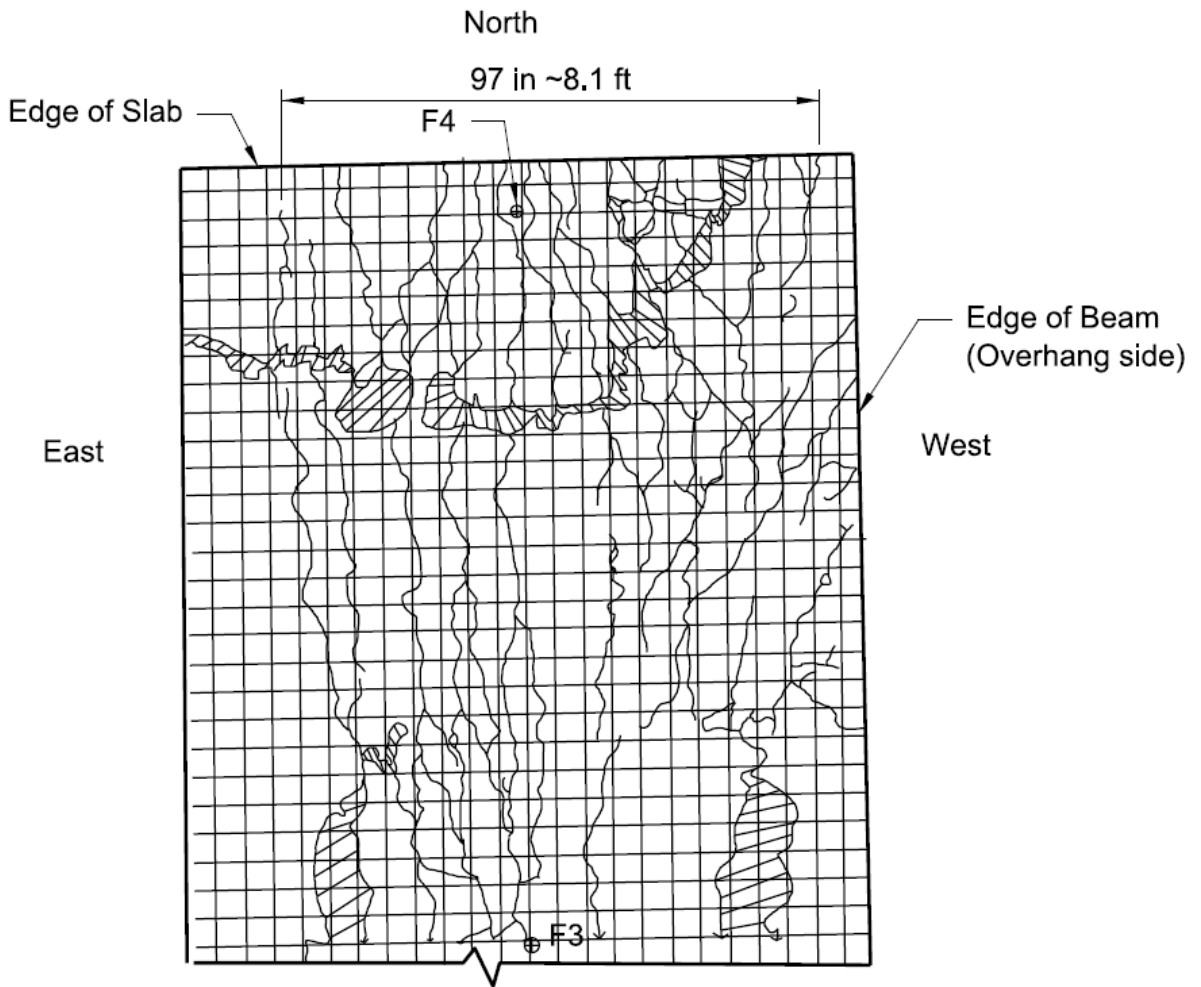
*Cracking Mapping for F2 Bottom of Slab (5 inch grid)*



*Crack Mapping F3 Top of Slab (5 inch grid)*



*Crack Mapping for F4 Top of Slab (5 inch grid)*

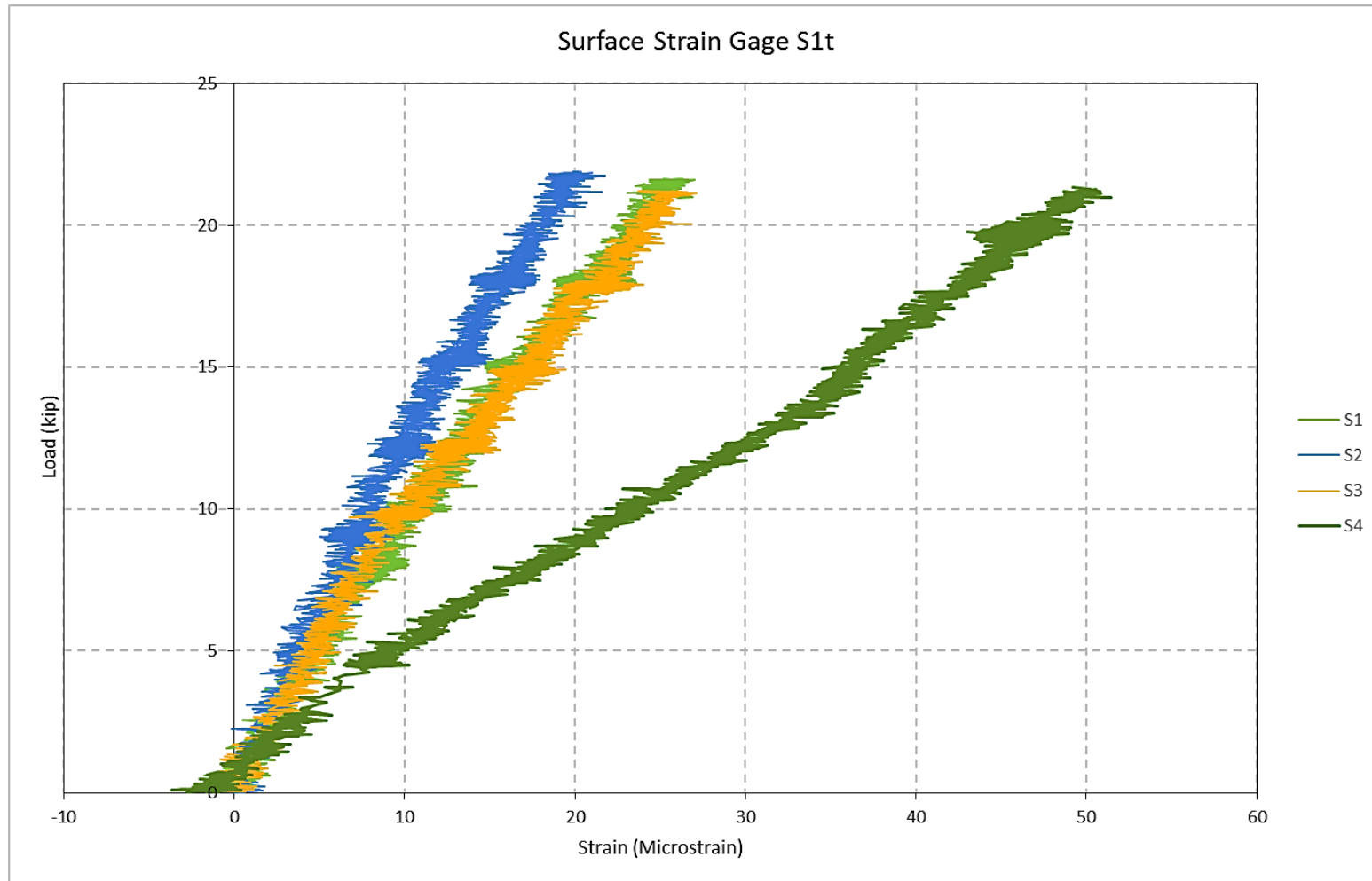


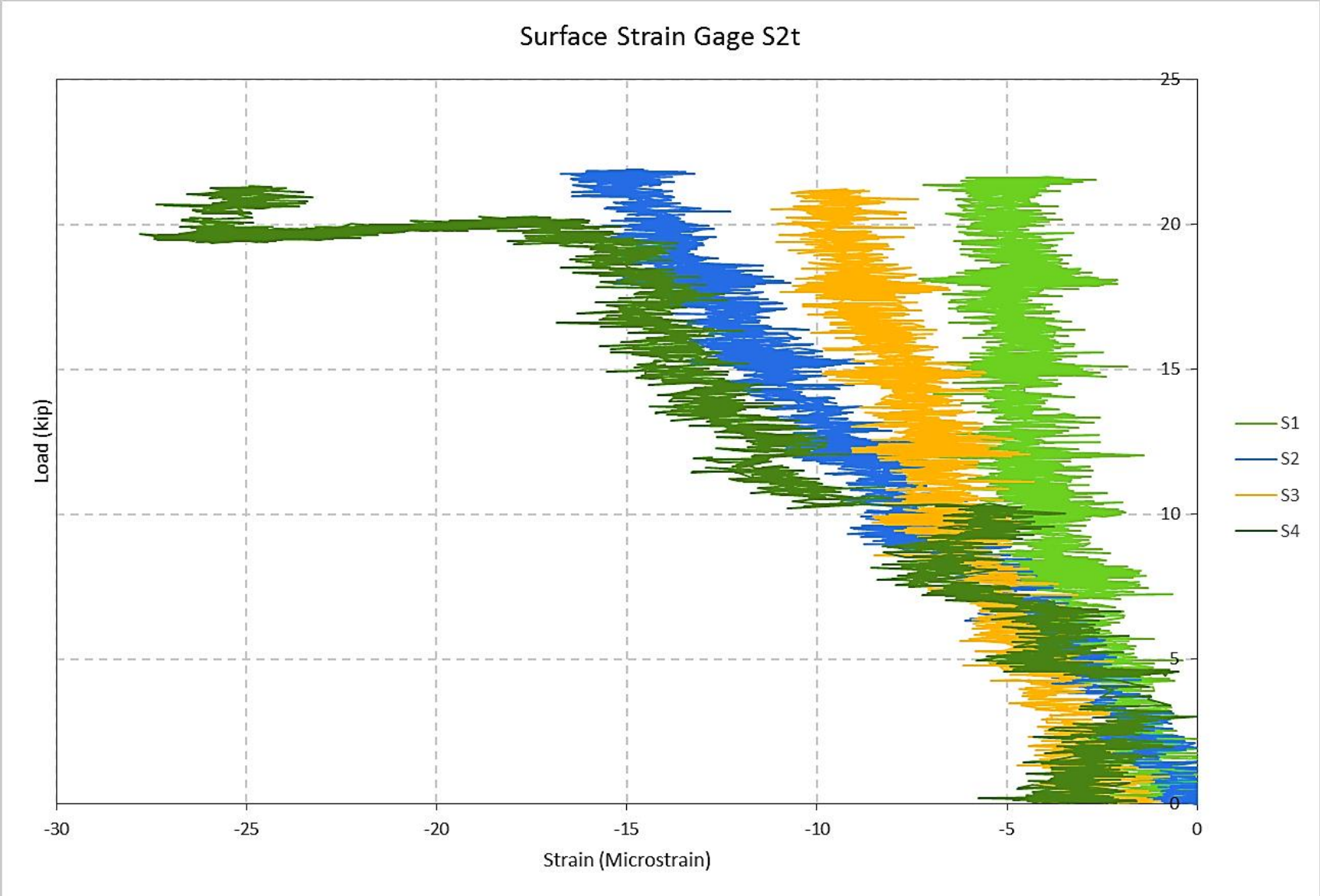
F4 Bottom of Slab  
 Striped areas denote exposed aggregate

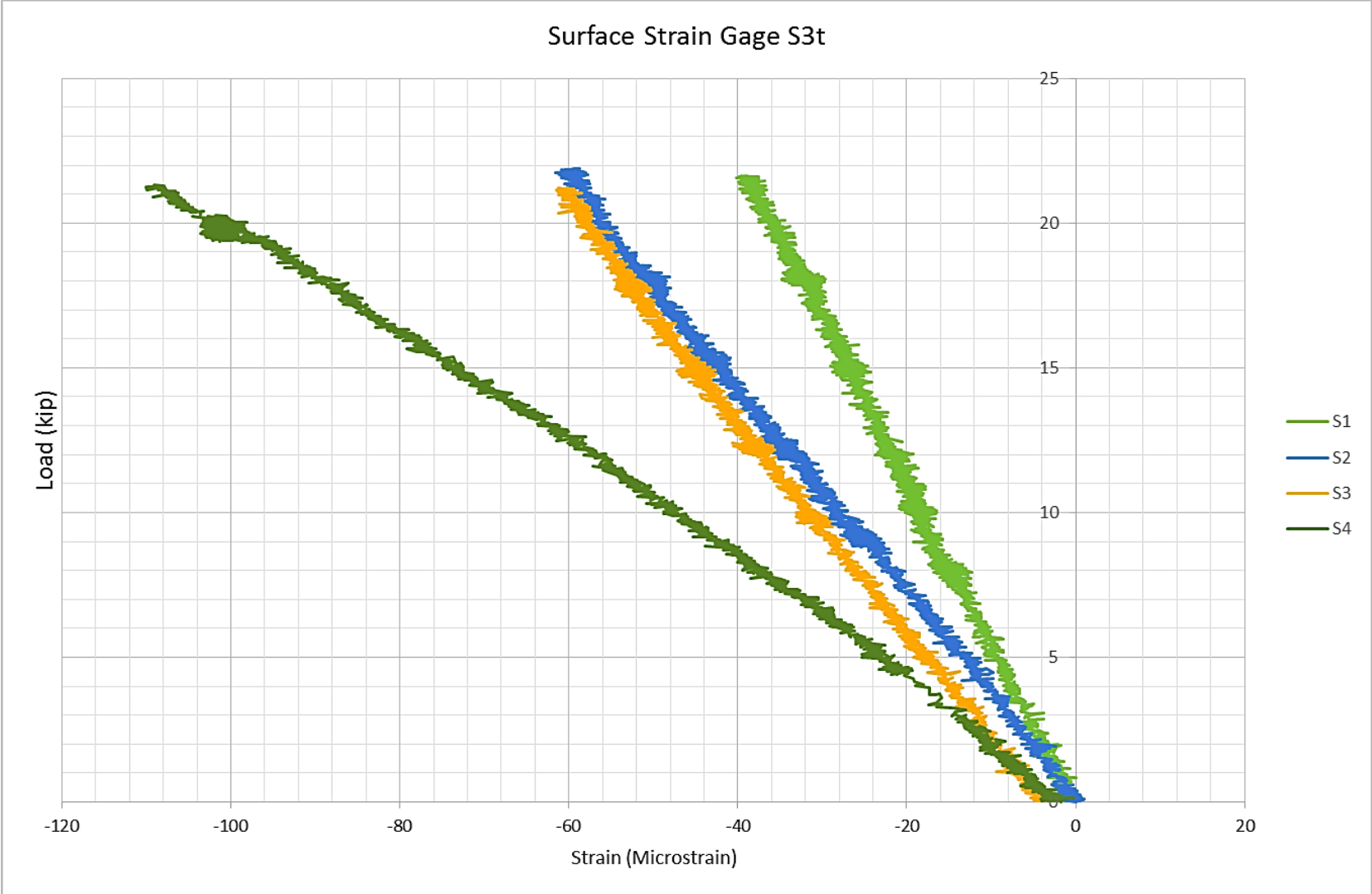
*Crack Mapping for F4 Bottom of Slab (5 inch grid)*

# APPENDIX VIII: SERVICE PLOTS

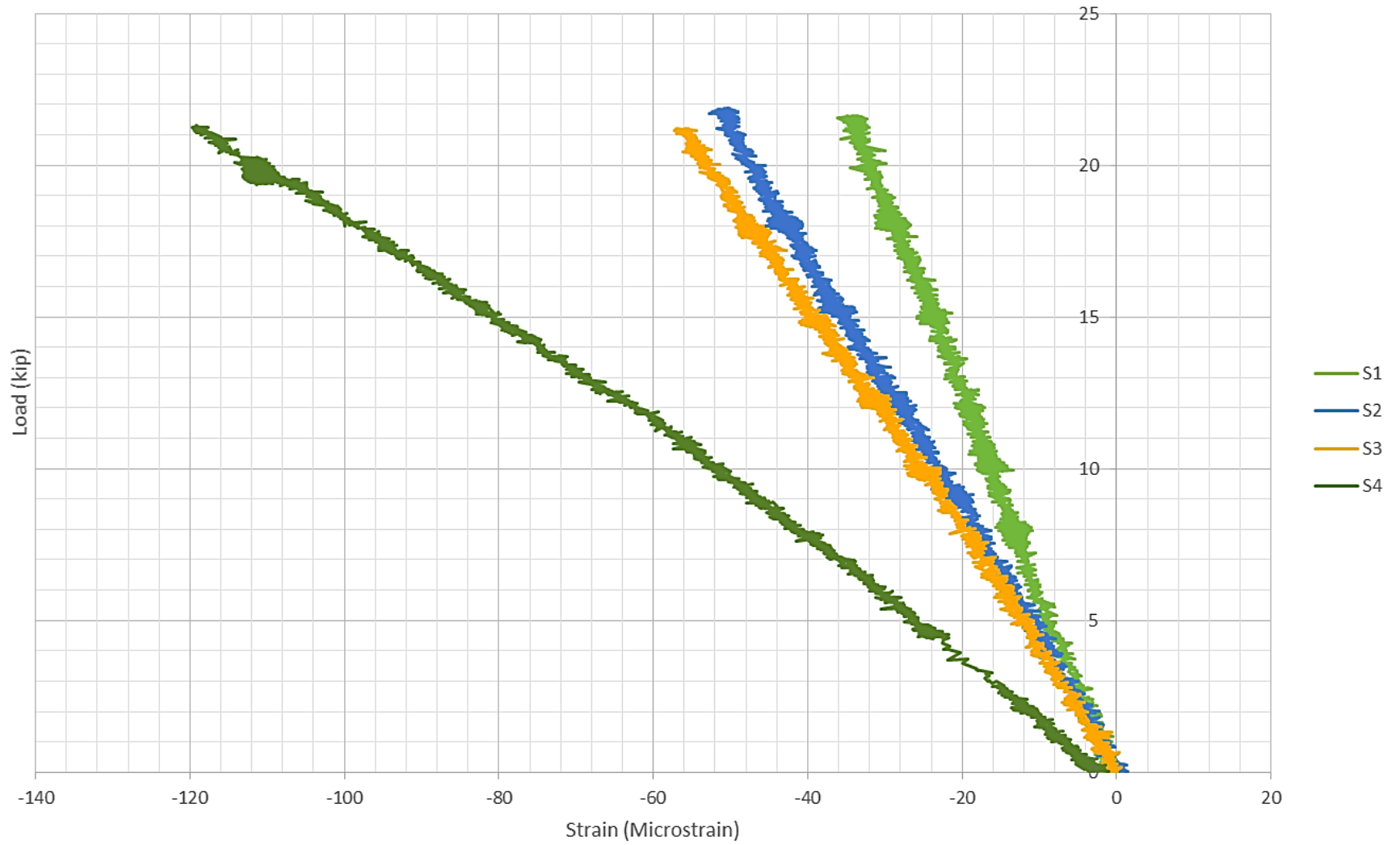
## Surface Gauges



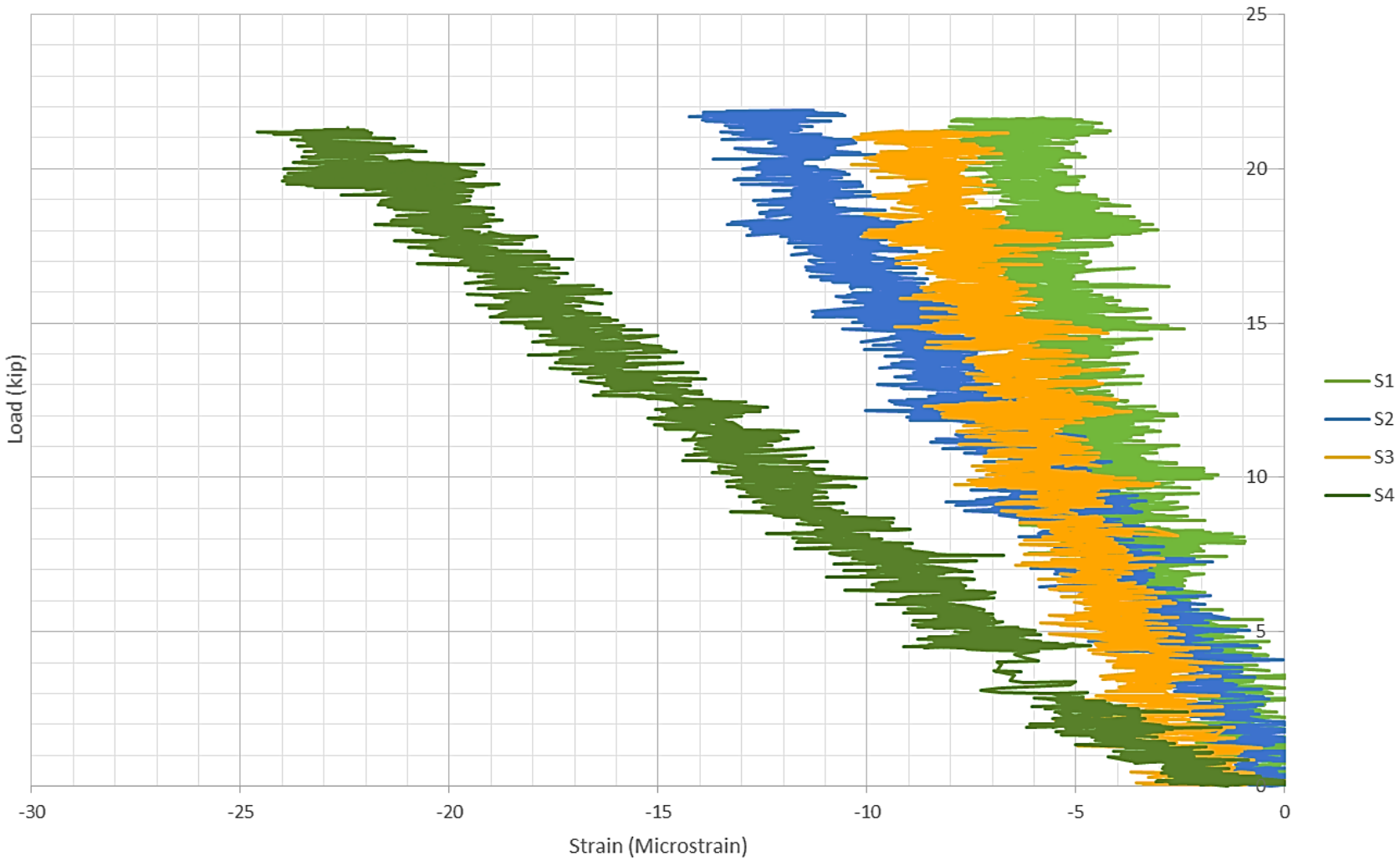


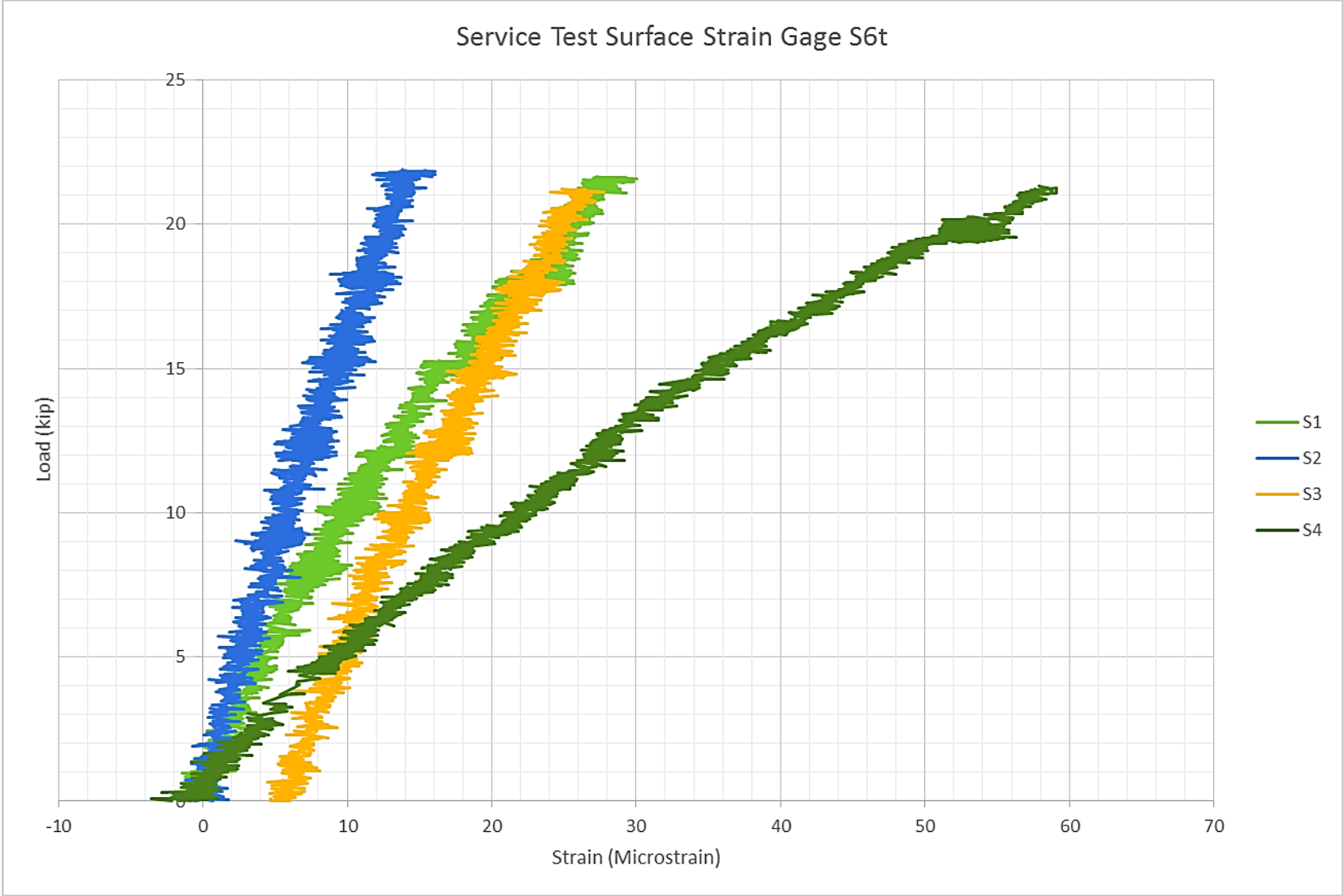


Surface Strain Gage S4t

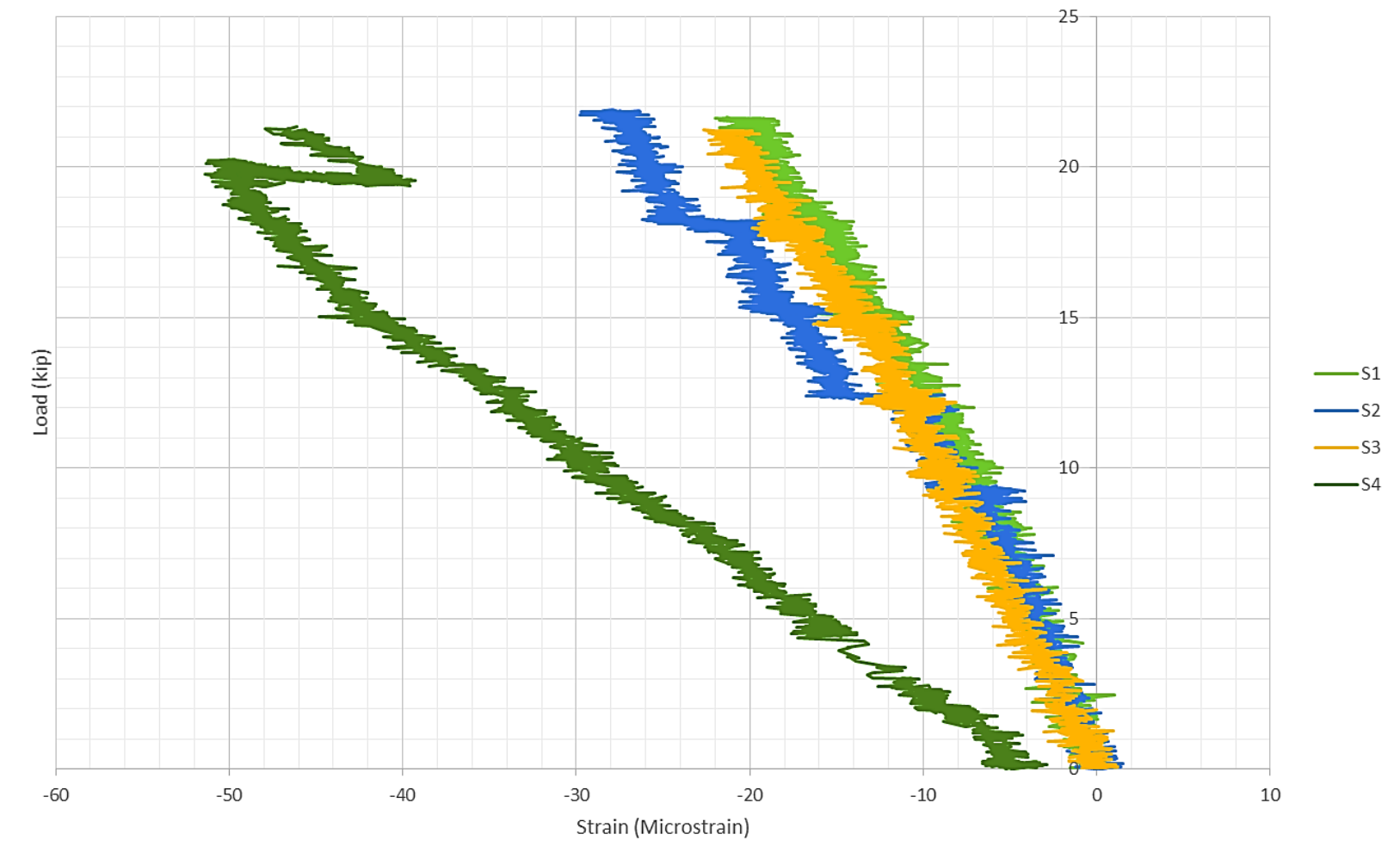


Surface Strain Gage S5t

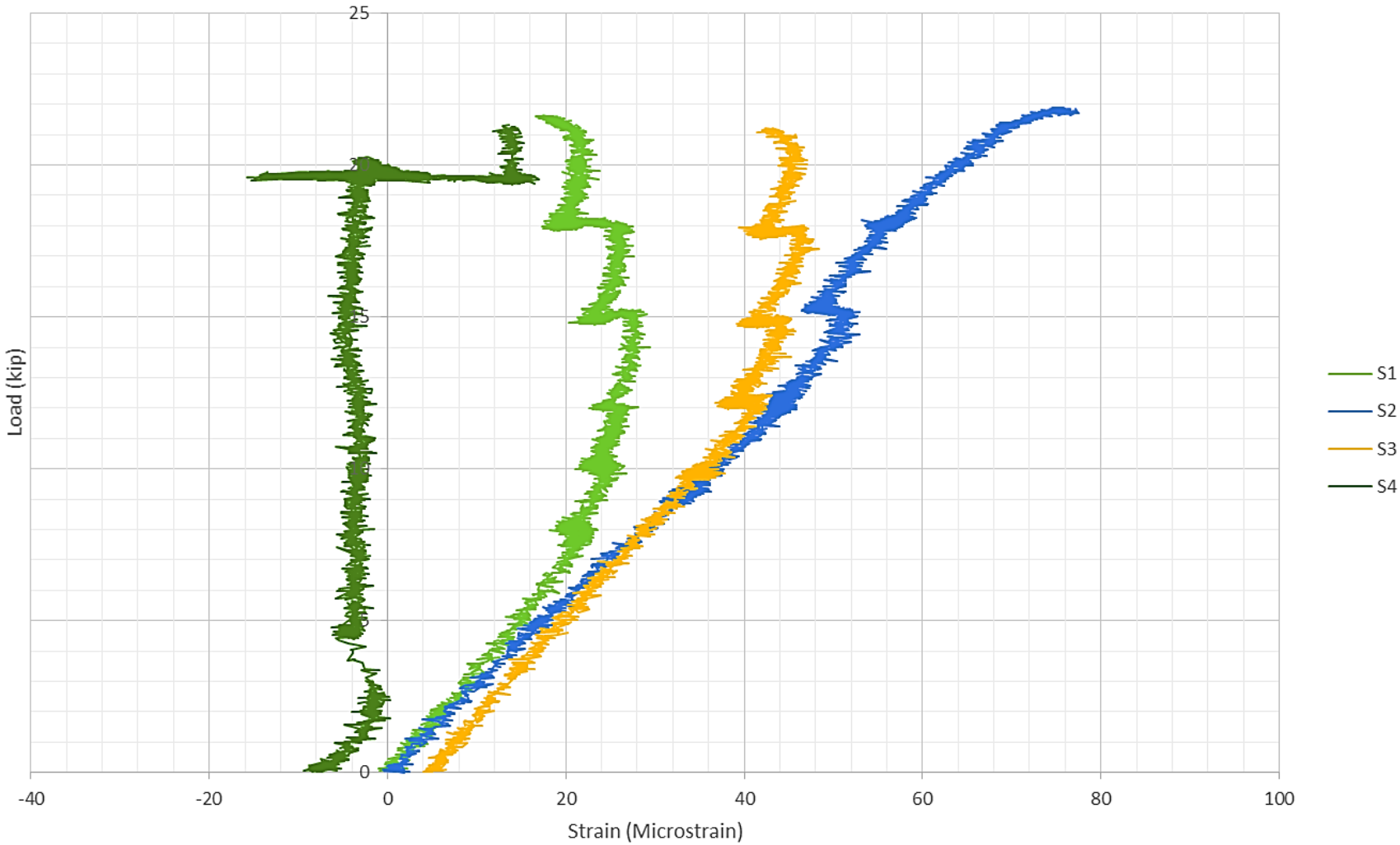




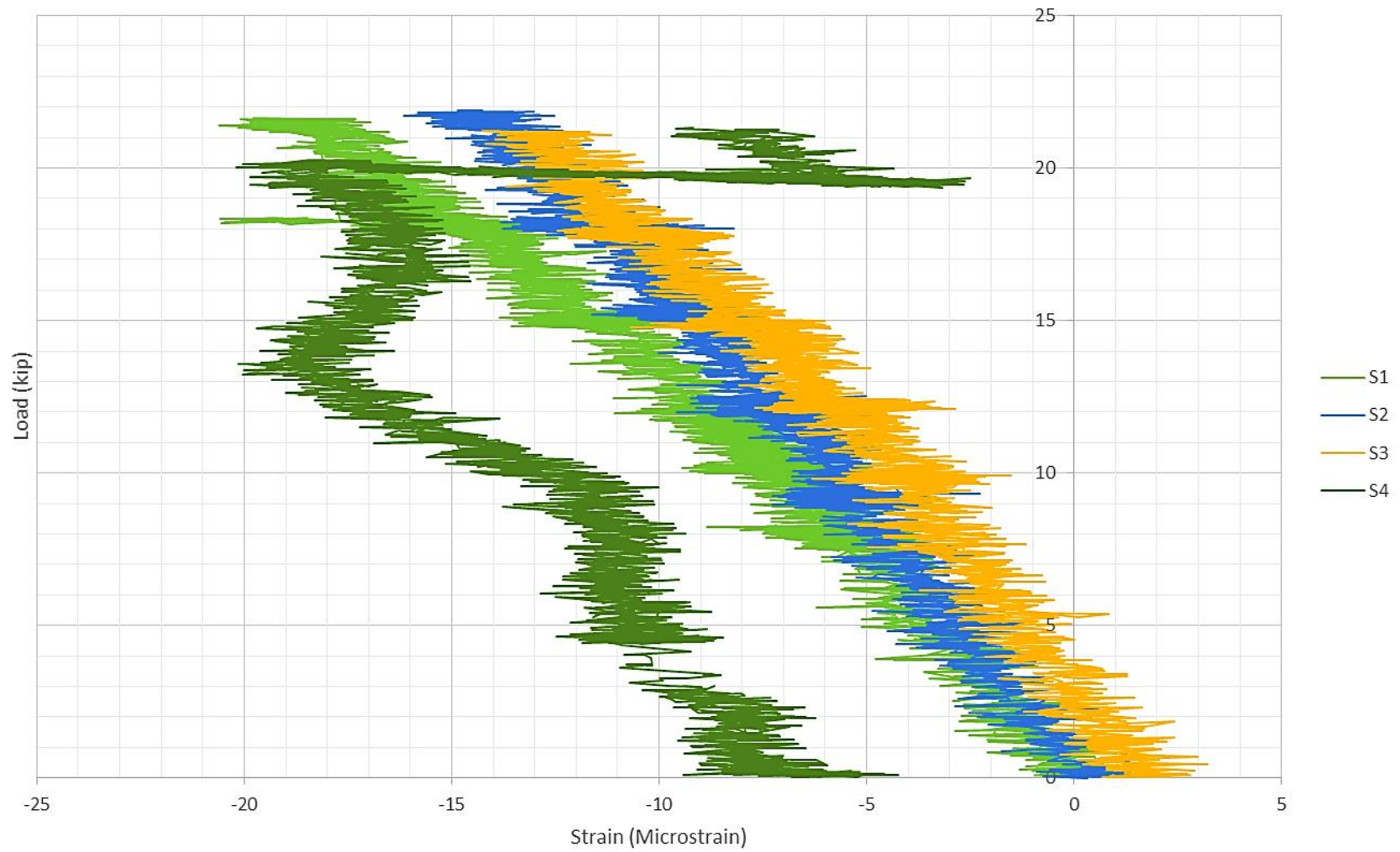
Service Test Surface Strain Gage S7b



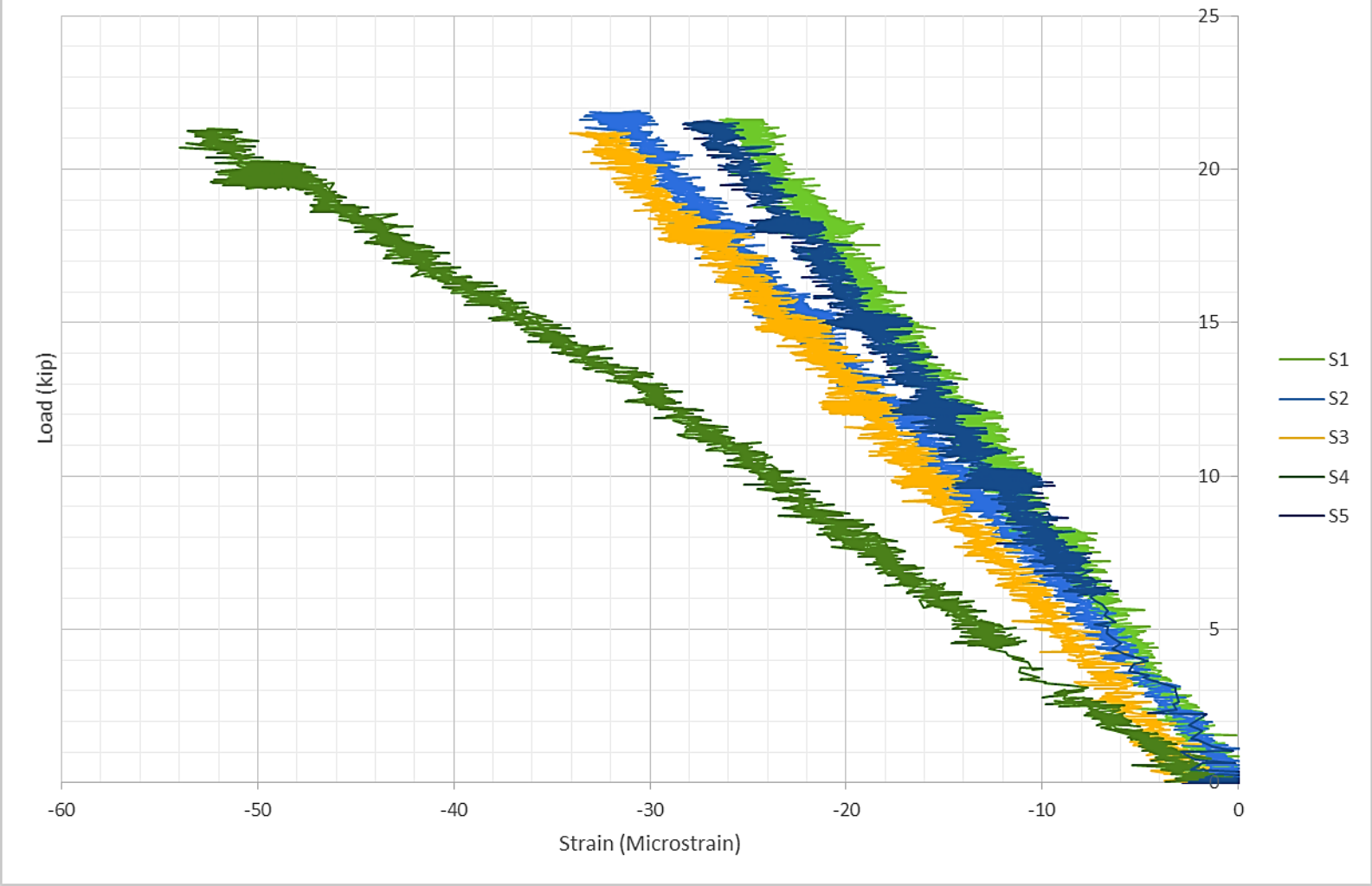
Service Test Surface Strain Gage S8b



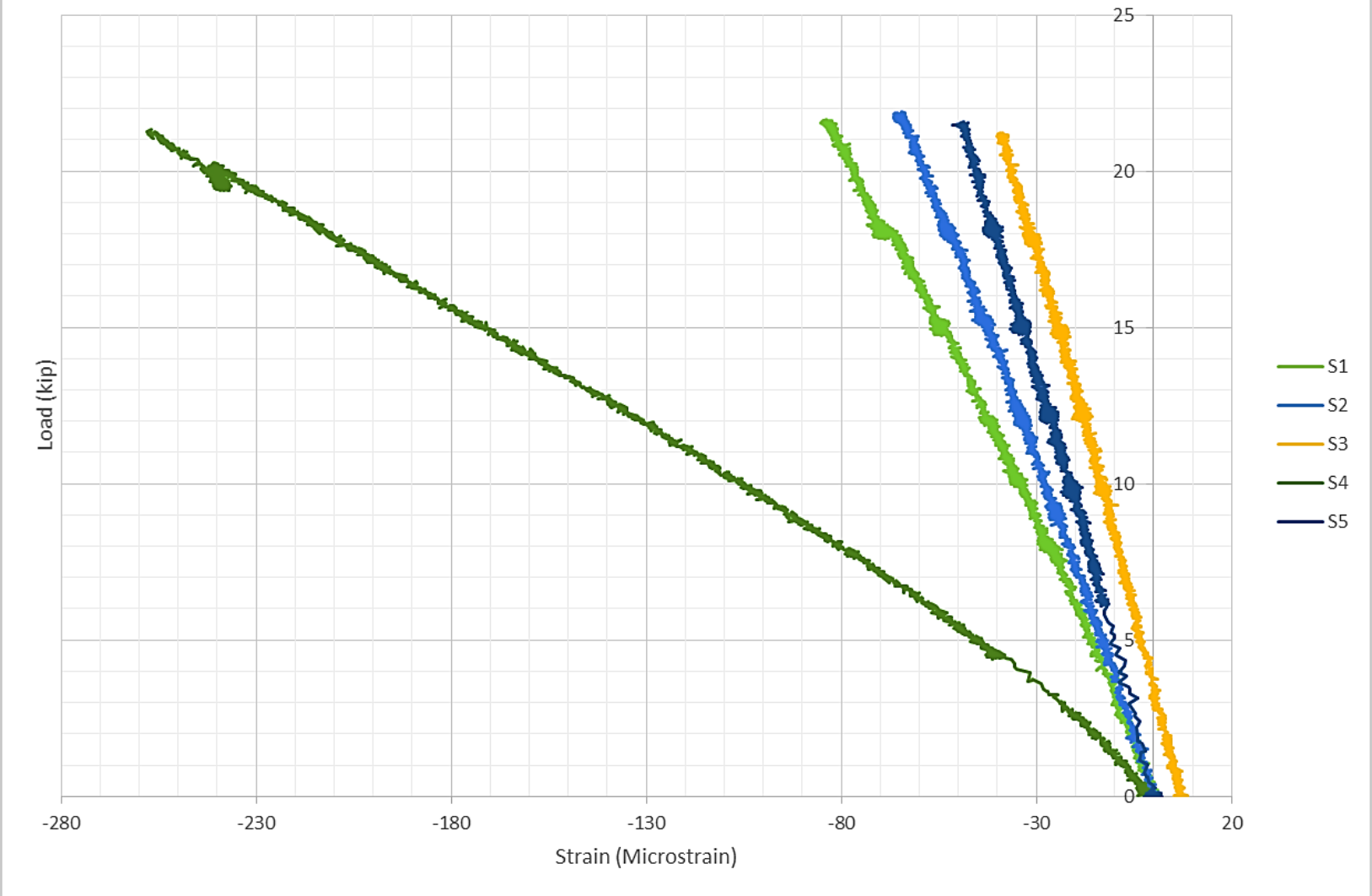
Service Test Surface Strain Gage S9b



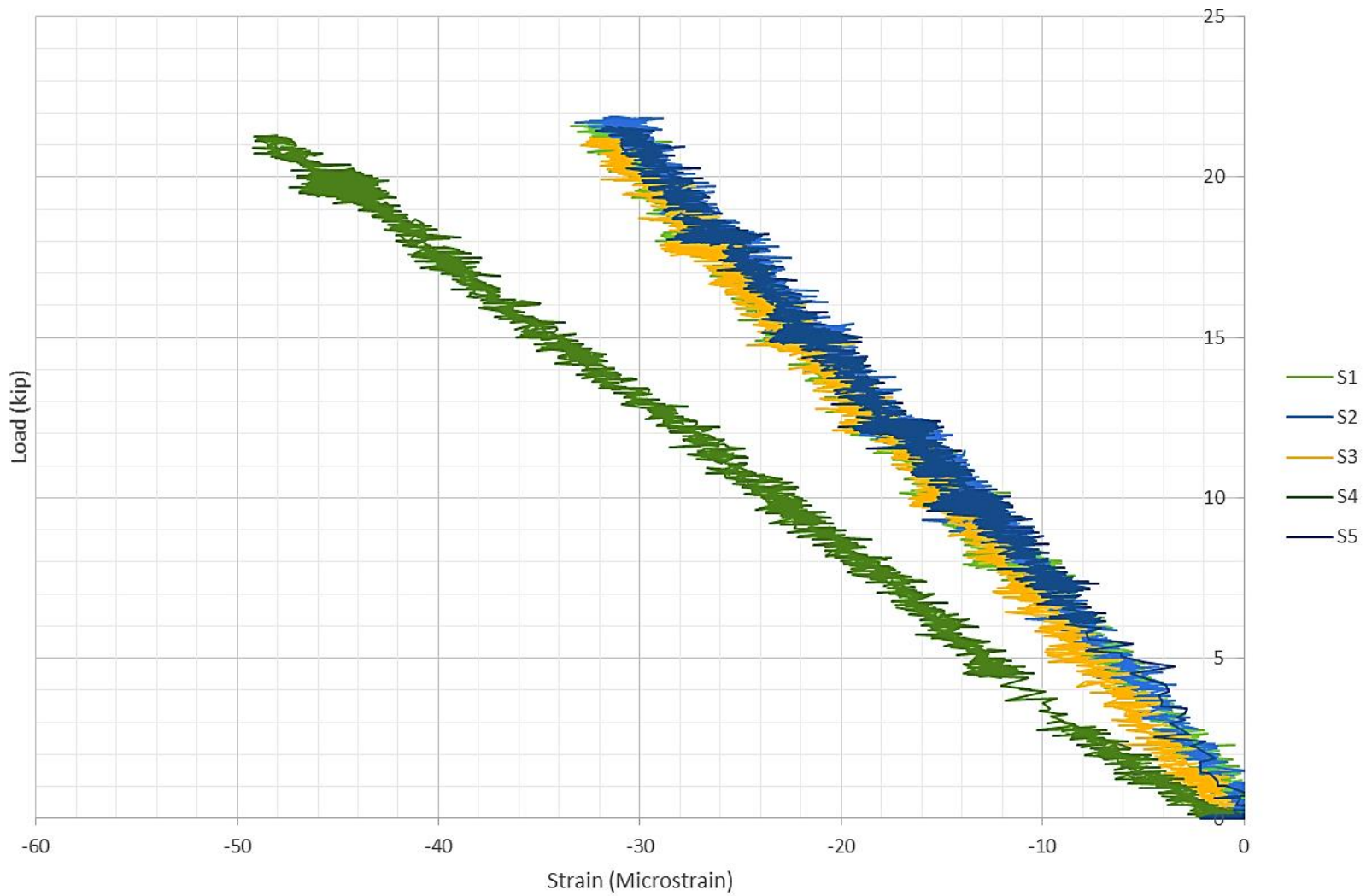
Service Test Surface Strain Gage S10t



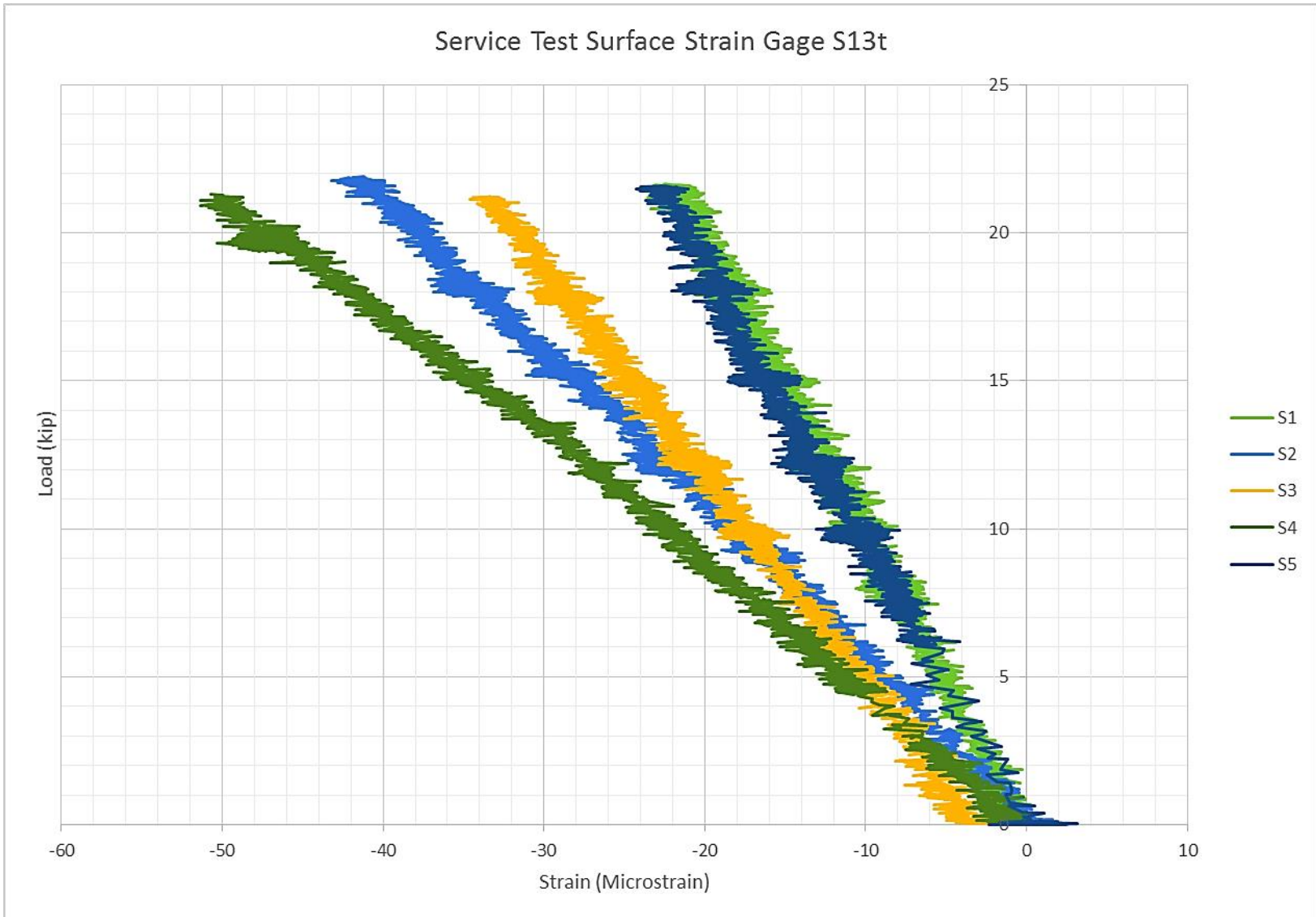
Service Test Surface Strain Gage S11t

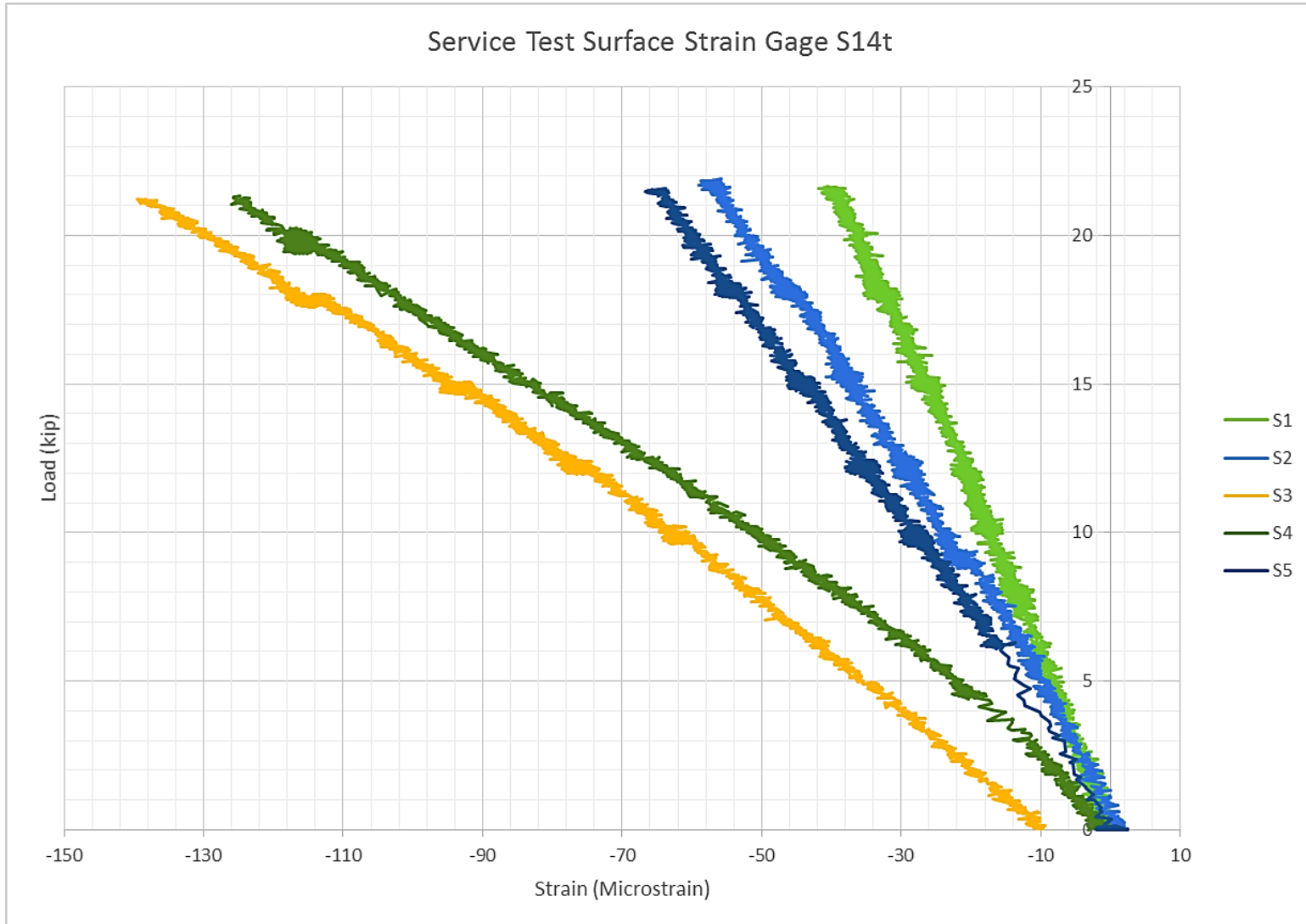


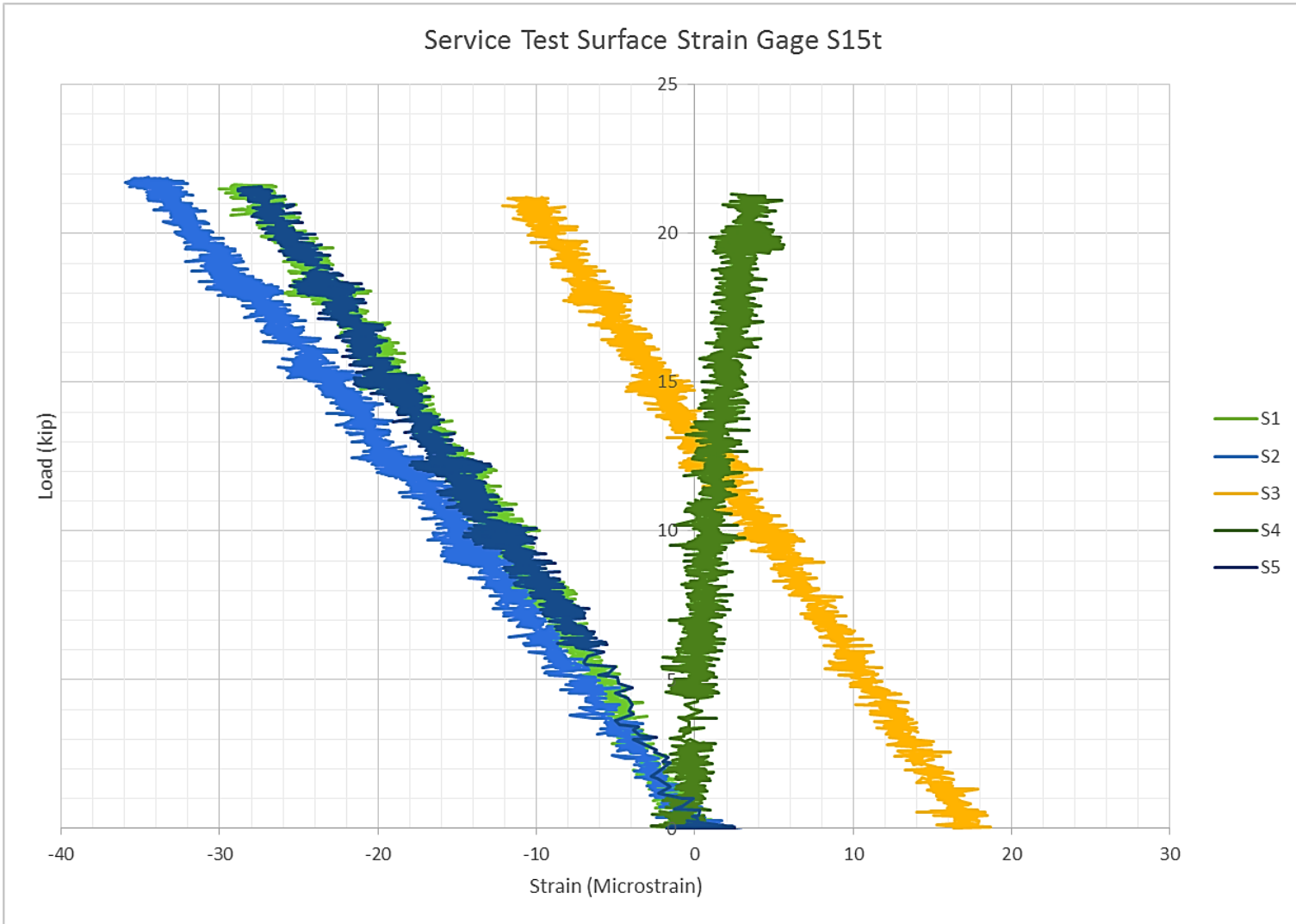
Service Test Surface Strain Gage S12t



Service Test Surface Strain Gage S13t

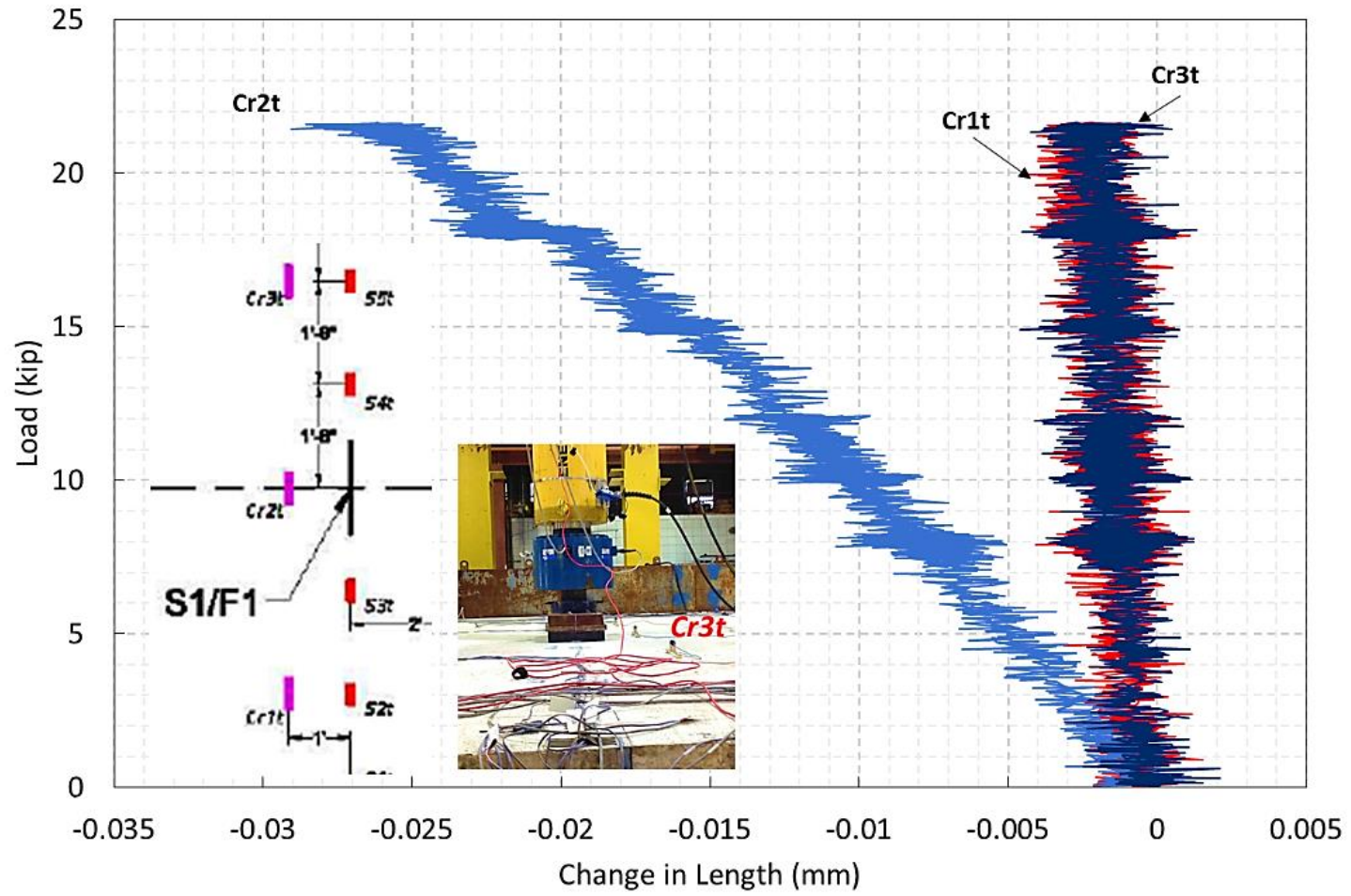


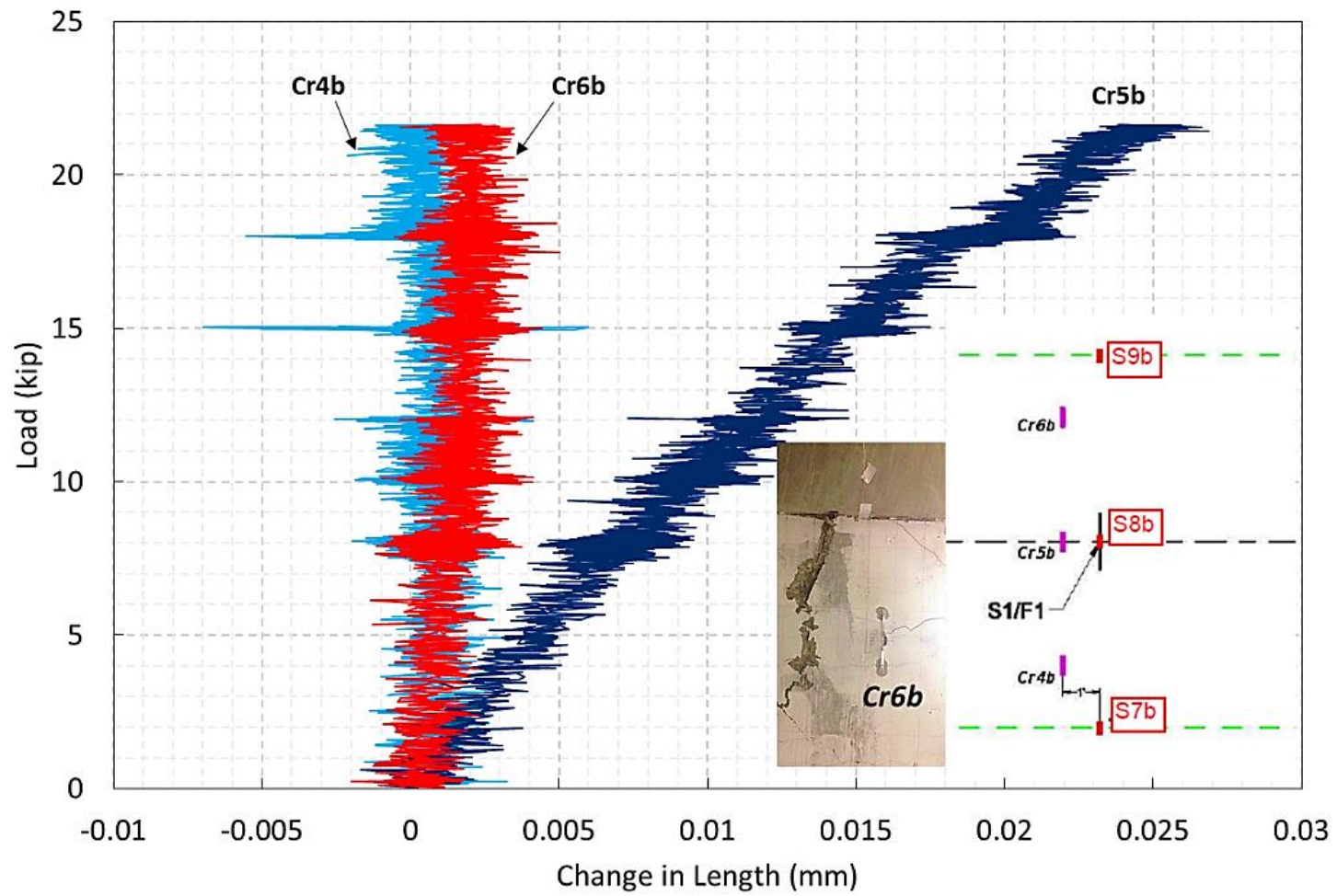




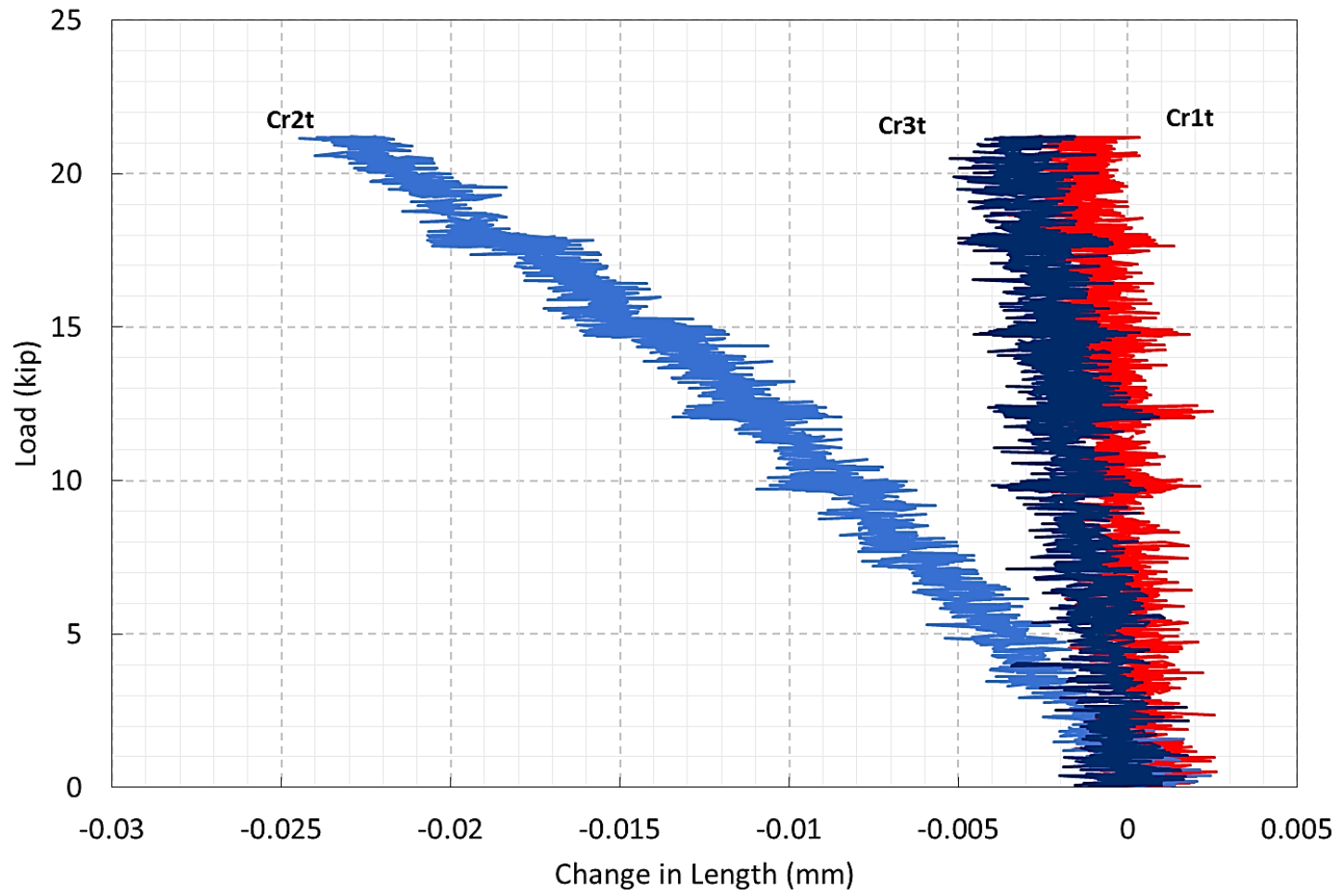
Crack Gauges

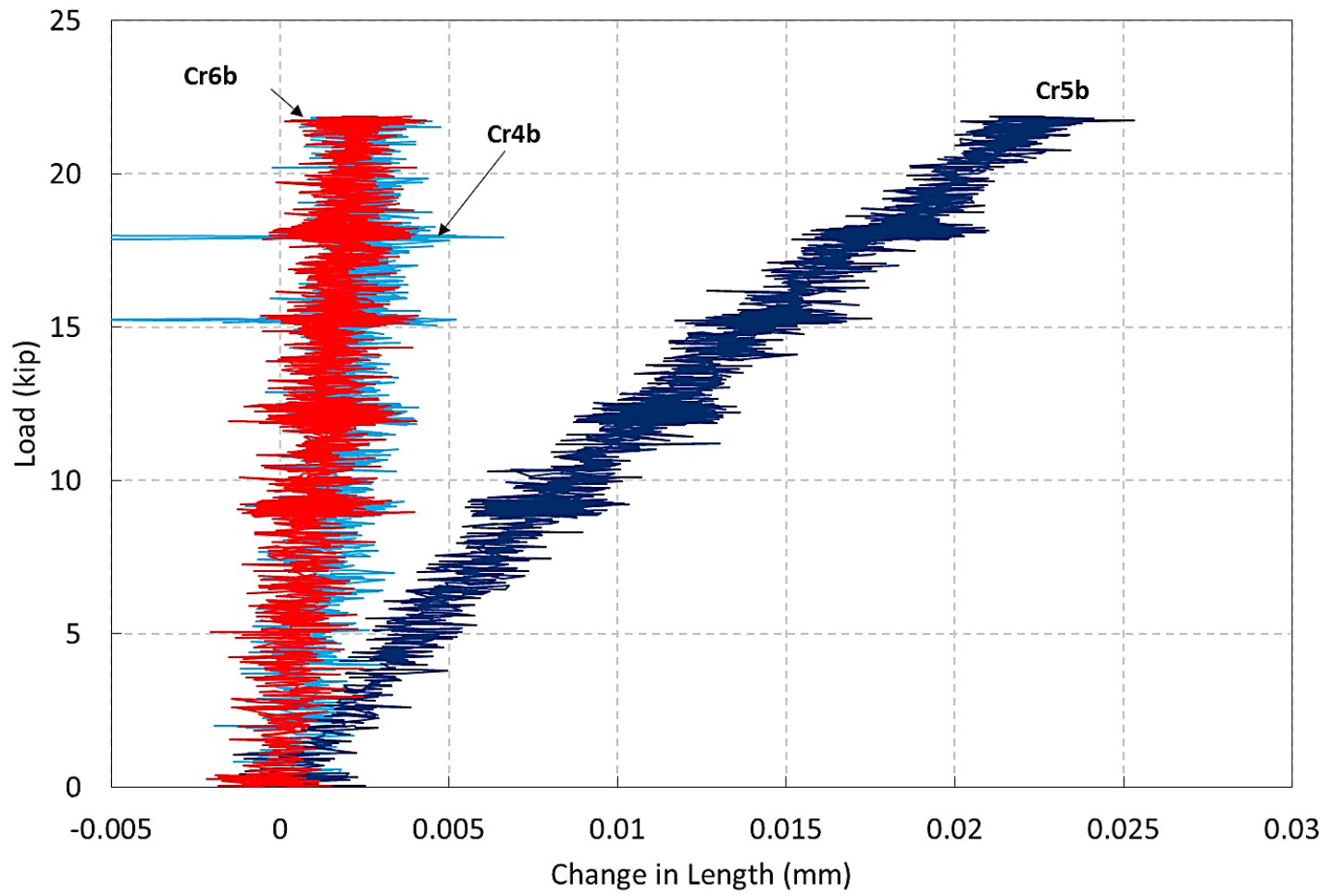
S1



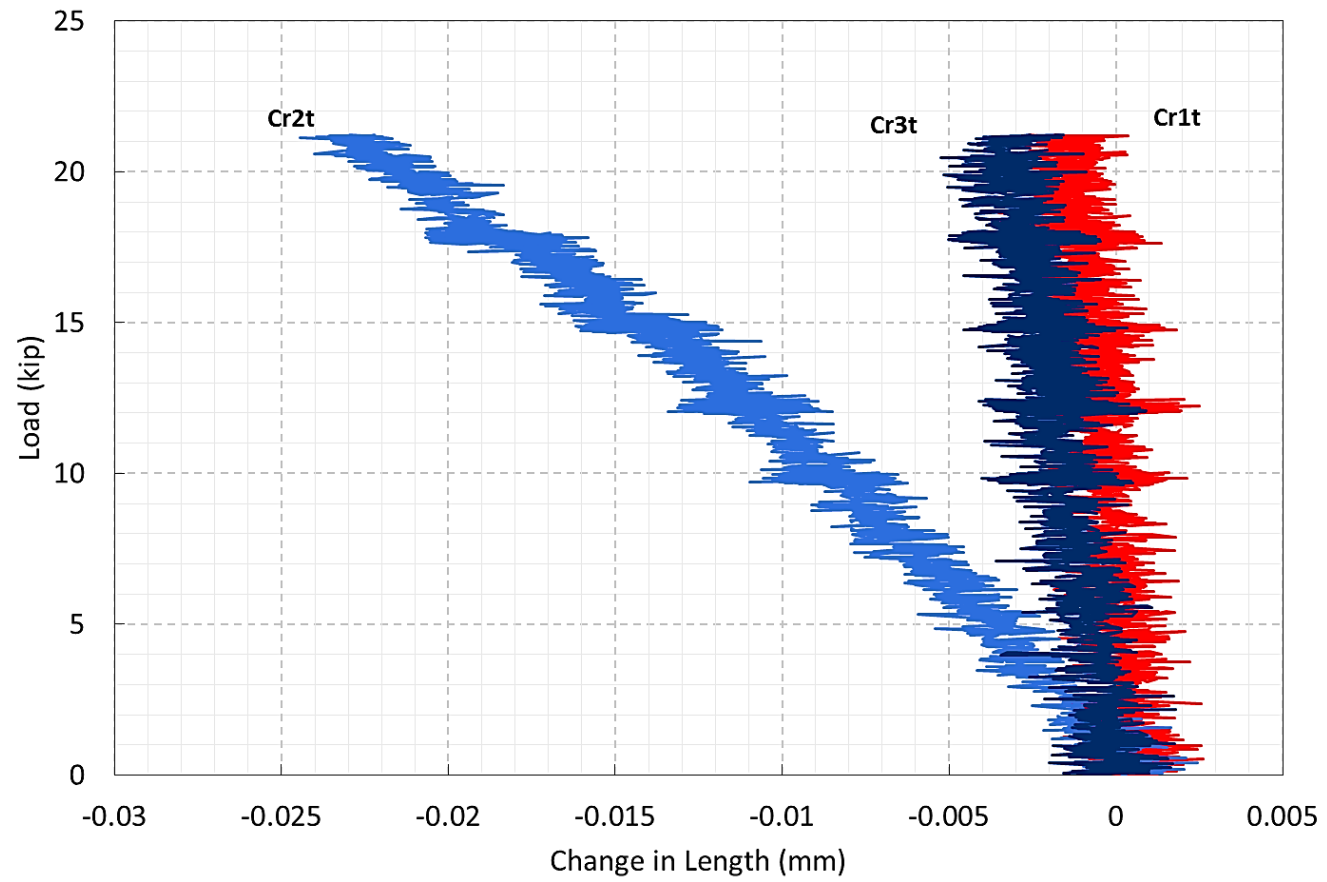


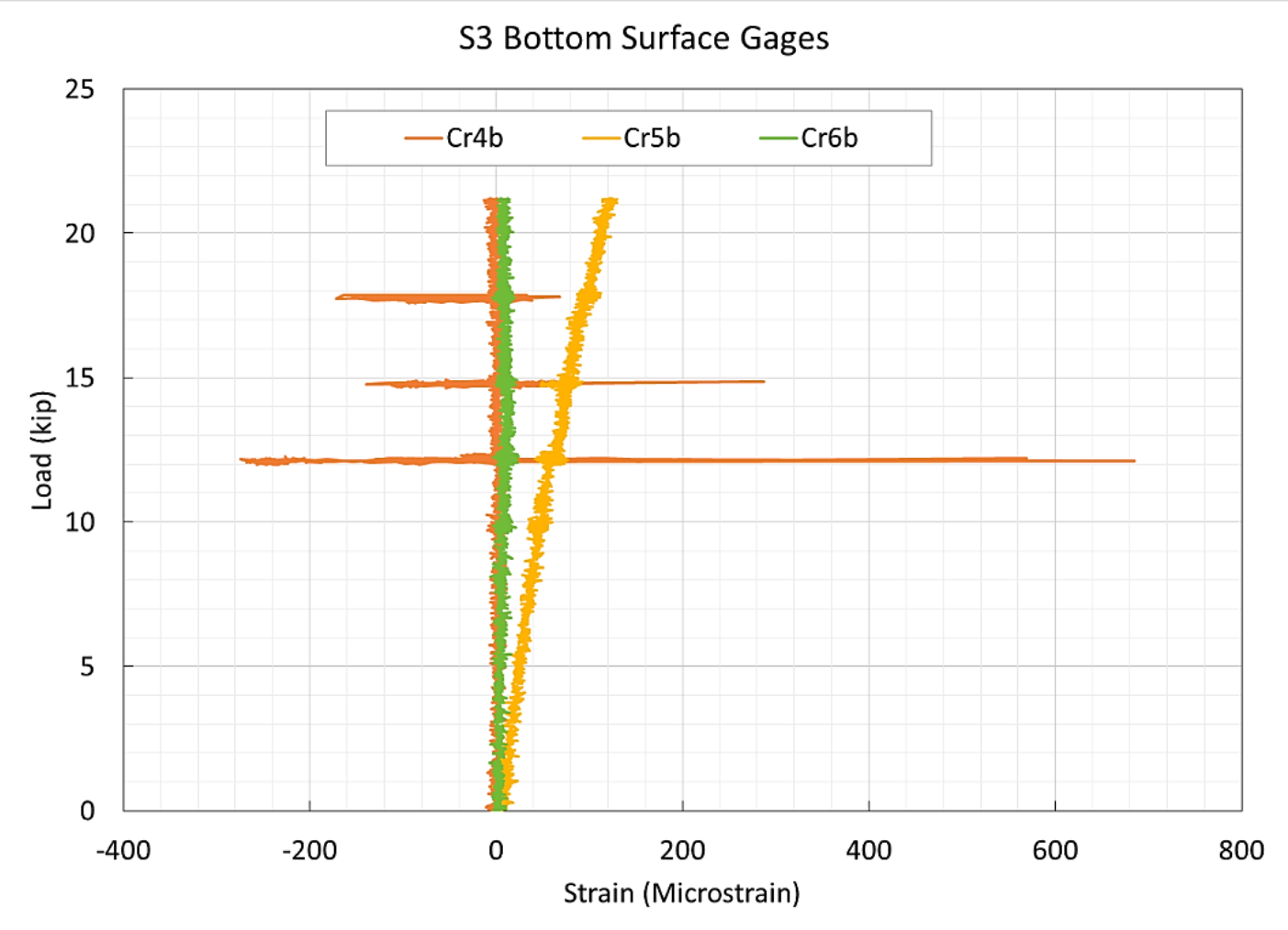
S2



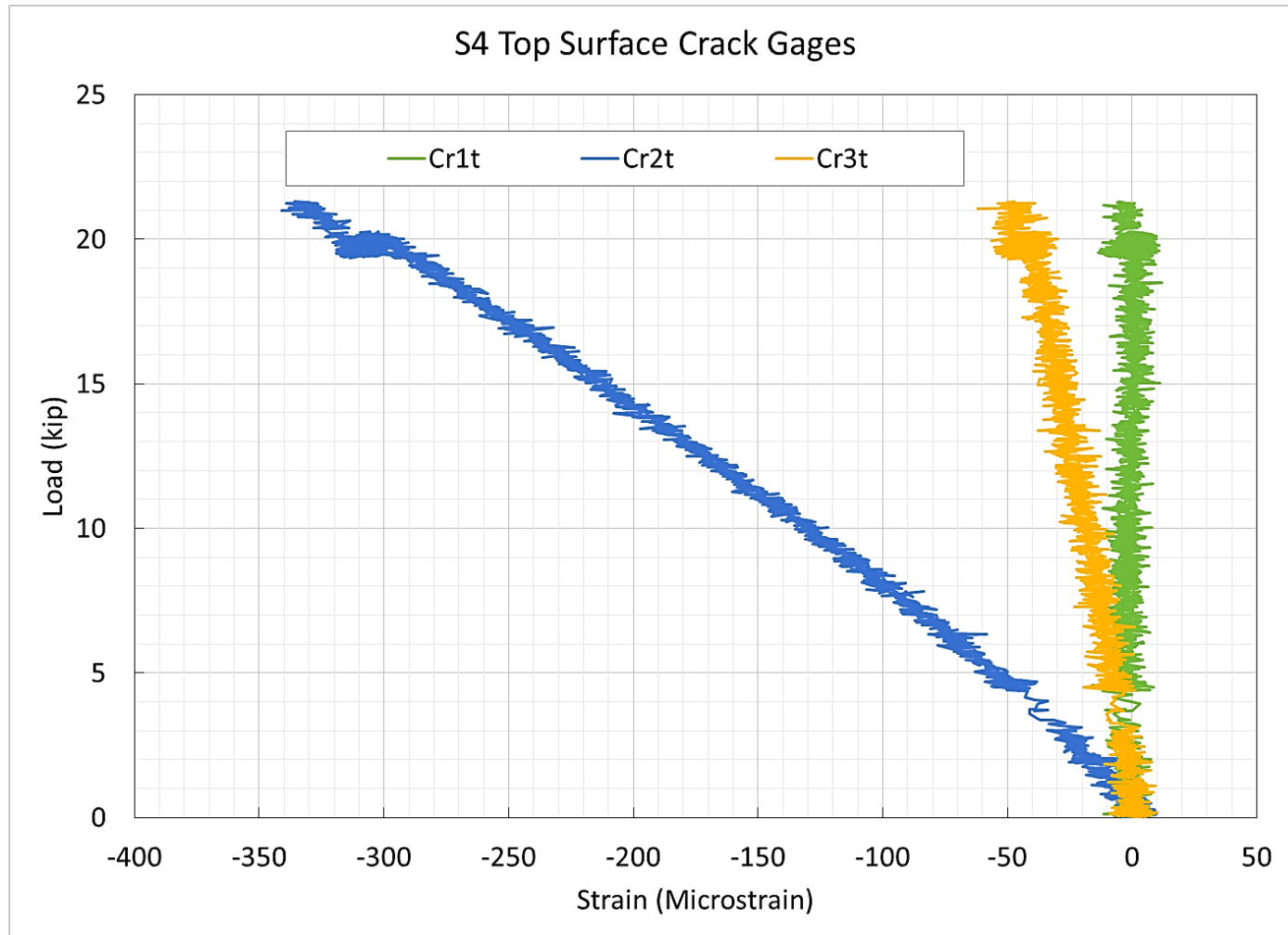


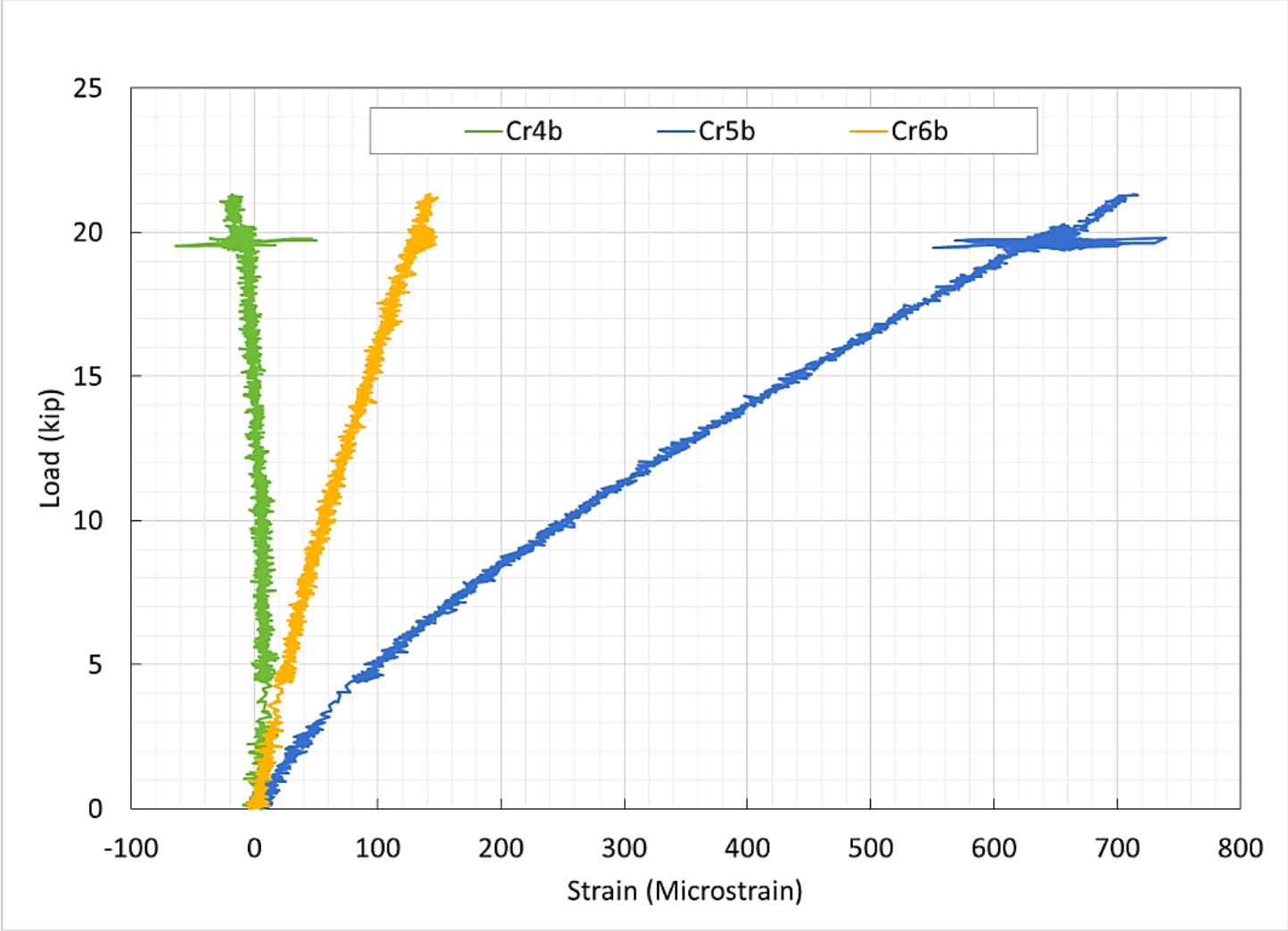
S3





S4

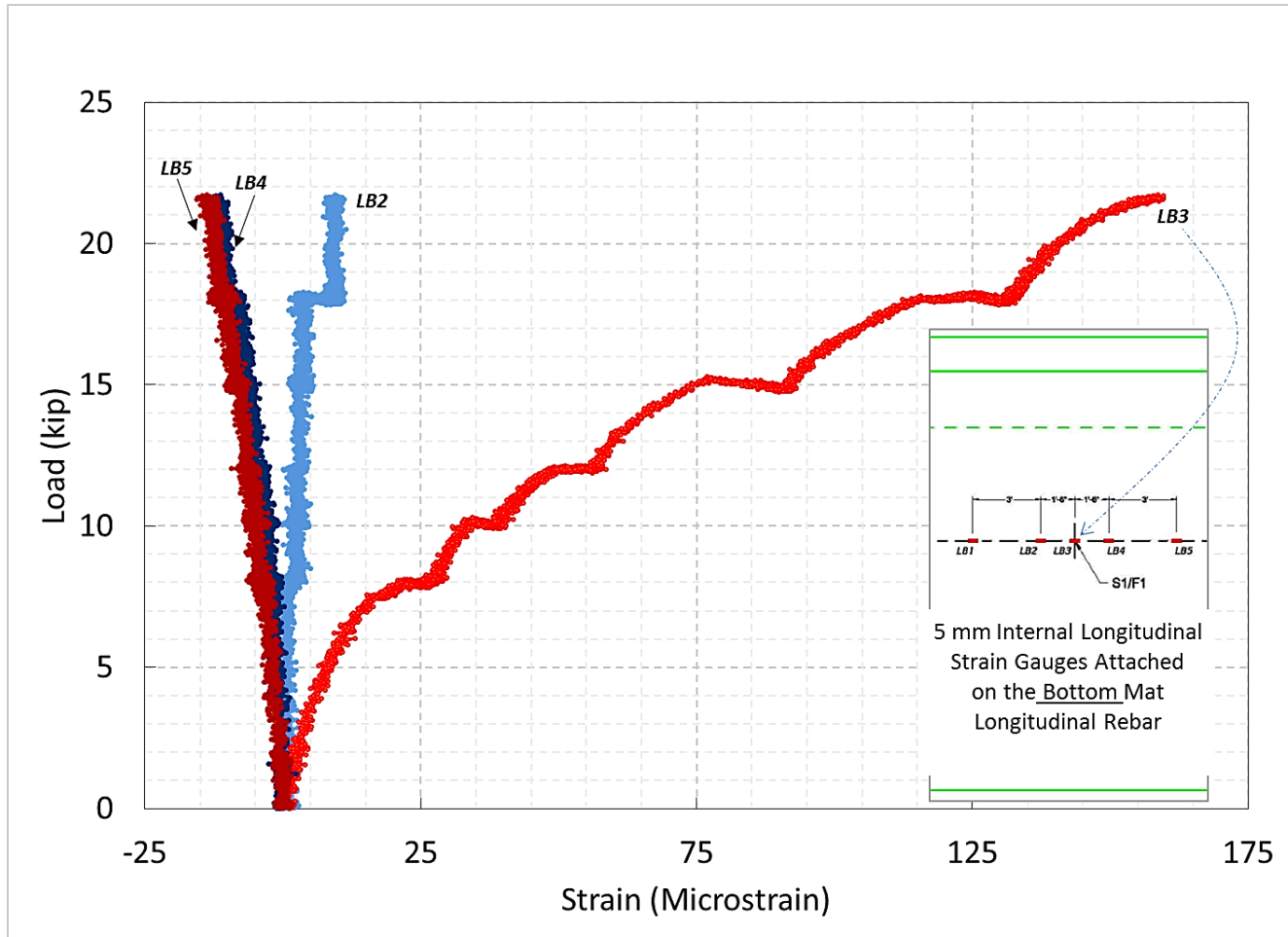




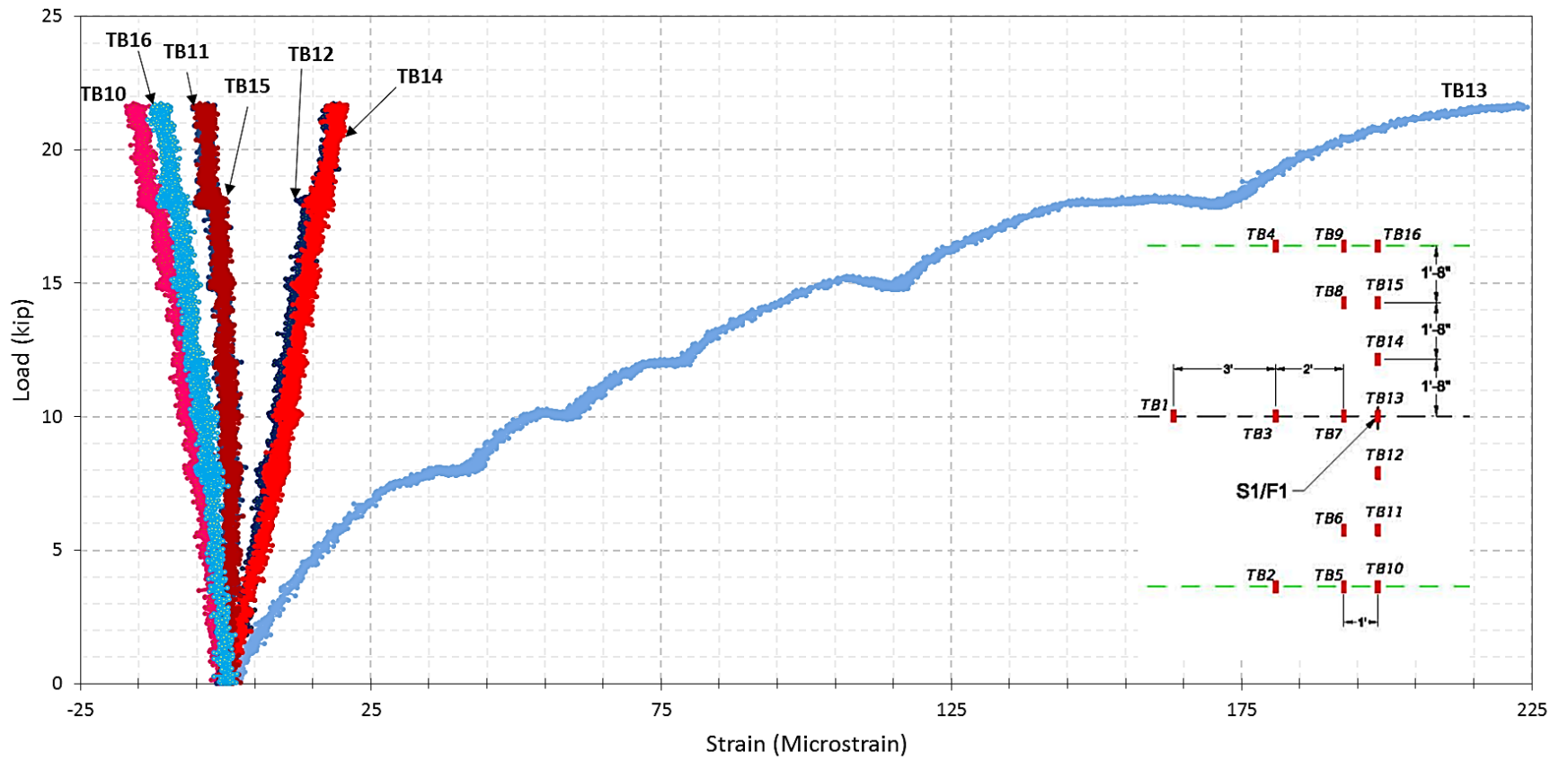
Strains

S1

Longitudinal Strain

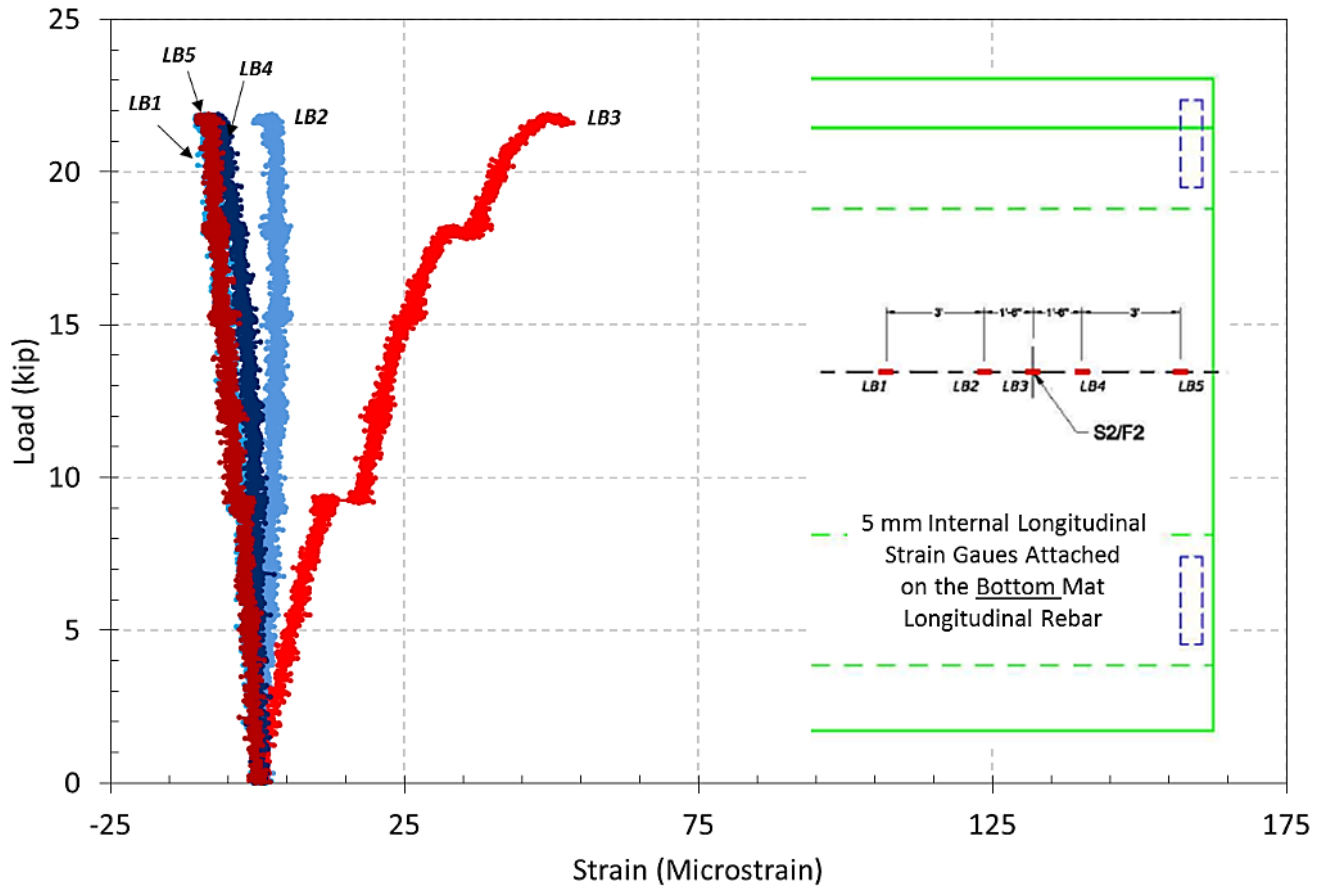


# Transverse Strain

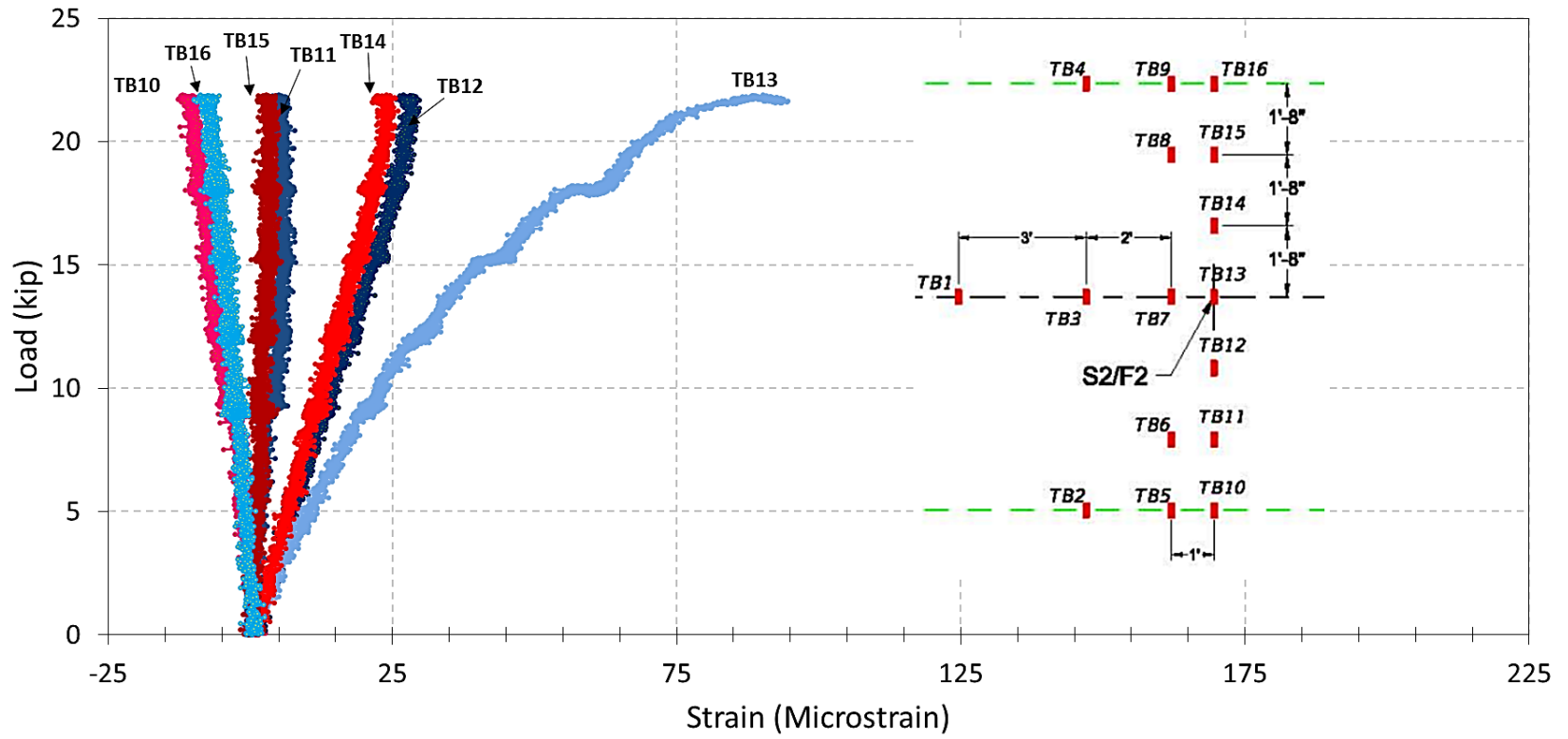


S2

Longitudinal Strain

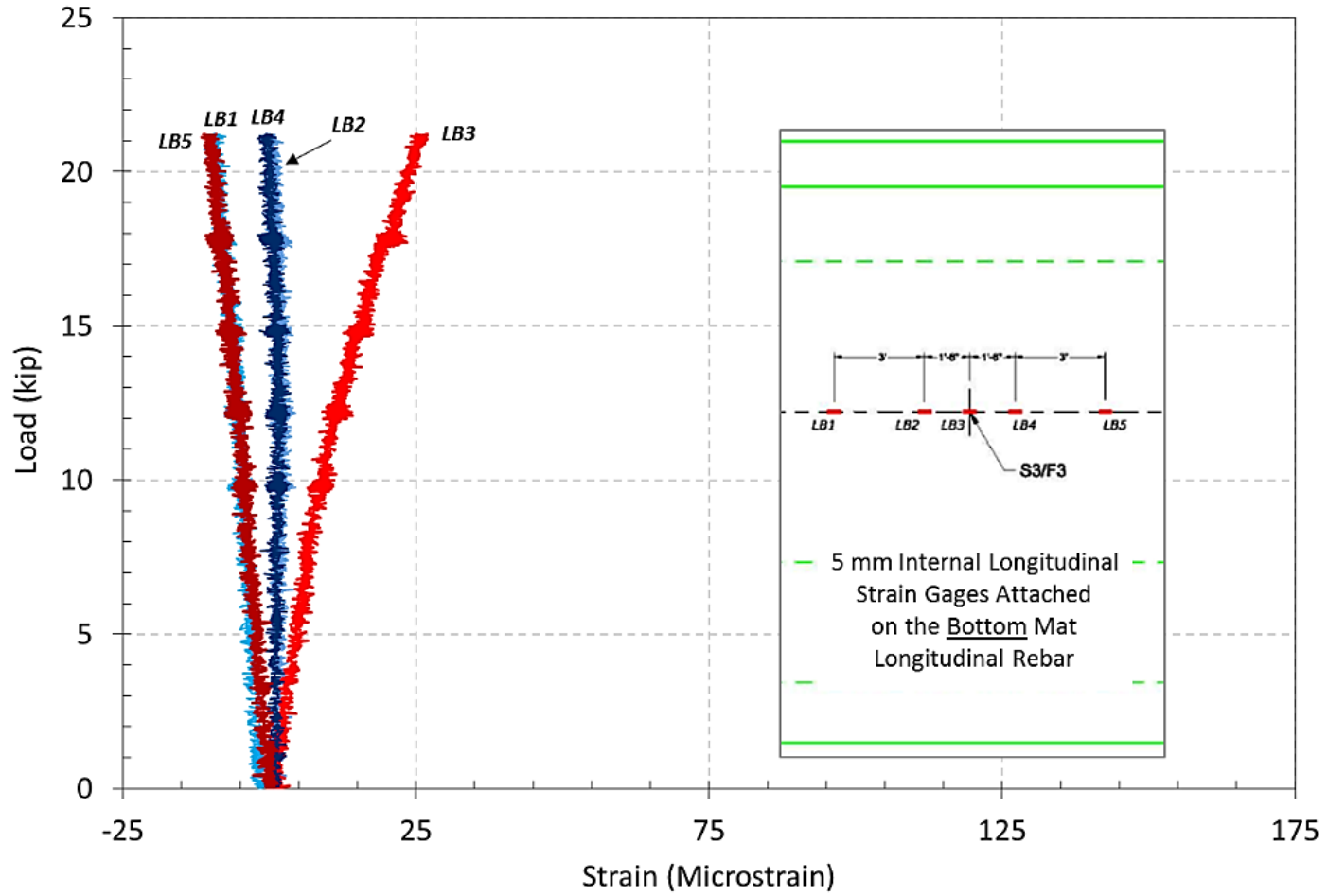


# Transverse Strain

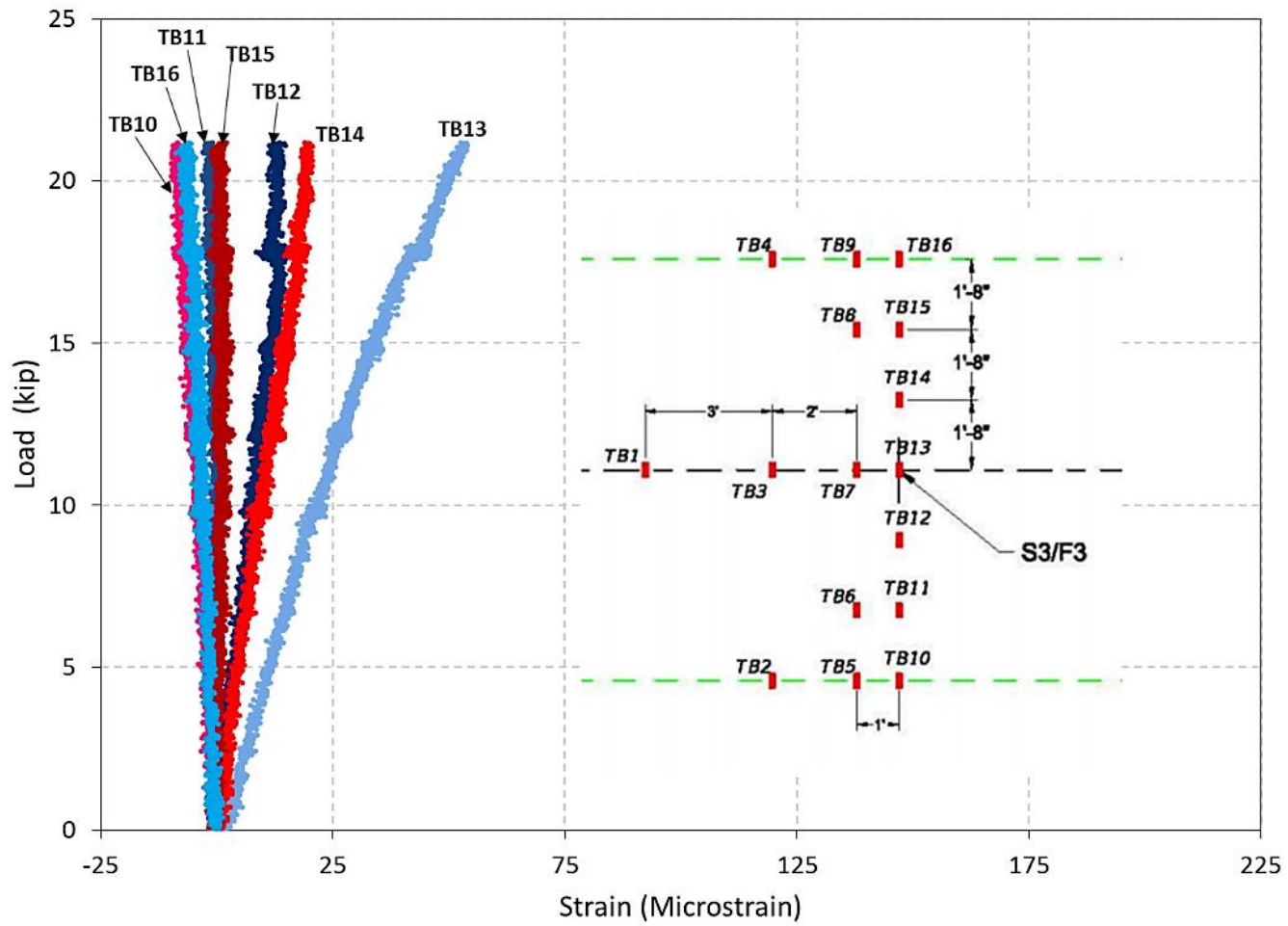


S3

Longitudinal Strain

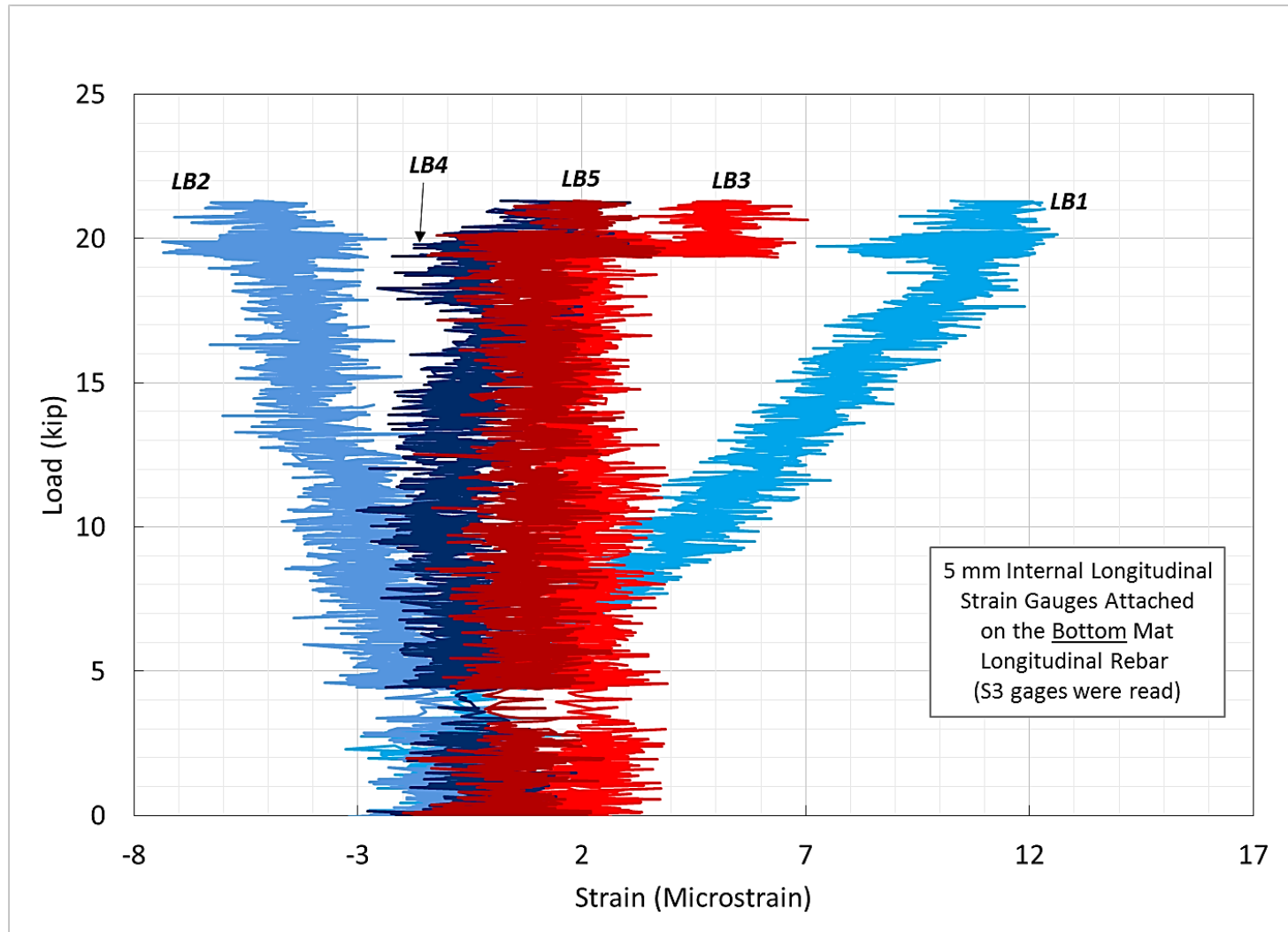


Transverse Strain

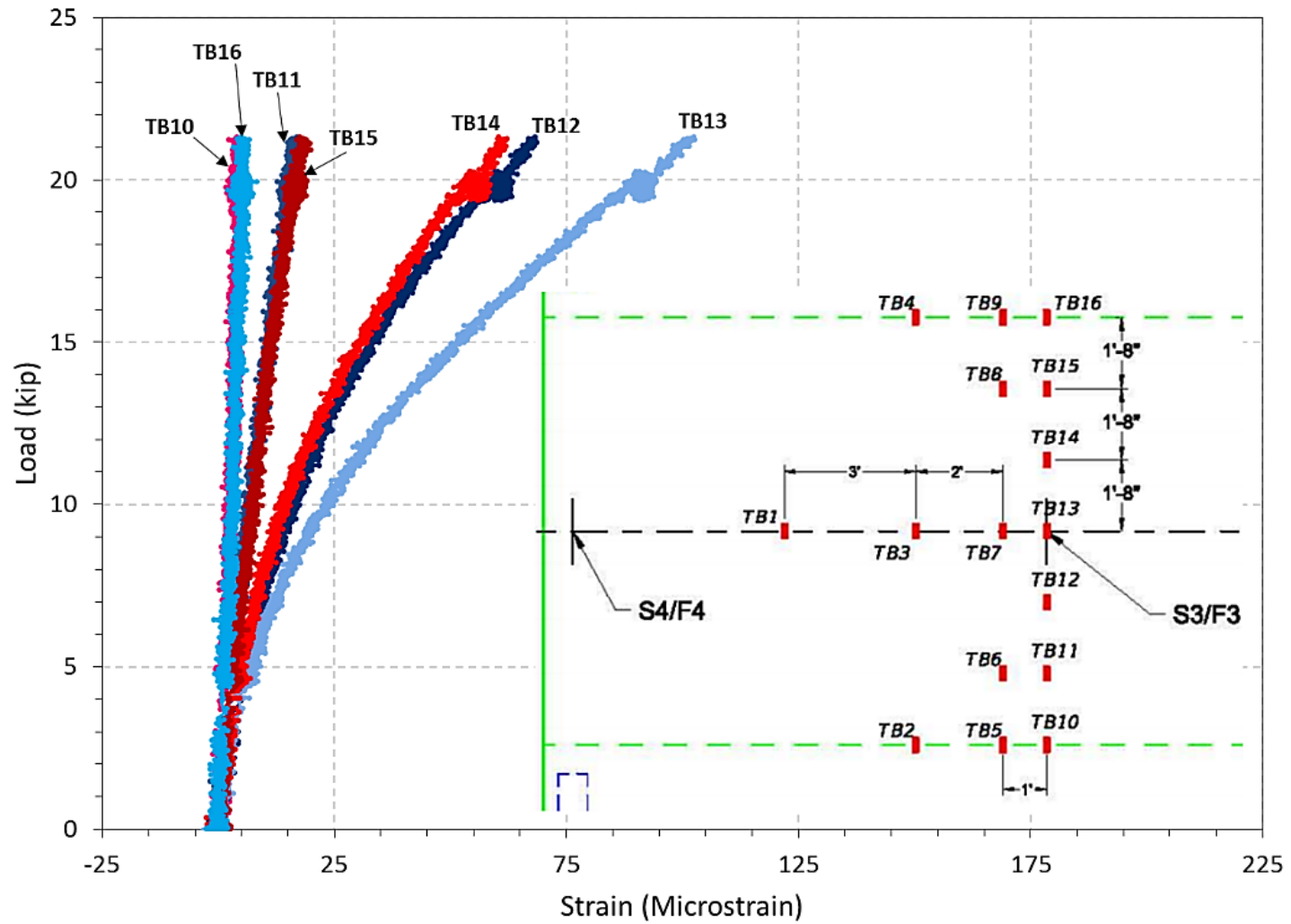


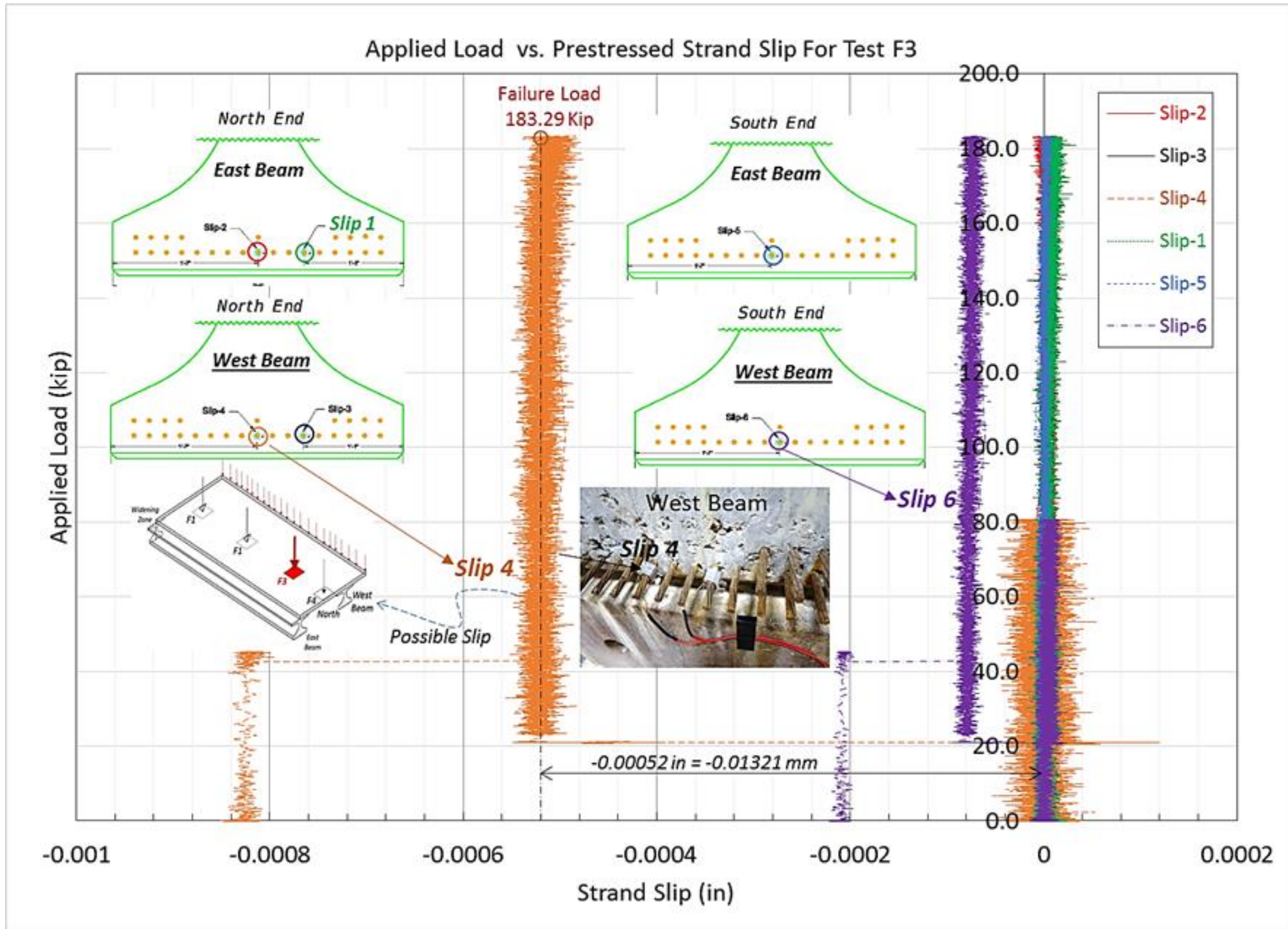
S4

## Longitudinal Strain



# Transverse Strain





# Crack and Surface Gauges

